Order Number 8908455

C-S-Fe correlation of shales hosting sedimentary manganese deposits

Liu, Tiebing, Ph.D.

University of Cincinnati, 1988

U·M·I
300 N. Zeeb Rd.
Ann Arbor, MI 48106

C-S-Fe CORRELATION OF SHALES HOSTING SEDIMENTARY MANGANESE DEPOSITS

A dissertation submitted to the

Division of Graduates Studies and Research
of the University of Cincinnati

in partial fulfillment of the
requirements for the degree of

DOCTOR OF PHILOSOPHY

in the Department of Geology
of the college of Arts and Sciences

1988

by

Tiebing Liu

A.B., Nanking University, 1976

M.S., Graduate School of Science and Technology
of University of China, 1982

UNIVERSITY OF CINCINNATI

December 1 19 88

I hereby recommend that the thesis prepared under my supervision by Tiebing Liu

entitled C-S-Fe Correlation of Shales Hosting Sedimentary Manganese Deposits

be accepted as fulfilling this part of the requirements for the degree of Doctor of Philosophy

Approved by:

ABSTRACT

Organic carbon (C) and sulfide sulfur (S) contents of host rocks and ore bodies selected from four manganese carbonate deposits were tested and plots of carbon against sulfur of the type proposed by Berner were used to distinguish depositional environments.

Taojiang, a manganese deposit of south China, occurs in the Middle Ordovician Modaoxi Formation. The ore body consists of well-crystallized rhodochrosite and is hosted by interbedded black and gray shales and gray mudstone. The plots of carbon versus sulfur show that the host rocks below the ore body are euxinic marine products, whereas the gray mudstone above the ore body is normal marine.

Xiangtan manganese deposit of South China occurs in the Lower Sinian Liantuo Formation. The hanging wall and footwall of rhodochrosite ore body are black shales with high organic carbon and sulfide sulfur contents. The plots of carbon versus sulfur suggest an euxinic environment throughout the whole ore-bearing sequence.

Molango, in the east-central Mexico, is the largest of the four deposits examined. The ore bed of the Molango manganese deposit is the basal unit of the Chipoco facies (Taman Fm., Kimmeridgian) and is underlain by laminated black shales of the "Santiago" Formation (Oxfordian). C-S plots suggest the black shale of the "Santiago" Formation

formed under an euxinic marine environment. The manganese ore bed consists of very finely laminated Mn-carbonate and has a low content of sulfide sulfur. The upper part of the Chipoco facies consists of organic-rich limestones and interbedded black shales. Both lithologies have a positive correlation between organic carbon and sulfide sulfur and may have been euxinic, although less so than the "Santiago".

Manuel's River prospect is a thin but widespread bed of rhodochrosite in eastern Newfoundland, Canada. The ore bed is the basal unit of the Middle Cambrian Chamberlain's Brook Formation. Host rocks consist of sideritic gray shale, gray shale, and black shale above the ore body and green shale and gray shale below the ore body. Both the ore body and host rocks contain very low organic carbon and sulfide sulfur which indicate normal marine conditions.

ACKNOWLEDGEMENTS

It is a great pleasure and privilege to acknowledge the many people and organizations who have aided my research efforts. I owe a great debt to those mentioned below.

My first thanks go to Dr. J. Barry Maynard who served as my chief advisor. I sincerely appreciate his encouragement and guidance in all stages of my doctoral program and research. This work and my growth as a scientist have benefitted greatly from the many hours of discussion with Dr. Maynard. I am also very grateful to Dr. W. A. Pryor and Dr. Holly Hucky who made up the rest of my committee. Their interest, constructive criticism, and encouragement are sincerely appreciated.

I am grateful to Drs. L. Ye and D. Fan, and colleagues at the Taojiang and Xiangtan mines for useful suggestions and support during the field work in China. I also thank Mr. X. Rao who worked with me during the field work in China.

Field work by Professor Maynard in Mexico was aided by Alfonso Martinez, and in Canada by Robert Stevens and David Strong. Special thanks are also due Dr. P.M. Okita and Dr. M. Lewan for offering part of organic carbon and sulfide sulfur analytical data and isotope analytical data. I would like to thank Drs. B.R. Bolton and J. Leventhal who reviewed a manuscript which based on this research, gave

useful suggestions, and arranged for it to be published.

Financial support was received from the Department of Geology, University of Cincinnati, University of Cincinnati Sedimentology Fund, from Cia. Minera Autlan, and from the Chinese Academy of Sciences in the form of tuition, teaching and research stipends, field and laboratory expenses.

Finally, a special thanks is owed to my wife Yan Hu. During the past four years, she has taken a great care to my parents and my son in China and supported me to finish my study in the U.S.A.

TABLE OF CONTENTS

LIST OF TABLES

LIST OF FIGURES

CHAPTER 1. INTRODUCTION

Shale is a fine-grained argillaceous sedimentary rock, consisting mainly of clay minerals. It forms more than 60% of the world's sedimentary rocks (Potter, et al., 1980). Because many types of economic deposits such as oil, natural gas, coal, uranium, and many metallic ore deposits occur in shales or have close relationships with shales, it is important to study the conditions of shale formation and the association between ore bodies and hosting shales. Total organic carbon (TOC), sulfide sulfur (S), and iron content of modern sediments and ancient rocks are considered to be sensitive indicators of geochemical environments (Sweeny, 1972; Leventhal, 1983; Berner and Raiswell, 1983; Berner, 1985; Raiswell and Berner, 1985). The purpose of this research is to investigate the TOC-S-Fe correlations of shales that host sedimentary manganese deposits and of manganese carbonate ore bodies in order to obtain a better understanding of the geochemical environments of formation of shales and thus of the manganese mineralization. Ore bodies studied are Taojiang and Xiangtan deposits of south China, Molango deposit of east-central Mexico and Manuel's River deposit (a prospective of manganese deposit) of Newfoundland of eastern Canada.

Economically significant, large accumulations of manganese are found on land (Verentsov and Grasselly, 1980; Roy, 1981), and covering a sizable portion of the modern ocean floor (Bonatti et al., 1972). Exploitation of the latter deposits is currently hindered by technological and political barriers (Assessment of Manganese Nodule Resources, 1982; Analysis of Exploration and Mining Technology for Manganese Nodules, 1984). Consequently, all manganese production is from land-based deposits which are commonly composed mainly of Mn-oxides. The primary pre-weathering Mn-bearing minerals of these deposits may have been oxides, carbonates, or a mixture of both.

Manganese deposits of economic importance can be grouped into two general categories: (1) supergene deposits formed by weathering of manganiferous rocks and (2) primary deposits, which include volcanogenic and non-volcanogenic sedimentary deposits. The deposits of Gabon and Brazil (National Materials Advisory Board, 1981) and those of India (Roy, 1981) are examples of important supergene deposits. By far the most important type of primary deposit is the shallow marine sedimentary deposit (Cannon and Force, 1983). Sedimentary manganese mineralization is the result of syngenetic or diagenetic precipitation of manganese. Examples of this type of deposit include Nikopol and Chiatura in the Soviet Union (Gryaznov and

Danilov, 1980), Groote Eylandt in Australia (McIntosh, et al., 1975), Kalahari in South Africa (de Villiers, 1971), and the Molango deposit in Mexico (Tavera and Alexandri, 1972; Canon and Force, 1983; Alexandri and Martinez, 1986; Okita, 1987).

All four deposits selected for this study are marine sedimentary manganese carbonate deposits. Among them, the Molango deposit, which is the largest manganese deposit in the North America and occurs in Jurassic black shales and organic-rich limestones, is well studied both in terms of geochemical features of the ore body and environmental analysis of the host rocks (Cannon and Force, 1983; Okita, 1987; May, 1988). Both the Taojiang deposit, occurring in a Middle Ordovician black and gray shale sequence, and the Xiangtan deposit, occurring in Precambrian black shale sequence, are important manganese carbonate deposits in China, but are rarely reported in English-language literature (Ye, et al, 1987). The Manuel's River prospect of the Newfoundland is not well studied. It occurs in a Cambrian gray shale and black shale sequence with a manganese carbonate ore horizon.

In deep and strictly anaerobic marine basins, manganese has an appreciable solubility. Iron precipitates in the reduced condition as pyrite with black shale, whereas manganese can be moved in reduced seawater or mobilized

from sediments by diffusion and dissolution. If this manganese-rich, iron depleted ore-forming solution moves to the basin margins or onto some submarine topographic high, manganese can be precipitated as manganese carbonate or manganese oxides at the interface of oxidizing and reducing conditions. Manganese oxide-facies deposits are preserved on oxic substrates in shallow water. Manganese carbonate-facies deposits apparently can form either on these oxic substrates or on reduced substrates in slightly deeper water. Based on this scheme, a stratified-basin margin model (also called bath-tub-ring model) was proposed by Cannon and Force (1983) that emphasized oxygen gradients in the basin water.

This model is generally appropriate for explaining many aspects of the large sedimentary deposits in which the ore bodies consist mainly of manganese oxides (Mn^{+4}), but difficulties exist with its detailed application to the deposits of this study in which all of the primary ore is a carbonate. The model does not explain the abundance of Mn-carbonates, because manganese is held in carbonate phases in the reduced (Mn^{+2}) state. In order to refine this model, it is very important to decipher the depositional environments of each of the manganese carbonate bearing sequence of four deposits mentioned above by studying and comparing the stratigraphic, petrographic, mineralogic, and

geochemical features of host rocks as well as the manganese carbonate ore bodies.

A geochemical method of measuring total organic carbon (TOC), sulfide sulfur (S), DOP (degree of pyritization of iron), and sulfur isotopes of modern sediments and ancient rocks, proposed by Leventhal (1983), Berner (1985), and Raiswell and Berner (1985), has been used to distinguish depositional environments. In marine depositional environments, many biological and chemical processes are dependent on the availability of reactive C and S species. Organic Creduces dissolved sulfate (SO_4^{-2}) in seawater to sulfide species (H_2S) (Berner, 1972), a reaction that occurs only under strictly anaerobic conditions, as a result of bacterially mediated C oxidation (Berner, 1982, 1984). The sulfide produced from the reduction of sulfate reacts with ferrous iron (Fe^{2+}), and is precipitated as pyrite (FeS_2) (Berner, 1967, Goldhaber, 1983).

In normal marine sediments (those deposited in oxygenated bottom waters), pyrite formation is limited by the concentration and reactivity of organic matter, whereas in euxinic (sulfidic, usually deep water condition) basins, pyrite formation is limited by the abundance and reactivity of detrital iron minerals. In non-saline swamp and lake sediments, pyrite formation is limited by the low levels of dissolved sulfate found in fresh water. Because of these

differences in limiting factors, these three depositional environments can be distinguished in both modern sediments and ancient rocks by plots of organic carbon versus sulfide sulfur (Berner, 1985). The degree of pyritization of iron (DOP), which is expressed as Fe_{pyrite}/Fe_{total}, is used to determine whether pyrite formation in a given sample was iron-limited (euxinic condition) or organic carbon-limited (normal marine) (Raiswell and Berner, 1985). The sulfur isotope data can provide information about the openness of a restricted basin to the open ocean. The TOC-S-Fe correlation and sulfur isotope composition, already used to study terrigenous modern sediments and ancient rocks (Berner, 1970; Sweeney, 1972, Garrels and Perry, 1974; Berner and Raiswell, 1983, 1984; Garrels and Lerman, 1984; Raiswell and Berner, 1985; Gibson, 1985; Raiswell and Berner, 1986; Fisher, 1986; Jenkyns, 1986; Hennessee, et al., 1986; Gautier, 1986, 1987; Anderson, et al., 1987; Leventhal, 1987; Raiswell and Berner, 1987; Sweeney, et al., 1987; Fisher and Hudson, 1987; Donnelly, et al., 1988), can also be extended to the study of manganese carbonate-bearing sequences to provide more information about depositional conditions and thus of manganese mineralization.

The objective of this research is to investigate the correlation among organic carbon, sulfide sulfur, and DOP

of shales that host sedimentary manganese carbonate mineralization selected from the Taojiang and the Xiangtan deposits of south China, the Molango deposit of east central Mexico, and the Manuel's River deposit in Newfoundland, eastern Canada, to help reveal paleo-environmental conditions of sedimentation and thus of the ore-forming processes, and to further refine the stratified-basin-margin model.

CHAPTER 2. STUDY METHODS AND EXPERIMENTAL PROCEDURES

The study methods for this research include field work in two Chinese manganese deposits, petrographic study, whole rock X-ray diffraction analysis, organic carbon and sulfide sulfur content measurements, and acid soluble iron determination. Fifteen samples from three stratigraphic levels of the Taojiang manganese deposit, South China were sent to U.S. Geological Survey for isotope analysis of sulfur, carbon, and oxygen determined by Dr. Patrick M. Okita and to Amoco Production Company Research Center for chemical analysis of organic matter determined by Dr. Michael D. Lewan.

Sample Collection and Preparation

Samples for this research were collected from two major sources: (1) field samples and (2) the University of Cincinnati's Geology Department sample collection. In the summer of 1986, field samples were collected in Taojiang and Xiangtan manganese deposits, Hunan Province, South China. Ninety-eight samples, including black shales, gray shales, mudstones, Mn-limestones, and rhodochrosite ores were collected from these two deposits. Two stratigraphic sections of ore-bearing sequences in two underground mining areas and one surface stratigraphic section above the ore-bearing sequence were measured in the Taojiang deposit and

one stratigraphic section of ore-bearing sequence was measured in the Xiangtan deposit. Another 70 samples, representing the Molango manganese deposit, east-central Mexico and a prospective manganese deposit in Manuel's River of Newfoundland, eastern Canada, were selected from the Geology Department's collection. Published data of organic carbon and sulfide sulfur contents of normal marine shales and euxinic marine shales were also used.

Representative samples of each kind of lithology and from rhodochrosite ores were selected and cut for making normal petrographic thin sections, polished thin sections, and polished chips for both transmitted light and reflected light microscope observations. Samples were powdered to less than 125 microns (<200 mesh) for X-ray diffraction analysis, organic carbon and sulfide sulfur contents and acid soluble iron measurements. Fifteen samples were selected from one underground stratigraphic section of the Taojiang manganese deposit for analysis of organic matter and isotopes of sulfur, carbon, and oxygen. In order to measure organic carbon content, each sample was weighed before and after treatment with 10% (weight) warm HCl. The percentage of acid soluble minerals (mostly carbonates) was calculated for each sample and the residues were subjected to analysis for organic carbon content. For sulfide sulfur

content and isotope analysis, samples were powdered shortly before the measurements.

Whole Rock X Ray Diffraction Analysis

A Siemens-Allis D 500 X-ray diffractometer with copper radiation was used for determining major mineral phases of whole rock powdered samples (Fig. 1). The working conditions of the X-ray diffractometer were as follows: X-ray tube voltage -- 40 kv, current -- 30 mA, and scanning speed -- 0.05 degree per second. For shales, the scanning range is from 1 degree (2 theta) to 90 degrees; for carbonates, from 1 degree to 80 degrees. The X-ray diffraction (XRD) data were analyzed based on comparison with the JCPDS (Joint Committee on Powder Diffraction Standards) files (Carver, 1971).

Organic Carbon Content Measurement

A Perkin Elmer 240 combustion elemental analyzer was used for measuring total carbon and organic carbon contents of all samples (Krom and Berner, 1983). The Model 240 Elemental Analyzer (Fig. 2) accurately determines carbon, hydrogen, and nitrogen contents of whole rock samples by detecting and measuring their combustion products (CO_2, H_2O, and N_2). For this study, only carbon content of samples is concerned.

Figure 1. The Siemens-Allis D 500 X ray diffractometer.

Figure 2. The Perkin Elmer 240 combustion elemental analyzer.

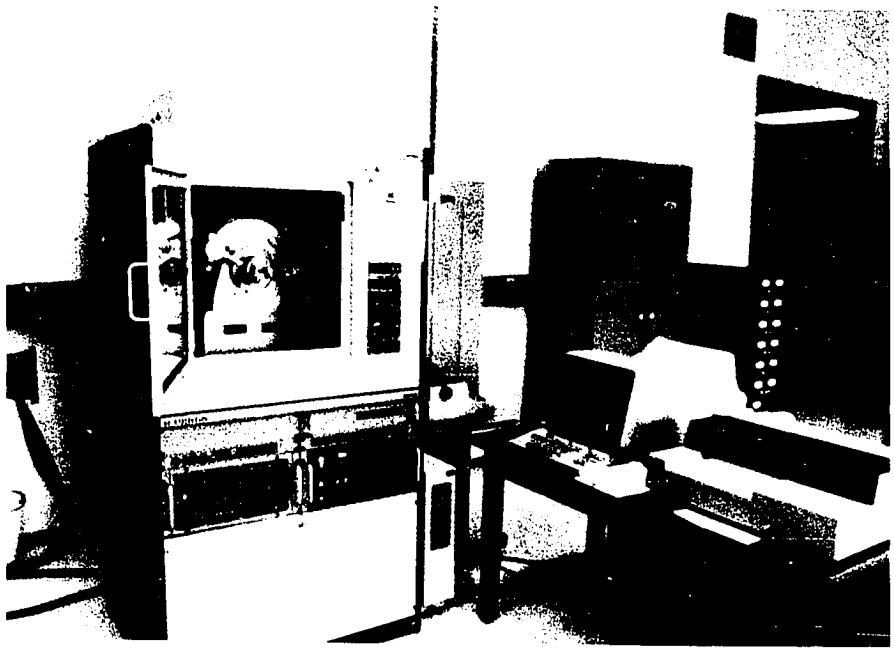

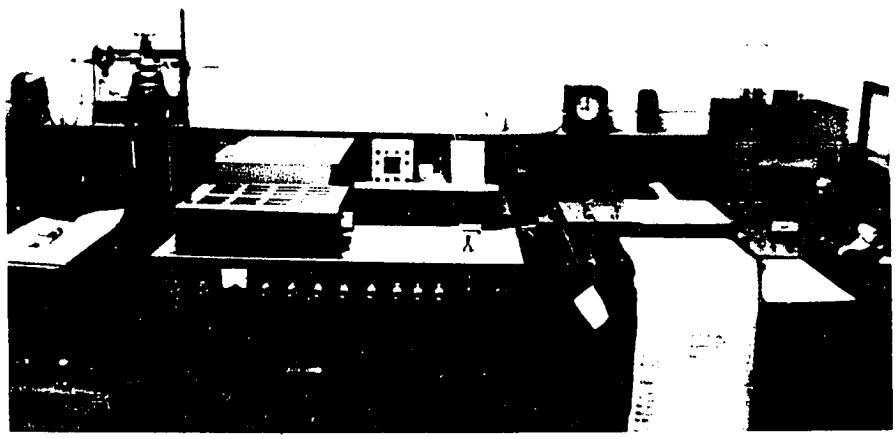

Ohio Devonian shale was used as the standard sample, which is of carbon content 6.9% (weight) as measured by U.S. Geological Survey. The result of measurement of the standard sample is the voltage difference between blank run and standard sample (6.9 weight-percent carbon). A K value (2.86) was obtained by dividing the voltage difference over 6.9 and sample weight. This K value can then be used to convert the voltage difference recorded by the machine to weight percentages of carbon of unknown samples. The experimental error is approximately 0.1 - 0.5 per cent of carbon content based on duplicate samples run during this study. Each day, after several blank runs were run for warming up the machine, the standard sample was tested at least three times to ensure reproducible results. Finally, other samples could be measured continuously. Some samples were tested twice or three times for controlling the system's accuracy.

Sulfide Sulfur Content Measurement

Sulfur can be found in modern sediments and ancient rocks as pyrite, elemental sulfur, sulfate and organic sulfur (Zhabina and Volkov, 1978). For this study, the chromium reduction technique described by Canfield et al. (1986) and modified by Okita (1987) was used to determine reduced inorganic sulfide sulfur.

The general procedure involves digesting 1 to 2 grams of sample in two steps. First, removal of carbonate and acid soluble sulfides is accomplished using hot 6N HCl. Second, conversion of pyrite to H_2S gas is performed by adding a solution of $CrCl_3$ reduced over zinc (a Jones Reductor) and heating for several hours. The evolved H_2S gas is bubbled into a silver nitrate solution and converted to silver sulfide. The entire process is carried out in a nitrogen atmosphere. The product silver sulfide was weighed and the weight used to calculate the sulfide sulfur content of the samples (see Appendix A for details).

Figure 3 shows a general setup scheme of sulfide sulfur determination as proposed by Canfield et al. (1986). Figure 4 shows the actual setup of the system used for this study. It was found that using zinc powder to reduce $CrCl_3$ solution (green) to $CrCl_2$ solution (blue) is more effective than using zinc shot as described by Okita (1987), because zinc powder can float on the surface of the solution and protect $CrCl_2$ solution from the air (Fig. 5).

Two methods were used to determine the accuracy of this sulfur determining system: (1) measuring single-crystal pyrite samples (the theoretical weight percent of sulfur in pyrite is 53.34), and (2) repeating tests of the same sample. The results indicate that the percentage

Figure 3. A general setup scheme of sulfide sulfur determination (based on Canfield et al., 1986).

Figure 4. The actual setup of the sulfide sulfur determining system of this research.

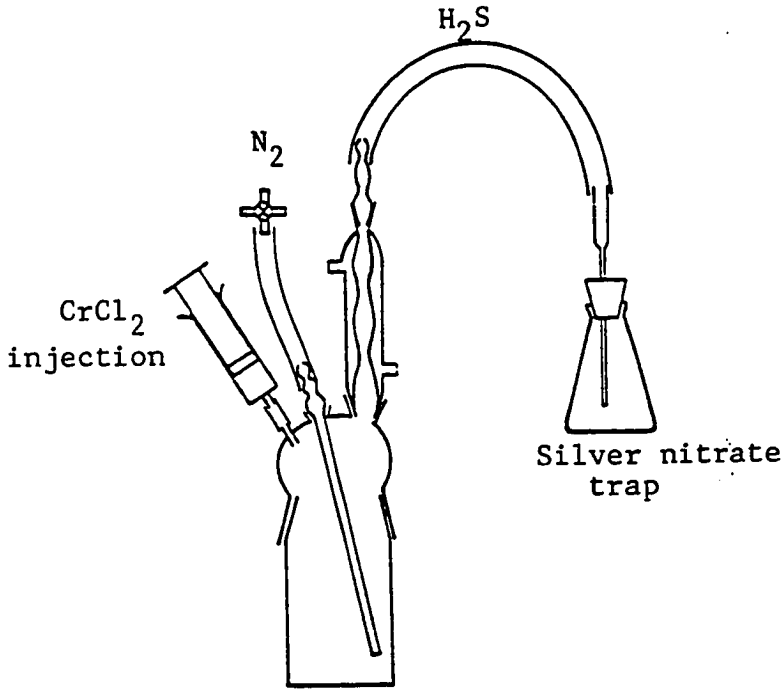

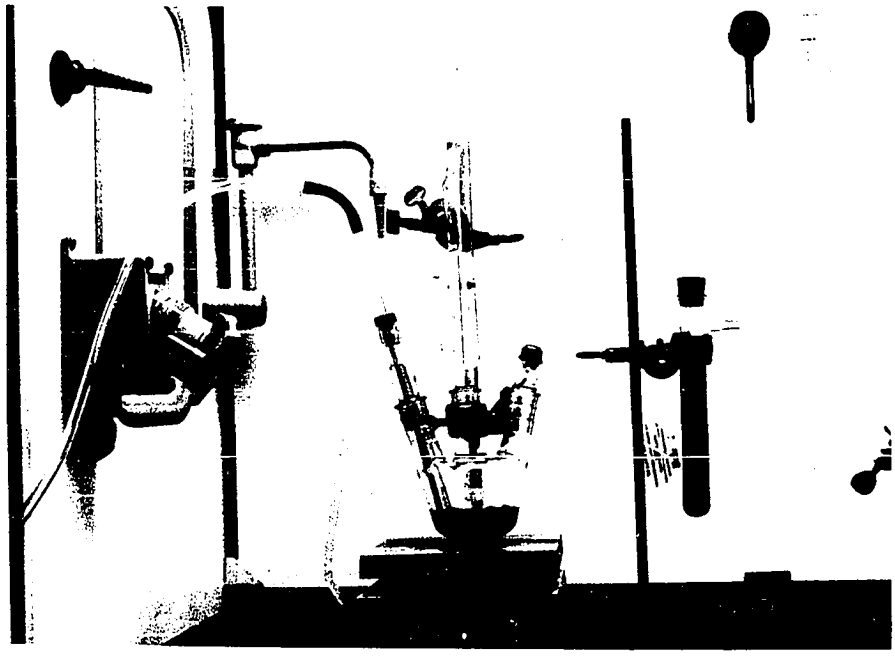

Figure 5. $CrCl_3$ reducing setup. Notice that zinc powder floated on the surface of the $CrCl_2$ solution which is blue in color.

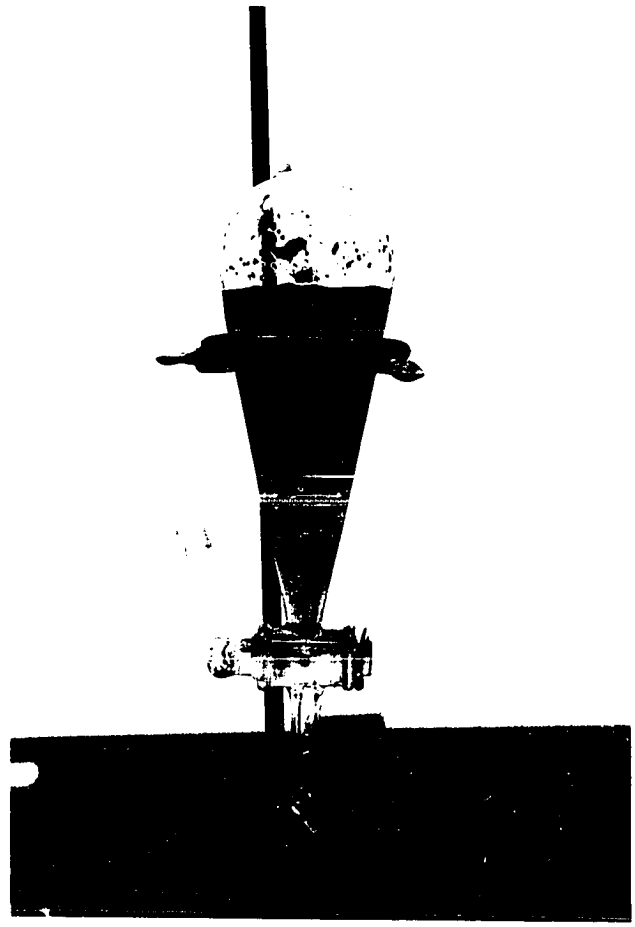

conversion of sulfur from pyrite is 97% (4 samples) and the average error of repeated tests for the same sample is about 0.1% of sample weight.

The time for complete conversion of pyrite to H_2S gas depends on the concentration of pyrite in the sample. Generally, two hours of reaction are necessary for pyrite-poor samples, four or more hours for pyrite-rich samples.

Acid Soluble Iron Determination

The degree of pyritization of iron (DOP) is expressed as $Fe_{pyrite} / Fe_{pyrite} + Fe_{HCl}$. Fe_{HCl}, which means acid soluble iron, was obtained by boiling each sample in 12 N HCl for one minute on a hot plate (Berner, 1970). This treatment was adopted because it extracts the most reactive (towards H_2S) iron compounds and is reproducible. Dissolved iron was determined by the 0-phenanthroline colorimetric method (Sandell, 1959, Taras, 1971) using a Beckman Model DU-2 spectrophotometer. In this study, both total and ferrous acid soluble iron were measured.

The principle of the colorimetry method is that (1) iron is dissolved into solution and reduced to the ferrous state by boiling with acid and hydroxylamine; and (2) treated with 1,10-phenanthroline at pH 3.2-3.3. Three molecules of phenanthroline chelate each atom of ferrous iron into an orange-red complex. The colored solution

obeys Beer's law; its intensity is independent of pH from 3 to 9 and is stable at least 6 months. A pH between 2.9 and 3.5 insures rapid color development in the presence of an excess of phenanthroline (Taras, 1971).

In this study, both ferric oxide (Fe_2O_3) and ferrous sulfate ($FeSO_4$), analytical compounds produced by Fisher Scientific Company, were used to make the standard solutions (200mg/l) by dissolving them in concentrated HCl and boiling for a minute on a hot plate. The standard solutions were diluted into different concentrations from 10mg/l to 1mg/l. The ferric oxide solutions were treated with hydroxylamine (100g/l) to reduce ferric iron to ferrous iron before coloring. The series of standard samples was then treated with ammonium acetate buffer and phenanthroline solution to develop color. The colored solutions were measured with a Beckman Model DU-2 spectrophotometer (selecting tungsten lamp source and 510 m wavelength) to obtain absorption values. A linear plot of absorption value versus concentration of standard solutions was made. The ratio of the concentration of solution versus the absorption value is 1.88. Each unknown for this study was treated with the same procedure. Two sample sets are necessary for each unknown. One set is treated with hydroxylamine to reduce all iron into ferrous state. In another sample set without hydroxylamine

treatment, only acid soluble ferrous iron will be colored by adding phenanthroline solution. The absorption value of each unknown read from the spectrophotometer was calculated based on the absorption value versus concentration diagram of standard solutions to obtain the actual acid soluble ferric and ferrous iron percentages in the rocks.

CHAPTER 3. GEOLOGICAL SETTINGS, AND STRATIGRAPHIC AND PETROGRAPHIC FEATURES OF THE MANGANESE DEPOSITS STUDIED

In this chapter, the geological settings and stratigraphic and petrographic features of four manganese deposits, Taojiang, Xiangtan, Molango, and Manuel's River prospect, are described. Descriptions of the two Chinese deposits are mainly based on my own field work; the Molango deposit and the Manuel's River prospect are mainly based on information from the literature and the samples collected by members of the geology department, University of Cincinnati.

Classification and Distribution of Manganese Deposits of China

Manganese deposits are widely distributed in China. Based on the features of regional tectonics and sedimentary environments as well as genetic characteristics, seven important metallogenic provinces can be identified. The commercial manganese deposits are distributed mainly on marginal areas of mobile platforms. The main metallogenic epochs of manganese deposition in China are Sinian (Late Proterozoic, 500 - 800 m.y.) and Devonian. (Ye, et al., 1988).

Based on their origins, manganese deposits in China can be divided into (1) sedimentary, (2) volcanic-sedimentary,

(3) metamorphosed sedimentary, (4) hydrothermally modified sedimentary, (5) hydrothermal, and (6) supergene deposits (Table. 1. Ye, et al., 1988).

An estimate of the percentage of original reserves of various deposits in China (Fig. 6), calculated on the basis of available data (Fu, 1983, personal communication), shows that sedimentary and supergene deposits are the most important manganese deposits for industry. About 70% of the total reserves of manganese deposits in China are sedimentary. Among them, marine sedimentary manganese is dominant, while lacustrine deposits are rarely seen. Marine sedimentary manganese deposits are distributed widely in age from Middle Proterozoic to Quaternary, and are especially abundant in Sinian (Late Proterozoic), Ordovician, Devonian, Permian, Triassic, and Quaternary rocks. According to the lithological association of ore-bearing sequences, such manganese deposits can further be divided into three types: (1) mudrock type; (2) "black shale" type, i.e. black shale series type, and (3) carbonate rock type (Ye, et al. 1988). Mudrock type manganese deposits have a siltstone and mudstone ore-bearing series. Black shale series type manganese deposits are hosted by a dark colored shale-chert-carbonate rock association. Finally, manganese deposits of carbonate rock

Table 1. Genetic Types of Manganese Deposits in China
(Based on Ye, et al., 1988)

Sedimentary ore deposits

(1) Mudrock type:
    1. Siltstone-mudrock association
       (Dounan; Middle Triassic)
    2. Siltstone-shale-limestone association
       (Wafangzi; Middle Proterozoic Tieling period)
(2) "Black shale" type
    1. Interglacial sandstone-black association
       (Xiangtan, Tangganshan, Minle, Datangpo etc., Early Sinian)
    2. Black shale-claystone association
       (Zunyi, Late Permian and Taojiang, Middle Ordovician)
    3. Black siliceous rock-shale association
       (Mugui, Late Devonian)
    4. Black shale-dolostone association
       (Gaoyan, Late Sinian and Jiaodingshan, Late Ordovician-Early Silurian)
    5. Black siliceous shale-limestone association
       (Dongxiangqiao, Early Permian)
(3) Carbonate rock type:
    1. Siliceous rock-mudstone-limestone association
       (Xialei, Late Devonian and Longtou, Early Carboniferous)
    2. Dolostone-limestone association
       (Baixian, Middle Triassic and Zhaosu, Early Carboniferous)
    3. Mudstone -dolostone association
       (Dongshuichang, Middle Proterozoic Gaoyuzhuang period)

Volcanic-sedimentary ore deposits

(1) Spilite-mudstone (phyllite) -carbonate rock association
    (Lijiaying, Early-Middle Sinian)
(2) Sandstone-mudstone-jasper association
    (Motuoshala, Early Carboniferous)
(3) Siliceous mudstone-volcanic rock association
    (Heixiakou, Middle Cambrian)

Hydrothermal modified sedimentary ore deposits

Fe-Mn-Pb-Zn-Au-Ag ore deposits in carbonate rocks
(Houjiangqiao, Late Devonian and Manaoshan, Middle Devonian)

Table 1. continued

Hydrothermal ore deposits

Ore deposits in contact zone of Magmatic and sedimentary rocks
(Hongshidong and Heishansi)

Supergene ore deposits

(1) Oxidized ore deposits
(Xialei, Dongping etc.)
(2) Leached ore deposits
(Mugui, Nanpengshan etc.)
(3) Accumulated ore deposits
(Sirong, Wuxuan etc.)

Metamorphosed sedimentary ore deposits

(1) Regional metamorphic type:
1. Phyllite-limestone association
(Huya, Early Triassic)
2. Spilite-mudstone (phyllite) -carbonate rock association
(Lijiaying)
(2) Contact metamorphic type:
1. Manganese silicate-oxide ore of Wanfanzi deposit
2. Alabandite ores of Tangganshan deposit

Figure 6. Percentage map of genetic types of manganese deposits in China based upon the data of Fu (1983). (1) Sedimentary, (2) Volcanic-sedimentary, (3) Metamorphosed sedimentary, (4) Hydrothermal modified sedimentary, (5) Hydrothermal, (6) Supergene. (Ye, et al., 1988).

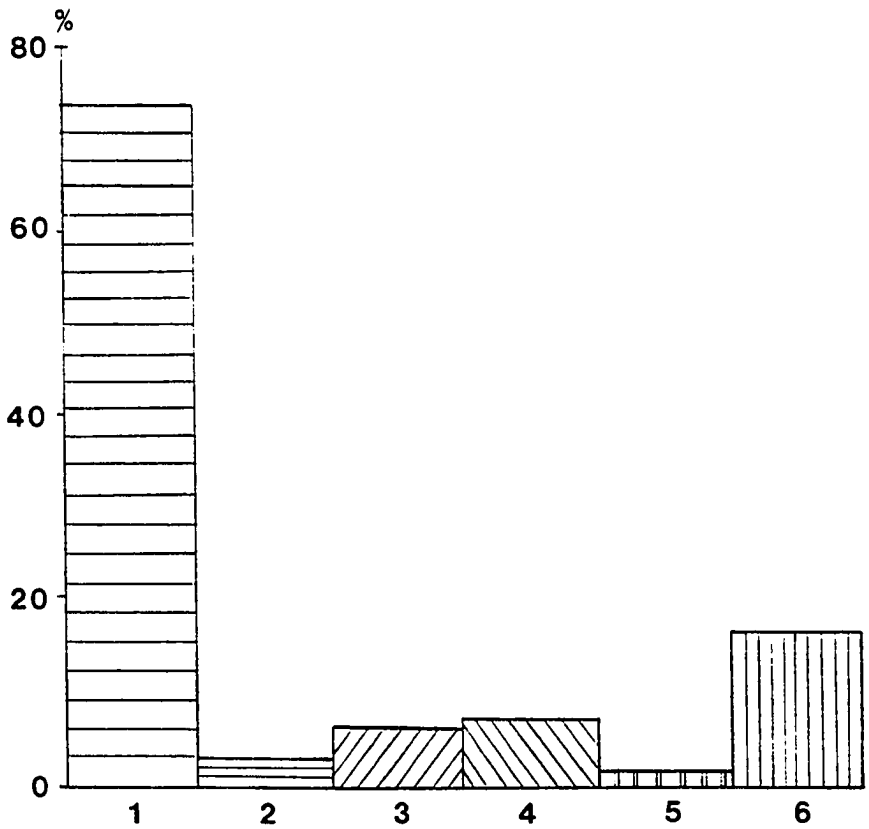

type are found in a dolostone-limestone dominated ore-bearing sequence.

Background of Taojiang and Xiangtan Manganese Deposits of Southern China

Both the Taojiang and the Xiangtan manganese deposits studied in this research belong to the black shale type sedimentary manganese deposits and occur on the margin of the Yangzi Platform (Ye, et al., 1988). The Taojiang manganese deposit is middle Ordovician in age, while the Xiangtan manganese deposit is early Sinian. The ore bodies of both districts consist of manganese carbonates (rhodochrosite, kutnohorite, Mn-dolomite, etc.) and are hosted by black shale dominated sequences. The Taojiang manganese deposit is moderate sized and has been mined for 20 years. On the other hand, the Xiangtan manganese deposit is the largest manganese carbonate deposit in China and has a longer mining history.

Taojiang Manganese Deposit

Taojiang manganese deposit is a gray mudstone, black shale, gray shale, and Mn-limestone hosted manganese carbonate deposit in northern Hunan Province of south China, occurring in middle Ordovician strata (Xu, 1980, Rao, 1988). The center of this district is situated

approximately 75 km northwest of Changsha, the capital city of Hunan Province (Fig. 7). There is one moderate sized deposit, which has been mined for 20 years and is of about 6 million ton reserves at 20% average manganese. Two other smaller deposits occur in the Taojiang district.

The Taojiang district is located in the zone of transition from the Yangzi Platform to the Hunan fold zone, belonging to the Xiazhou east-west structural zone. The rocks found in this district belong to the Sinian, Cambrian, Ordovician, and Silurian systems, being nearshore to offshore marine sediments. Previous workers believed that the Taojiang manganese deposit formed in a restricted shallow marine environment (Xu, 1980).

Stratigraphy

The rocks of the Taojiang district and vicinity present a discontinuous geological record from Pre-Sinian to lower Silurian. Younger rocks are not found, except granitic intrusions, occurring in the north and south parts of the district. The rocks can be divided into Pre-Sinian metamorphic basement, Sinian marine rocks, Cambrian marine rocks, Ordovician marine rocks, and Silurian marine rocks (Table 2).

Pre-Sinian metamorphic basement -- The oldest rocks found in the district are Pre-Sinian metamorphic rocks. As observed in the field and documented in the literature,

Table 2. Stratigraphy of the Taojiang Area

(Based on Xu, 1980)

S				Upper part consists of
I	L			gray to yellowish gray
L	O	Zhoujiaxi	250-500m	siltstone and thinly bedded
U	W	Formation		black shale.
R	E			Lower part consists of
I	R			organic-rich black shale.
A				
N				
	U			
	P	Wufen		Thinly bedded organic-rich
	P	Formation	15-25m	black shale and siliceous
	E			black shale.
O	R			
R				Gray to dark gray thickly
D	M	Modaoxi		bedded mudstone, Mnlimestone,
O	I	Formation	8-35m	rhodochrosite ore, inter-
V	D			bedded gray and black shale.
I	D			(Contains Taojiang Deposits)
C	L	Hule	4-40m	Thinly bedded organic-rich
I	E	Formation		pyritic black shale.
A				
N	L	Yanxi		Gray silty shale and black
	O	Formation	110-250m	shale.
	W			
	E	Baishuixi	70-200m	Gray silty shale and
	R	Formation		calcareous shale.

Table 2 Continued

CAMBRIAN	UPPER	Tanxi Group	300m	Muddy limestone, dolostone and calcareous shale.
	LOWER	Xiaoyanxi Formation	120-250m	Thinly bedded, organic-rich black shale with siliceous shale interbeds.
SINIAN	UPPER	Liuchanpo Formation	40-50m	Thickly bedded black siliceous shale.
		Doushantuo Formation	20-60m	Thinly bedded black shale with limestone lenses.
	LOWER	Nantuo Tillite	50-150m	Gray to green thick tillites
		Liantuo Formation	30-170m	Thinly bedded black shale, Mn-limestone, rhdochrosite, sandstone. (Contains Xiangtan Deposit)

Figure 7. Location of Taojiang and Xiangtan deposits.

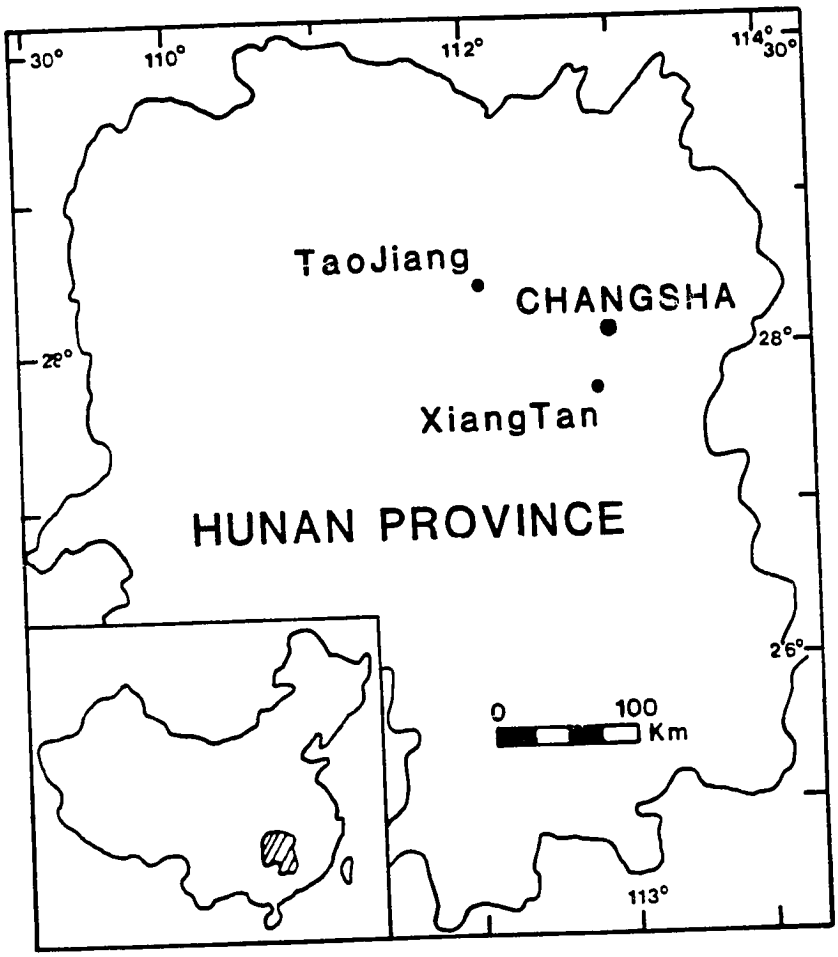

these rocks are slate and phyllite called the Banxi Group. They occur mainly in the northern part of the Taojiang district.

Sinian rocks -- Sinian (Late Proterozoic) includes early Sinian and late Sinian. There are two formations of early Sinian age, the Liantuo Formation and the Nantuo Tillite. The Liantuo Formation consists of thinly bedded black shale, Mn-limestone and manganese carbonate horizons in the upper part, and of sandstone in the lower part. The Liantuo Formation is a very important manganese ore-bearing horizon in northern Hunan Province and contains the Xiangtan deposit which will be discussed later in this chapter. The Nantuo Tillite consists of gray to green thick tillite beds. There is a black tillite at the bottom of the formation. The Upper Sinian contains two formations: (1) the Doushantuo Formation, being thinly bedded black shale with siliceous shales interbeds, dolostone and Mn-Limestone lenses at the upper part and pyrite lenses at the bottom; (2) the Liuchapo Formation, being thickly bedded black siliceous shales.

Cambrian rocks -- Cambrian rocks consist of the Xiaoyanxi Formation and the overlying Tanxi Group. The Xiaoyanxi Formation is thinly bedded, organic-rich black shale with siliceous shale interbeds. It has phosphate concretions and very organic-rich black shale (locally

called stone coal) layer at the bottom of the formation. The Tanxi Group is composed of muddy limestone, dolostone, and calcareous shale with trilobites.

Ordovician rocks -- The Lower Ordovician has two formations, the Baishuixi Formation and the Yanxi Formation. The Baishuixi Formation (70 - 200m) consists of gray silty shale and calcareous shale with a few graptolites and trilobites. The Yanxi Formation (110 - 250m) is of gray silty shale and black shale with Pteroagraptus elegansele, Didymorgraptus ellesae and D.deflexus.

The Middle Ordovician was an important epoch of manganese formation in the Taojiang district and has two formations, the Hule Formation and the Modaoxi Formation. The Hule Formation (0 - 40m) consists of thinly bedded black shale, rich in pyrite and organic matter. The Modaoxi Formation (8 - 35m) is composed of gray to dark gray thickly bedded mudstone, Mn-limestone, rhodochrosite ore beds, black shale, and interbedded black and gray shales. The shales and Mn-limestones contain ostracodes, trilobites, and graptolites. The Upper Ordovician Wufen Formation consists of thinly bedded organic rich black shale and siliceous black shale with graptolites.

Silurian rocks -- Only the Lower Silurian Zhoujiaxi Formation (200 - 250m) is visible in the Taojiang district.

The lower part of the Zhouziaxi Formation is of thinly bedded, organic-rich black shales with Monograptus aff. gemmmatus, Climacograptus angrustus, Glyptograptus cf. tamariscus, Pristiograptus sp. The upper part of the Zhoujiaxi Formation consists of gray to yellowish gray muddy siltstone and thin black shale interbeds with Monograptus sp.

Structural Features

Folds in the Taojiang district are related to a syclinorium that trends nearly east-west, and contain smaller folds superimposed on the larger structures. Faults are abundant and consist mainly of east-west normal faults with an average throw of about 5 meters. In addition, there are some lamprophyric dikes in this district.

Stratigraphic and Petrographic Observations

The following descriptions of stratigraphy and petrology of the Taojiang manganese deposit are based on three stratigraphic sections measured during field work and observations of the samples collected from the working area (Fig. 8, 9, 10, 11, 12). Not all of the stratigraphic units mentioned above can be found in this working area. Three stratigraphic sections were measured during the field work, covering the upper-most Lower Ordovician Yanxi Formation, the Middle Ordovician Hule and ModaoXi

Figure 8. The simplified geological map of Taojiang area (according to the geological map of Geological Survey of Hunan Province, 1979).

1. Stratigraphic sections measured for this research; 2. Lower Ordovician (Yangxi Formation); 3. Middle Ordovician, manganese ore-bearing horizon (Hule Formation and Modaoxi Formation); 4. Upper Ordovician (Wufen Formation); 5.Silurian (Zhoujiaxi Formation) ; 6. anticline; 7. syncline.

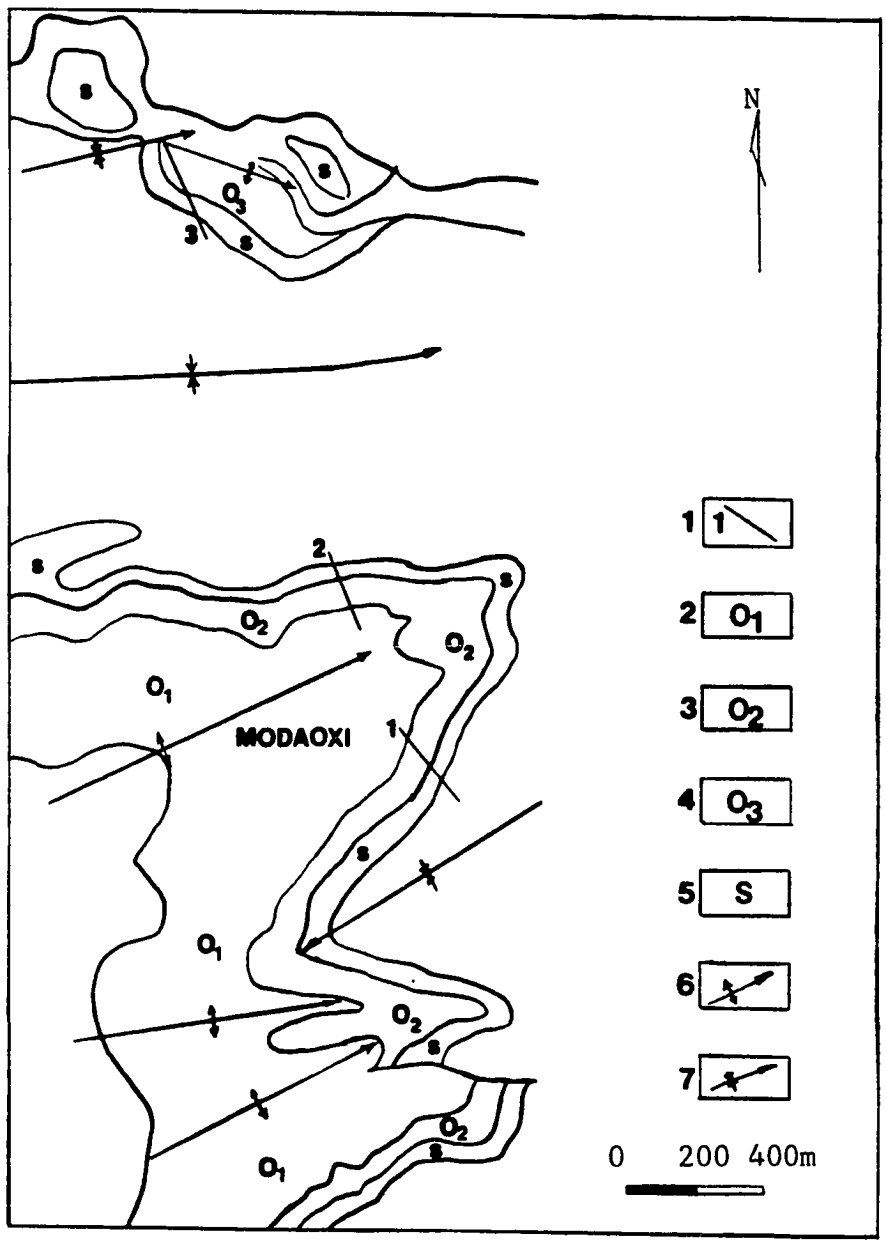

Figure 9. The general stratigraphic column of the Taojiang district and the coverages of the stratigraphic sections measured during the field work. No stratigraphic thicknesses are implied.

Taojiang Manganese Deposit
(not to scale)

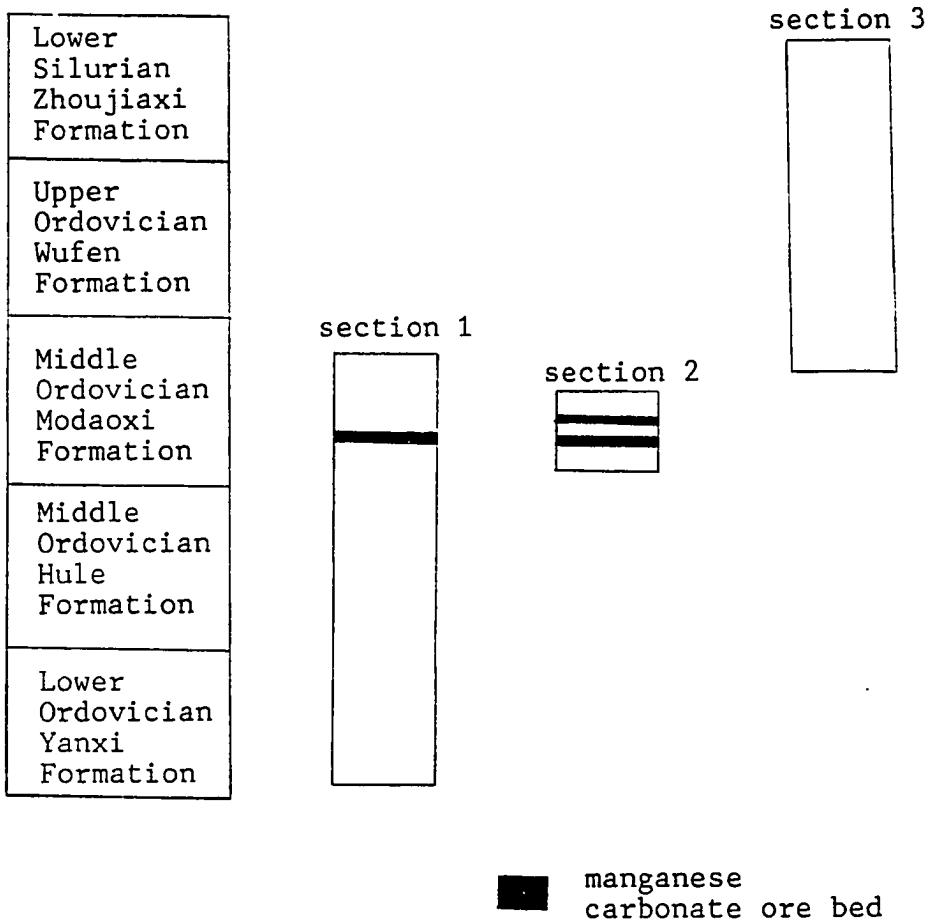

Figure 10. The stratigraphic column of the Taojiang manganese deposit, based on measured section 1 (see Figure 8,9). Total thickness is 12 meters.

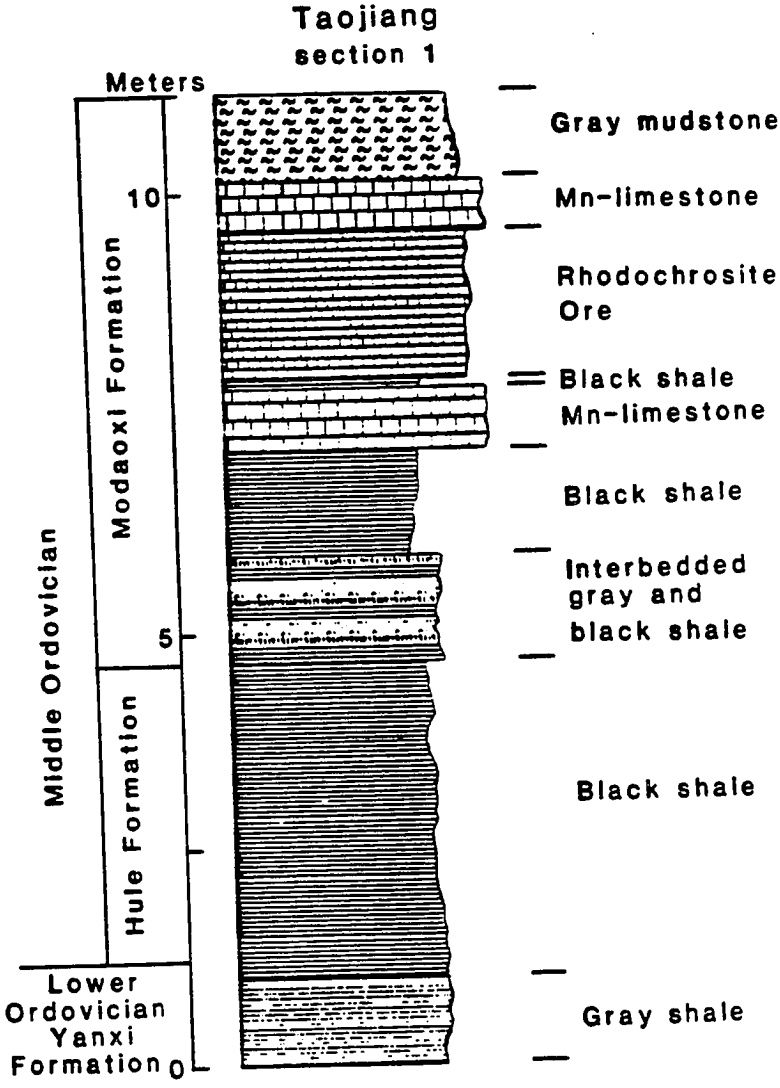

Figure 11. The stratigraphic column of the Taojiang manganese deposit, based on measured section 2 (see Figure 8,9). Total thickness is 7.5 meters.

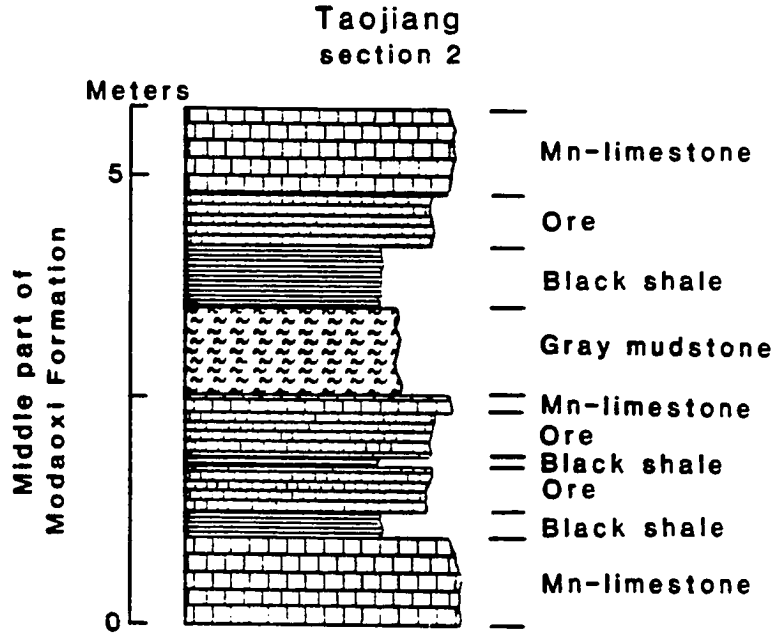

Figure 12. The stratigraphic column of the Taojiang manganese deposit, based on measured section 3 (see Figure 8,9). Total thickness is 60 meters.

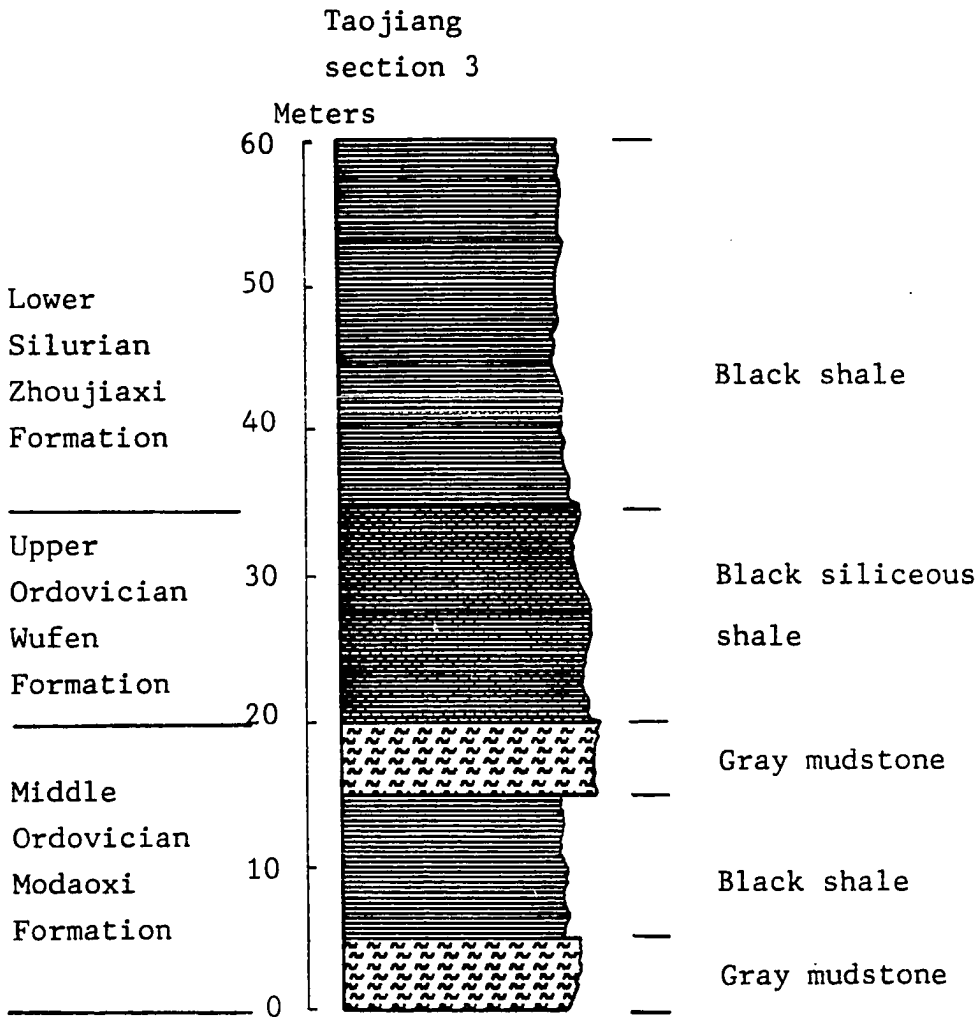

Formations (major ore bearing sequence, stratigraphic columns 1 and 2), the Upper Ordovician Wufen Formation, and the lower part of the Lower Silurian Zhouziaxi Formation (stratigraphic column 3) (Fig. 9).

Stratigraphic Observations

Yanxi Formation -- only the upper-most 10 meters of the Yanxi Formation were observed during the field work. The rocks are dark gray, well-laminated shales. The upper Yanxi Formation is widely distributed in the Taojiang district and is a consistent lithology, so it is a good indicator of pre-ore formation. The boundary between the Yanxi Formation and the Hule Formation is sharp.

Hule Formation -- the Hule Formation, lower part of the Middle Ordovician, is about 3.5 meters thick on average and contains very thinly bedded, organic rich, well laminated black shale. The distribution of the Hule Formation is irregular. In the western part of the district, the thickness of the Hule Formation is about 40 meters, whereas in the eastern part of the district it is less than 1 meter thick or completely absent. The Hule Formation is conformably overlain by the Modaoxi Formation.

Modaoxi Formation -- the Modaoxi Formation is the major manganese ore-bearing formation and can be divided according to petrographic features into three sections. From bottom to top they are: (1) a lower section of

interbedded black and gray shales; (2) a middle section of rhodochrosite ore body with Mn-limestone and thin interbeds of black shale; and (3) an upper section of thickly bedded gray mudstone with a few black shale interbeds.

The lower section of the Modaoxi Formation is about 3 meters thick, consisting of interbedded, well laminated, organic rich black shale and poorly laminated, organic poor, gray to dark gray shales. The thickness of individual beds is about 2 to 5 centimeters. At the bottom of this horizon, the gray shale beds are thicker than black shale beds. Toward the upper part of this horizon, black shale beds gradually become thicker than gray shale beds and the horizon grades into totally black shale at the top.

The middle section of the Modaoxi Formation is the rhodochrosite ore body with Mn-limestone hanging wall and footwall. Several very thin black shale interbeds occur within the ore body and Mn-limestones. The total thickness of this part is about 3 meters and the average thickness of the rhodochrosite ore body is about 1.7 meters (stratigraphic section 1, Fig. 10). In the northern part of the working area (stratigraphic section 2, figure 8, 9), the ore body splits into two horizons (Fig. 11). The total thickness of ore is up to 3 meters. The footwall of the ore body is Mn-limestone 1 meter thick. There is a very thin (10 centimeters) black shale layer between the

rhodochrosite ore body and the Mn-limestone footwall. The hanging wall is 1 meter thick Mn-limestone and has a sharp contact with the top of the rhodochrosite ore body.

The upper section of the Modaoxi Formation consists of thickly bedded, poorly laminated, organic poor gray mudstone with a few thin interbeds of black shales. The total thickness of this part is about 10 to 20 meters.

Wufen Formation -- the Wufen Formation of Late Ordovician age consists of siliceous black shale and organic rich, thinly bedded black shale with graptolites (Fig. 12). The outcrops of the Wufen Formation are very poor. According to the literature (Xu, 1980, Rao, 1988), there is a 1 to 3 meters thick conglomerate bed overlying the Modaoxi Formation at the contact with the Wufen Formation.

Zhoujiaxi Formation -- the Zhoujiaxi Formation of Early Silurian age consists of two sections. The lower section consists of thinly bedded, well laminated, organic rich black shale with graptolites, and is 30 meters thick. The upper section consists of gray to yellowish siltstone with thin black shale interbeds. The total thickness of the Zhoujiaxi Formation is about 400 meters. Only the lower section of this formation was investigated during the field work.

Petrographic Observations

Yanxi Formation -- The hand samples of the Yanxi Formation are dark gray in color and well-laminated. The thickness of laminae are 0.1 to 0.3 mm with dark gray to very light gray color changes among the laminae. No pyrite can be observed in hand sample. Some laminae are wavy, indicating depositional compaction.

In thin section, the rock is very fine-grained and consists of clay minerals, very fine-grained detrital quartz (1 - 10 microns in diameter), a small amount of disseminated small pyrite crystals (some of them are framboidal pyrites), and organic matter (Fig. 13). The laminae are mainly defined by clay mineral-rich layers and quartz-rich layers. Organic matter and pyrite occur mostly in the boundaries between the different laminae. Pyrite occurs as (1) framboids along the laminae, (2) small pyrite crystals disseminated in the rock with crystal sizes from less 1 micron to 3 microns, and (3) larger euhedral pyrite crystals, ranging 10 to 50 microns in diameter and occurring mostly in the quartz-rich layers. Total pyrite in the rock averages less than one volume per cent, but locally ranges to 3 per cent.

Hule Formation -- The hand samples of the Hule Formation are well laminated, organic- and pyrite-rich, black shale. In thin section, organic matter gives the

Figure 13. The gray shale of the Lower Ordovician Yanxi Formation (sample DL1). Transmitted light.

Figure 14. The black shale of the Middle Ordovician Hule Formation (sample DL8). Transmitted light.

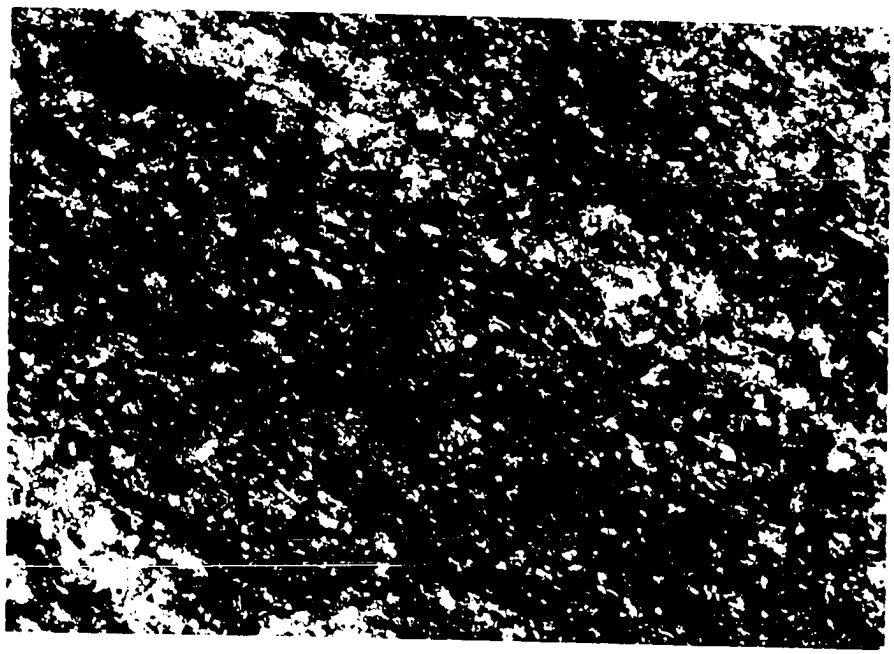

0.2mm

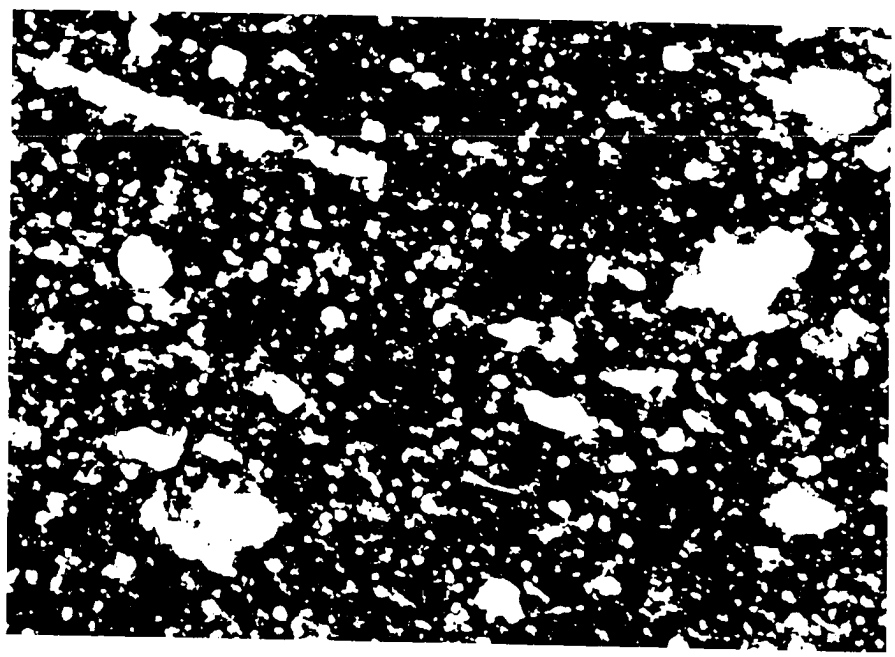

0.2mm

whole thin section an almost opaque appearance, except for very fine-grained detrital quartz grains (Fig. 14). Under reflected light, sulfide minerals including pyrite framboids, small pyrite crystals, and large euhedral pyrite crystals associated with marcasite and sphalerite can be identified (Fig. 15, 16). Sulfide minerals comprise an average of 5 per cent (volume) of the rock and locally to 10 per cent.

Modaoxi Formation -- As mentioned above, there are five lithotypes in the Modaoxi Formation -- black shale, gray mudstone, gray shale, Mn-limestone, and rhodochrosite ores.

The lower section of Modaoxi Formation consists of interbedded gray and black shales, grading into black shale toward the upper part. In thin section, the gray shale layer is very fine-grained and poorly laminated with much less organic matter than the black shale (Fig. 17). Pyrite crystals are small and euhedral. They are commonly concentrated as small nodules (1 to 5 mm in diameter). The upper contact of gray shale with black shale is gradational. The bottom contact of gray shale with underlying black shale is sharp and exhibits a deformed pattern at the top of the black shale layer. The black shale layers are well laminated with much organic matter and pyrite (Fig. 18). Each lithology change from gray shale to black shale may represent a depositional cycle,

Figure 15. An example of euhedral pyrite crystal (at right corner) and framboidal pyrite assemblages on the left (sample DL8). Reflected light.

Figure 16. Higher power view of the framboidal pyrite assemblages seen in figure 15. Reflected light.

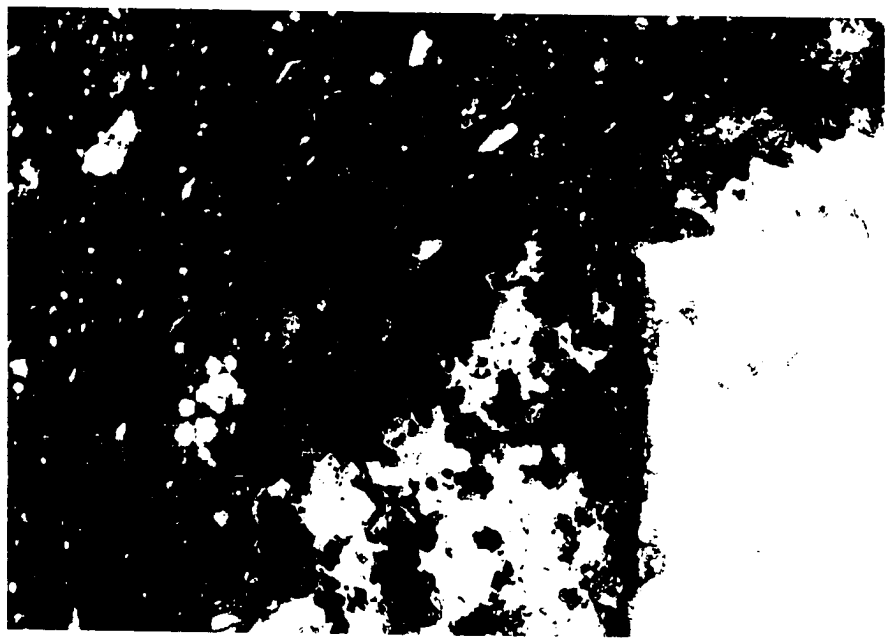

0.2mm

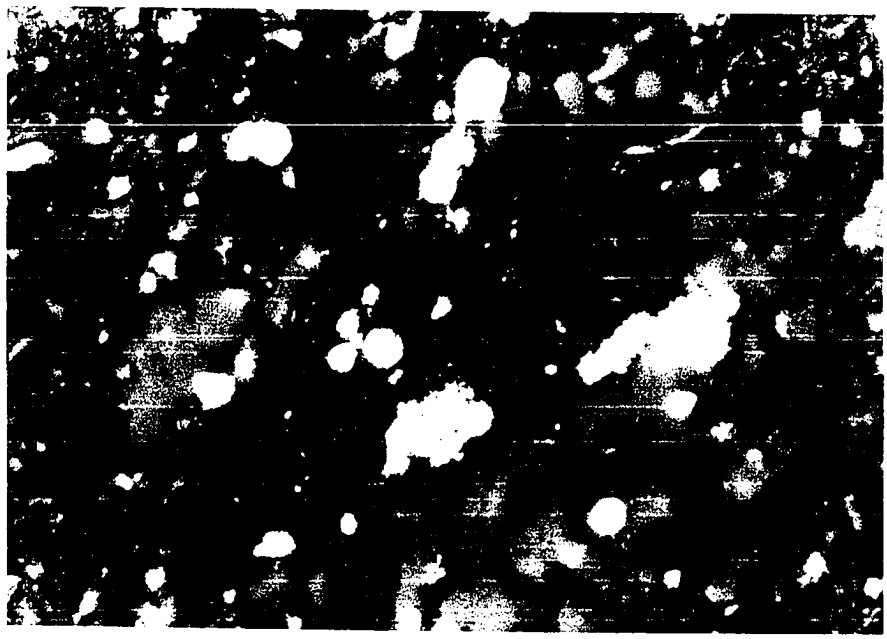

0.2mm

Figure 17. Lower part of the Modaoxi Formation. The interbedded gray and black shale (sample NS9). The gray shale layer is on the right and black shale layer on the left. Transmitted light.

Figure 18. The black shale layer of the same sample as figure 17. Transmitted light.

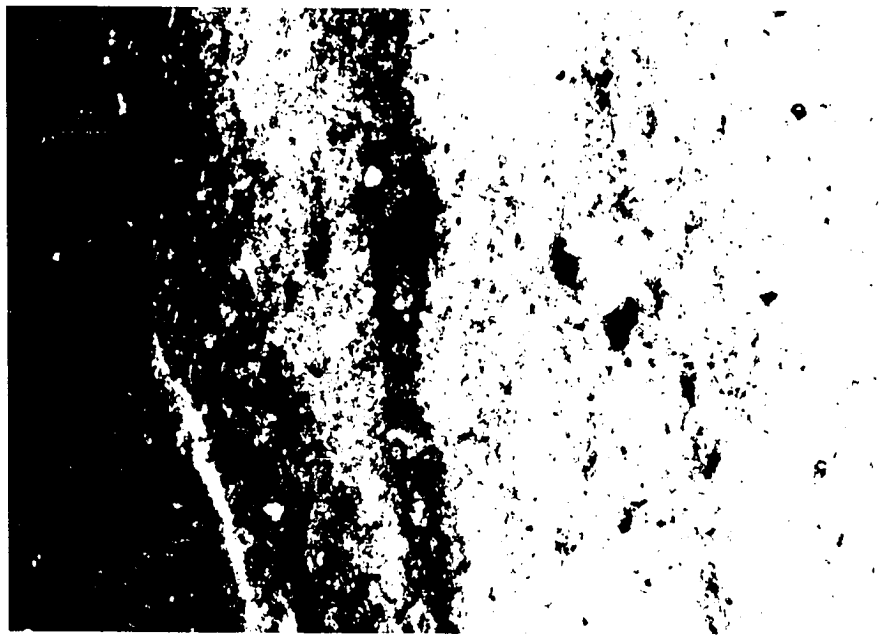

0.2mm

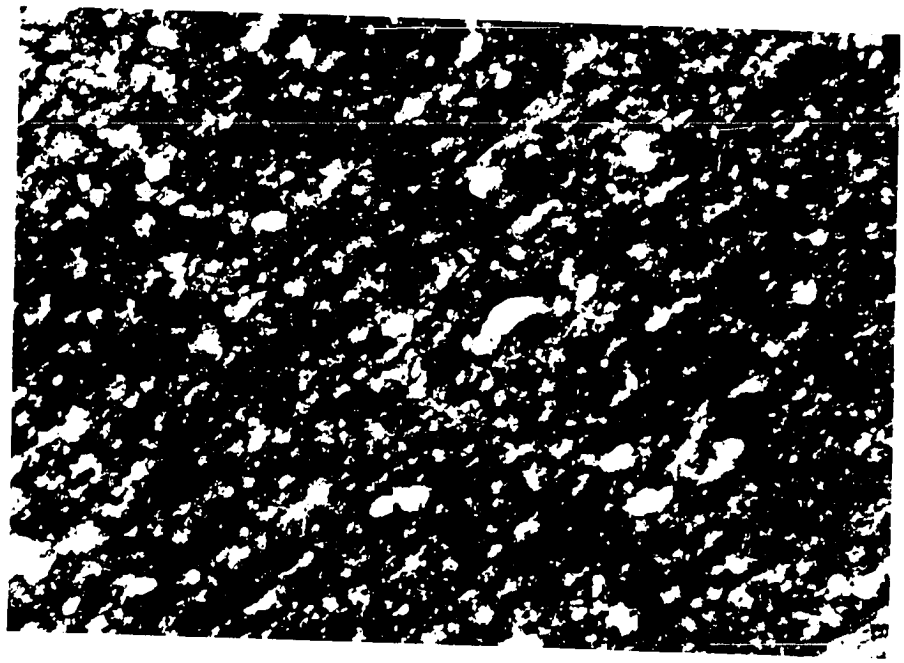

0.2mm

being from a reducing to moderately oxidizing depositional condition.

The middle section of the Modaoxi formation contains three major kinds of rocks. They are Mn-limestone as the hanging wall and footwall of the manganese ore body; the rhodochrosite ore body itself; and thin black shale interbeds within both the Mn-limestones and the rhodochrosite ore body. The hand samples of Mn-limestones are very dark gray in color and well crystallized. In thin section, the Mn-limestone consists of carbonate grains, carbonate cements, fossil fragments, and a small amount of organic matter and pyrite. The fossil fragments include trilobites, echinoderms, and ostracodes, making up 20 per cent of the whole rock (Fig. 19). Organic matter is concentrated in stylolites. Pyrite occurs with organic matter or within small late veins of calcite.

Rhodochrosite ore samples are well crystallized and light gray, gray, or light pink in color. In thin section, rhodochrosite ores form mosaic structures with small quartz veins (Fig. 20). Rhodochrosite ores contain very small amount of organic matter and small scattered pyrite crystals. No fossil fragments can be found.

The black shales interbedded within rhodochrosite ore and Mn-limestone are very thin (a few centimeters) and

Figure 19. An example of limestone (sample DL20) with fossil fragments in the Modaoxi Formation, from the hanging wall of the rhodochrosite ore body. Transmitted light.

Figure 20. An example of the rhodochrosite ore (sample NS5). Transmitted light.

0.2mm

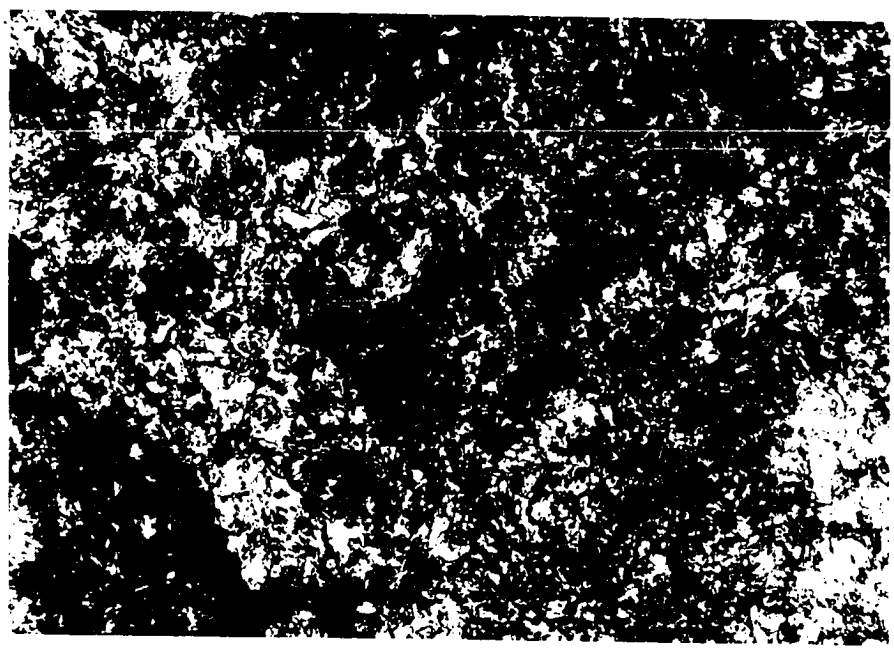

0.2mm

difficult to make into thin sections. However, these black shales are rich in organic matter and pyrite.

The upper part of the Modaoxi Formation consists of gray, poorly laminated mudstone overlying the Mn-limestone hanging wall of the ore body. In thin section, these gray mudstone are very fine-grained (averaging about 0.5 microns), contain little organic matter and pyrite, and are structureless (Fig. 21).

Wufen formation -- The rocks of the Wufen Formation are black, organic rich, well laminated, thinly bedded shales. In thin section, the black shale is very fine-grained and consists mainly of clay minerals and mica. The detrital quartz grains are very fine (1 - 5 micron in diameter). Pyrite is rare and very fine-grained. Organic matter, however, is abundant (Fig. 22).

Zhoujiaxi Formation -- The hand samples from the lower Zhoujiaxi Formation are black, well laminated, and contain abundant organic matter and pyrite with graptolites. In thin section, the black shales are very fine-grained and organic-rich. In the samples of the lower part of the lower Zhoujiaxi Formation, pyrite is rare in thin sections, while toward the upper part of the lower Zhoujiaxi Formation, disseminated small pyrite crystals are common (Fig. 23).

Figure 21 The gray shale of the upper part of the Modaoxi Formation (sample DL23). Transmitted light.

Figure 22. The black shale of the Upper Ordovician Wufen Formation (sample TM16). Transmitted light.

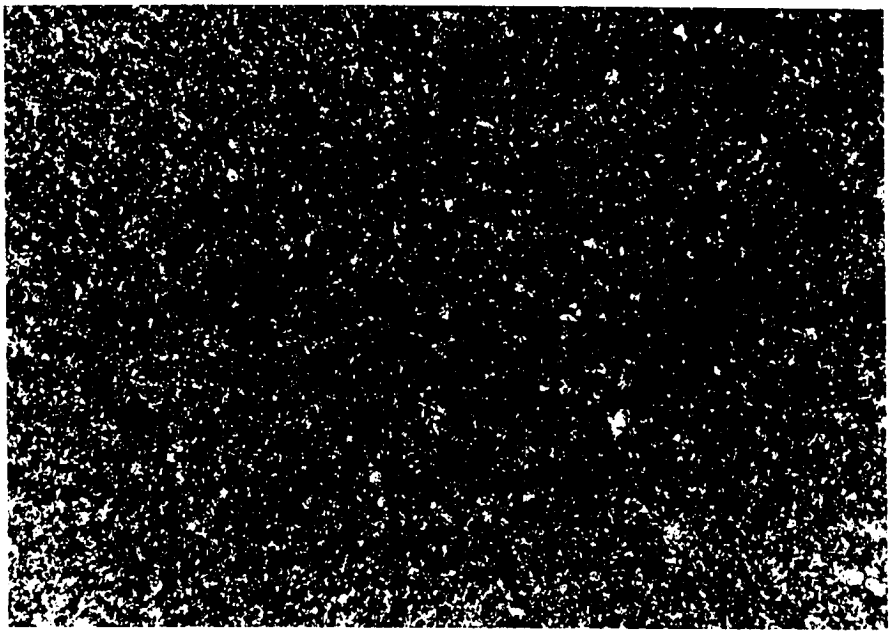

0.2mm

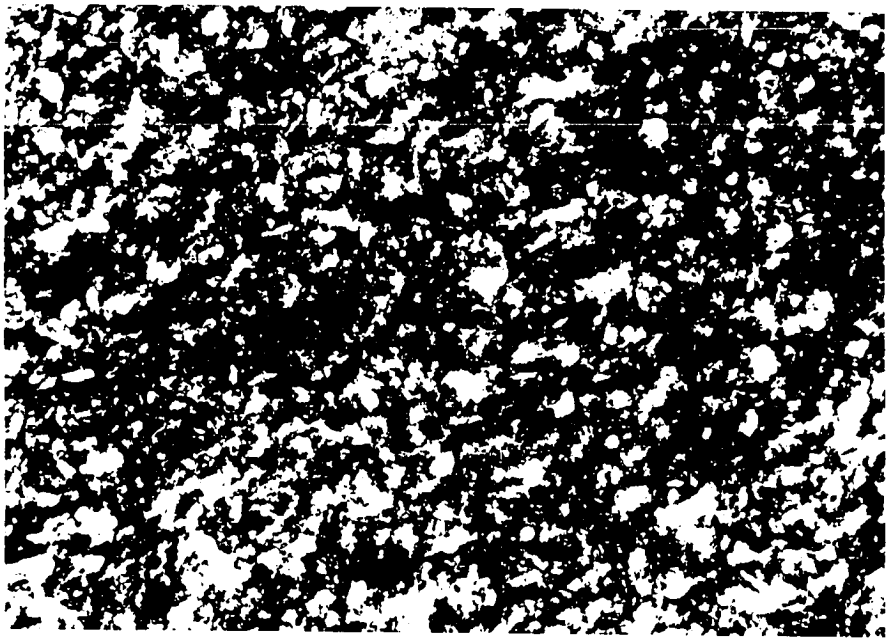

0.2mm

Figure 23. The black shale of the upper portion of the Lower Silurian Zhoujiaxi Formation of the Taojiang manganese deposit. Transmitted light.

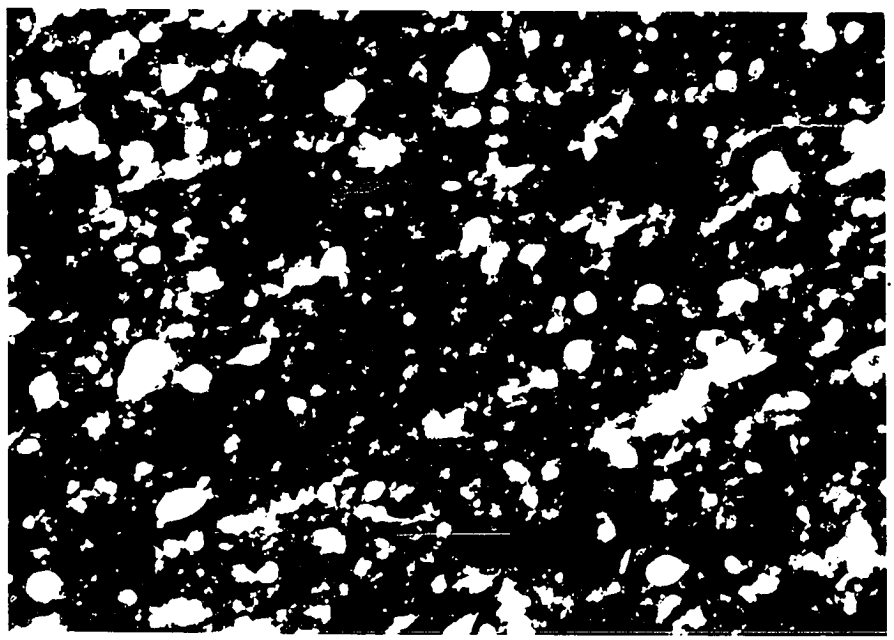

0.2mm

Paleo-geography during Middle Ordovician to Early Silurian

The Middle Ordovician was the main period of manganese formation in the Taojiang district. The organic- and pyrite-rich black shales of the Hule Formation of the early middle Ordovician, which indicate more reducing conditions, perhaps sulfidic (Berner, 1981, Maynard, 1982), preceded manganese mineralization. This organic-rich, well-laminated pyritic, black shale is the product of a deeper water restricted basin. The Modaoxi Formation begins with interbedded black and gray shales, shales that reflect fluctuating depositional conditions between more and less reducing environments. These interbedded gray and black shales represent, perhaps, slope turbidites. The sea level may have been rising and falling, which would have caused more or less circulation with the open ocean. However, the black shale becomes dominant toward the rhodochrosite ore body. In the entire ore-bearing sequence, only the ore body and its direct hanging wall and footwall are carbonates (rhodochrosite and Mn-limestones). No petrographic evidence was found to determine whether manganese carbonates replaced manganese oxides. The rhodochrosite ore body and its hanging wall and footwall limestones contain fossil fragments and low organic matter. This indicates a less reducing condition near the oxic/ anoxic water interface at the slope. Above the ore body,

the host rocks are organic poor, structureless (which was caused by bioturbation) gray mudstone with a few thin black shale interbeds. This gray mudstone represents more circulation with the open ocean, possibly caused by sea level rise. This ore-bearing sequence (the Hule Formation and the Modaoxi Formation) reflects a depositional environment that changed from anoxic to oxic, and the ore itself occurred during the transition (Fig. 24).

The Upper Ordovician Wufen Formation and the Lower Silurian Zhoujiaxi Formation consist of organic-rich black shale with much less pyrite compared with the black shales of the Hule Formation and the Modaoxi Formation. Considering that these organic-rich and pyrite poor black shales contain many graptolites and well-developed lamination, a reducing marine depositional environment should be concluded.

Xiangtan Manganese Deposit

The Xiangtan manganese deposit is an organic rich, black shale-hosted manganese carbonates deposit in the north of Hunan Province, of early Sinian age. The center of this district is situated about 40 km southwest of the Changsha City (Fig. 7). Supergene enrichments of manganese oxides were mined here during the 1930s. In the 1950s, the primary manganese carbonate ores were found and interpreted

Figure 24. Generalized paleo-geographic model of Taojiang manganese deposit during middle Ordovician.

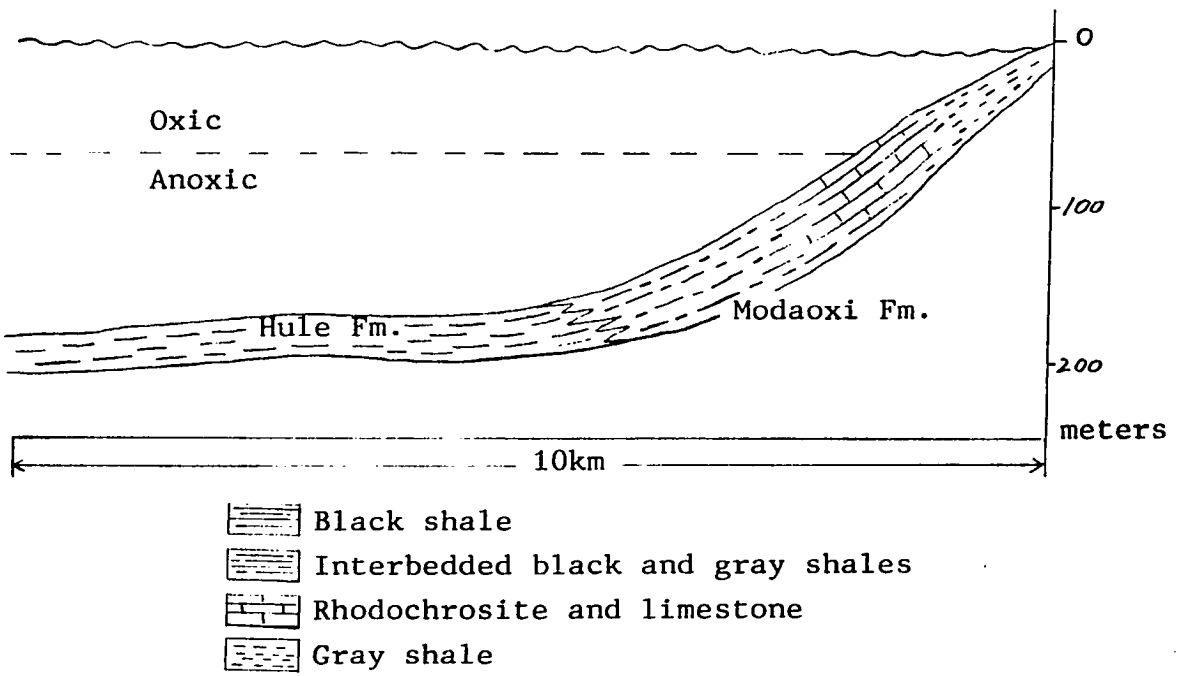

Figure 25. A simplified geological map of the Xiangtan area (after Song, 1985).

1. Lower Sinian, manganese ore-bearing horizon (Liantuo Formation and Nantuo Tillite)); 2. Upper Sinian; 3. Cambrian; 4. Ordovician; 5. Devonian; 6. Pre-Sinian; 7. Eogene.

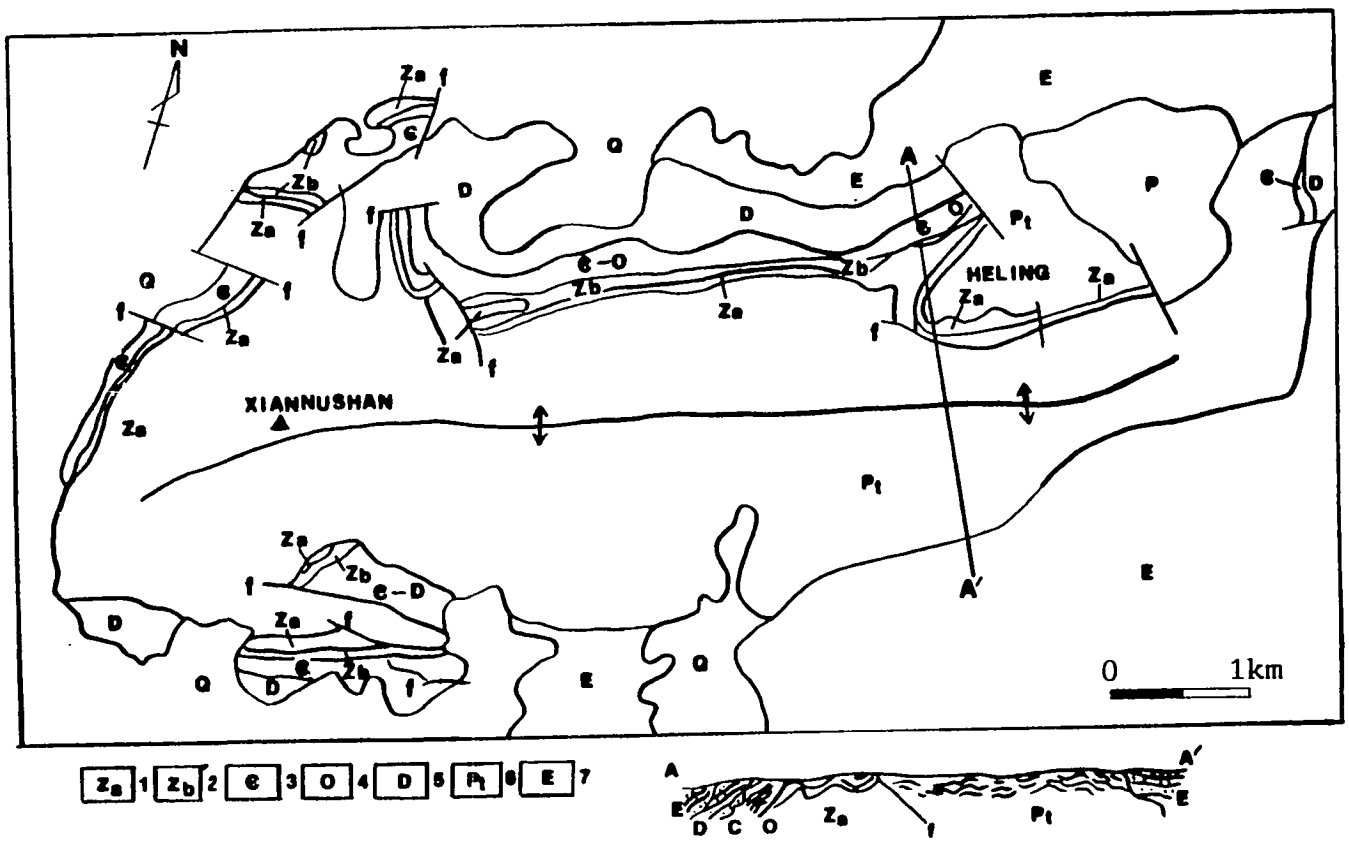

to be of a interglacial shallow water marine origin (Ye. et al., 1988). There are seven mines in the Xiangtan district. The ore beds, with 23 weight-percent manganese (as MnO) are rather persistent, being 26 kilometers long from east to west and 1.5 to 2.5 meters thick on average.

During a very short visit in the summer of 1986, one underground mining area near Heling was investigated (Fig. 25) which included the manganese ore body and its direct hanging wall and footwall black shales.

Stratigraphy

As mentioned earlier in this chapter, the stratigraphy of the Xiangtan district is similar to the Taojiang district and consists of the Pre-Sinian metamorphic basement, the early Sinian Liantuo Formation and Nantuo Tillite, and the Late Sinian Doushantuo Formation and Liuchapo Formation (Table 2). Cambrian, Ordovician, Devonian, and Permian rocks are also present, but are poorly exposed and do not appear to contain manganese mineralization (Song, 1985). Here, the description of stratigraphy will mainly emphasize the manganese ore-bearing sequence ---- the early Sinian Liantuo Formation and Nantuo Tillite (Fig. 26).

Liantuo Formation: The Liantuo Formation can be divided lithologically into three parts (from bottom to top): (1) basal sandstones, which unconformably overlie the Pre-

Figure 26. The stratigraphic column of the Xiangtan manganese deposit, measured at an underground mining area near Heling (see figure 24). The total thickness is 18m.

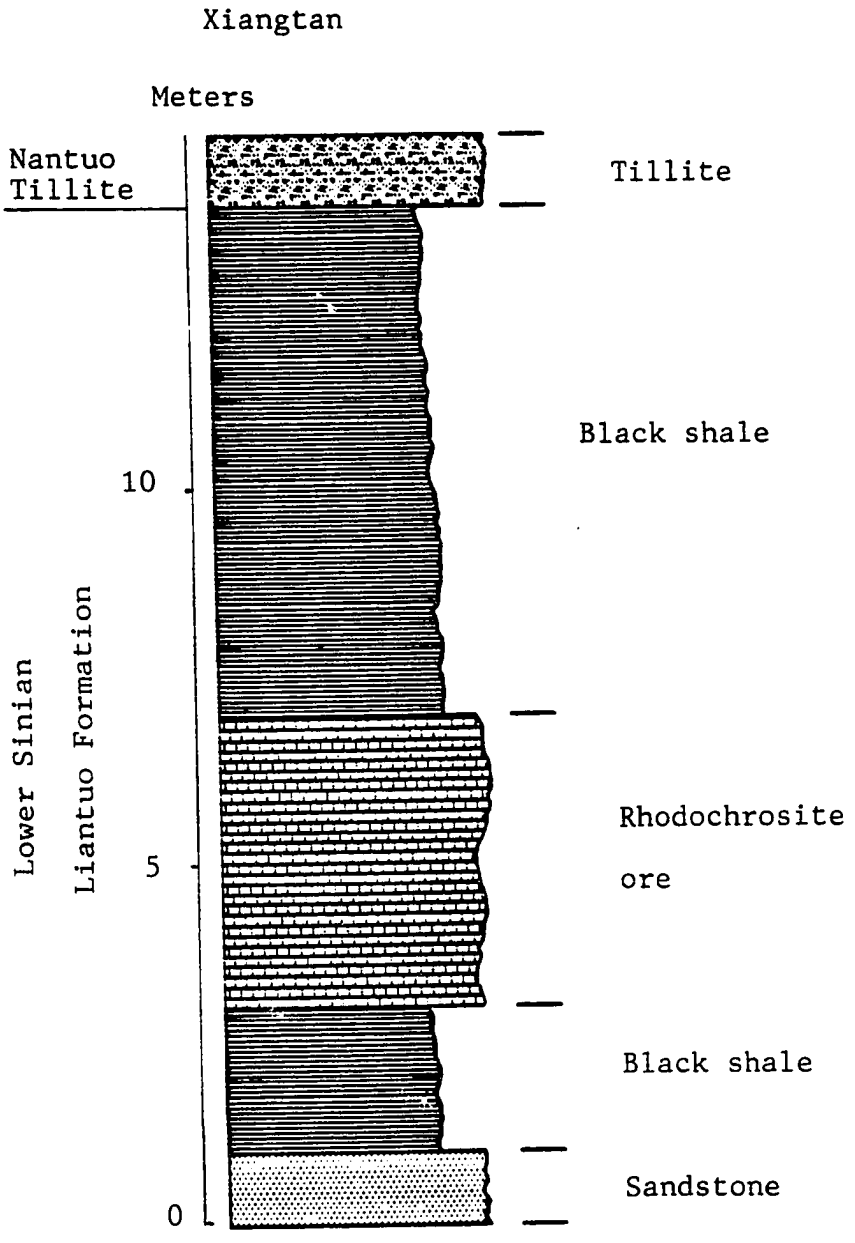

Sinian metamorphic basement; (2) black shale with ore-grade rhodochrosite; (3) an upper black shale, which has an unconformable contact with the overlying Nantuo Tillite.

The basal sandstone is about 5 meters thick. The bottom of the basal sandstone bed is yellowish, medium grained and contains a small amount of conglomerate scattered throughout. The middle part of the sandstone bed is light brown in color and consists of fine-grained quartz and feldspar. Toward the top, the sandstone becomes dark gray and more fine-grained. At the upper contact of the sandstone, very fine-grained sandstone is in contact conformably with overlying blacks shales.

The black shale with rhodochrosite ore horizon is about 4 meters thick, consisting of well-laminated, organic-rich pyritic black shale in the lower part, and about 2 meters of well-laminated dark gray manganese carbonates in the upper part.

The upper black shale is about 30 meters thick and consists of very soft, thinly bedded, pyrite-rich black shale in the hanging wall of the manganese ore body and grades into thickly bedded, more siliceous black shale toward the top.

Nantuo Tillite: The NanTuo Tillite is widely distributed in the area, but the thickness changes greatly from 5 to 50 meters. The tillite is gray in color and

consists of clasts of slate, siliceous sedimentary rocks and granite with a matrix of poorly sorted sands and rock fragments.

Petrographic Observations

The direct hanging wall and footwall of the ore body are organic and pyrite-rich, well-laminated black shales. In thin section, the black shale consists of clay minerals, a small amount of mica, abundant organic matter, pyrite and detrital, silt sized quartz (about 10 to 50 microns in diameter) (Fig. 27). The pyrite in the black shale occurs as both framboids and small, disseminated, subhedral crystals (Fig. 28). Larger pyrite crystals formed by overgrowth on framboidal pyrite. The average amount of pyrite is about 5 volume per cent.

Rhodochrosite ores of the Liantuo Formation are gray in color and well-laminated. The laminae are 0.1 to 1 mm in thickness. In thin section, the lamination is caused by organic-rich and carbonate-rich layers (Fig. 29). X-ray diffraction data show that the carbonates are mainly rhodochrosite (see Chapter 4). Pyrite (about 5%) occurs as small framboidal assemblages and small anhedral crystals disseminated in the ore. A small amount of detrital quartz (5 - 20 microns in diameter) is also present.

The Xiangtan deposit contrasts with the Taojiang deposit in several ways. First, the rhodochrosite ore body

Figure 27. Silty black shale of the Lower Sinian Liantuo Formation (sample XT1). Transmitted light.

Figure 28. Euhedral pyrite crystal and small framboidal pyrites of the same sample as figure 27. Reflected light.

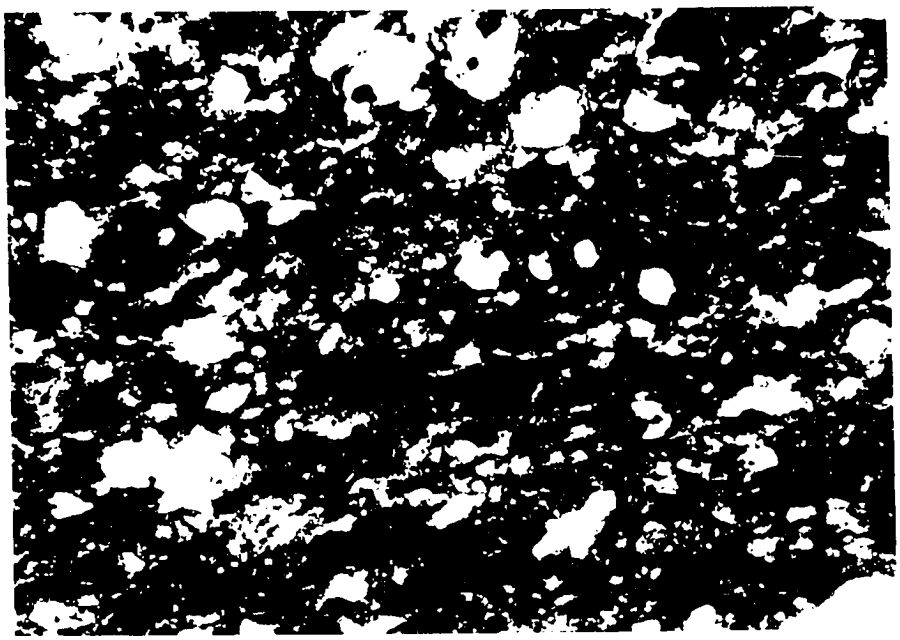

0.2mm

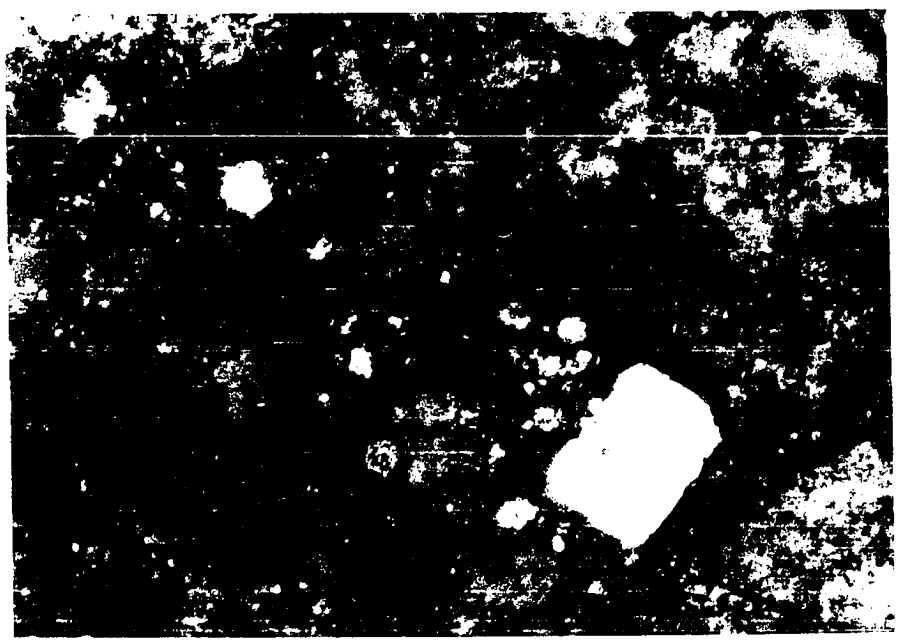

0.04mm

Figure 29. The rhodochrosite ore of the Liantuo Formation. Transmitted light.

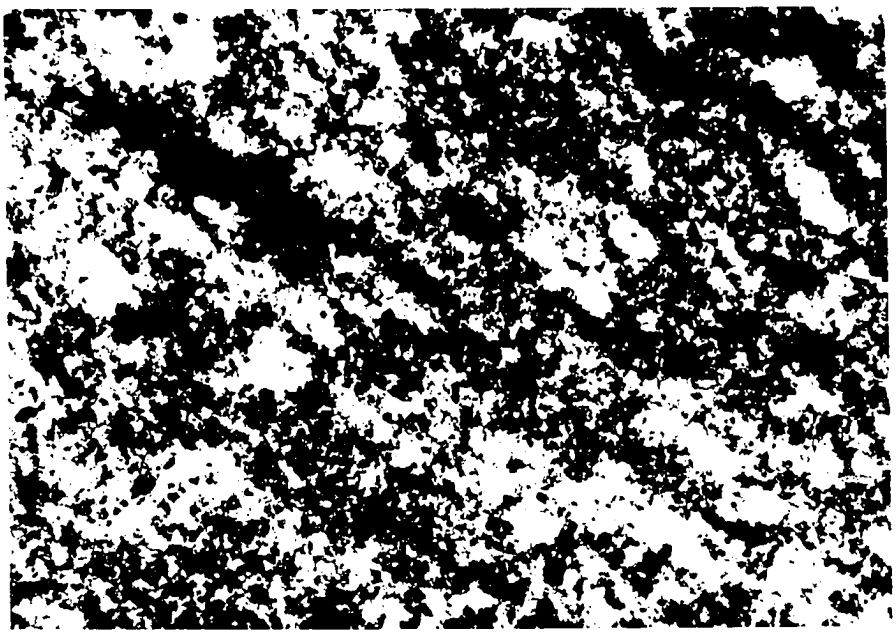

0.2mm

is well laminated and very fine-grained with relatively significant organic matter and pyrite. Second, both the hanging wall and footwall of the ore body are organic-rich, pyritic black shales. Third, the entire ore bearing sequence represents a continuously reducing depositional environment.

Paleo-geography during Liantuo

The Liantuo Formation represents a interglacial sedimentary sequence. There are two major hypotheses of paleo-geography of the Xiangtan deposit from Chinese literature. Most people believe that organic-rich, pyritic black shale of the Liantuo Formation formed in an euxinic, deep water basin. The well-laminated, organic and pyrite bearing rhodochrosite ore also formed under reducing conditions, perhaps, deep water. Another hypothesis proposed is that rhodochrosite ore formed in shallow water based on the discovery of blue-green algae in the rhodochrosite ore (Ye, et al. 1988). Both hypotheses propose that interglacial processes should control manganese formation. It is reported that an iron and manganese oxide deposit of the Urucum district in Brazil (Urban and Stribrny, 1985; Leeuwen, 1987; Leeuwen and Graf, 1987) has a similar age to the Xiangtan deposit and is also associated with glacial strata. In the Urucum district, most of the iron and manganese ore were precipitated as

chemical sediments in a partly ice-covered, fjord-like basin. It is possible that the source of manganese in Xiangtan deposit came from glacial processes on land and manganese deposited as carbonate in an euxinic basin which is different from the Urucum iron- and Mn-oxide deposit. It is obvious that the manganese formation of Precambrian deposits are different from Paleozoic manganese deposits.

Molango Deposit, Eastern Central Mexico

The Molango manganese deposit occurs in an upper Jurassic black shale and limestone sequence, and is the largest manganese carbonate deposit in the North America. Descriptions of this deposit have been made by Cannon and Force (1983), Alexandri and Martinez (1986), Okita (1987), Force and Cannon (1988), and May (1988).

The Molango manganese deposit is located in northeastern Hidalgo State, with a currently known outcrop area of roughly 25 km (west-east) by 50 km (north-south) in size, encompassing the mines (Fig. 30). The center of this district is situated approximately 150 km northeast of Mexico City and about the same distance southwest of Tampico. The deposit was discovered in 1960, and first production began in 1968 (DeYoung, et al., 1984).

Figure 30. Location of the Molango district, eastern-central Mexico (from Okita, 1987). The Tetzintla mine is the source of samples for this study.

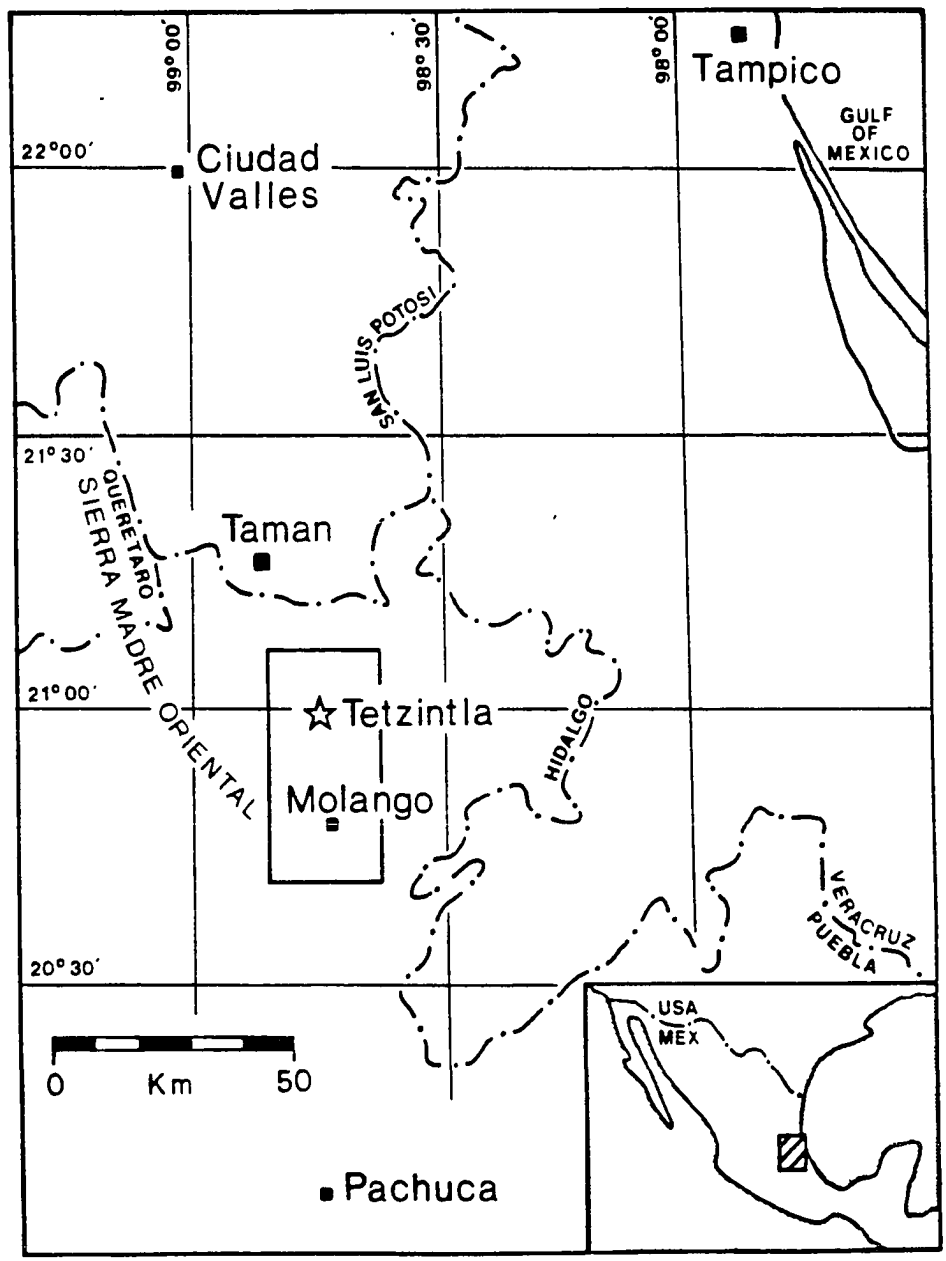

Four mine locations: Acoxcotlan, Naopa, Nonoalco, and Tetzintla, occur in the Molango manganese district; the latter two are currently active. The Nonoalco site is being mined for supergene, battery grade oxides and is purported to be the largest such accumulation in the world (Okita, 1987). The Tetzintla mine is producing primary carbonate ore. The manganese mineralization of the whole district occurs as a single stratiform ore zone ranging in thickness from less than one meter to approximately 10 meters and having a known strike length in excess of 50 kilometers (Okita, 1987). Proven reserves of the current workings are in excess of 3 million tons, which at current production rates should last about 30 years; district reserves exceed 200 million tons (Martino, 1986, p. 567). The samples for this research are from the Tetzintla mine collected by Okita and May in 1986.

Rocks of the Molango district and vicinity present a discontinuous record of geologic history from Precambrian to Tertiary age (Fig. 31). These rocks can be separated into four general groups: Precambrian Basement, Permian Marine Sequence, Mesozoic Non-marine and Marine Rocks, and Tertiary Igneous Rocks. Because the manganese mineralization is related to the upper Jurassic "Santiago" Formation and the Taman Formation (Manganese Horizon and Chipoco facies) and the samples of this study are from one

Figure 31. Generalized stratigraphic column of the rocks found in the Molango district. No stratigraphic thicknesses are implied (from Okita, 1987).

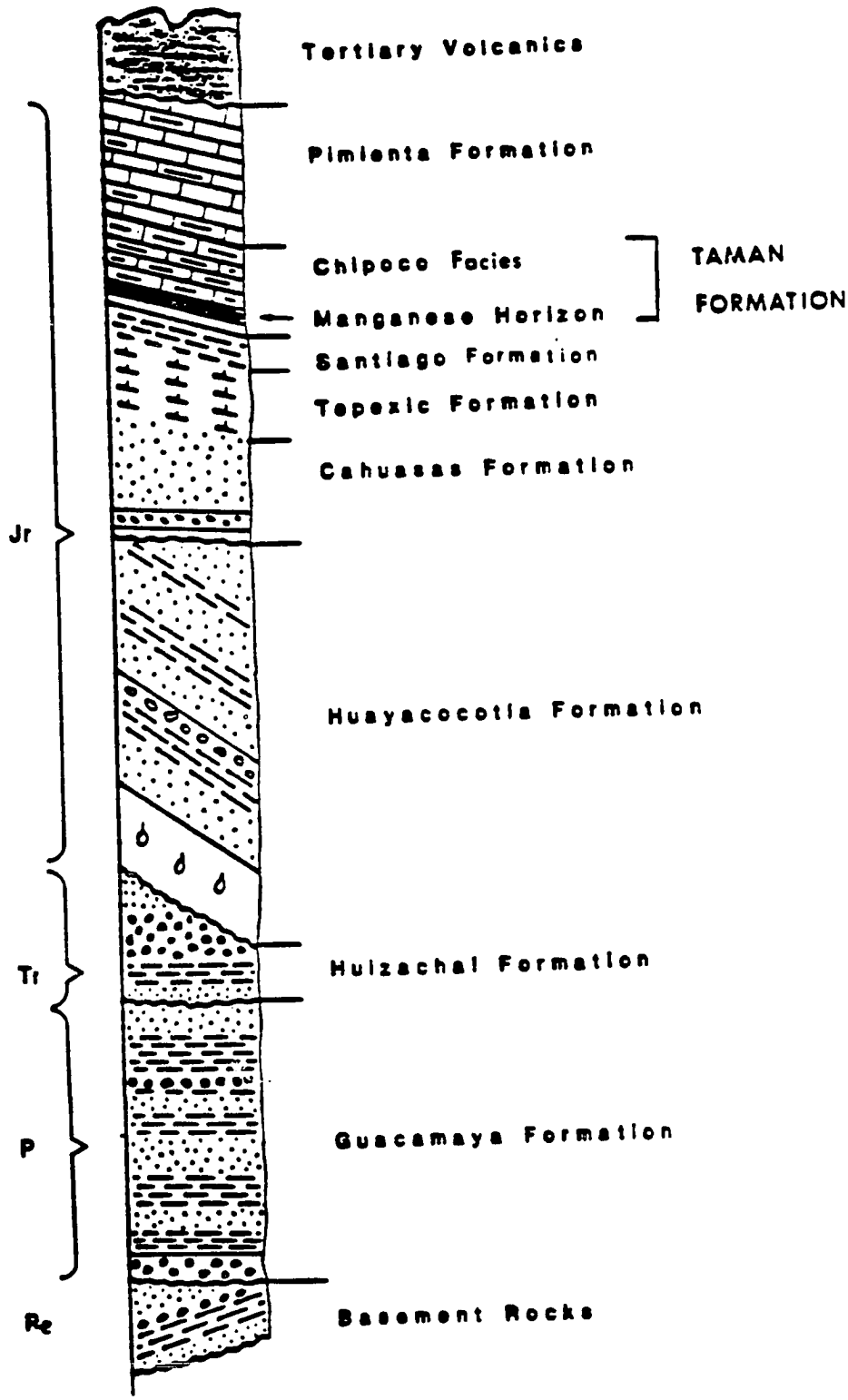

Figure 32. The "Frente B" measured section from underground and open-pit mapping (from Okita, 1987).

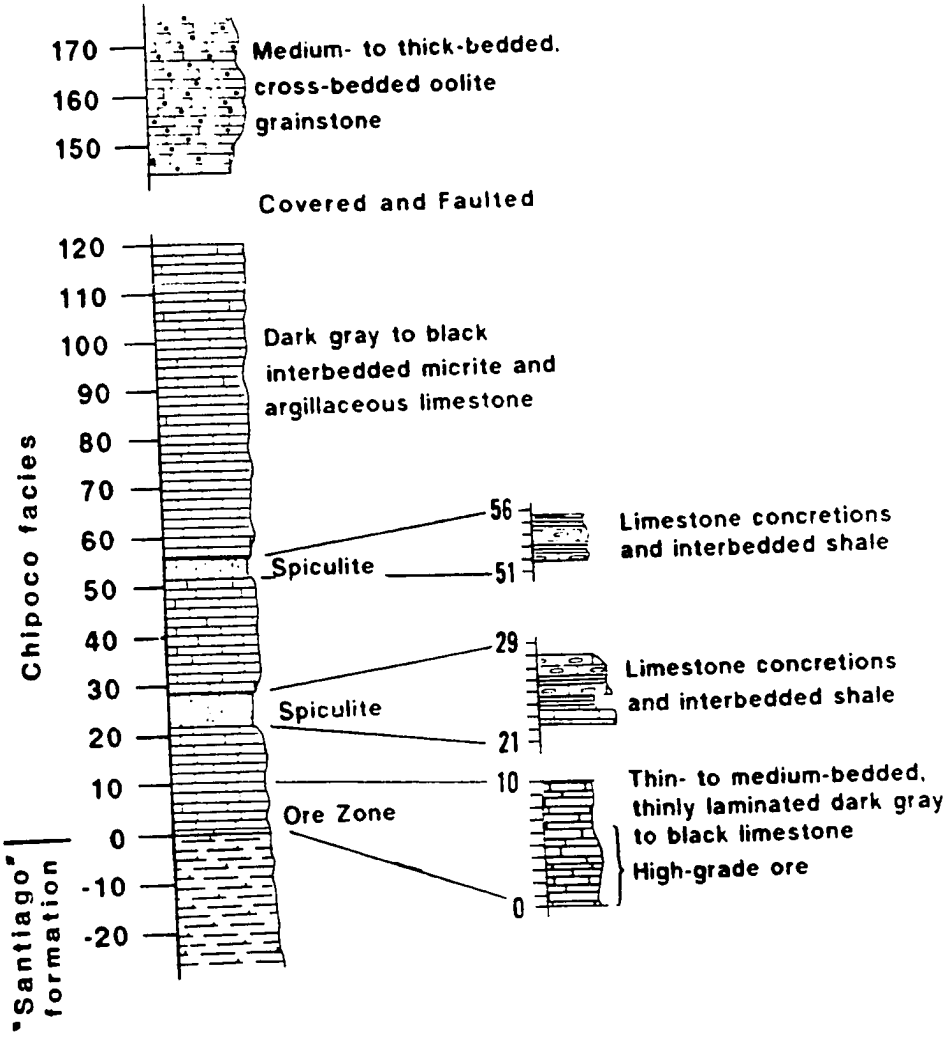

stratigraphic section (the Frente B section) measured underground and in outcrop at the Tetzintla mine (Fig. 32), the stratigraphic and petrographic description is concentrated on the upper Jurassic "Santiago" Formation, Manganese Horizon, and Chipoco facies. For a detailed description of the regional geology of the Molango district see Okita (1987).

Stratigraphic and Petrographic Description

"Santiago" Formation

The "Santiago" Formation consists of a lower black shale and upper calcareous shale with a total thickness of about 360m (Alexandri and Martinez, 1986). The lower part of the "Santiago" Formation is a sooty black, laminated, fissile, unfossiliferous, and slightly calcareous shale with thickness about 200 meters (Okita, 1987). There are no samples available from this part for further description.

The upper part of the "Santiago" Formation consists of a thinly bedded (i.e. 5 to 10 cm thick), calcareous black shale to argillaceous wackstone. In the uppermost 2 to 5 meters, it commonly contains whole ammonites, Gryphea shell beds, and limestone concretions (Okita, 1987).

In thin section, the rock of the uppermost "Santiago" Formation (i.e. the last 25 meters) is a dark brown to black, silty, calcareous shale. The rock contains local

concentrations of pyrite, 10 to 15% by visual estimate, and between 5 and 50% silt-sized (< 0.05mm) quartz as equant, angular disseminated grains. Well-developed lamination is absent; however, a sub-parallel orientation of the rock constituents is readily evident.

Chipoco facies

The contact between the "Santiago" Formation and Chipoco facies appears to be a fault contact at the Tetzintla, and can be characterized as a bedding plane or extremely low angle fault. The occurrence of a fault at this contact may be governed in part by the evident physical difference between the two units. The basal Chipoco facies, which contains the mineralized zone, is significantly harder than either the underlying "Santiago" Formation or the superjacent unmineralized zone.

Above the contact, there is a 45 centimeter thick, hard, calcite-veined, pyritiferous, manganese carbonate layer, called the "A - Bed". The "A - Bed" has abundant calcite veins, which exhibit no orientation. Pyrite is abundant in the "A - bed" and occurs in the form of small pods, thin laminae, and 2 to 3 centimeter thick beds. In thin section, a large part of the rock consists of brown micrite which possesses a distinctly crenelated to wavy lamination and contains abundant irregularly shaped clots. Black- to dark-brown pelloids and coated grains (i.e.

ooids, pellets, shells) are common and often contain abundant pyrite, both in their centers and margins. Framboidal pyrites and small euhedral pyrite crystals are abundant (Fig. 33).

Immediately overlying the "A - Bed" is the base of the high grade ore zone. These rocks have a blocky fracture and contain 30 weight-percent manganese (as MnO). They consist of dark gray to black, laminated, non-effervescent, slightly argillaceous carbonate. Pyrite is noticeably absent in the basal 3 meters of the ore zone but is present in the upper portion of the ore zone. Upward to a distance 21.6 meters above the contact between the "Santiago" Formation and Chipoco facies, the lithology is similar to that described for the ore zone, but the manganese content decreases.

In thin section, the ore zone is finely laminated. The laminations appear as alternating light and dark brown to black, parallel laminae, which often show evidence of soft sediment deformation from gravity sliding (Fig. 34). No evidence of bioturbation is present. Manganese mineralization occurs as microcrystalline rhodochrosite in light brown layers. The manganese carbonate can be in the form of discrete layers (i.e. parallel upper and lower boundaries) or in clotted structures.

Figure 33. An example of framboidal pyrites from the "A - Bed", Tetzintla mine, Molango (sample T+0.1). Reflected light.

Figure 34. An example of the rhodochrosite ore from the Tetzintla mine (sample T+4.5). Transmitted light.

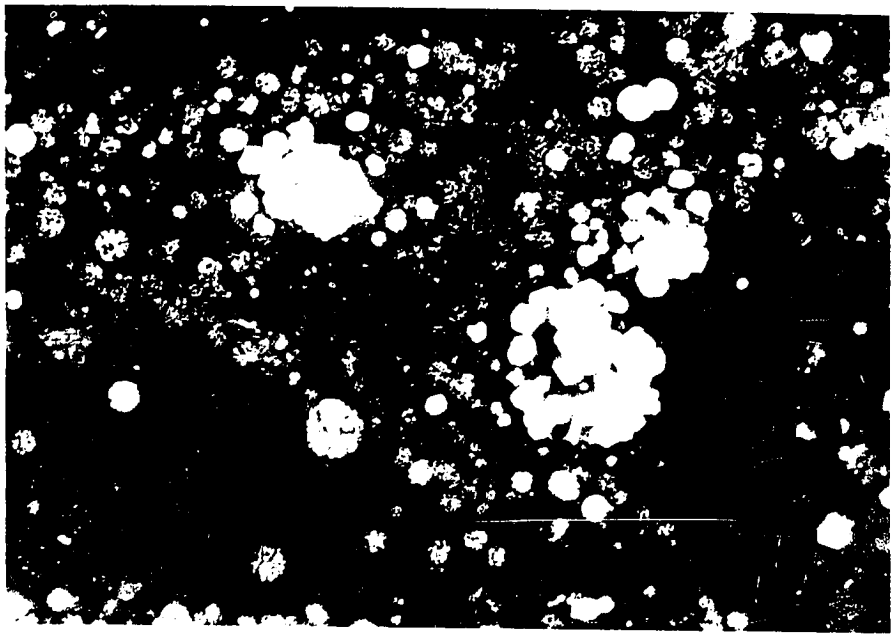

0.04mm

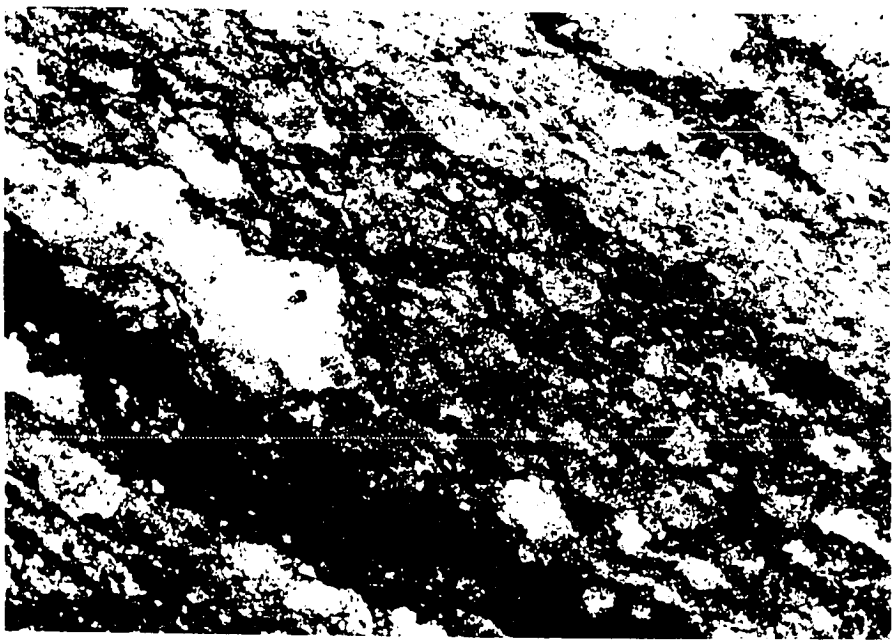

0.2mm

From the top of the ore zone (21.6 meters) upward to a second fault (about 140m above the contact between "Santiago" Formation and Chipoco facies, Fig. 31), the dominant lithology is a dark gray, thin- to medium-bedded, argillaceous limestone with three spiculite intervals, which are composed of shaley, silty, and concretionary beds. In thin section, the limestone exhibits well-developed planar, fine lamination with scattered, silt-sized quartz and irregularly shaped and laterally discontinuous carbonate masses (Fig. 35).

Above the fault, the Chipoco facies consists of oolitic, pelloidal packstone and grainstones. This coarse-grained interval has a minimum thickness of about 30 meters and is characterized as a light gray, locally cross-bedded, poorly sorted but normally graded grainstone. In thin section, the allochems include: silt-, sand-, and gravel-sized intraclasts, micritized ooliths, pellets, algal material, and mollusk and gastropod fossils (Fig. 36). Non-carbonate material is dominated by silty- to coarse-sand sized quartz and feldspar grains. Quartz grains are present as single crystals, polycrystalline grains and as the constituents of rock fragments.

Paleo-geography during "Santiago" and Chipoco

The black shales of the "Santiago" Formation represent a period when water levels were low enough that circulation

Figure 35. An example of the limestone of the middle part of the Chipoco facies (sample T+28.5). Transmitted light.

Figure 36. An example of the limestone of the upper part of the Chipoco facies (sample T+47). Transmitted light.

0.2mm

0.2mm

with the open ocean was restricted creating an euxinic condition in the basin (May, 1988). The contact with the Chipoco facies represents a change in the style of deposition from dominantly clastic to dominantly carbonate, possibly reflecting a rise in sea level to a position where adjacent highs were covered by seawater and began shedding carbonate debris (May, 1988). The Chipoco facies was probably deposited under oxygen-depleted conditions based on the scarcity of bioturbation. The oolitic wackstone and grainstone of the upper part of the Chipoco facies are interpreted to be allochthonous accumulations derived from a shallower shelf setting (Fig. 37; Okita, 1987; May, 1988).

Manuel's River Prospect

The Manuel's River manganese prospect occurs in Cambrian rocks of eastern Newfoundland. Associated lithologies are gray shale, sideritic gray shale, and black shale. The outcrops of this prospect area are located about 20 km west of St. John's, on the Avalon peninsula of Newfoundland, Canada. As mentioned above, the Manuel's River prospect is not well studied and has the least information available comparing with other deposits studied. The samples were collected by Dr. Maynard during a field trip in 1980. Figure 38 shows the location of this

Figure 37. Generalized paleo-geographic model of the Molango manganese deposit during "Santiago" and Chipoco.

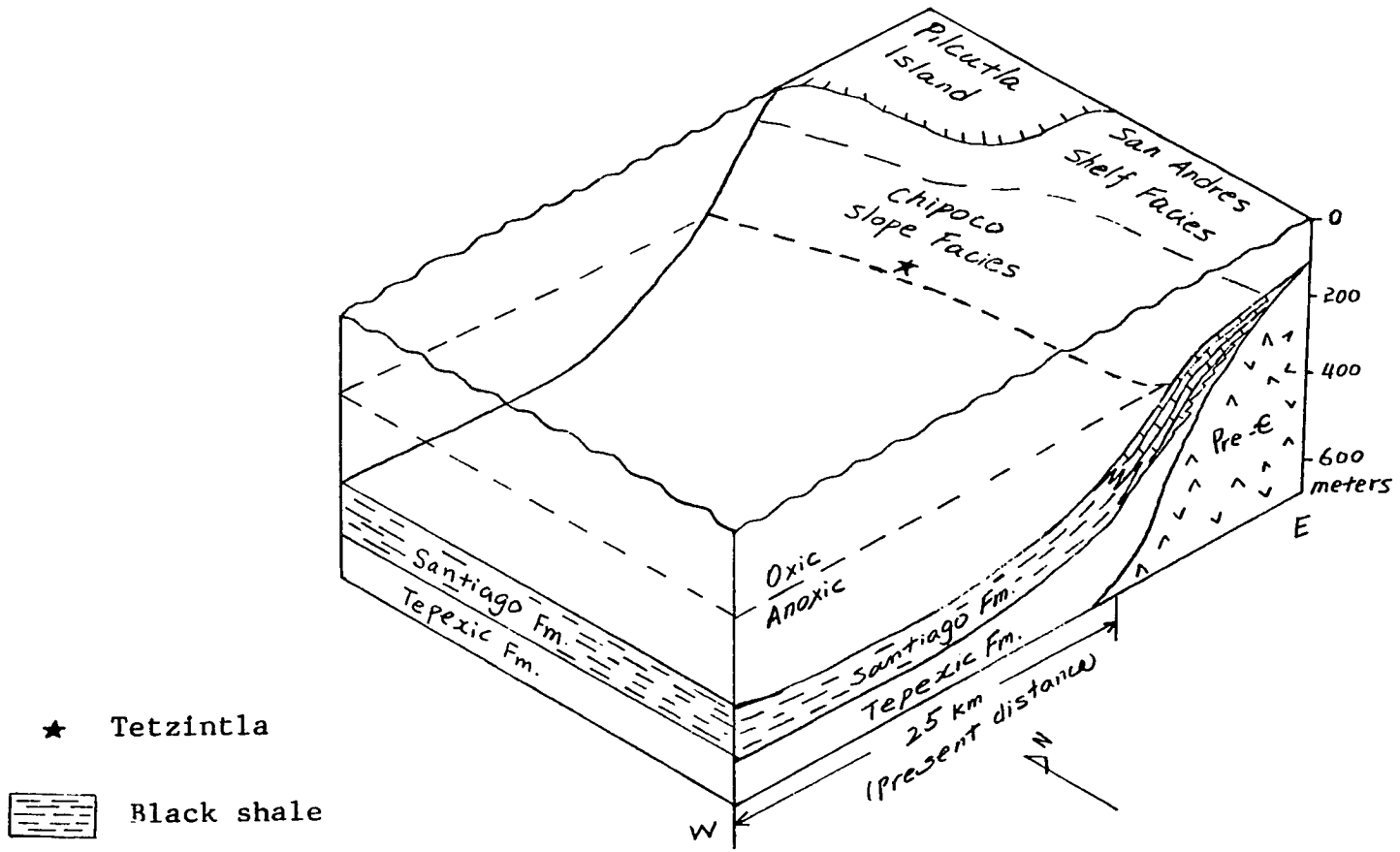

Figure 38. Location of the Manuel's River Respect, eastern Newfoundland (after Douglas, 1983). The samples of this research are from the Manuel's River.

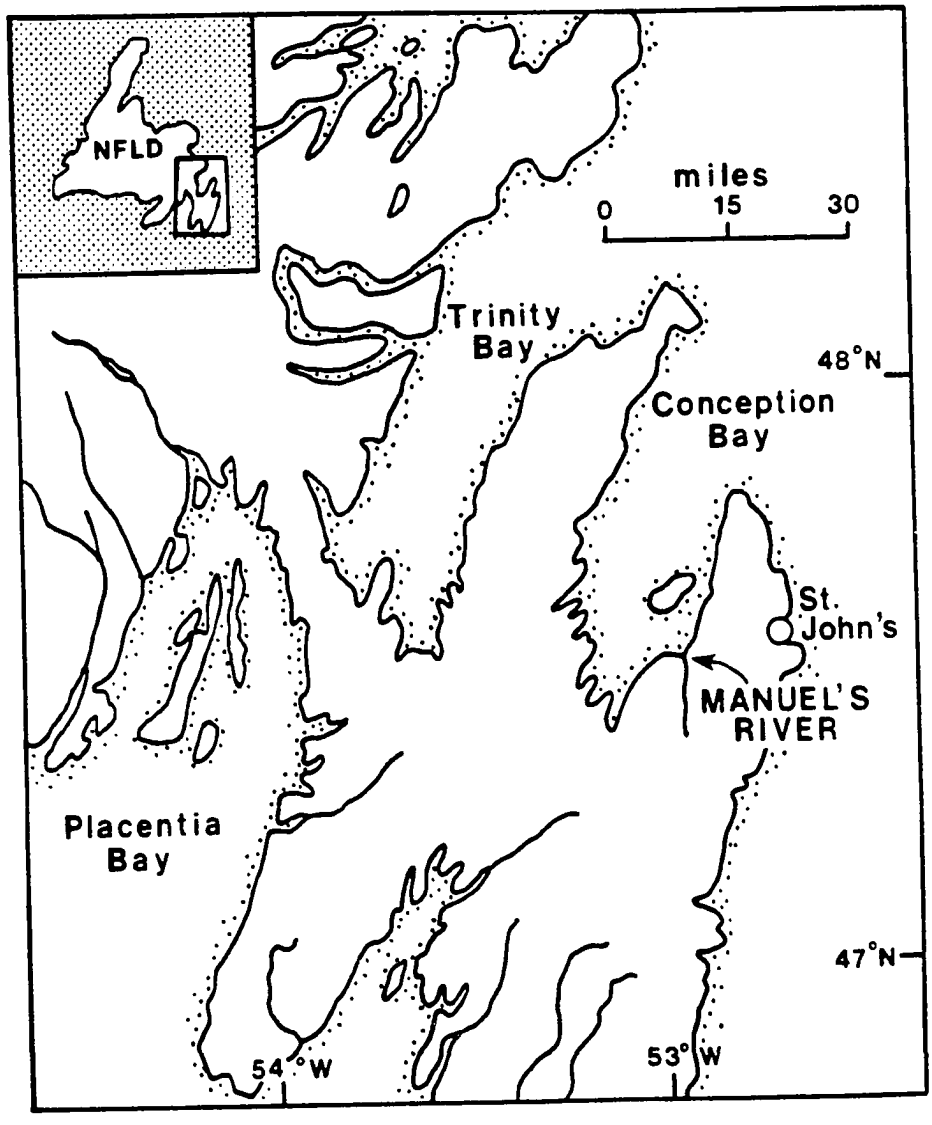

area (Douglas, 1983); Manuel's River is the source of hand samples and thin sections for this study.

Stratigraphic and Petrographic Features

The rocks of the Manuel's River prospect include Holyrood Granite basement overlain uncorformably by Cambrian rocks. Cambrian rocks are divided into the Lower Cambrian Brigus Formation, the Middle Cambrian Chamberlain's Brook and Manuel's River Formations, and the Upper Cambrian Eliott Cove Formation (Fig. 39). At the boundary between the Chamberlain's Brook Formation and Manuel's River Formation, there is a bentonite bed (about 20 cm thick), which also divides the Cambrian rocks into the Adeyton Group (100 meters thick) and the Harcourt Group (200 meters thick).

The Lower Cambrian Brigus Formation locally contains a 5 to 6 meters thick, basal conglomerate. Above the conglomerate bed, the rocks consist of green and gray shales with few limestone interbeds. The thickness of these shales is about 20 meters.

The Middle Cambrian has two formations. The Chamberlain's Brook Formation consists of thickly bedded gray shale in the upper portion and sideritic gray shale with red mudstone restricted to the lower part of the formation (Douglas, 1983). Nodular limestone beds are intercalated with the shales. The manganese carbonate

Figure 39. Generalized stratigraphic column of the rocks found in the Manuel's River district. The thickness of minor lithologies such as the manganese horizon has been exaggerated for emphasis.

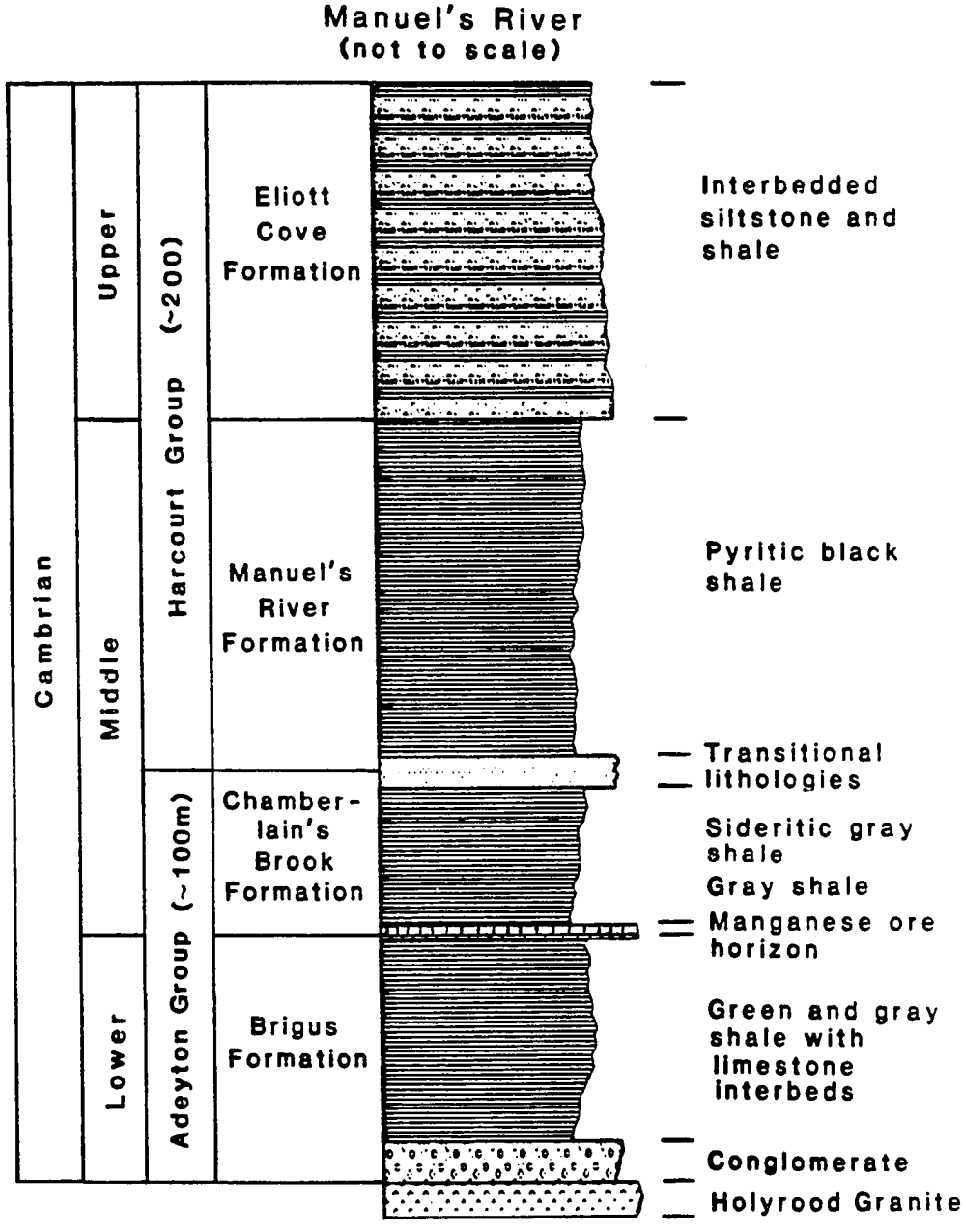

horizon is at the base of the Chamberlain's Brook Formation, being one meter thick. Overlying the Chamberlain's Brook Formation, the upper Middle Cambrian Manuel's River Formation consists of pyritic black shales with a basal bentonite bed (few centimeters thick) which separates these two formations.

The upper Cambrian Eliott Cove Formation consists of thinly interbedded siltstone and gray shale. It is about 200 meters thick.

Manganese Horizon

The manganese horizon occurs at the base of the Middle Cambrian Chamberlain's Brook Formation. This horizon is about 1 meter thick and widely spread in the area.

Manganese horizon samples consist of a mixture of argillaceous material and of carbonate minerals (Fig. 40). Some samples contain euhedral crystals of pyrite, barite and magnetite; and others contain phosphatic nodules. Identifiable minerals in the argillaceous portion of these rocks include chlorite, quartz, and hematite. X- ray diffraction data show that the major manganese carbonate is rhodochrosite (see Chapter 4). Figure 41 shows the gray shale just above the rhodochrosite ore horizon.

Summary

In contrast to the other three manganese deposits studied, the manganese horizon of Manuel's River is thin

Figure 40. An example of the rhodochrosite ore from the Manuel's River prospect. Transmitted light.

Figure 41. An example of the gray shale which lies immediately above the rhodochrosite ore horizon. Transmitted light.

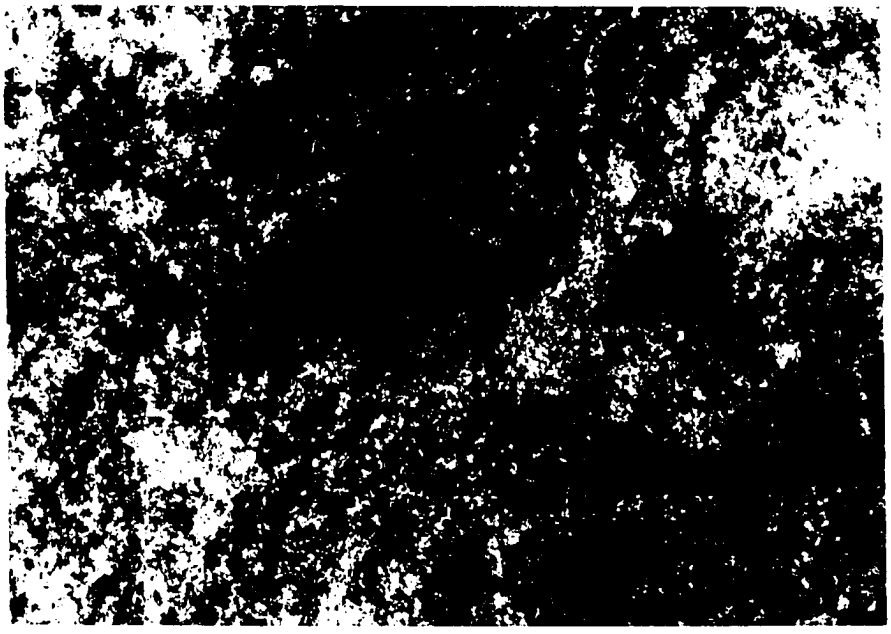

0.2mm

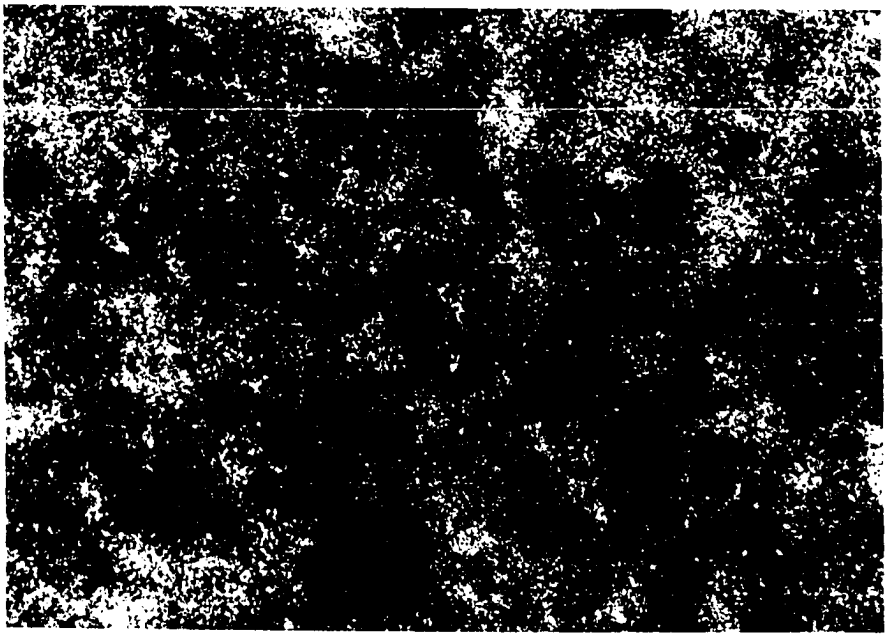

0.2mm

and impure and overlies a green and gray shale sequence, which represents a rather oxidized condition, possibly a normal marine shelf. The rocks above the manganese horizon, the Chamberlain's Brook Formation, also represents an oxidized condition, based on the occurrence of sideritic gray shale and gray shale. Only the upper Middle Cambrian Manuel's River Formation consists of pyritic black shale, representing an oxygen-depleted condition. Because there is no euxinic basin developed before the ore zone, the manganese source possibly was very far away and very small and a thin rhodochrosite ore bed was formed. A brief comparison of the major characteristics of these four manganese deposits is given in Table 3.3.

Comparison of major features of the manganese deposits

	Manuel's River prospect	Taojiang deposit	Molango deposit
Age	Middle Cambrian	Middle Ordovician	Upper Jurassic
Host rocks above ore	Gray Sh.	Mn-limestone gray mudstone	limestone
Mn-ore bed Thickness	<1m	1.7 - 3m	9m
Lithology	Fine-grained Rho.	well-crystallized Rho. with minor Py. and organic matter	laminated Rho. with minor Py. and organic matter
Host rocks below ore	Gray and green Sh.	Black Sh. Gray Sh.	Black Sh.
Thickness of black Sh.	0m	10-30m	360m
Redox condition	Moderately oxidized throughout	From more reducing to less reducing upward	From more reducing to less reducing upward

CHAPTER 4. WHOLE ROCK X-RAY DIFFRACTION, ISOTOPE, AND ORGANIC MATTER ANALYSES

Whole Rock X-Ray Diffraction analysis

Mineralogy of representative samples from each deposit studied, except the samples of the Molango manganese deposit, was determined with an X-ray diffractometer. X-ray diffraction data from the Molango Deposit from the dissertation of Okita (1987) are available for comparison. The major mineral phases found are quartz, illite and chlorite in shales, and rhodochrosite, kutnahorite, dolomite and calcite in carbonate rocks. Pyrite is present in black shales and some rhodochrosite ores. More detailed X-ray diffraction data of each sample determined are presented in Appendix D.

Taojiang Manganese Deposit

The lithologies of the ore-bearing sequence of the Taojiang manganese deposit consist of black shale, gray mudstone, limestone, and rhodochrosite ore. X-ray diffraction patterns of the black shales below the ore body show that the major mineral phases are quartz, illite, chlorite, and pyrite (Fig. 42, 43). The direct footwall and hanging wall of the rhodochrosite ore body are limestones. The X-ray diffraction pattern shows that calcite is the major mineral phase with a small amount of quartz (Fig. 44). The edge of the ore body consists of low

Figure 42.

X-ray diffraction patterns of black shale (sample DL7) of the Hule Formation, Taojiang Deposit.

Abbreviations used:

Q = Quartz
Ill = Illite
Ch = Chlorite
Py = Pyrite

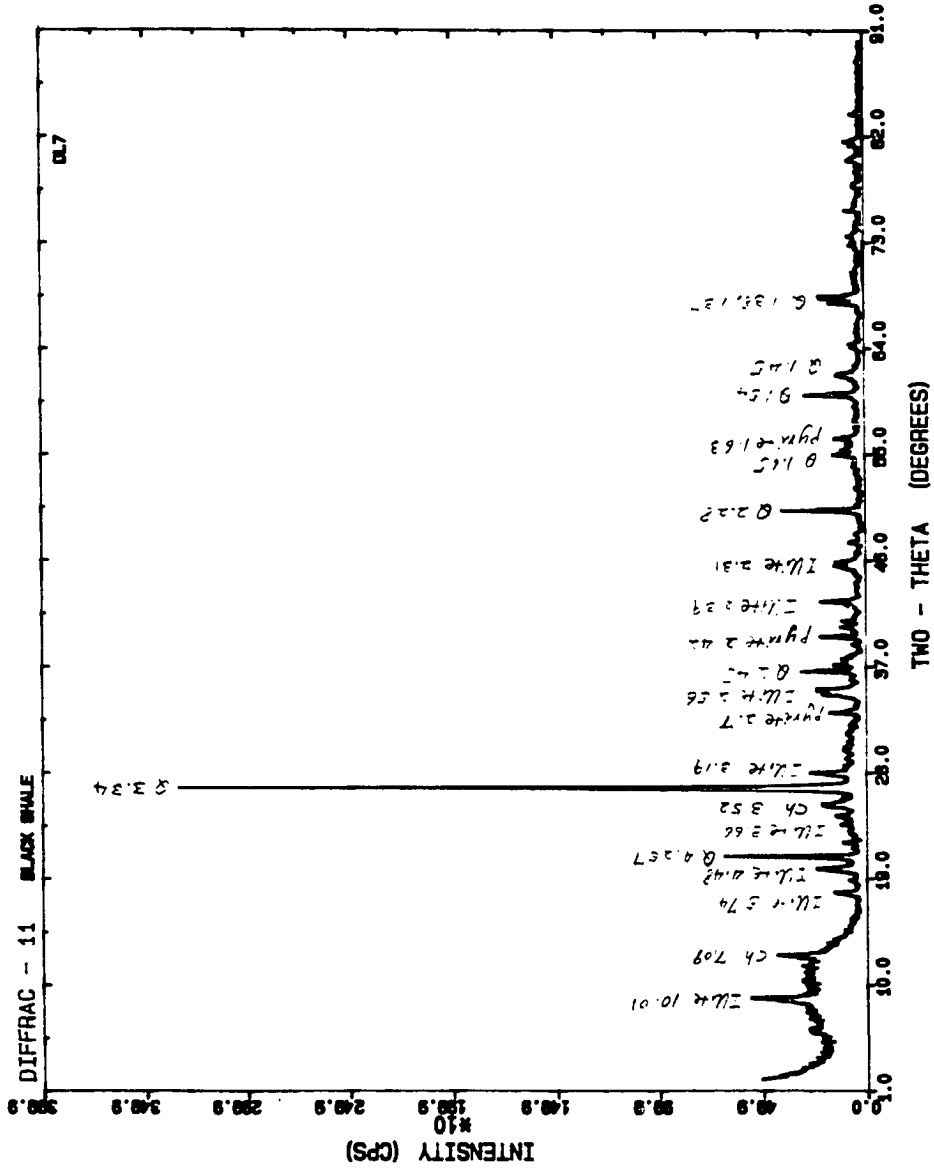

Figure 43.

X-ray diffraction pattern of black shale (sample NS2) of the middle Modaoxi Formation, Taojiang Deposit.

Abbreviations used:

Q = Quartz
Ill = Illite
Ch = Chlorite
Py = Pyrite

Figure 44.

X-ray diffraction pattern of limestone (sample DL13) of the Modaoxi Formation, Taojiang Deposit.

Abbreviations used:

D = Dolomite
C = Calcite
Q = Quartz

grade rhodochrosite ore. The X-ray diffraction pattern shows that dolomite and kutnahorite are major carbonate minerals with a small amount of quartz, illite, and chlorite (Fig. 45). The center of the ore body consists of a rather pure rhodochrosite phase with a very small amount of quartz (Fig. 46). The host rocks above the ore body are gray mudstones. The X-ray diffraction pattern shows that clay mineral phases, illite and chlorite, become dominant (Fig. 47). Quartz and pyrite are also present in small amounts.

Xiangtan Manganese Deposit

The lithologies of the ore-bearing sequence of the Xiangtan manganese deposit consist of black shales and rhodochrosite ores. The X-ray diffraction patterns of black shales, which are the footwall and hanging wall of the ore body, show that quartz, illite, and pyrite are major mineral phases. The X-ray diffraction pattern of a sample of black shale within the ore body shows rhodochrosite, illite, quartz, and pyrite mineral phases (Fig. 48). This indicates a kind of low-grade rhodochrosite ore formed by the mixing of Mn-carbonate and silicate minerals. Figure 49 shows the X-ray diffraction pattern of a high grade rhodochrosite ore sample. Rhodochrosite is the major mineral phase with small amounts of pyrite and quartz. The significant pyrite is found in

Figure 45.

X-ray diffraction pattern of low grade rhodochrosite ore (sample DL18) of the middle Modaoxi Formation, Taojiang Deposit.

Abbreviation used:

D = Dolomite
K = Kutnahorite
C = Calcite
Q = Quartz
Ill = Illite
Ch = Chlorite

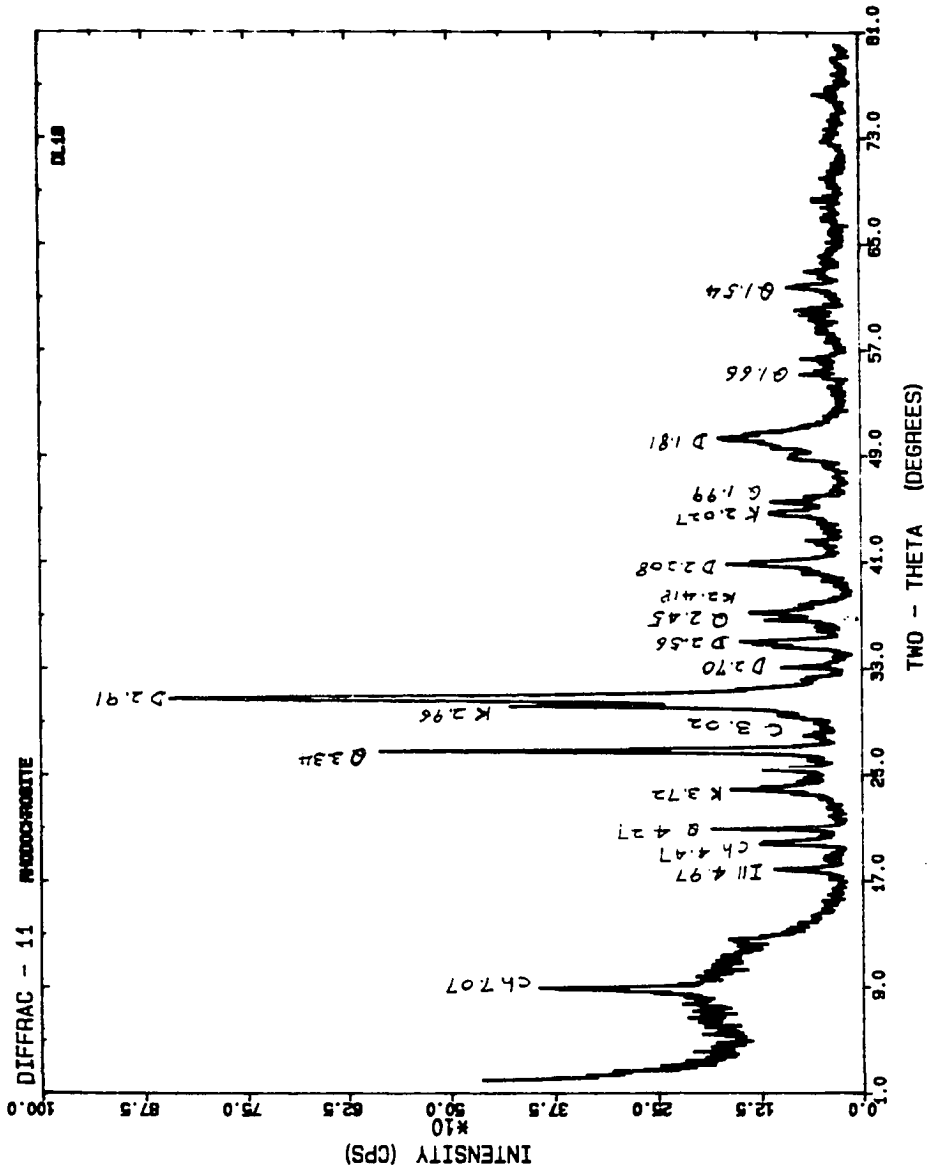

Figure 46.

X-ray diffraction pattern of rhodochrosite (sample NS5a) of the middle Modaoxi Formation, Taojiang Deposit.

Abbreviations used:

Rho. = Rhodochrosite
Q = Quartz

Figure 47.

X-ray diffraction pattern of gray mudstone (sample DL23) of the upper Modaoxi Formation, Taojiang Deposit.

Abbreviations used:

Ill = Illite
Q = Quartz
Py = Pyrite

Figure 48.

X-ray diffraction pattern of black shale (sample XT5) within the rhodochrosite ore body of the Liantuo Formation, Xiangtan Depcsit.

Abbreviations used:

Rho = Rhodochrosite
Q = Quartz
Ill = Illite
Py = Pyrite

Figure 49.

X-ray diffraction pattern of rhodochrosite ore (sample XT7) of the Liantuo Formation, Xiangtan Deposit.

Abbreviations used:

Rho = Rhodochrosite
Q = Quartz
Py = Pyrite

rhodochrosite ore only in the Xiangtan deposit for this study.

Molango Manganese Deposit

Three representative X-ray diffraction patterns of samples from upper, middle, and basal portions of ore zone in the lower Chipoco facies of the Molango manganese deposit are shown here (Fig. 50 -- 52; Okita, 1987). The X-ray diffraction pattern of the samples from the upper, low-grade portions of the ore zone shows kutnahorite, dolomite, rhodochrosite, manganoan calcite, calcite, magnetite, maghemite, pyrite, and quartz mineral phases (Fig. 50). Among them, kutnahorite and dolomite are the major mineral phases. The X-ray diffraction pattern from the high grade ore zone shows that rhodochrosite is the major mineral phase, with associated maghemite (Fig. 51). The sample from the basal Chipoco facies consists of dolomite, calcite, and quartz. The X-ray diffraction pattern shows that dolomite is the major mineral phase (Fig. 52).

Manuel's River prospect

The rhodochrosite ore horizon occurs in the basal portion of the Chamberlain's Brook Formation, Middle Cambrian, and is hosted by gray shales. The X-ray diffraction pattern of the rhodochrosite ore shows rhodochrosite, hematite, quartz, calcite, and chlorite

Figure 50.

Representative X-ray diffraction pattern of samples from upper, lower grade portions of the ore zone in lower Chipoco facies, Molango Deposit (Okita, 1987).

Abbreviation used:

Q = Quartz
P = Pyrite
K = Kutnahorite
D = Dolomite
R = Rhodochrosite
Mn= Manganoan Calcite
C = Calcite
M = Magnetite
m = Maghemite

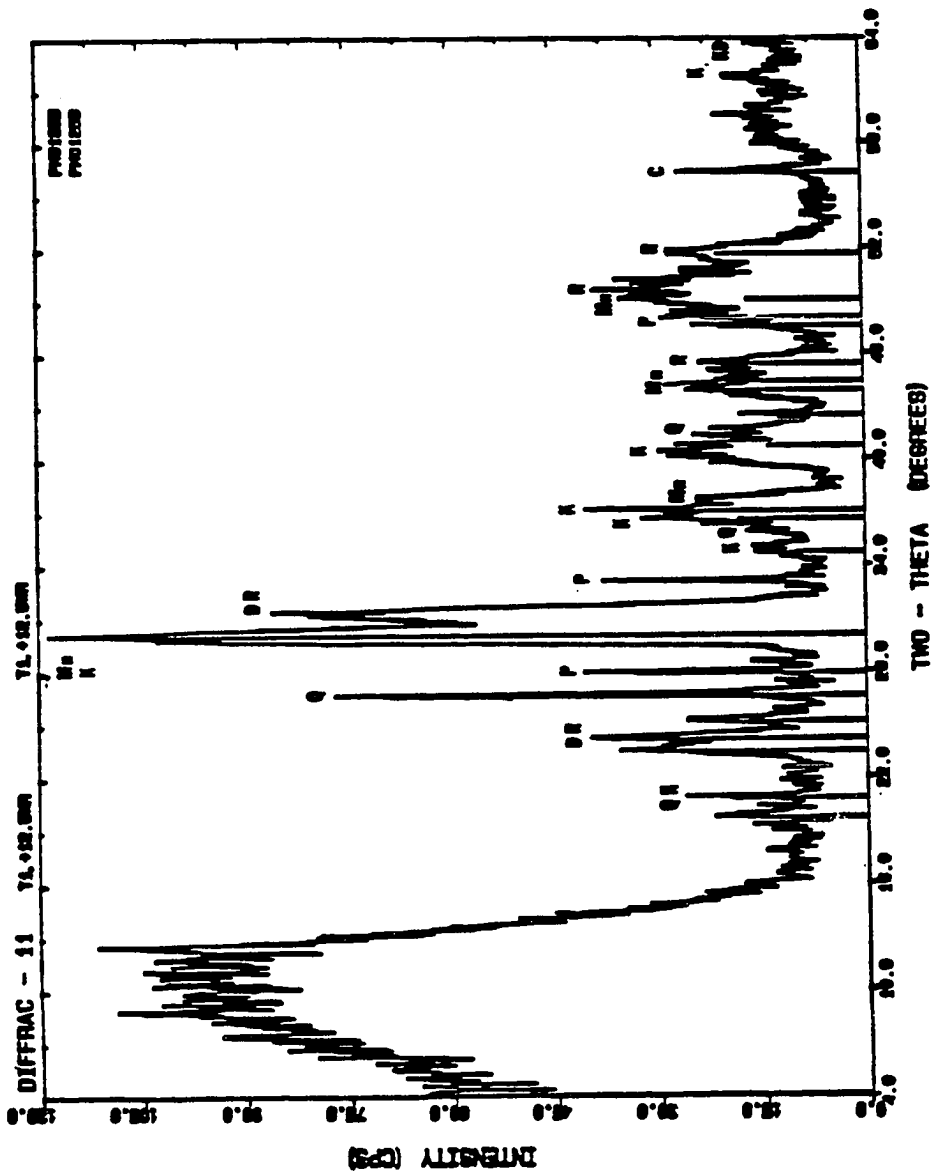

Figure 51.

X-ray diffraction pattern from the high grade ore zone of Lower Chipoco facies, Molango Deposit (Okita, 1987). Note sharp peek definition and absence of other mineral phases besides rhodochrosite.

Abbreviation used:

R = Rhodochrosite
m = Maghemite

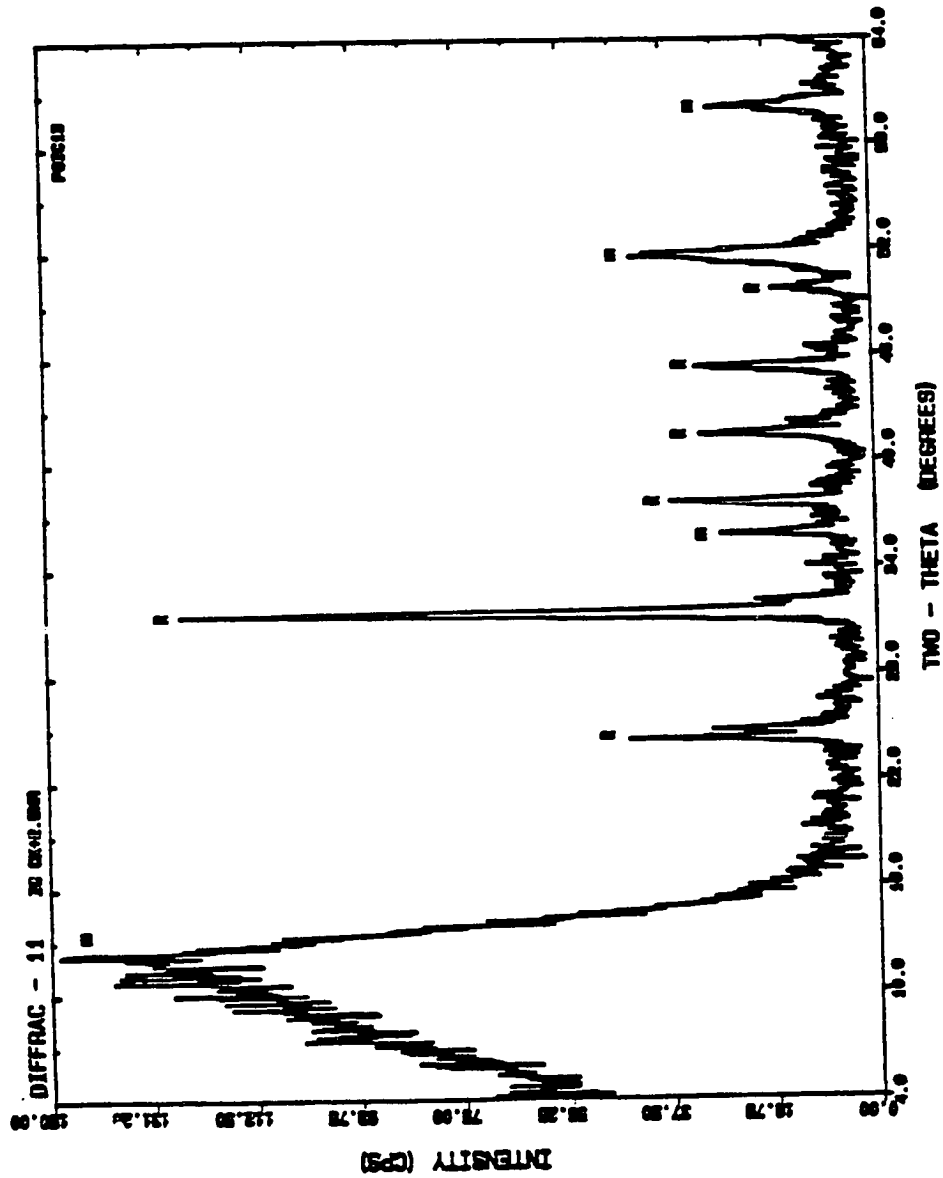

Figure 52.

X-ray diffraction pattern from basalmost Chipoco facies showing the presence of quartz and dolomite. * = order reflections for dolomite (Okita, 1987).

Abbreviation used:

Q = Quartz
D = Dolomite
C = Calcite

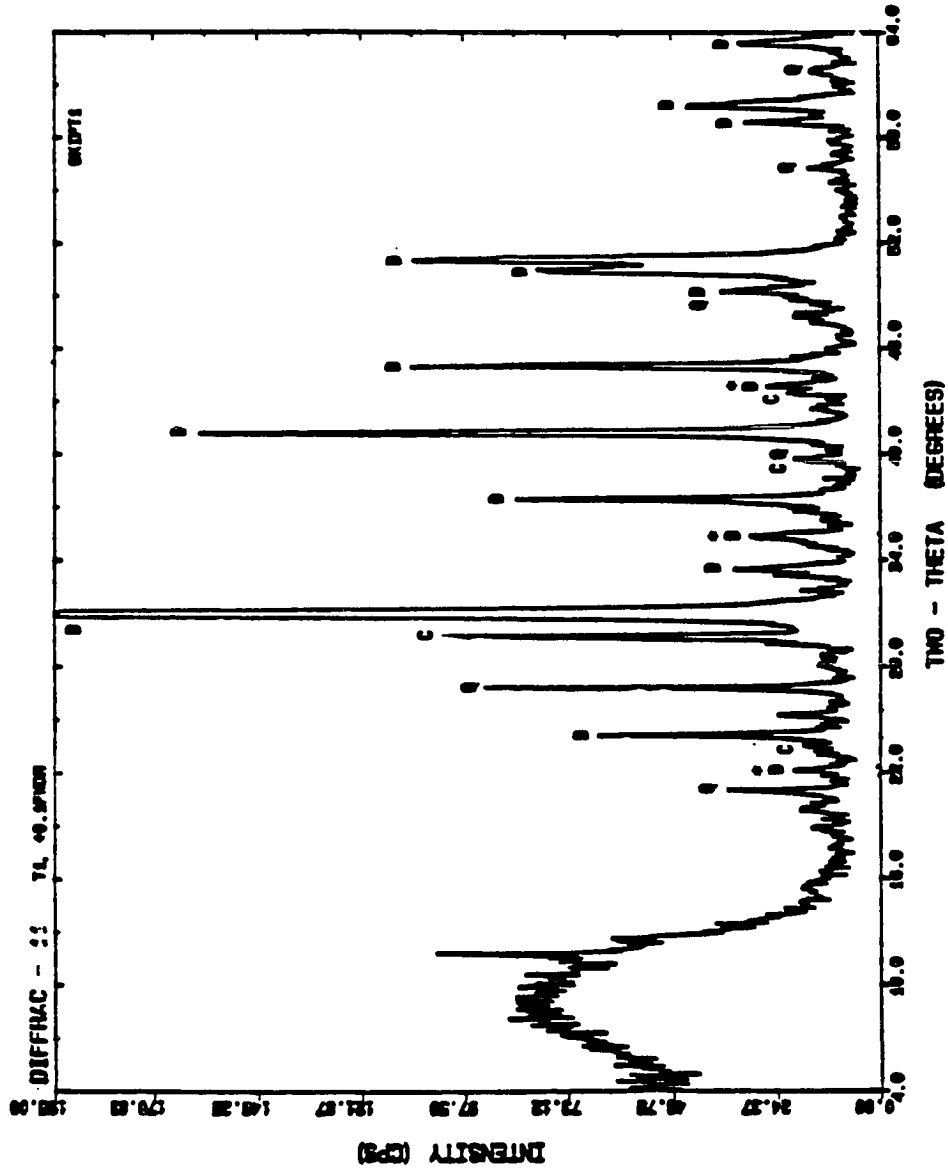

mineral phases (Fig. 53). The hematite is found in low-grade rhodochrosite ore only in the Manuel's River prospect for this study. The X-ray diffraction pattern of gray shale hosting the rhodochrosite ore bed shows quartz, illite and chlorite mineral phases (Fig. 54).

Summary

The major mineral phases of ore-bearing rocks of these manganese deposits are similar. Shales consist mainly of quartz and a mixture of illite and chlorite. Pyrite is usually present in black shales. The gray shale above the ore body of the Taojiang manganese deposit consists of more clay minerals (illite and chlorite) than black shale below the ore zone does. Rhodochrosite is a major manganese bearing mineral phase in these four deposits studied. The center of each rhodochrosite ore body consists of a pure rhodochrosite phase, whereas low-grade edges of the ore (low grade) consists of kutnahorite and dolomite (Taojiang and Molango), or rhodochrosite mixed with silicate mineral phases (Xiangtan). Pyrite is present in high grade rhodochrosite ore bodies only at the Xiangtan deposit. Magnetite and maghemite are abundant in the high grade rhodochrosite ore body of the Molango deposit, but not elsewhere. Hematite is found in the rhodochrosite ore body of Manuel's River prospect only. In the high grade rhodochrosite ore body of the Taojiang deposit, no iron

Figure 53.

X-ray diffraction pattern of rhodochrosite ore (sample F343) from the Manuel's River prospect, Newfoundland.

Abbreviation used:

Q = Quartz
Rho = Rhodochrosite
He = Hematite
Ch = Chlorite

Figure 54.

X-ray diffraction pattern of gray shale (Sample F344) hosting rhodochrosite ore bed of the Manuel's River prospect, Newfoundland.

Abbreviation used:

Q = Quartz
Ill = Illite

oxide mineral phases can be found. These indicate that rhodochrosite can be stable with iron sulfide or iron oxides during deposition and diagenesis.

Isotope and organic matter analysis of Taojiang deposit

As mentioned in Chapter 2, 15 samples of the Taojiang manganese deposit were sent to the U.S. Geological Survey and Amoco Production Company Research Center for sulfur and carbon isotopes and organic matter analysis respectively. Table 4 shows the analytical data for sulfur and carbon isotopes, and sulfur weight percent of the samples of the Taojiang manganese deposit at the U.S.G.S.

The data of sulfur isotope of pyrite show that gray and black shales have negative $\delta^{34}S$ values (-23 to -32 ‰). Low $\delta^{34}S$ values and high pyrite contents in the unmineralized zones suggest that pyrite formed from normal seawater by bacteriogenic SO_4 reduction. In contrast, pyrite from Mn-bearing horizon has very heavy $\delta^{34}S$ value (-2 to +23 ‰), in some cases approaching the value for contemporaneous seawater. Pyrite content is anomalously low in the mineralized zone (< 0.5 wt. %). The $\delta^{34}S$-enriched pyrite from the ore zone indicates that pyrite formed in a nearly closed system that underwent extensive SO_4 reduction. It is not clear whether this system was limited to local porewaters or involved the entire sedimentary basin. A few carbon isotope data from shales

Table 4.

Sulfide sulfur, sulfur isotope and carbon isotope data of the Taojiang manganese deposit

Sample #	Name	wt.% sulfur	S^{34}/S^{32} CDT ‰	C^{13}/C^{12}PDB ‰
Yanxi Formation				
DL1	Gray shale	0.091	-23.474	-18.00
DL3	Gray shale	0.218	-28.176	
Hule Formation				
DL6	Black shale	1.992	-29.508	
DL7	Black shale	2.082	-32.246	
DL9	Black shale	1.261	-26.498	
Modaoxi Formation				
DL10	Gray shale	0.051	-21.207	
DL12	Black shale	1.556	-22.599	-11.90
DL13	Mn-limestone	0.279	+23.245	-5.80
DL15	Black shale	3.276	-28.234	-17.80
DL17	Rhodochrosite			-10.50
DL20	Mn-limestone	0.132	-2.085	
DL22	Gray mudstone	0.058	-14.188	
NS5	Rhodochrosite	0.046	-8.575	

Analyzed by Okita, 1987

and Mn-carbonates show that Mn-bearing carbonates have negative $\delta^{13}C$ values: -5 to -18 °/oo (PDB) and the most negative values occur in high grade ore (i.e., rhodochrosite rich). These data indicate that a significant proportion of the carbon in Mn carbonates was derived from organic matter via diagenetic reactions involving SO_4 or MnO_2 reduction. Pyritiferous black shales have $\delta^{13}C$ values as negative as Mn-bearing carbonates. The carbon isotopic results suggests that this Mn-bearing sequence formed as early diagenetic and syngenetic products in dysaerobic to anoxic marine environments.

The carbon isotope data of the Molango deposit made by Okita (1987) show similar characteristics as those of the Taojiang deposit. The rhodochrosite ore of the Molango deposit shows very negative $\delta^{13}C$ isotopic values, raging from approximately -8.0 to -16.43 °/oo. The hosting rocks below and above the ore zone are generally characterized by $\delta^{13}C$ values of about +1.0 °/oo.

Only four samples that have a high organic carbon content (4.5 to 2.3 wt. %) were examined for vitrinite reflectance and carbon isotopes of kerogen (Table 5, 6). Figure 55 shows results of vitrinite reflectance analysis. The average value of these four pyritiferous, organic-rich black shales is 3.704 % R_o (3.51 to 3.88 %), which are the same as the data of the samples of the Molango deposit

(3.36 to 3.39 % Ro) made by Okita (1987). The practice employed in interpreting these histograms is to assume that the lowest % R_o values are produced by autochthonous organic material (Tissot and Welte, 1984, p. 516). The higher reflective component is the result of the incorporation of reworked vitrinite. Considering the higher % R_o values of these samples, it is possible that organic matter is composed of a relatively large fraction of reworked vitrinite. An alternative interpretation of %R_o values of about 4.00 is that the organic matter has been subjected to near or incipient metamorphic (i.e. greenschist, T - 400° C) conditions. However, this is not the case, because metamorphism does not appear to have severely affected the organic matter of the black shales studied.

The $\delta^{13}C$ values of kerogen (Table 6) in all five samples are nearly uniform: -32.30 to -31.50 °/oo PDB, which are close to $\delta^{13}C$ values of kerogen of the average data of the Molango deposit made by Okita (1987): -27 °/oo PDB. These data are within the range of values which delimit the L-amorphous kerogen variety of Lewan (1986). Such isotopic compositions have been found to be a characteristic of restricted basins overlain by stratified shallow water (<200 m) where the prevailing source of carbon in the photic zone is organically derived CO_2.

Table 5. Chemical analysis of organic carbon

AMOCO PRODUCTION COMPANY
RESEARCH CENTER

OFFICE
TECHNICAL SERVICE NUMBER DISTRICT 871873

ROCKEVAL PYROLYSIS DATA
TABLE 2.
DATE 10/12/87

SAMPLE NUMBER	TOP OF INTERVAL FEET	FORMATION	TOTAL ORGANIC CARBON WT% [redacted] TOC	PPM VOLATILE HYDROCARBONS (S1 X 1000)	VOL/ TOC	PPM GENERATED HYDROCARBONS (S2 X 1000)	GEN/ TOC	TEMP OF MAX GEN	VOL/ VOL + GEN
			LECO TOC						
STATE FOREIGN OPERATOR			COUNTY CHINA /EXCL LEASE	TAIWAN/ TAO JIANG		WELL LOCATION OUTCROPS			
DL-1		YANXI	0.4	< 10	< 0.01	< 10	< 0.01	NR	< 0.01
DL-6		HULE	3.5	< 10	< 0.01	< 10	< 0.01	NR	< 0.01
DL-7		HULE	4.5	30	< 0.01	70	< 0.01	NR	0.30
DL-9		HULE	4.4	10	< 0.01	< 10	< 0.01	NR	1.00
DL-10		MO DAOXI	0.3	< 10	< 0.01	10	< 0.01	NR	< 0.01
DL-12			2.3	< 10	< 0.01	< 10	< 0.01	NR	< 0.01
DL-13			0.4	10	< 0.01	< 10	< 0.01	NR	1.00
DL-15			2.5	< 10	< 0.01	< 10	< 0.01	NR	< 0.01
DL-17			0.2	20	0.01	< 10	< 0.01	NR	1.00
DL-19			0.5	< 10	< 0.01	< 10	< 0.01	NR	< 0.01
DL-20			0.5	< 10	< 0.01	< 10	< 0.01	NR	< 0.01
DL-22			0.3	< 10	< 0.01	< 10	< 0.01	NR	< 0.01
NS-5			0.2	< 10	< 0.01	< 10	< 0.01	NR	< 0.01
NS-12			0.4	< 10	< 0.01	< 10	< 0.01	NR	< 0.01

NR indicates "not reliable"

Table 6. Kerogen analysis of organic carbon

AMOCO PRODUCTION COMPANY
RESEARCH CENTER

OFFICE
TECHNICAL SERVICE NUMBER 871873 DISTRICT

KEROGEN DATA
TABLE 5.
DATE 10/12/87

LAB SAMPLE NUMBER	FIELD NO. OR DEPTH FEET TOP***BOTTOM	FORMATION	NORM. ELEMENTAL ANALYSIS, WT. % CARBON	HYDROGEN	OXYGEN	NITROGEN	% REC	SULFUR WT. %	ASH WT. %	ATOMIC RATIO O/C	ATOMIC RATIO H/C	CARBON ISOTOPE KEROGEN
STATE FOREIGN OPERATOR		COUNTY	CHINA /EXCL TAIWAN/ LEASE TAO JIANG		WELL LOCATION OUTCROPS							
DL-6		HULE	95	0.0	3.8	1.1	65			0.03	0.00	-31.70
DL-7		HULE	96	0.0	3.2	1.2	70			0.03	0.00	-31.90
DL-9		HULE	96	0.0	3.1	1.2	70			0.02	0.00	-32.30
DL-12			95	0.0	3.5	1.0	60			0.03	0.00	-31.80
DL-15												-31.50

Figure 55.

Histograms of vitrinite reflectance data.

VITRINITE REFLECTANCE ANALYSIS

OUTCROP SAMPLES FROM AN UNKNOWN LOCATIONSAMPLES DL-6, DL-7, DL-9, DL-12, & DL-15

LOCALITY 871873 9-30-87 GEO-STRAT, INC.

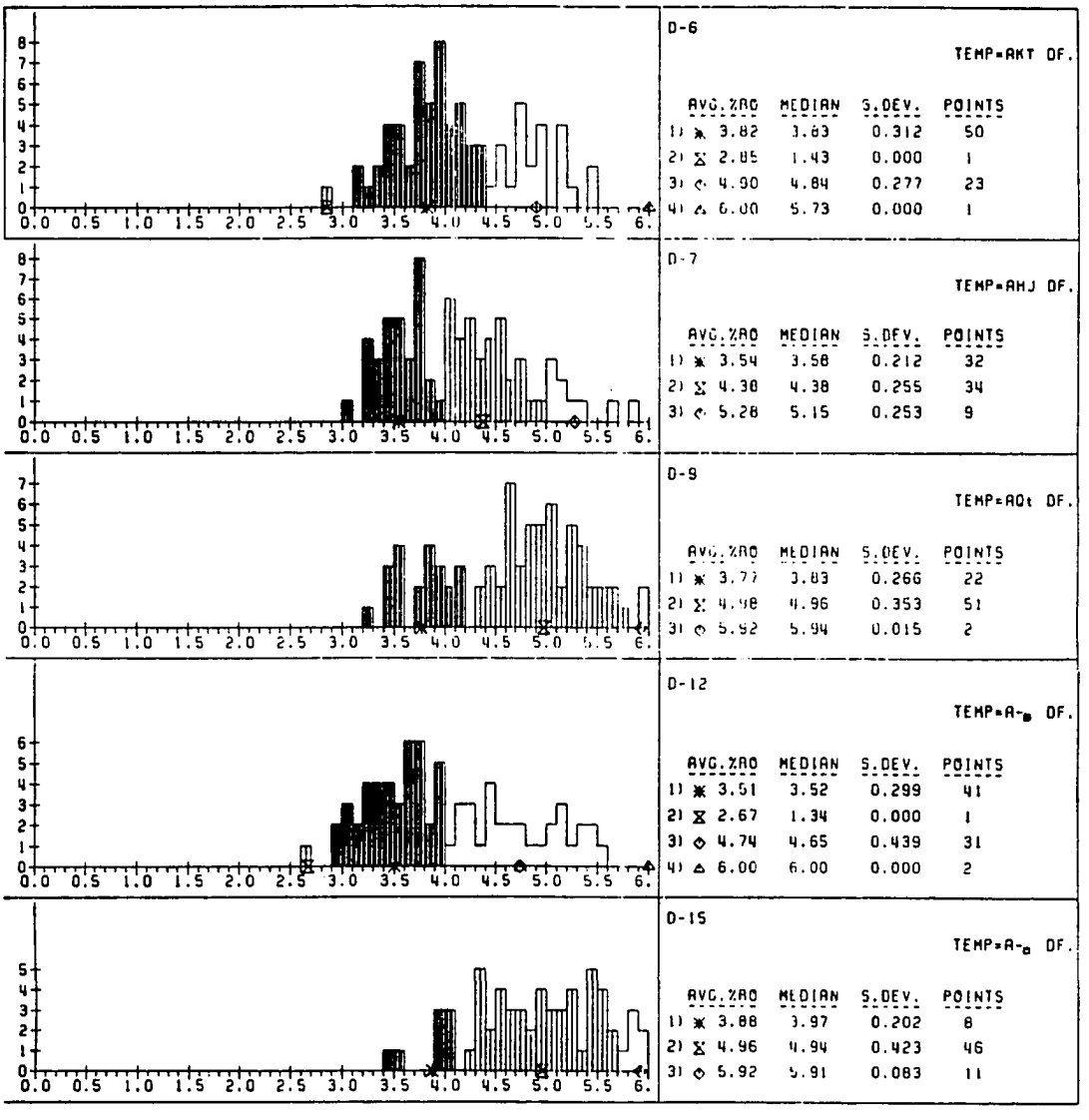

D-6

TEMP=AKT DF.

	AVG.%RO	MEDIAN	S.DEV.	POINTS
1)	3.82	3.83	0.312	50
2)	2.85	1.43	0.000	1
3)	4.90	4.84	0.277	23
4)	6.00	5.73	0.000	1

D-7

TEMP=AHJ DF.

	AVG.%RO	MEDIAN	S.DEV.	POINTS
1)	3.54	3.58	0.212	32
2)	4.38	4.38	0.255	34
3)	5.28	5.15	0.253	9

D-9

TEMP=AQt DF.

	AVG.%RO	MEDIAN	S.DEV.	POINTS
1)	3.77	3.83	0.266	22
2)	4.98	4.96	0.353	51
3)	5.92	5.94	0.015	2

D-12

TEMP=A-$_e$ DF.

	AVG.%RO	MEDIAN	S.DEV.	POINTS
1)	3.51	3.52	0.299	41
2)	2.67	1.34	0.000	1
3)	4.74	4.65	0.439	31
4)	6.00	6.00	0.000	2

D-15

TEMP=A-$_e$ DF.

	AVG.%RO	MEDIAN	S.DEV.	POINTS
1)	3.88	3.97	0.202	8
2)	4.96	4.94	0.423	46
3)	5.92	5.91	0.083	11

X-AXIS = PERCENT REFLECTANCE OF VITRINITE (%RO)

Y-AXIS = FREQUENCY

AVERAGE %RO FOR POP.1 = 3.71

CHAPTER 5. TOC-S-Fe CORRELATION AND DEPOSITIONAL ENVIRONMENTS

Introduction

TOC-S-Fe correlation of modern terrigenouse sediments and ancient rocks can be used to distinguish depositional environments (Sweeny, 1972; Leventhal, 1983; Berner and Raiswell, 1984; Berner, 1985; Raiswell and Berner, 1985). In this chapter, the principles of studying TOC-S-Fe correlation of modern sediments and ancient rocks are introduced. Then, the data of total organic carbon (TOC), sulfide sulfur (S), Degree of Pyritization (DOP), total reactive iron, and ratios of ferrous iron versus total reactive iron of the samples studied in this research will be presented. These data are also plotted on TOC-S, TOC-DOP, TOC-total reactive iron, and TOC-Fe^{2+}/Fe_{total} diagrams to analyze depositional environments using the principles discussed below.

Pyrite Formation and Depositional Environments

In marine depositional environments, many biological and chemical processes, ranging from the flow of energy in food chains to early diagenetic changes in the sediments, are dependent on the availability of reactive carbon and sulfur species. Organic carbon plays a major role in controlling the redox potential of the sediments, and

thereby regulates the behavior of the other chemical species, especially manganese and iron. Organic carbon reduces dissolved sulfate (SO_4^{2-}) in the sea water to sulfide species (H_2S; Berner, 1972). The reaction can be written as $2CH_2O + SO_4^{2+} = H_2S + 2HCO_3^-$. This reaction, which occurs only under strictly anaerobic conditions (below the sediment-water interface in most sediments), results from bacterially-mediated carbon oxidation. The sulfide produced from the reduction of sulfate reacts with ferrous iron (Fe^{2+}) and is precipitated as iron monosulfide (FeS). Over time, the iron monosulfide is converted to pyrite (FeS_2) by reaction with elemental sulfur (Berner, 1967). Figure 56 shows a general process of pyrite formation (Berner, 1985). The three principal factors that ultimately limit how much pyrite may form are (1) the amount and reactivity toward sulfate reduction of organic matter supplied to the sediments; (2) the amount and reactivity toward H_2S of detrital iron minerals supplied to the sediment; and (3) the availability of dissolved sulfate (Berner, 1985). Based on these three parameters, pyrite formation in sediments can be used to distinguish depositional environments by plotting organic carbon versus sulfide sulfur (most by pyrite) correlation of sediments and ancient rocks.

Figure 56.

Schematic diagram summarizing the major steps in sedimentary pyrite formation (Berner, 1985).

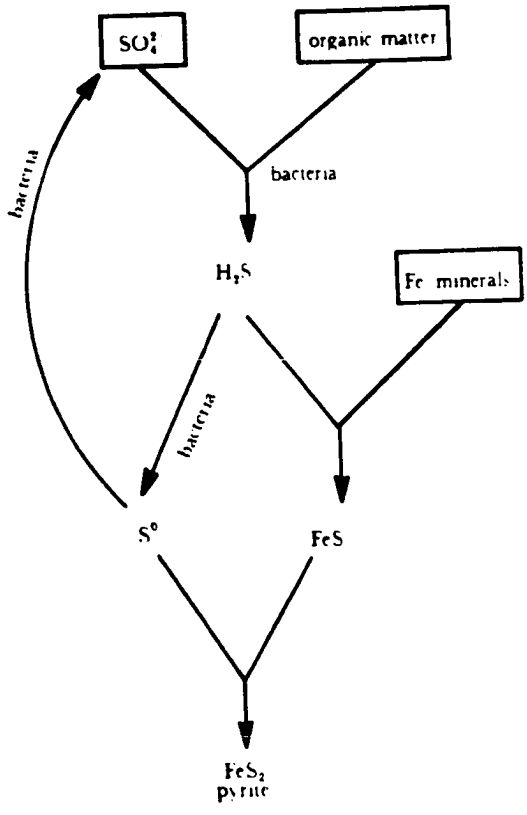

In normal marine environments (oxygenated bottom waters), the bacterial sulfate reduction is dominantly controlled by organic matter availability (Berner, 1978; Westrich and Berner, 1984; Berner, 1985; Raiswell and Berner, 1985). There is sufficient detrital iron present, except for those sediments consisting almost entirely of biogenic silica or calcium carbonate, to ensure that pyrite formation is not limited by iron. This is demonstrated by the presence of excess iron at depth in these sediments after all the pyrite has formed. In this case the pyrite formation in sediments is diagenetic (after deposition) in normal marine environments. Higher rates of H_2S production, by organically-controlled sulfate reduction, allow a greater proportion of the iron minerals present to be transformed to pyrite. A good positive correlation between sulfide sulfur and residual organic carbon, with zero intercepts for both, is exhibited by normal marine sediments (Fig. 57; Berner, 1985).

In euxinic environments where H_2S is present in the bottom waters (e.g. Black Sea; Berner, 1985) pyrite can form at locations where no organic matter is deposited. In fact, in euxinic basins organic matter falling toward the bottom is rapidly introduced to anoxic, sulfidic waters before appreciable oxic decomposition can take place. As a result more reactive organic compounds become available for

Figure 57.

Plot of pyrite sulfur (S) in percentage by mass versus percentage of organic carbon (TOC) for modern normal marine sediments. Plotted points represent preferred values as summarized by Leventhal (1983) from the compilation of Sweeney (1972) and Goldhaber & Kaplan (1974) (Berner, 1985).

Figure 58.

Plot of pyrite sulfur versus organic carbon for euxinic, deep-water sediments of the Black Sea. Data from Rozanov et al. (1974).

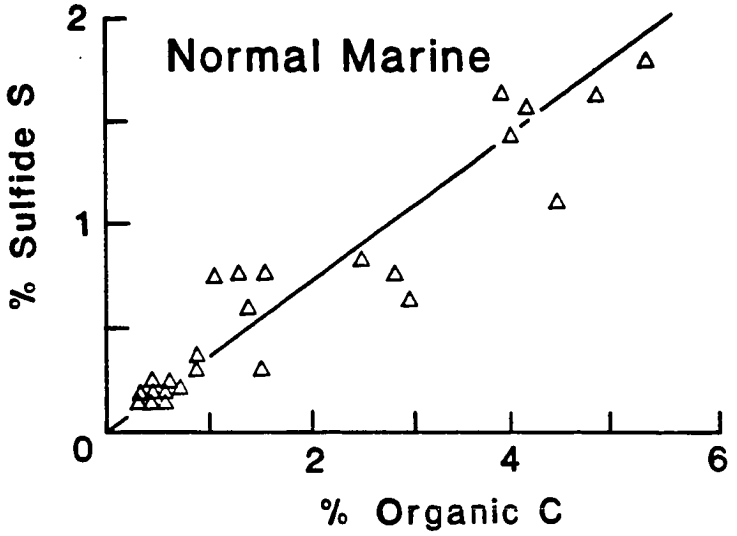

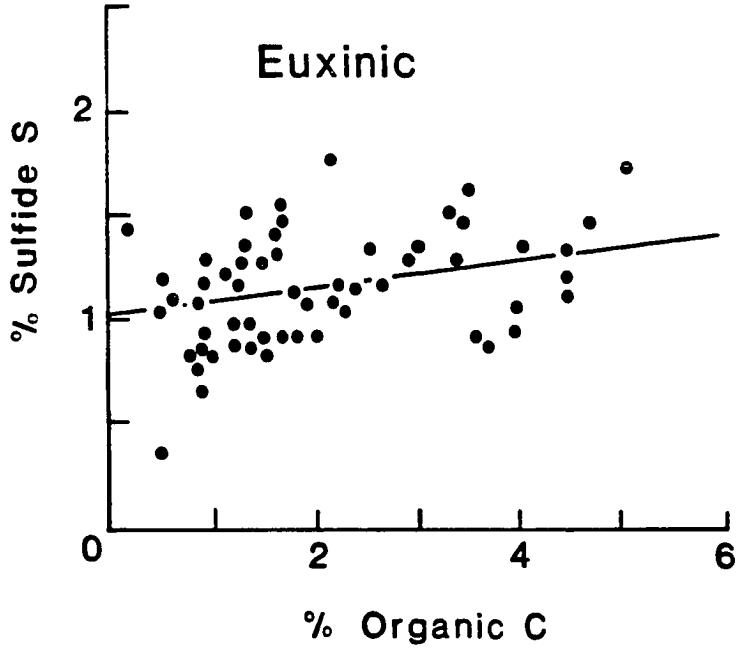

bacterial sulfate reduction both in the deep portions of the water column and on the bottom. In this case, H_2S is present above the sediment-water interface as well as within the sediments. Consequently, pyrite can form from sedimenting detrital iron minerals before burial, both in the water column and at the sediment-water interface. Thus pyrite formation in euxinic sediments is syngenetic, which leads to a greater proportion of H_2S for each C atom sedimenting to the bottom than occurs in normal marine environments (Berner, 1985). Because of abundance of H_2S, pyrite formation in euxinic basins is limited by the amount and reactivity of iron minerals. Consequently, a good correlation between sulfide sulfur and organic carbon is generally not found (Fig. 58). Poor TOC-S correlation occurs because appreciable pyrite can form at low concentrations of organic carbon as explained above. A high sulfide sulfur content at low organic carbon values and a regression line with a positive intercept on the sulfur axis of TOC-S plots of euxinic modern sediments and ancient rocks provides a ready way to distinguish euxinic from normal marine sediments (Berner, 1985; Raiswell and Berner, 1985).

Carbon-sulfur-iron relationships in euxinic sediments are, however, sometimes complicated by formation of additional diagenetic pyrite after burial. The diagenetic

pyrite is carbon-limited (as is the case for normal-marine sediments) as opposed to the original syngenetic pyrite which is not (Raiswell and Berner, 1985). One way to separate the effects of iron and organic carbon limitations on sedimentary pyrite formation is the parameter DOP, the degree of pyritization (Berner, 1970), which is defined as:

DOP = pyrite iron / total iron

(In actual practice pyrite-Fe plus Fe soluble in hot concentrated HCl, Fe_R, is often substituted for total Fe, Fe_T, in the definition of DOP -- giving rise to DOP_R and DOP_T respectively. The remaining HCl-insoluble iron is unlikely ever to react with H_2S to form pyrite -- see Berner, 1970). Use of DOP eliminates the effect of differences total iron among sediments and puts the focus more properly on the reactive iron and the production of H_2S. The overall reasoning is that the higher the concentration of H_2S, and/or the greater the reactivity of the iron minerals, and /or the longer the time that H_2S remains in contact with the iron minerals, then the higher will be the value of DOP (Raiswell and Berner, 1985).

In euxinic environments, where pyrite is syngenetic and Fe-limited, the DOP will be constant in a plot of DOP versus organic carbon (Fig. 59). In contrast, for environments with very low O_2 in bottom water, which Raiswell and Berner (1985) termed semi-euxinic environment,

Figure 59.

Idealized plots of pyrite sulfur (S) and degree of pyritization of iron (DOP) versus organic carbon (TOC) for a hypothetical euxinic sediment. In (A) resulting from the formation of Fe-limited syngenetic pyrite alone, as indicated by a uniform DOP with increasing TOC content in (B). (Raiswell and Berner, 1985).

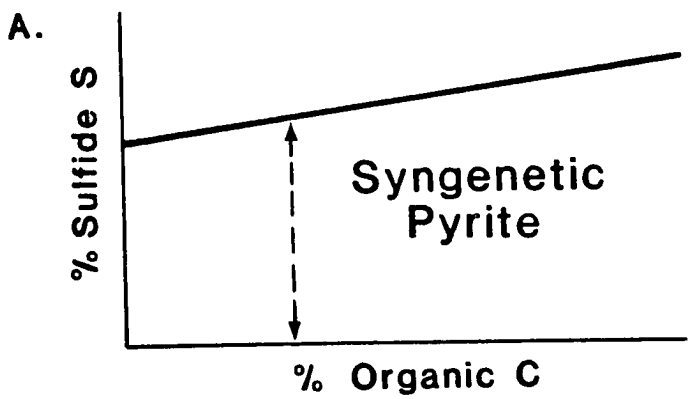

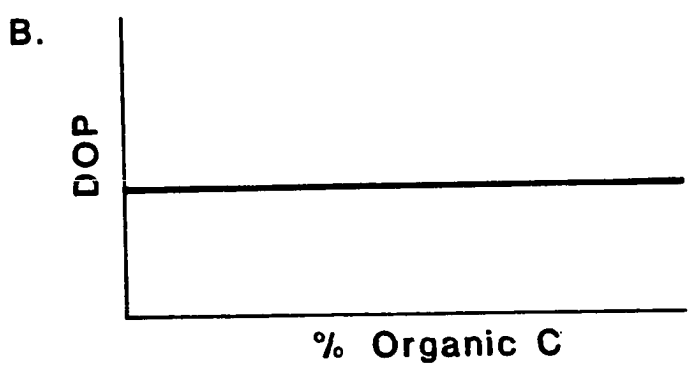

pyrite formation in sediments is syngenetic plus diagenetic. As a result, the DOP of such sediments has a positive correlation with organic carbon content (Fig. 60). In this way, two depositional environments can be separated by DOP versus organic carbon (Raiswell and Berner, 1985).

In this research, total reactive iron (pyritic iron plus hot HCl soluble iron) and the ratio of ferrous iron to total reactive iron were also determined. These can provide information about the reactive iron availability of rocks and the redox condition of depositional and/or diagenetic environments.

In contrast to the normal marine environment, sediments deposited in fresh water are depleted in dissolved sulfate. This occurs because the sulfate concentration in most fresh waters is hundreds of times lower than that found in sea water. Consequently, pyrite formation in freshwater lake and swamp sediments is limited by dissolved sulfate. The TOC-S plot of freshwater sediments shows a poor correlation between sulfide sulfur and organic carbon. Regardless of how much organic matter or iron is deposited, there simply is not enough sulfate available to form much pyrite (Fig. 61; Berner, 1985).

Figure 60.

The same idealized plots as in figure 59, but with the plot in (A) are shown results for the formation of extra TOC-limited diagenetic pyrite. This is indicated by the increase in DOP with TOC content in (B) (Raiswell and Berner, 1985).

A.

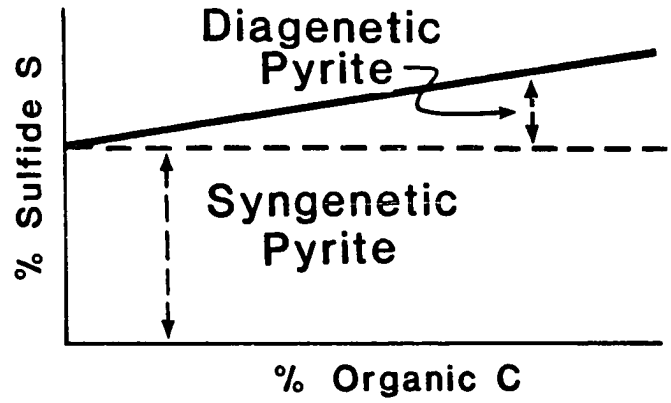

B.

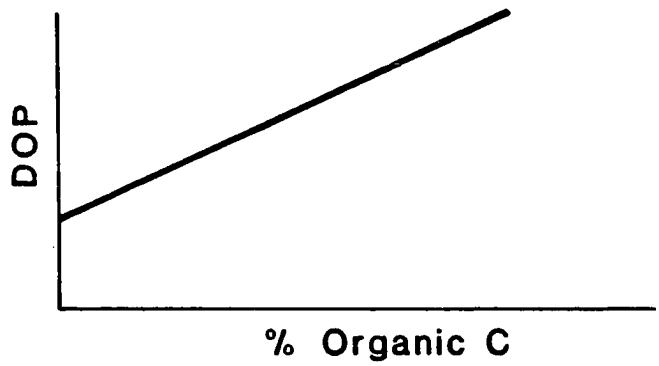

Figure 61.

Plot of reduced sulfur (mainly pyrite) versus organic carbon for freshwater lake sediments. The correlation line and limits for normal marine sediments from figure 57 are shown for comparison (Berner, 1985).

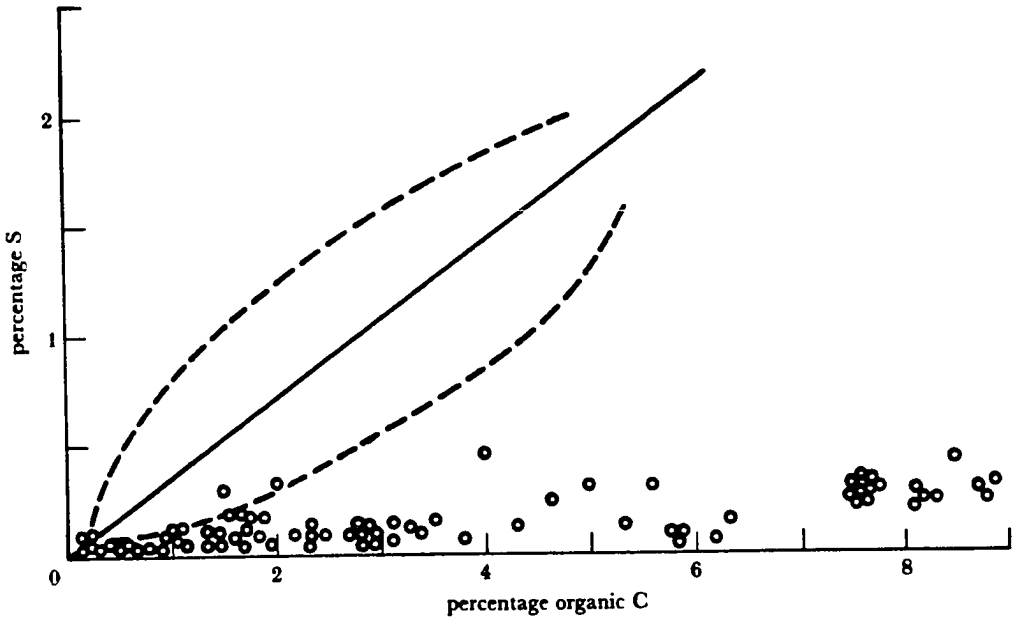

TOC-S-Fe Correlation of Samples Studied

This section presents the data for organic carbon, sulfide sulfur, DOP, total reactive iron (pyrite iron plus HTOCl soluble iron), and the ratio of ferrous iron versus total reactive iron of the samples studied. For each sample location, four groups of data were plotted based on the principles of environmental analysis mentioned above. The linear least square regression line of organic carbon versus sulfide sulfur of black shales was calculated and correlation coefficients were compared to levels of significance from tables in Davis (1986). A regression line of the modern normal marine sediments (S/TOC = 0.36) is plotted on each diagram of organic carbon versus sulfide sulfur for comparison. More detailed data tables of each studied area are in Appendix C.

Taojiang Manganese Deposit

As mentioned in chapter 3, three stratigraphic sections were measured in the Taojiang area, covering upper-most Lower Ordovician Yanxi Formation, Middle Ordovician Hule and Modaoxi formations, Upper Ordovician Wufen Formation, and the lowest Lower Silurian Zhoujiaxi Formation.

Table 7 shows the TOC-S-Fe data of section one, which was measured in an underground mining area, covering the upper-most Lower Ordovician Yanxi Formation, the lower

Table 7.

TOC-S-Fe data of Taojiang Manganese deposit, China
(Section 1)

Sample Number	Name	TOC%	SS%	DOP	Fe_{total} Reactive	Fe^{+2}/Fe_{total} Reactive
Yangxi Formation						
DL1	GS	0.60	0.09	0.04	1.95	0.97
DL2	GS	0.52	0.08	0.05	1.33	0.45
DL3	GS	0.72	0.22	0.08	2.53	0.53
DL4	LM	0.79	0.12	0.03	3.95	0.57
DL5	CALCITE	0.93	0.10	0.08	1.16	0.31
Hule Formation						
DL6	BS	3.00	2.00	0.41	4.24	0.56
DL7	BS	4.00	2.09	0.53	3.44	0.96
DL7'	BS	4.10	3.96	0.68	5.07	0.78
DL8	BS	3.82	1.45	0.50	2.51	0.67
DL9	BS	4.30	2.37	0.71	2.90	0.88
Modaoxi Formation						
DL10	GS	0.63	0.51	0.27	1.65	0.51
DL12	BS	2.09	1.56	0.51	2.66	0.57
DL13	LM	0.42	0.28	0.26	0.93	0.82
DL14	LM	0.34	0.15	0.06	2.22	0.48
DL15	BS	2.57	3.28	0.84	3.40	0.85
DL16	RH	0.32	0.47	0.38	1.08	0.59
DL17	RH	0.39	0.06	0.05	1.02	0.50
DL18A	RH	0.44	0.51	0.18	2.48	0.68
DL18B	RH	0.46	1.00	0.30	2.87	0.70
DL19	RH	0.75	0.21	0.05	3.80	0.49
DL20	LM	0.71	0.13	0.02	4.96	0.67
DL21	LM	0.76	0.12	0.04	2.69	0.59
DL22A	GM	0.87	0.06	0.02	2.51	0.65
DL22B	GM	0.42	0.05	0.01	2.76	0.67
DL23	GM	0.42	0.42	0.23	1.56	0.29
DL24	GM	0.53	0.14	0.03	4.32	0.58

TOC% -- Total organic carbon wt. per cent
SS% -- Pyritic sulfur wt. per cent
LM -- Limestone
RH -- Rhodochrosite ore
GS -- Gray shale
BS -- Black shale
GM -- Gray mudstone
Calcite -- Calcite vein

Middle Ordovician Hule Formation, and the upper Middle Ordovician Modaoxi Formation. This section includes gray shales and gray mudstones in the Yanxi Formation and upper part of the Modaoxi Formation, black shales in the Hule Formation and the lower part of the Modaoxi Formation, rhodochrosite ores in the middle part of the Modaoxi Formation, and limestones in the immediate hanging wall and footwall of the ore body.

The black shales have high organic carbon (2.09 - 4.3%) and sulfide sulfur (1.45 - 3.96%) contents. In the TOC-S plot (Fig. 62a), black shales plot basically above the normal marine regression line. The regression line of black shales is: $y = 0.23(x)+1.63$, $n = 7$, $r = 0.214$, which is not significant at 90% level (y = sulfide sulfur wt.%, x = organic carbon wt.%, r = correlation coefficient). The poor correlation between organic carbon and sulfide sulfur, and 1.63 intercept on the S axis indicate an euxinic environment pattern. The DOP of the black shales ranges from 0.41 to 0.84 and is poorly correlated with organic carbon: $y = 0.05(x)+0.546$, $n = 7$, $r = 0.085$, which is not significant at 90% level (Fig. 62b). The total reactive iron of the black shales ranges from 2.51 to 5.07%, and the ratio of ferrous versus total reactive iron is high and ranges from 0.65 to 0.96. The plot of total reactive iron versus organic carbon (Fig. 63a) shows a very poor positive

Figure 62.

A. Plot of organic carbon versus sulfide sulfur of the Taojiang manganese deposit samples from the upper-most Yanxi Formation, the Hule Formation, and the Modaoxi Formation. The solid line represents the regression line of black shales: $y=0.23(x)+1.63$, $n=7$, $r=0.214$, which is not significant at 90% level. The regression line of the modern normal marine sediments is also presented.

B. Plot of organic carbon versus DOP. The solid line represents the regression line of black shales: $y=0.015(x)+0.546$, $n=7$, $r=0.157$, which is not significant at 90% level.

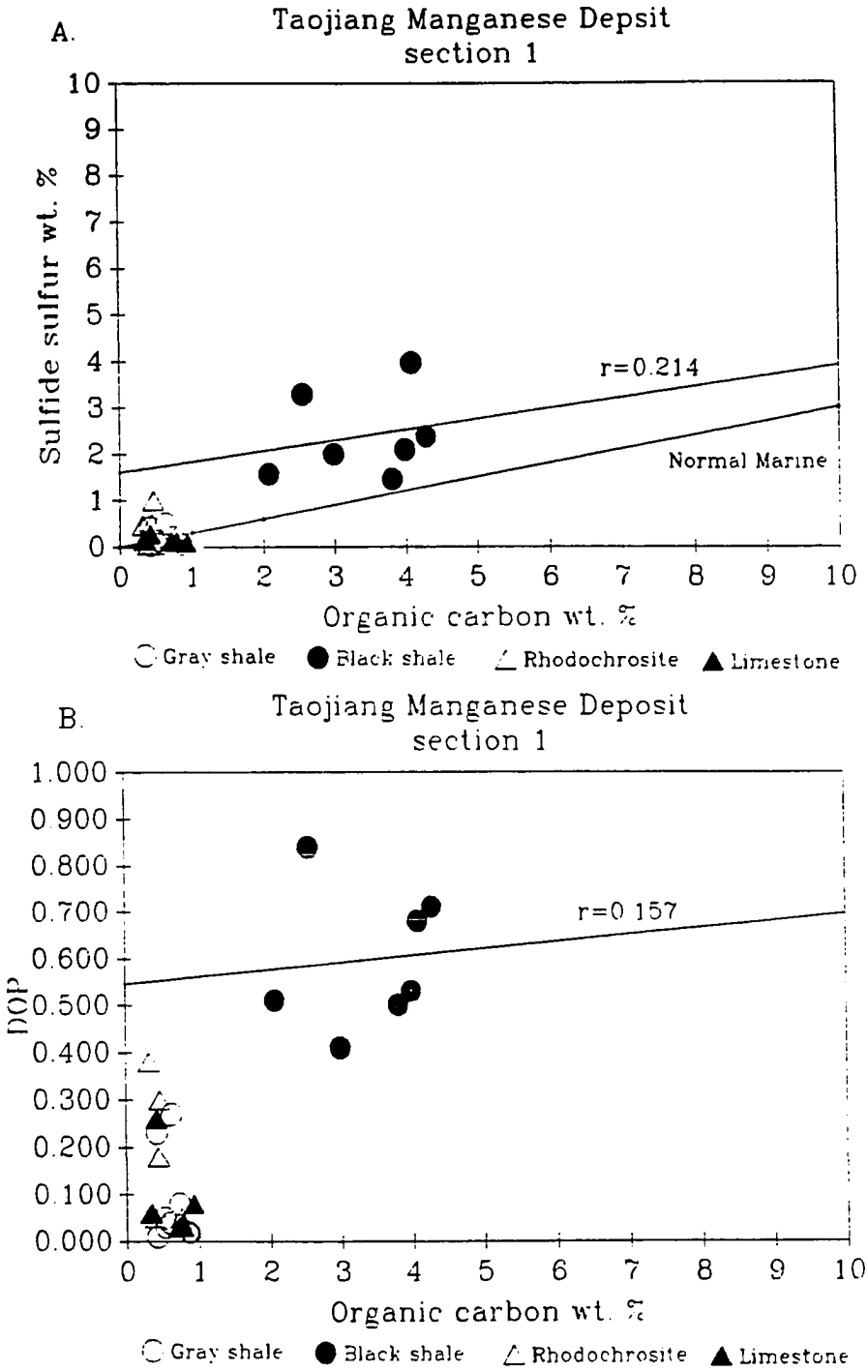

Figure 63.

A. Plot of organic carbon versus total (reactive) iron of the Taojiang manganese deposit samples from the upper-most Yanxi Formation, the Hule Formation and the Modaoxi Formation.

B. Plot of organic carbon versus Fe^{2+}/Fe_{total}.

A.

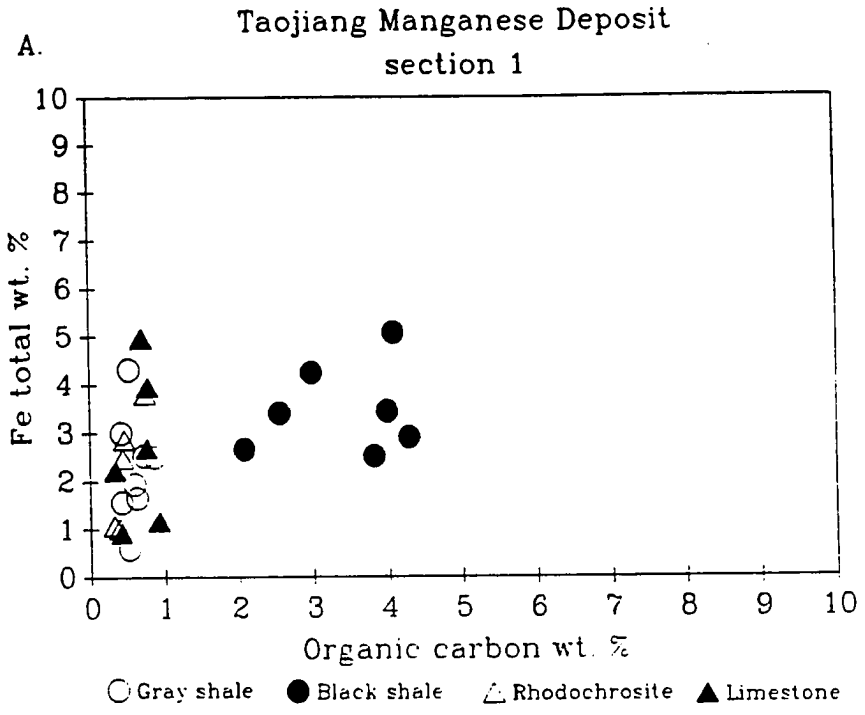

B.

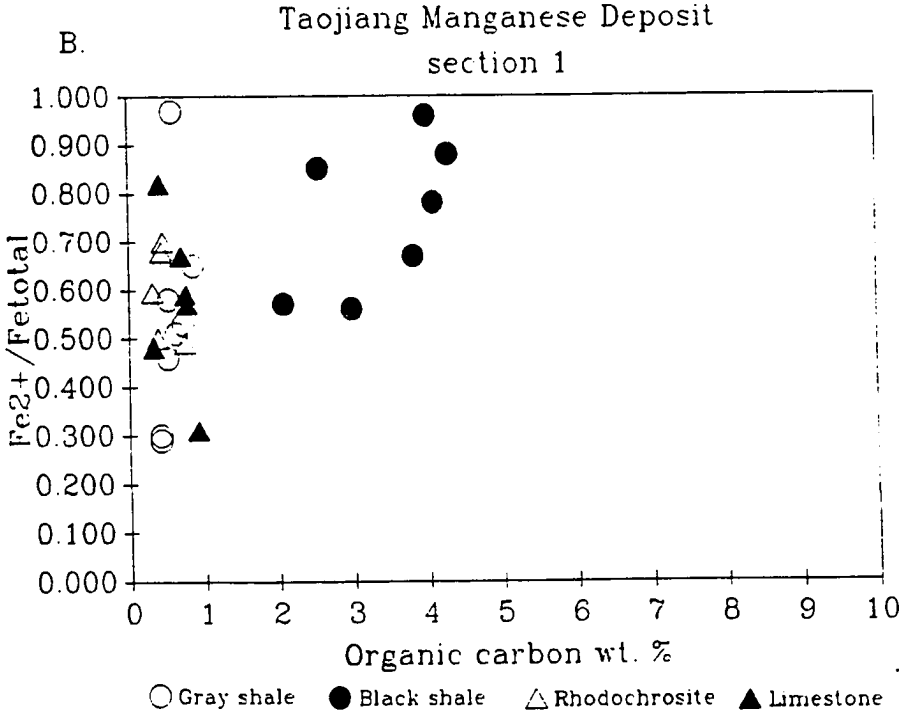

correlation. The plot of the ratio of ferrous iron versus total reactive iron versus organic carbon (Fig. 63b) shows a better positive correlation, r = 0.574 (n = 7 and not significant at 90% level). These indicate that most of the iron in the black shale comes from pyrite minerals and that the black shales of the Hule Formation and the lower Modaoxi Formation formed in an euxinic environment and possibly has some additional organic-limited diagenetic pyrite.

Gray shales of the upper-most Yanxi Formation and gray mudstones of the upper section of the Modaoxi Formation have low values both in organic carbon (0.42 - 0.87%) and sulfide sulfur (0.05 - 0.51%), and low DOP (0.01 - 0.23). The TOC-S plots of gray shales and gray mudstones are close to the normal marine regression line (Fig. 62a). Relatively high total reactive iron (1.33 - 4.32%) (Fig. 63a) and a high ratio of ferrous iron versus total reactive iron (0.29 - 0.97; Fig. 63b) indicate that pyrite formation was not limited by iron but rather was limited by organic carbon in a normal marine environment.

Carbonate rocks, limestones and rhodochrosite ores are found in the middle section of the Modaoxi formation. They contain low organic carbon (0.32 - 0.76%) and sulfide sulfur (0.06 - 1.00%) and are generally close to normal marine regression line on the TOC-S plot (Fig. 62a). The

DOP values of carbonates range from 0.02 to 0.34, which are much lower than the DOP value of black shales (0.41 - 0.83; Fig. 62b). Limestones and rhodochrosite ores have higher total reactive iron (1.02 - 4.96%; Fig. 63a) and high ratio of ferrous iron versus total reactive iron (0.48 - 0.85; Fig. 63b). Obviously, iron was trapped in carbonate minerals rather than forming more pyrite. Also, the pyrite formation in limestones and rhodochrosite ores was limited partially by organic carbon content. Because the precipitation of rhodochrosite as well as Mn-bearing limestones may possibly be unfavorable to pyrite formation (this will be discussed later), the TOC-S plots of rhodochrosite and limestones do not provide as much information about the depositional environments as they do for black shales and gray shales.

Table 8 presents TOC-S-Fe data of the section two which was measured in another underground mining area, including two enriched rhodochrosite ore horizons and gray mudstone and black shale interbeds in the middle section of the Modaoxi Formation (see chapter 3 for detailed description). The black shales contain 0.58 - 2.72% organic carbon and 0.13 - 1.86% sulfide sulfur. The DOP values of the black shales range from 0.06 - 0.51. The TOC-S plot (Fig. 64a) and TOC-DOP plot (Fig. 64b) of the black shale interbeds within the rhodochrosite ore horizons show a strong

Table 8.

TOC-S-Fe data of Taojiang Manganese Deposit, China
(Section 2)

Sample Number	Name	TOC%	SS%	DOP	Fe_{total} Reactive	Fe^{+2}/Fe_{total} Reactive
NS1	LM	0.93	0.04	0.14	0.28	0.25
NS2	BS	2.72	1.86	0.51	3.17	0.69
NS3	RH	0.39	0.11	0.12	0.78	0.41
NS4	BS	0.74	1.15	0.27	3.67	0.82
NS5	RH	0.15	0.05	0.07	0.58	0.29
NS6	LM	0.33	0.06	0.05	1.06	0.63
NS7	GM	0.27	0.06	0.02	3.15	0.61
NS8	GM	0.49	0.05	0.02	2.02	0.75
NS9A	BS	1.19	0.41	0.17	2.09	0.45
NS9B	GM	0.31	0.19	0.07	2.40	0.48
NS10	BS	1.12	0.68	0.29	2.02	0.58
NS11	BS	0.58	0.13	0.06	1.78	0.38
NS12	RH	0.40	0.06	0.12	0.48	0.51
NS13	LM	0.58	0.05	0.03	1.44	0.58

TOC% -- Total organic carbon wt. per cent
SS% -- Pyritic sulfur wt. per cent
LM -- Limestone
RH -- Rhodochrosite ore
BS -- Black shale
GM -- Gray mudstone

Figure 64.

A. Plot of organic carbon versus sulfide sulfur of the Taojiang manganese deposit samples from the middle section of the Modaoxi Formation. The solid line represents the regression line of black shales: $y=0.543(x)+0.424$, $n=4$, $r=0.748$, which is significant at 90% level. The regression line of normal marine sediments is also presented.

B. Plot of organic carbon versus DOP. The solid line represents the regression line of black shales: $y=0.142(x)+0.105$, $n=4$, $r=0.866$, which insignificant at 90% level.

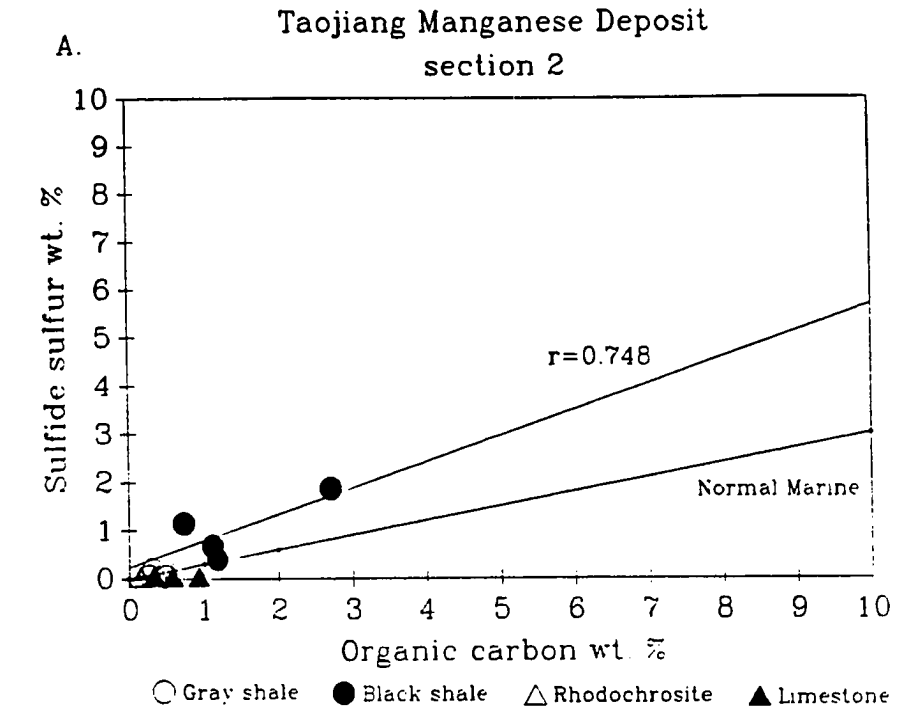

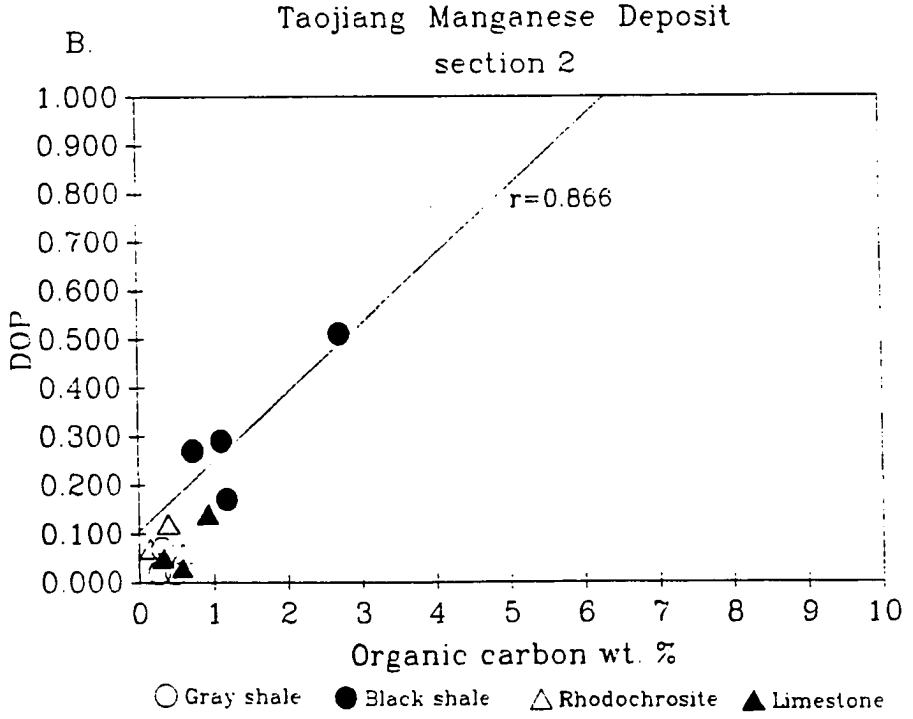

positive correlations: y = 0.543(X)+0.242, n = 4, r = 0.748, which is significant at 90% level; y = 0.142(x)+0.105, n = 4, r = 0.866, which is significant at 95% level, respectively. These plots indicate that pyrite formation in the black shales was mainly organic carbon-limited and formed in a semi-euxinic or near normal marine environment.

The gray mudstone interbeds within the rhodochrosite ore horizons have low organic carbon (0.27 - 0.49%) and low sulfide sulfur (0.05 - 0.19%) contents, and are close to the normal marine regression line, although poorly correlated (Fig. 64a). DOP values are very low (0.02 - 0.07) (Fig. 64b). The relatively higher total reactive iron (2.02 - 3.15%) indicates that pyrite formation was not iron-limited and so was probably limited by organic carbon (Fig. 65a).

Both the gray mudstones and the black shales are interbeds within the rhodochrosite ores and contain carbonate minerals (acid soluble carbonate ranges from 2.08 to 54.35 wt.% -- see Appendix C). The high ratio of ferrous iron versus total reactive iron (0.38 - 0.83 for the black shales and 0.48 - 0.75 for the gray mudstones) indicate that the iron was also possibly trapped in carbonates as ferrous iron (Fig. 65b).

Figure 65.

A. Plot of organic carbon versus total (reactive) iron of the Taojiang manganese deposit samples from the middle section of the Modaoxi Formation..

B. Plot of organic carbon versus Fe^{2+}/Fe_{total}.

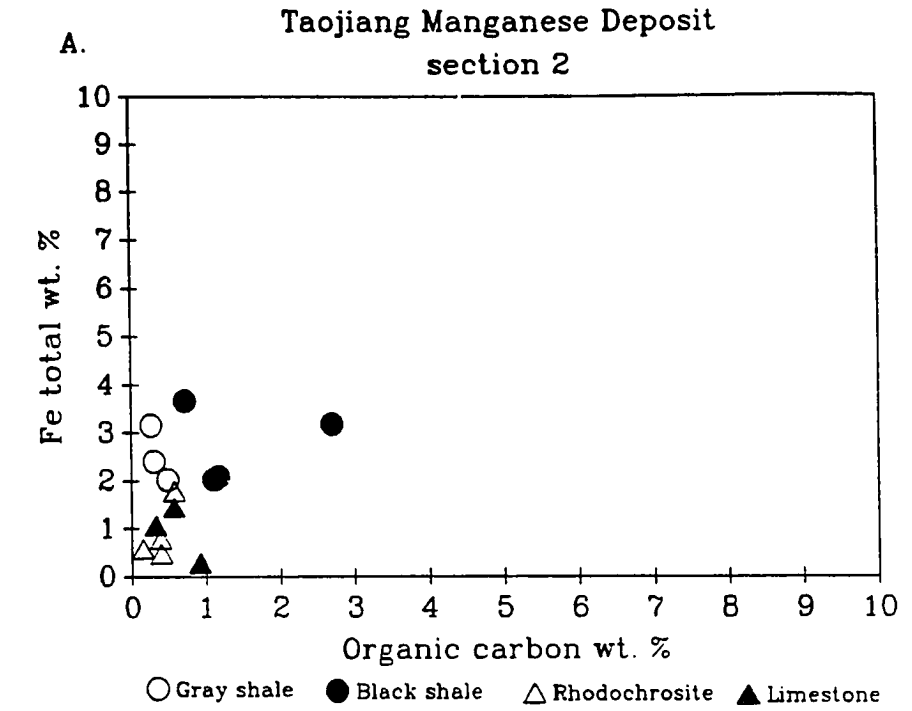

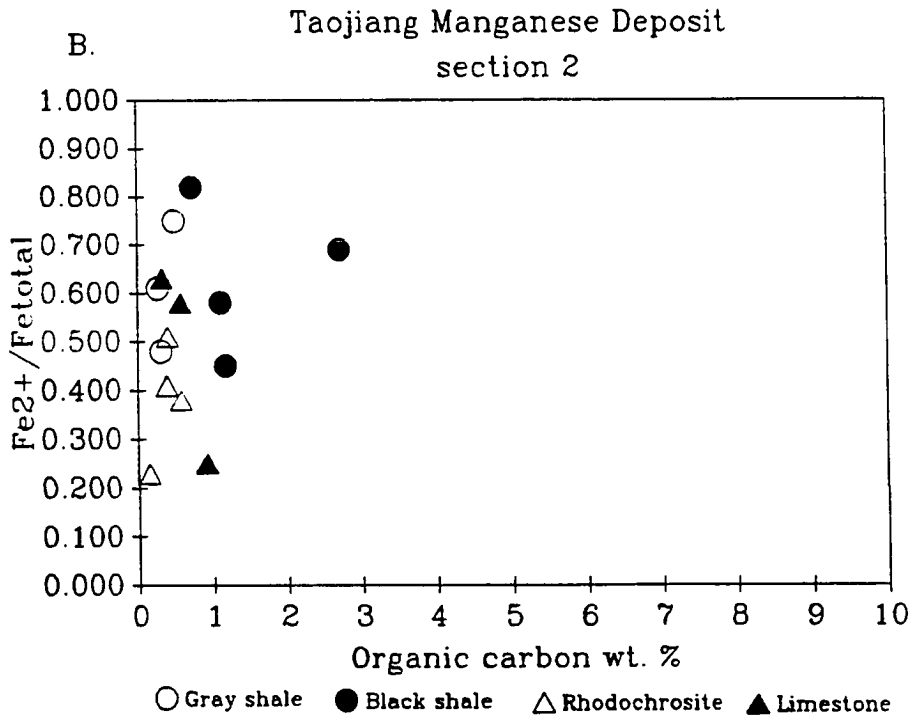

The rhodochrosite ores and limestones contain low organic carbon (0.15 - 0.93%) and sulfide sulfur (0.04 - 0.11%) contents. Their low DOP (0.03 - 0.14; Fig. 64b), higher total reactive iron (0.28 - 1.44; Fig. 65a). The ratio of ferrous iron versus total reactive iron (0.25 - 0.63; Fig. 65b) is the lowest among the lithologies sampled and shows that considerable Fe^{3+} is present. It indicates that the pyrite formation was limited by organic carbon rather than by iron. The TOC-S plots of the rhodochrosite ores and limestones are close to the normal marine regression line (Fig. 64a). Considering the TOC-S plots of gray shale and black shale interbeds of the ore horizon, the entire cross section reflects a normal marine depositional environment.

Section three was measured on the outcrops in Taojiang area including the upper-most Middle Ordovician Modaoxi Formation, the Upper Ordovician Wufen Formation, and the lower section of the Lower Silurian Zhoujiaxi Formation. The TOC-S-Fe data are shown in Table 9. Generally, these outcrop samples have high organic carbon content (black shales are around 4%, gray shales are around 0.8%), but low sulfur content (0.03 - 0.29%) and low DOP values (0.01 - 0.34). Four samples of black shales of the upper part of the Zhoujiaxi Formation, however, have relatively higher sulfur content (0.16 - 1.56%) and DOP value (0.28 - 0.65).

Table 9.

TOC-S-Fe Data of Taojiang Manganese Deposit, China (section 3)

Sample Number	Name	TOC%	SS%	DOP	Fe_{total} Reactive	Fe^{2+}/Fe_{total} Reactive
Upper Modaoxi Formation						
TM1	GS	0.67	0.03	0.01	4.40	0.53
TM2	BS	4.29	0.04	0.04	0.93	0.76
TM3	BS	4.70	0.14	0.19	0.66	0.59
TM4	BS	4.69	0.17	0.34	0.43	0.56
TM5	BS	4.56	0.08	0.26	0.28	0.68
TM6	BS	1.63	0.07	0.05	1.18	0.27
TM7	BS	1.01	0.05	0.02	1.67	0.07
TM8	GS	0.78	0.01	0.01	4.25	0.50
TM9A	GS	0.37	0.02	0.02	0.86	0.11
TM9B	GS	0.48	0.02	0.01	3.25	0.13
TM9C	GS	0.57	0.03	0.01	3.09	0.01
Wufen Formation						
TM10	BS	1.26	0.03	0.01	3.89	0.06
TM11	BS	0.67	0.11	0.45	0.20	0.85
TM12	BS	1.66	0.04	0.02	1.74	0.13
TM16	BS	1.35	0.29	0.37	0.67	0.42
TM17	GS	0.99	0.05	0.12	0.38	0.13
TM18	GS	0.97	0.08	0.10	0.70	0.18
TML9	GS	0.67	0.05	0.11	0.41	0.69
ZHouJiangXi Formation						
TM14	BS	4.34	0.04	0.12	0.32	0.40
TM15	BS	4.34	0.07	0.17	0.34	0.46
TM20	BS	5.51	0.06	0.21	0.24	0.23
TM22	BS	4.21	0.06	0.14	0.33	0.33
TM23	BS	4.68	0.06	0.19	0.30	0.20
TM24	BS	4.14	0.09	0.30	0.27	0.39
TM25	BS	4.23	0.04	0.10	0.30	0.25
TM26	BS	3.84	0.04	0.05	0.68	0.29
TM27	BS	3.67	0.48	0.53	0.79	0.61
TM28	BS	3.59	1.56	0.65	2.09	0.73
TM29	BS	3.23	1.45	0.56	2.25	0.63
TM30	BS	4.98	0.16	0.28	0.48	0.50
TM31	BS	3.67	0.86	0.41	1.82	0.65

TOC% -- Total organic carbon wt. per cent.
SS% -- Sulfide sulfur wt. per cent.
BS -- Black shale
GS -- Gray shale

Figure 66a. is the TOC-S plot of black shales and gray shales of the upper-most Modaoxi Formation and the Wufen Formation, which seems to follow a fresh water pattern. A poor correlation between organic carbon and DOP (Fig. 66b), relatively high total reactive iron (0.41 - 4.4%; Fig. 67a) and large ranges of the ratio of ferrous iron versus total reactive iron (Fig. 67b) indicate that iron was in excess for the samples which contain less than 2% organic carbon. For samples which contain more than 4% organic carbon, most of the reactive iron is from pyrite formation. Figure 68a. shows the TOC-S plot of the black shale of the Zhoujiaxi Formation. The samples have more than 4% organic carbon, but contain very low sulfur content (0.04 - 0.16%) and show poor correlation between sulfide sulfur and organic carbon. Four samples having less than 4% organic carbon contain higher sulfur content (0.48 - 1.56%) and their TOC-S plots are close to the normal marine regression line. The DOP values of these black shales increase with the organic carbon content (Fig. 68b). The plot of total reactive iron versus organic carbon (Fig. 69a) shows that most of the iron is from pyrite formation. Figure 69b. shows a large range for the ratio of ferrous iron versus total reactive iron of the samples, with abundant ferric iron. The four samples with higher sulfide sulfur content have the highest Fe^{2+}/Fe_{total} ratio.

Figure 66.

A. Plot of organic carbon versus sulfide sulfur of the Taojiang manganese deposit samples from the upper-most Modaoxi Formation and the Wufen Formation. The solid line represents the regression line of black shales: $y=0.065(x)-0.0027$, $n=9$, $r=0.414$, which is not significant at 90% level. The dashed line represents the regression line of gray shales: $y=0.0047(x)+0.088$, $n=9$, $r=0.094$, which is not significant at 90% level. The regression line of normal marine sediments is also presented.
B. Plot of organic carbon versus DOP. The solid line represents the regression line of black shales: $y=0.14(x)-0.00295$, $n=9$, $r=0.203$, which is not significant at 90% level. The dashed line represents the regression line of gray shales: $y=0.038(x)+0.039$, $n=9$, $r=0.432$, which is not significant at 90% level.

A.

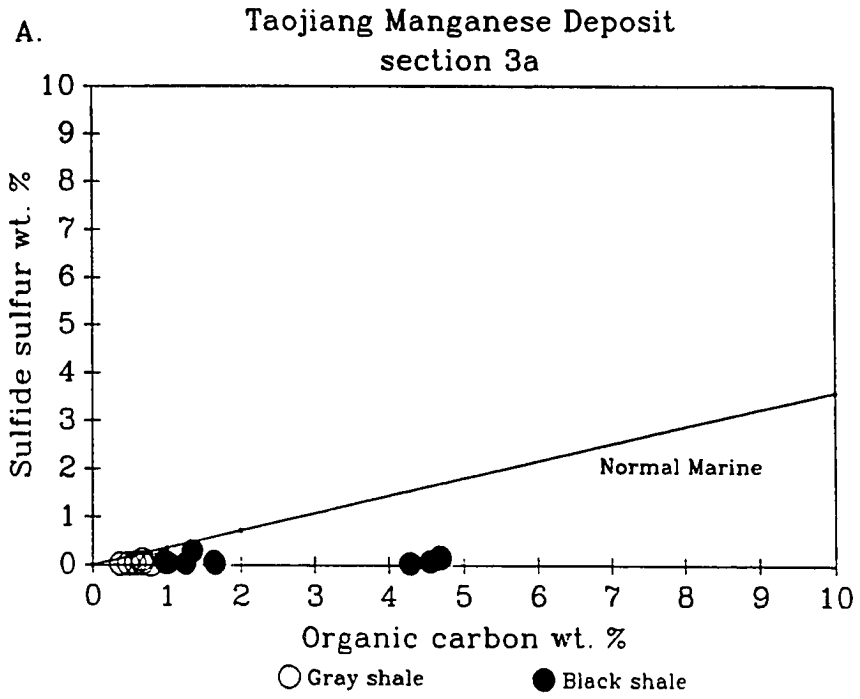

B.

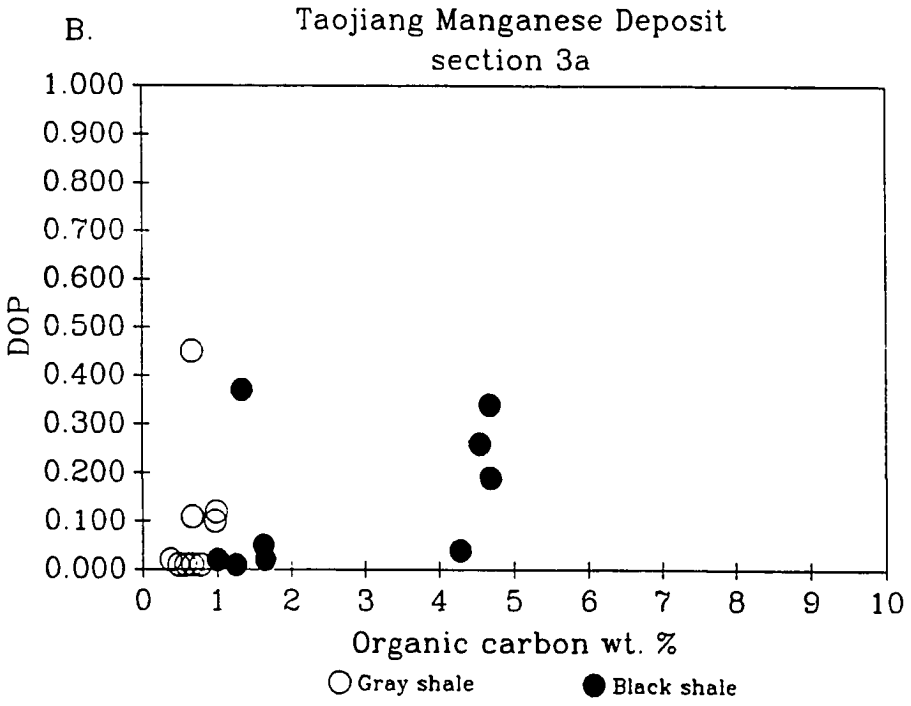

Figure 67.

A. Plot of organic carbon versus total (reactive) iron of the Taojiang manganese deposit samples from the uppermost Modaoxi Formation and the Wufen Formation..

B. Plot of organic carbon versus Fe^{2+}/Fe_{total}.

A.

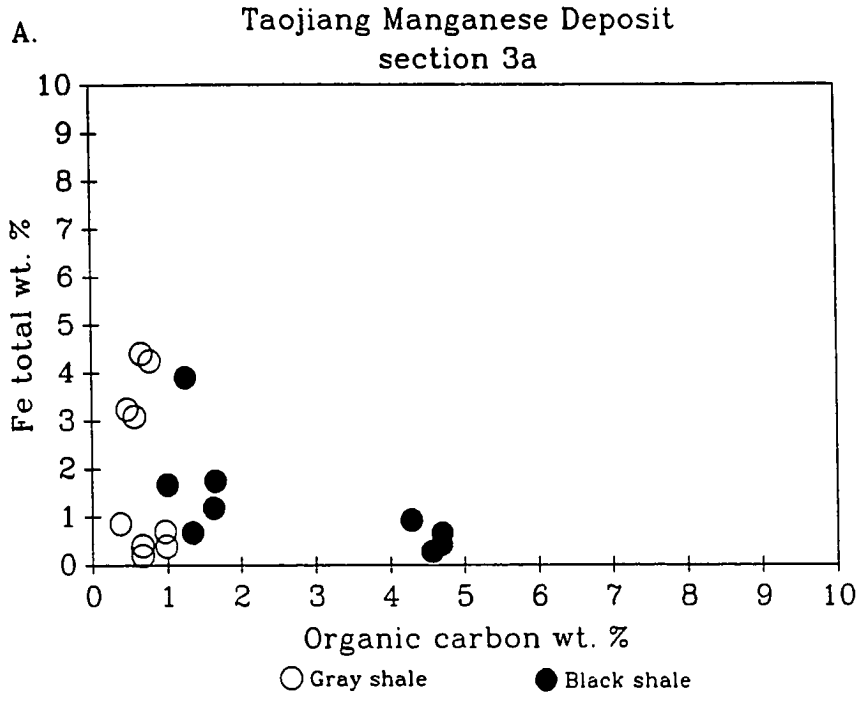

B.

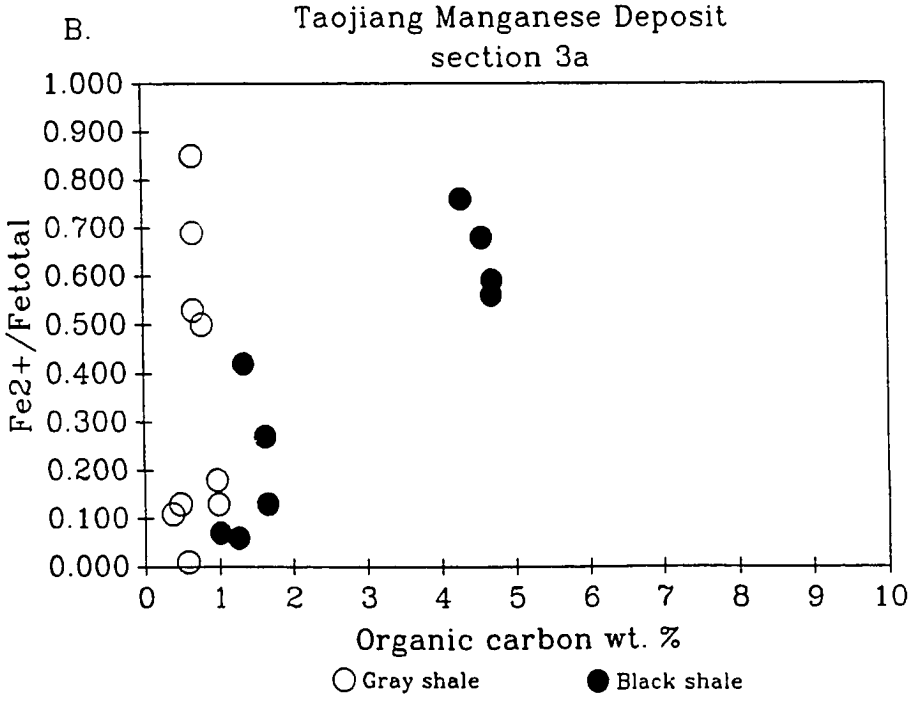

Figure 68.

A. Plot of organic carbon versus sulfide sulfur of the Taojiang manganese deposit samples from Zhoujiaxi Formation. The regression line of normal marine sediments is also presented.

B. Plot of organic carbon versus DOP.

A.

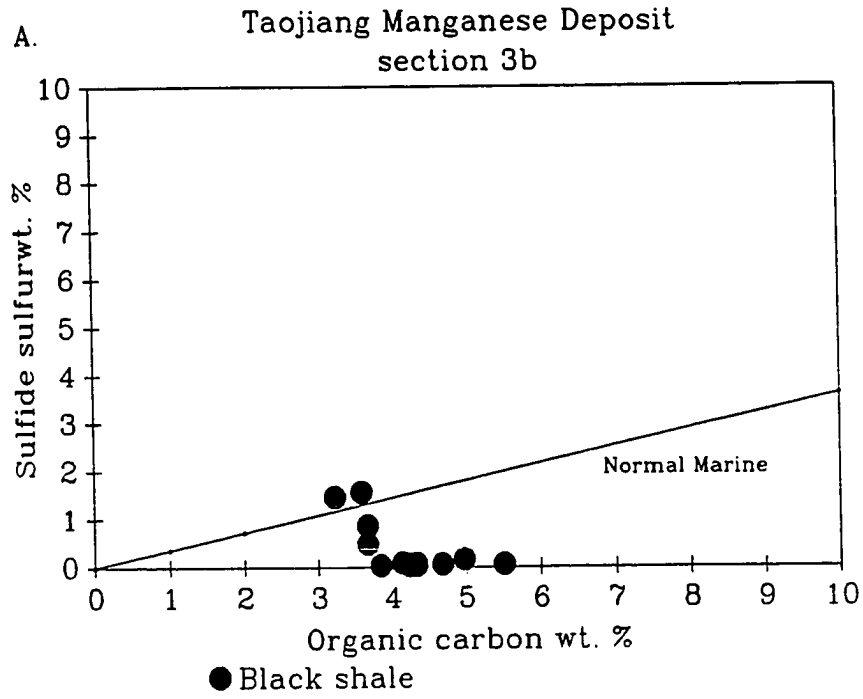

B.

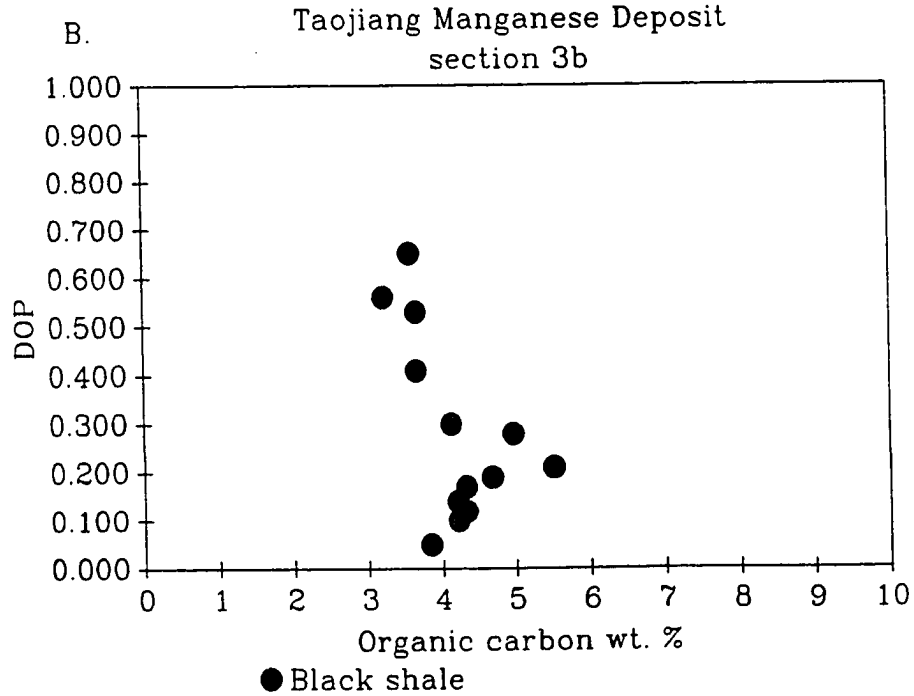

Figure 69.

A. Plot of organic carbon versus total (reactive) iron of the Taojiang manganese deposit samples from Zhoujiaxi Formation.

B. Plot of organic carbon versus Fe^{2+}/Fe_{total}.

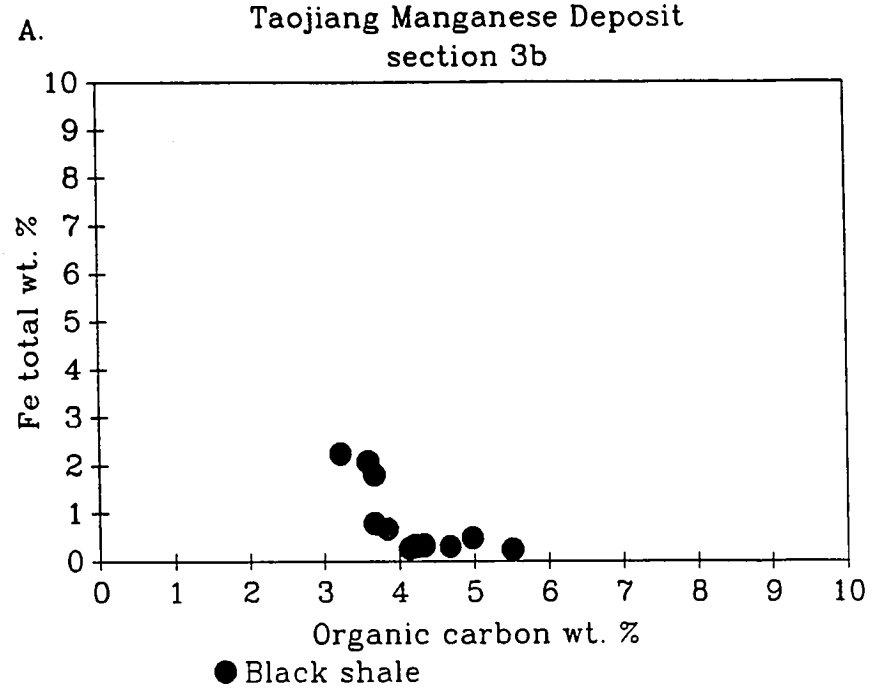

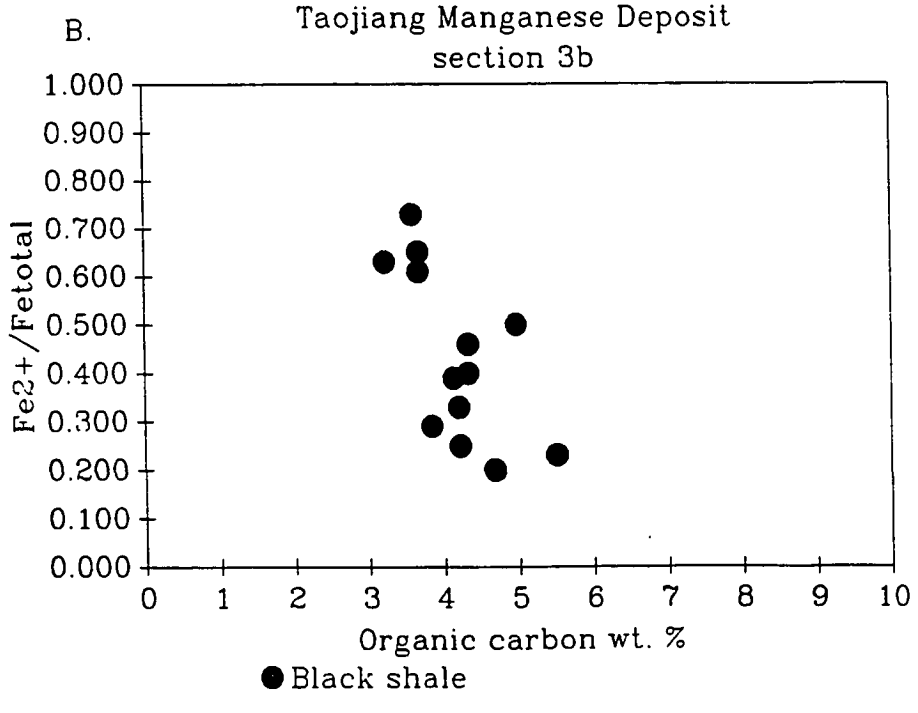

In summary, TOC-S-Fe correlations of samples of the Taojiang manganese deposit indicate that the black shales of the Hule Formation and the lower section of the Modaoxi Formation which are below the rhodochrosite ore horizon formed in an euxinic to semi-euxinic environment. The black shale and gray mudstones interbeds within the rhodochrosite ore bodies formed in a semi-euxinic to near normal marine environment. Gray shales of Yanxi formation and upper section of Modaoxi formation were deposited under rather oxidized normal marine condition. Limestones and rhodochrosite ores formed when the environments shifted from euxinic to more oxidized normal marine.

The gray shales and black shales of the uppermost Modaoxi Formation, the Wufen Formation, and the lower section of the Zhoujiaxi Formation are outcrop samples and possibly weathered which causes low sulfur content. However, high organic carbon content possibly indicate low degree of weathering. If the later is true, the pyrite formation may have been limited by the small reactive iron supply in a rather reduced condition. A sulfate limiting condition (fresh water) is another possible explanation of low sulfur and high carbon content. However, considering the petrographic features of these gray and black shales which contain abundant graptolites, a normal marine depositional environment should be concluded. Thus, the

most likely reason for high organic carbon and low sulfide sulfur contents of these black shales is surface weathering.

Xiangtan Manganese Deposit

As mentioned in chapter 3, the Xiangtan manganese deposit occurs in Pre-cambrian organic-rich black shales. Only rhodochrosite ores and direct hanging-wall and foot-wall black shales were collected from this deposit (Table 10).

In the TOC-S diagram (Fig. 70a), the black shales and the rhodochrosite ores plot above the normal marine regression line. One limestone sample has low sulfur (0.62%) but high carbon content (4.63%). The black shales contain 1.11 - 5.41% organic carbon and have a rather constant sulfur content (1.69 - 3.25%; except one sample with a very high sulfur content: 7.98%) and almost no correlation with organic carbon: $y = 0.003(x)+2.289$, $n = 7$, $r = 0.093$, which is not significant at 90% level. The DOP values of the black shales are high (0.56 - 0.88) and have a positive correlation with organic carbon: $y = 0.03(x)+0.607$, $n = 7$, $r = 0.501$, which is not significant at 90% level (Fig. 70b). These indicate that the pyrite formation of the black shales was syngenetic in an euxinic environment with additional diagenetic, organic-limited pyrite formation. Figure 71a. and 71b. indicate that

Table 10.

TOC-S-Fe Data of Xiangtan Manganese Deposit, China

Sample Number	Name	TOC%	SS%	DOP	Fe_{total} Reactive	Fe^{+2}/Fe_{total} Reactive
XT1	BS	1.11	1.75	0.68	2.25	0.97
XT2	BS	1.13	3.25	0.70	4.06	0.87
XT3	BS	4.33	7.98	0.75	9.27	0.81
XT4	RH	2.53	3.47	0.66	4.60	0.72
XT5	RH	0.75	0.45	0.25	1.58	0.54
XT7	RH	3.34	2.47	0.52	4.17	0.68
XT8	RH	1.83	1.16	0.47	2.16	0.54
XT9	RH	1.66	1.52	0.56	2.35	0.65
XT10	BS	4.80	2.57	0.71	3.14	0.76
XT11	LM	4.63	0.62	0.64	0.84	0.70
XT12	BS	5.41	2.78	0.88	2.75	0.89
XT13	BS	3.60	2.31	0.66	3.05	0.70
XT15	BS	3.30	1.69	0.56	2.61	0.61

TOC% -- Total organic carbon wt. per cent
SS% -- Sulfide sulfur wt. per cent
LM -- Limestone
RH -- Rhodochrosite ore
BS -- Black shale

Figure 70.

A. Plot of organic carbon versus sulfide sulfur of the Xiangtan manganese deposit samples from the Liantuo Formation. The solid line represents the regression line of black shales: y=0.033(x)+2.289, n=7, r=0.093, which is not significant at 90% level (ignoring one black shale sample which has higher sulfur content caused by late diagenetic pyrite layer). The dashed line represents the regression line of rhodochrosite ores: y=0.971(x)-0.15, n=5, r=0.971, which is significant at 95% level. The regression line of normal marine sediments is also presented.

B. Plot of organic carbon versus DOP. The solid line represents the regression line of black shales: y=0.03(x)+0.67, n=7, r=0.501, which is not significant at 90% level. The dashed line represents the regression line of rhodochrosite ores: y=0.108(x)+0.273, n=5, r=0.692, which is significant at 90% level.

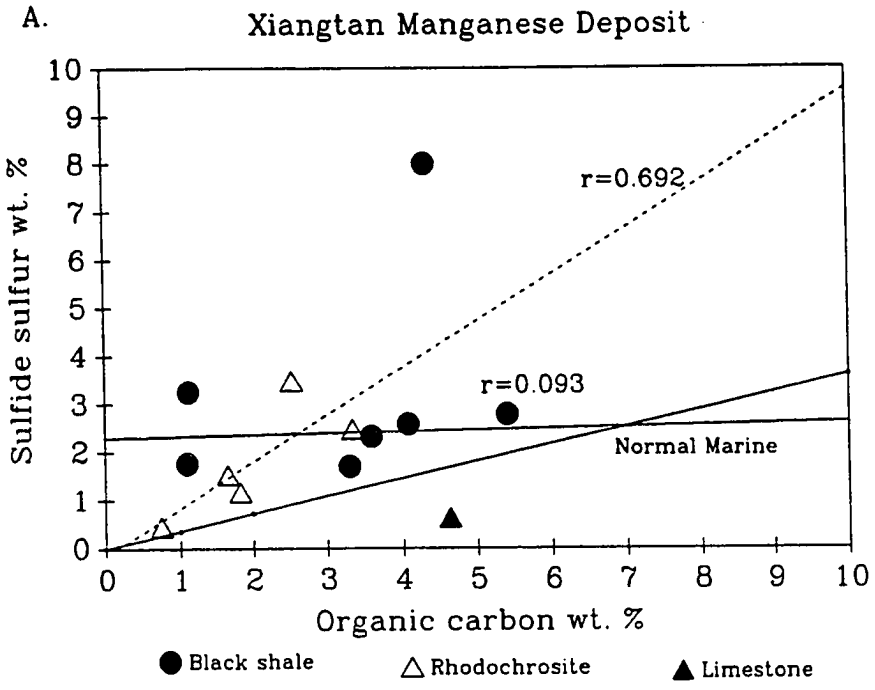

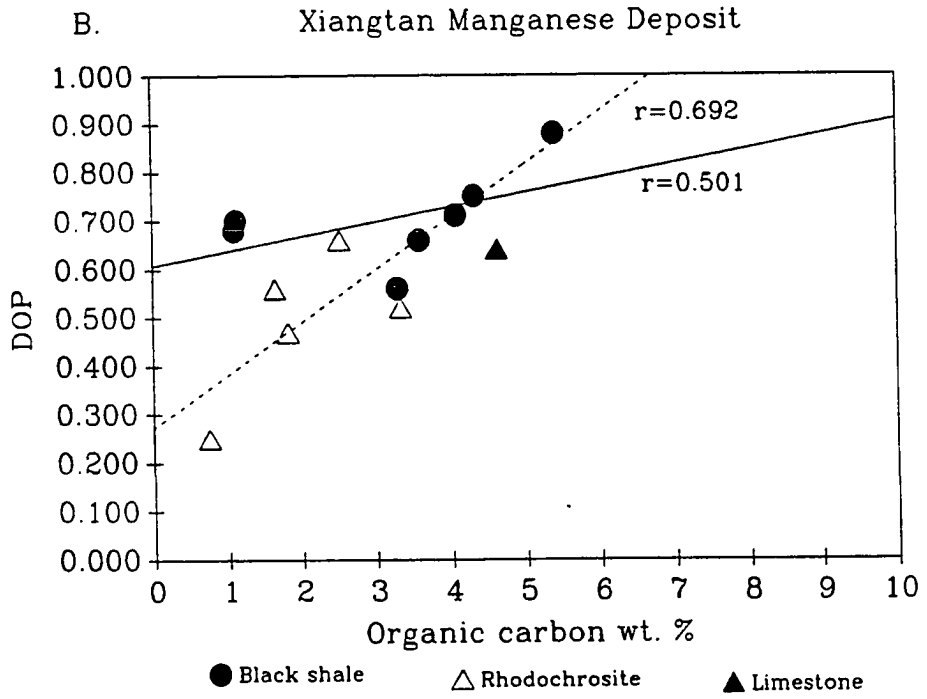

Figure 71.

A. Plot of organic carbon versus total (reactive) iron of the Xiangtan manganese deposit samples from the Liantuo Formation.

B. Plot of organic carbon versus Fe^{2+}/Fe_{total}.

A. Xiangtan Manganese Deposit

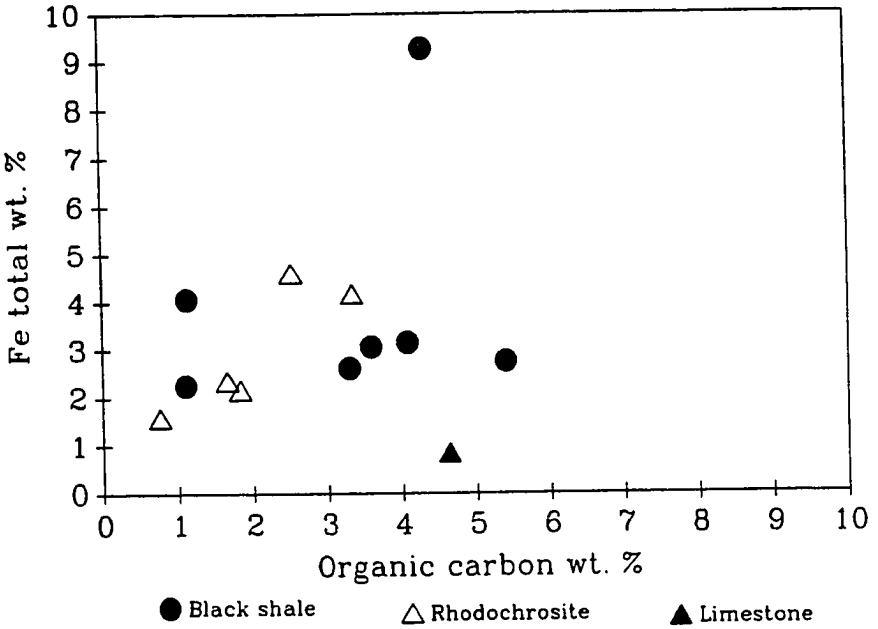

B. Xiangtan Manganese Deposit

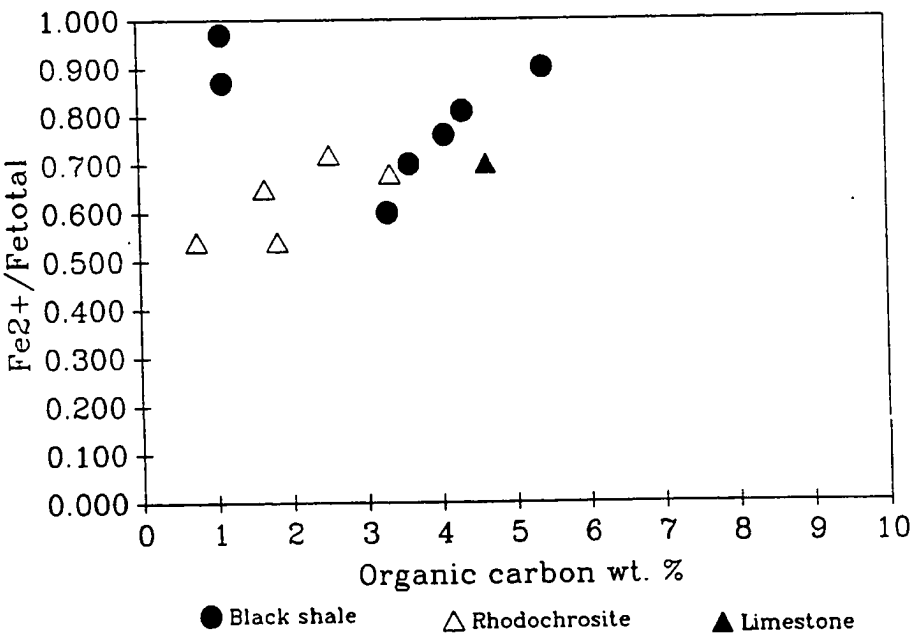

reactive iron of the black shales comes mostly from pyrite formation, and the Fe^{2+}/Fe_{total} ratio shows that virtually all of the reactive iron present is in the reduced state.

The values of organic carbon and sulfide sulfur of rhodochrosite range from 0.75 to 3.33% and 0.45 to 3.47% respectively. This is very different from the other manganese deposits studied. The rhodochrosite ores have good positive correlation of TOC-S (Fig. 70a): $y = 0.971(x)-0.15$, $n = 5$, $r = 0.971$ (significant at 95% level), and good positive correlation of TOC-DOP (Fig. 70b): $y = 0.108(x)+0.273$, $n = 5$, $r = 0.692$, which is significant at 90% level. The total reactive iron (1.58 - 4.60%) and the ratio of ferrous iron versus total reactive iron (0.54 - 0.72) versus organic carbon plots indicate the iron content of rhodochrosite ores mainly occurs as pyrite (Fig. 71a,b). The pyrite formation of rhodochrosite was limited by organic carbon, possibly in a normal marine environment.

Molango Manganese Deposit

The samples collected from Molango manganese deposit are black shales of the "Santiago" Formation, rhodochrosite ores of the lower part of the Chipoco facies, and limestones with black shale interbeds of the upper part of the Chipoco facies (Table 11).

Table 11.

TOC-S-Fe Data of Molango Manganese Deposit, Mexico

Sample Number	Name	TOC%	SS%	DOP	Fe_{total} Reactive	Fe^{+2}/Fe_{total} Reactive
"Santiago" Formation						
T1-24.9	BS	1.36	2.54	0.76	2.90	0.92
T1-20.4	BS	2.23	3.01	0.69	3.83	0.78
T1-20.3	BS	2.27	3.79	0.76	4.36	0.79
T1-20.35	BS	0.88	8.68	0.73	10.35	0.77
T1-19.0	LM	1.04	2.87	0.76	3.28	0.83
T1-17.1	BS	1.77	3.06	0.67	3.96	0.75
T1-13.8	BS	1.45	2.73	0.73	3.27	0.83
T1-7.2	BS	2.01	3.17	0.76	3.65	0.84
T1-3.9	BS	1.54	3.48	0.82	3.68	0.89
T1-0.1	BS	2.11	5.78	0.89	5.66	0.91
T1+0.0	BS	2.43	9.27	0.87	9.24	0.89
Chipoco facies						
T1+0.1	LM	0.94	0.88	0.72	1.07	0.85
T1+0.45	ORE	0.31	5.93	0.53	9.70	0.67
T1+0.5	ORE	1.13	0.11	0.03	3.28	0.07
T1+1.5	ORE	0.54	1.02	0.48	1.84	0.71
T1+2.0	ORE	1.06	0.05	0.01	11.17	0.50
T1+2.5	ORE	0.96	0.10	0.02	4.24	0.56
T1+3.0	ORE	0.46	0.36	0.07	4.74	0.43
T1+3.4	ORE	0.93	0.12	0.02	5.79	0.43
T1+4.0	ORE	0.79	0.38	0.07	4.58	0.32
T1+4.5	ORE	1.04	0.10	0.01	13.99	0.17
T1+5.9	ORE	0.66	0.15	0.03	4.44	0.37
T1+8.5	ORE	0.67	4.65	0.82	4.95	0.87
T1+8.9	LM	0.63	0.38	0.27	1.25	0.83
T1+12.5	LM	0.92	0.95	0.19	4.38	0.29
T1+19	LM	0.97	0.94	0.48	1.69	0.53
T1+21.7	LM	0.44	0.54	0.40	1.17	0.55
T1+22.2	BS	0.88	0.45	0.32	1.23	0.42
T1+22.3	LM	0.73	3.29	0.61	4.67	0.66
T1+27.5	BS	0.90	1.38	0.70	1.71	0.73
T1+38.7	LM	1.01	1.26	0.68	1.60	0.73
T1+45.3	LM	0.91	0.44	0.66	0.58	0.73
T1+58.4	BS	3.16	2.88	0.91	2.77	0.91
T1+71.5	LM	1.24	2.09	0.82	2.22	0.83

Table 11. Continued

Sample Number	Name	TOC%	SS%	DOP	Fe^{t}_{total} Reactive	Fe^{+2}/Fe_{total} Reactive
T1+87.9	LM	1.39	2.55	0.86	2.57	0.88
T1+101	BS	1.74	2.75	0.81	2.95	0.82
T1+102.6	LM	3.32	1.75	0.75	2.04	0.75
T1+124	LM	0.89	2.54	0.84	2.63	0.91
T1+130.6	LM	0.99	1.31	0.75	1.52	0.76
T1+135	BS	2.39	1.69	0.42	3.53	0.48
T1+140.6	LM	0.28	0.29	0.39	0.66	0.47
T1+151.8	LM	1.81	1.38	0.62	1.92	0.65
T1+161.5	LM	0.25	0.15	0.37	0.36	0.47
T1+171	LM	0.43	0.24	0.39	0.52	0.49
T1+223.5	LM	0.50	0.36	0.03	9.75	0.48

TOC% -- Organic carbon wt. per cent
SS% -- Sulfide sulfur wt. per cent
LM -- Limestone
BS -- Black shale
Ore -- Rhodochrosite ore

The black shales of the "Santiago" Formation have high sulfur contents (2.54 - 9.27%) and relatively low organic carbon contents (0.88 - 2.43%). The TOC-S plot shows a good positive correlation (ignoring three samples with very high sulfur content which caused by late diagenetic pyrite layers; Fig. 72a): $y = 0.439(x)+2.386$, $n = 8$, $r = 0.704$, which is significant at 90% level. This is a typical euxinic TOC-S plot pattern. The DOP values of the black shales are high (0.67-0.89) and roughly constant, with a very poor correlation with organic carbon (Fig. 72b). Figure 73a. and 73b. show that the total reactive iron comes mostly from pyrite in the black shales. These results indicate this pyrite formation was syngenetic in a typical euxinic environment.

Above the "Santiago" formation, the lower part of the Chipoco facies consists of rhodochrosite ores with low sulfide sulfur (0.1- 1.02%), low organic carbon (0.67 - 1.13%) and low DOP values (most < 0.1). Three exceptions are samples which are located in the lower-most and upper-most parts of the ore body and have high sulfide sulfur content and DOP values. The TOC-S plots of rhodochrosite ores are close to the normal marine regression line (Fig. 74a). The relatively high total reactive iron and very low DOP values of rhodochrosite ores indicate the existence of Fe-carbonates or Fe-oxides. The presence of appreciable

Figure 72.

A. Plot of organic carbon versus sulfide sulfur of the Molango manganese deposit samples from "Santiago" Formation. The solid line represents the regression line of black shales: y=0.439(x)+2.386, n=8, r=0.704, which is significant at 90% level (ignoring three black shale samples which have high sulfide sulfur content caused by late diagenetic pyrite layer). The regression line of normal marine sediments is also presented.

B. Plot of organic carbon versus DOP (Mean = 0.767).

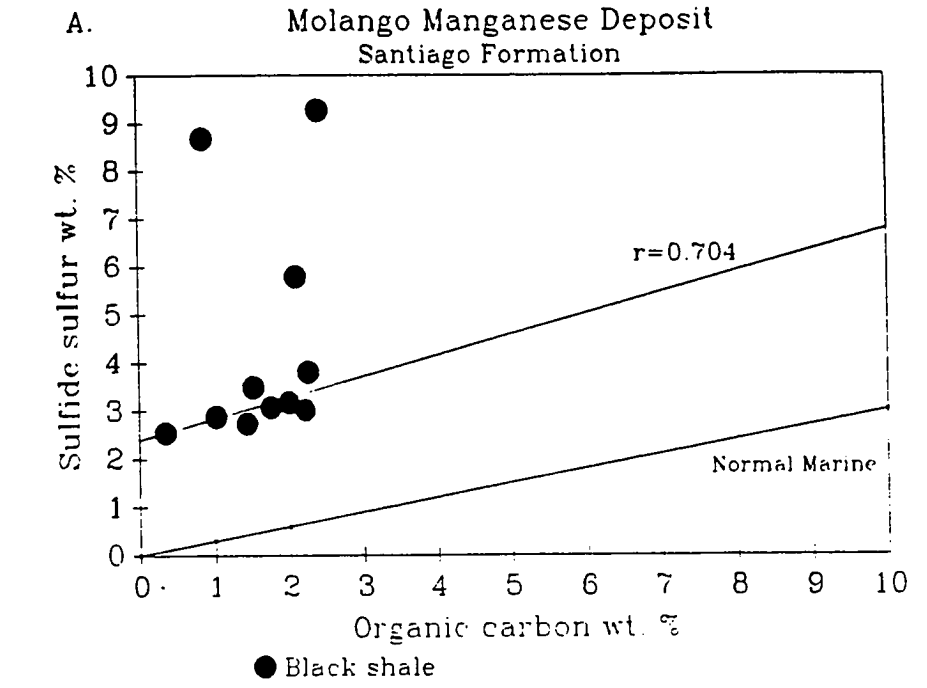

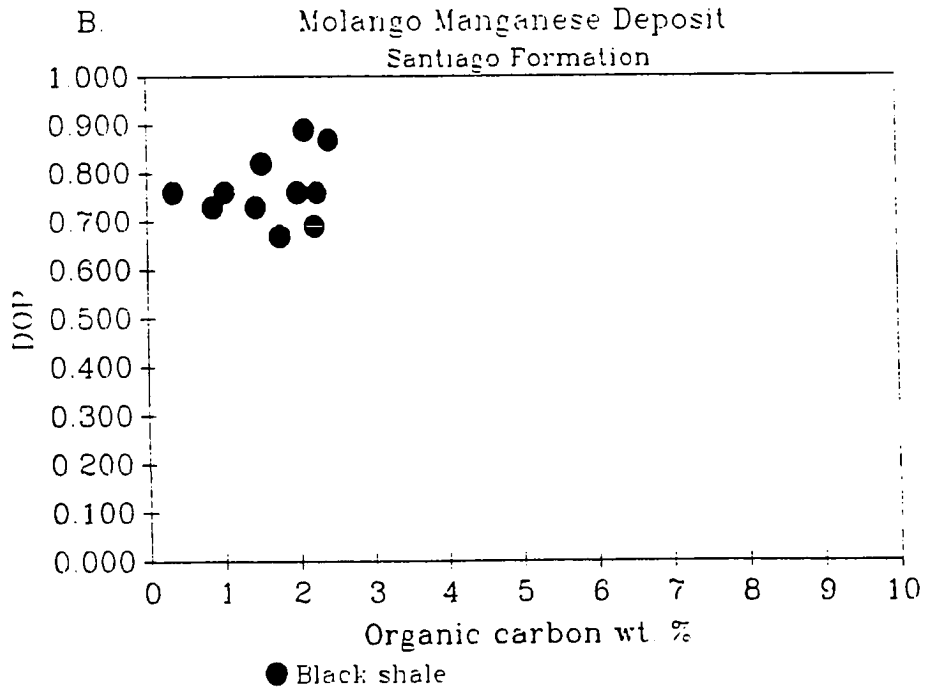

Figure 73.

A. Plot of organic carbon versus total (reactive) iron of the Xiangtan manganese deposit samples from the Liantuo Formation.

B. Plot of organic carbon versus Fe^{2+}/Fe_{total}.

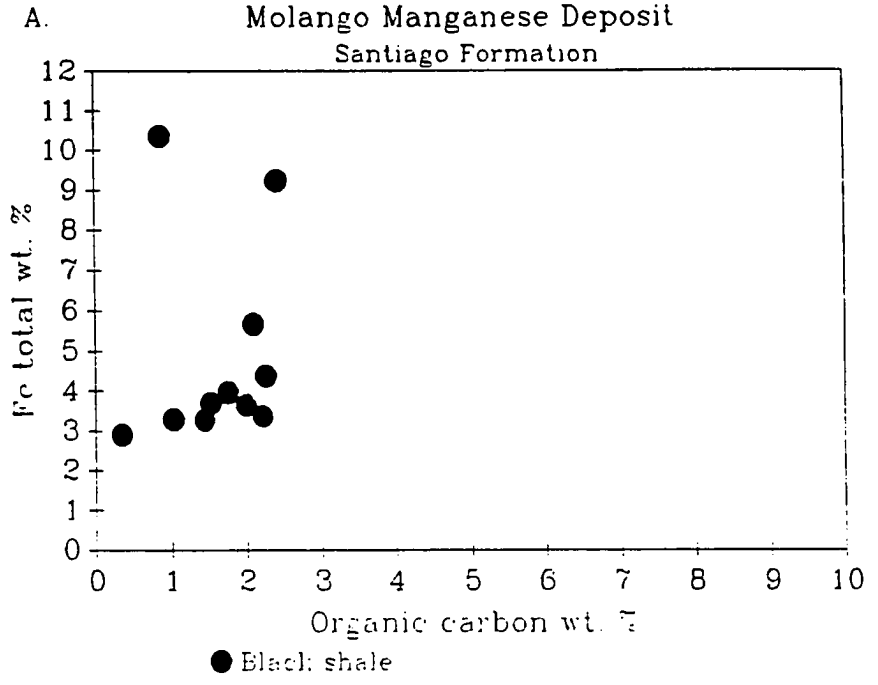

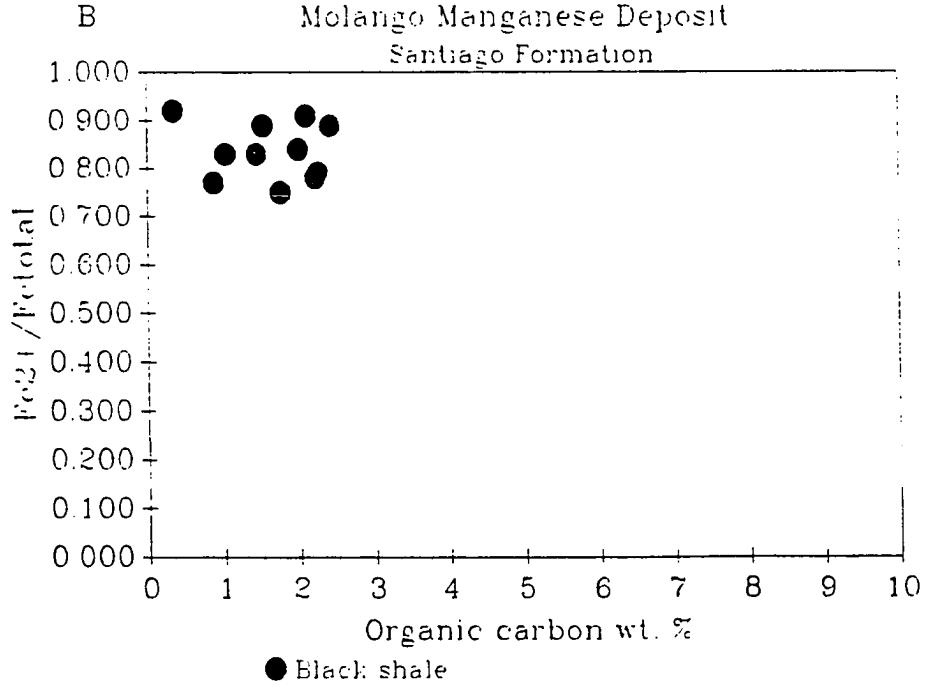

Figure 74.

A. Plot of organic carbon versus sulfide sulfur of the Molango manganese deposit samples from Chipoco facies. The solid line represents the regression line of black shales: $y=0.796(x)+0.436$, $n=5$, $r=0.748$, which is significant at 90% level. The regression line of normal marine sediments is also presented.

B. Plot of organic carbon versus DOP. The solid line represents the regression line of black shales: $y=0.121(x)+0.412$, $n=5$, $r=0.471$, which is not significant at 90% level.

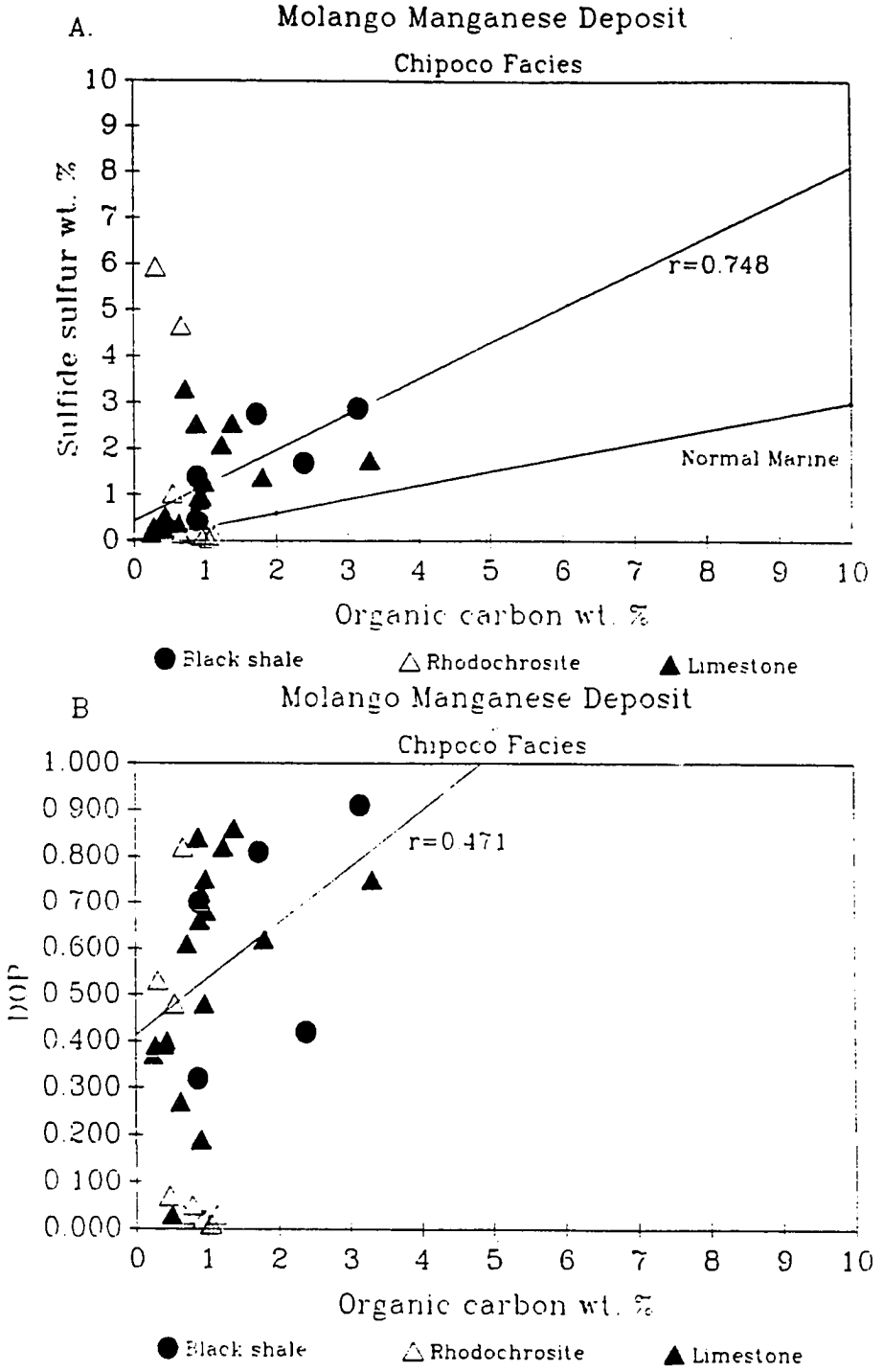

ferric iron in the ore bed is consistent with Okita's (1987) report of the common occurrence of magnetite (Fig. 74b, 75a,b). Three samples located at the lowermost and uppermost ore zone have very high sulfur content (about 5%) and high DOP value. This is caused by the existence of late diagenetic pyrite layers.

The upper part of the Chipoco facies consists of limestones and thin black shale interbeds. On the TOC-S plot, the black shales present a positive correlation of sulfur and carbon: $y = 0.796(x)+0.436$, $n = 5$, $r = 0.748$, which is significant at 90% level (Fig. 74a). Three black shale samples have high DOP value and positive correlation with organic carbon. Two black shale samples have lower DOP values, but they still show a positive correlation with organic carbon (Fig. 74b). Fig 75a. and 75b. show that reactive iron comes from pyrite in the black shale interbeds, indicating a semi-euxinic environment and syngenetic pyrite formation with organic carbon-limited diagenetic pyrite. Limestones of the Chipoco facies contain rather high carbon and sulfur contents. Compared with rhodochrosite ores, limestones have higher DOP values and lower total reactive iron (Fig. 75a), this indicates most iron of limestones come from pyrite. Poor positive correlation both in TOC-S and TOC-DOP plots of limestones of the upper Chipoco facies indicate possibly a semi-

Figure 75.

A. Plot of organic carbon versus total (reactive) iron of the Molango manganese deposit samples from Chipoco facies.

B. Plot of organic carbon versus Fe^{2+}/Fe_{total}.

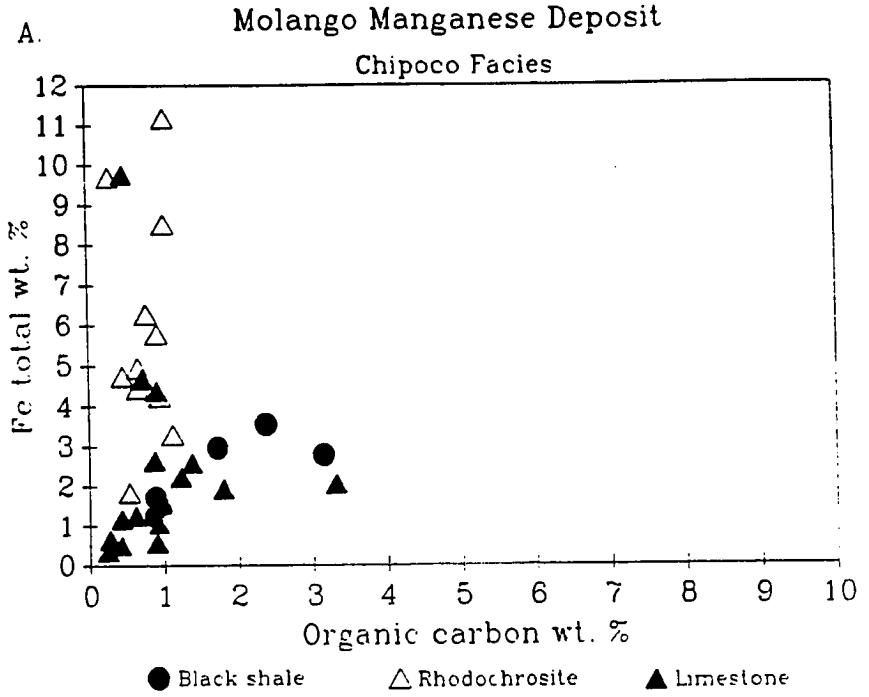

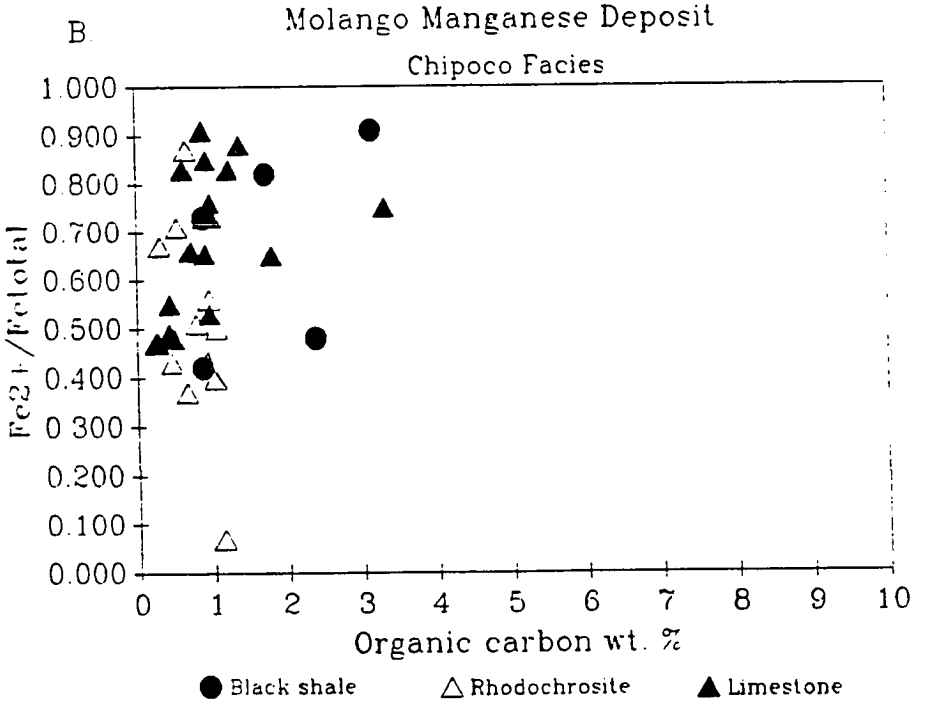

euxinic environment and that pyrite formation in limestones was syngenetic with additional carbon-limited diagenetic pyrite.

Manuel's River Manganese Prospect

The stratigraphy of the Manuel's River Manganese prospect of Newfoundland consists of pyritic black shale of the Manuel's River Formation and sideritic gray shale of the Chamberlains Brook Formation above ore bed; a rhodochrosite bed; and gray and green shales with limestone interbeds of Brigus Formation below the ore bed. Table 12 shows the TOC-S-Fe data of Manuel's River Prospect. Generally, data set shows that the different lithologies contain low organic carbon, low sulfide sulfur, and low DOP, but have higher total reactive iron and large ranges of the ratio of ferrous iron versus total reactive iron.

The gray shales below the rhodochrosite ore bed contain low organic carbon (0.32 - 0.49%), low sulfide sulfur (0.05 - 0.08%) and low DOP (0.01 - 0.02). The total reactive iron (6.24 - 3.75%) and the ratio of ferrous iron versus total reactive iron (0.92 - 0.36) are high. The TOC-S plot of these gray shales is close to normal marine regression line (Fig. 76a). Their low DOP and high total reactive iron indicate that pyrite formation was limited by organic carbon in a normal marine environment (Fig. 76b, 77a). Table 12.

TOC-S-Fe Data of Manuel's River prospect, Newfoundland

Sample Number	Name	TOC%	SS%	DOP	Fe_{total} Reactive	Fe^{+2}/Fe_{total} Reactive
F339	SS	0.36	0.06	0.01	3.83	0.40
F341	GS	0.32	0.08	0.02	3.75	0.36
F342	GS	0.49	0.05	0.01	6.24	0.92
F343 red	HR	0.21	0.04	0.01	3.60	0.44
F343	GS	0.33	0.03	0.02	1.65	0.06
F344	GS	0.55	0.04	0.01	5.97	0.83
F346 red	HR	0.25	0.02	0.01	2.51	0.11
F347 red	HR	0.34	0.05	0.01	3.25	0.23
F347	GS	0.33	0.11	0.01	6.67	0.48
F348 Siderite		0.80	0.05	0.01	6.63	0.37
F349	BS	0.54	0.10	0.02	3.93	0.48
F350	BS	1.11	0.14	0.03	4.49	0.33
F351 Siderite		0.76	0.10	0.02	5.14	0.47
F352	GS	0.37	0.08	0.01	5.46	0.11
F354	BS	2.19	1.41	0.21	5.87	0.68
F355	GS	0.33	0.23	0.08	2.69	0.77
F356	BS	0.50	1.84	0.44	3.65	0.58

TOC% -- Total organic carbon wt. per cent
SS% -- Pyritic sulfur wt. per cent
HR -- Rhodochrosite ore
GS -- Gray shale
BS -- Black shale
Siderite -- Sideritic nodules

Figure 76.

A. Plot of organic carbon versus sulfide sulfur of Manuel's River manganese deposit samples. The regression line of normal marine sediments is also presented.

B. Plot of organic carbon versus DOP.

A. Manuel's River Manganese Prospect

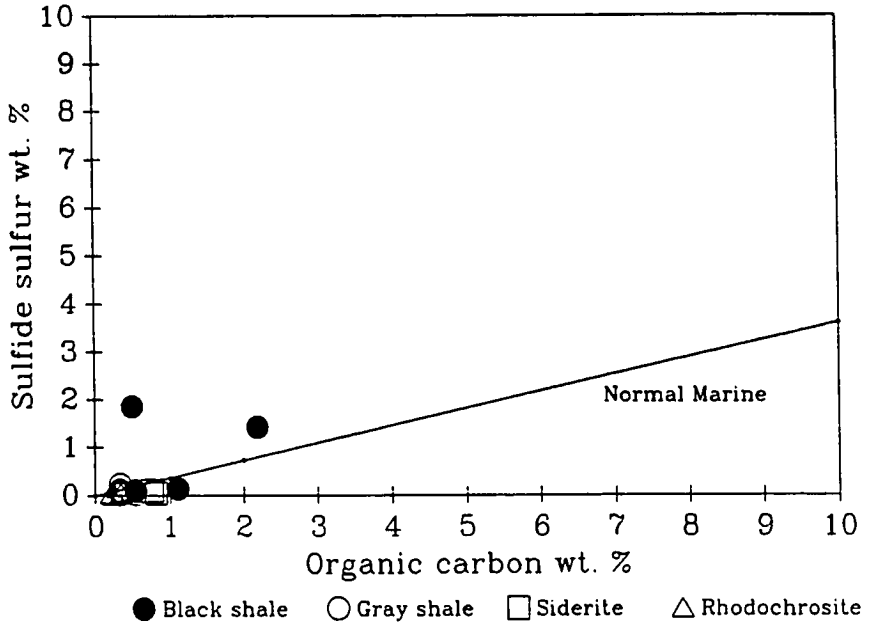

B. Manuel's River Manganese Prospect

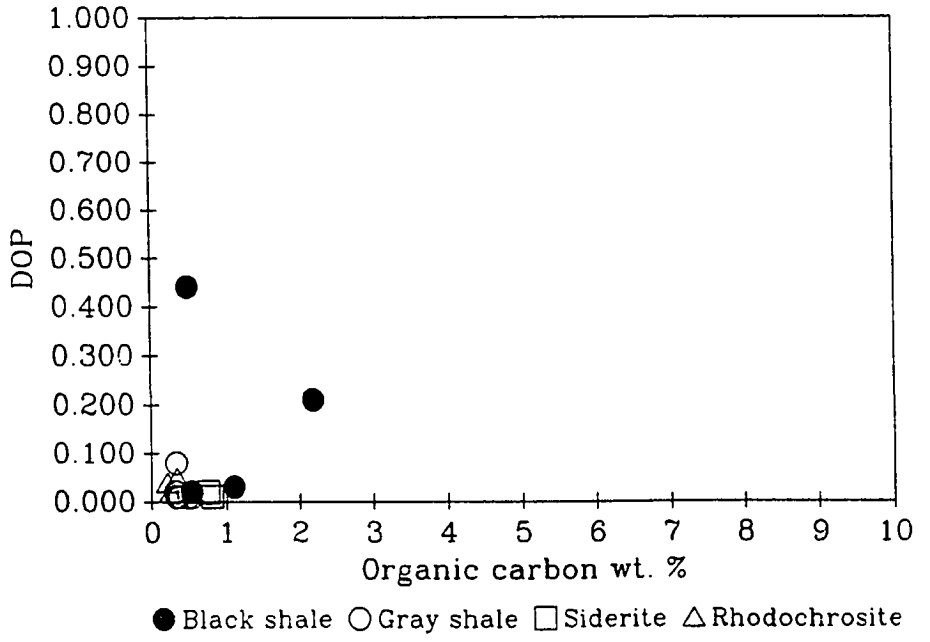

Figure 77.

A. Plot of organic carbon versus total (reactive) iron of Manuel's River manganese deposit samples. The solid line represents of regression line of black shales: $y=1.248(x)+3.131$, $n=4$, $r=0.995$, which is significant at 95% level.

B. Plot of organic carbon versus Fe^{2+}/Fe_{total}.

A. Manuel's River Manganese Prospect

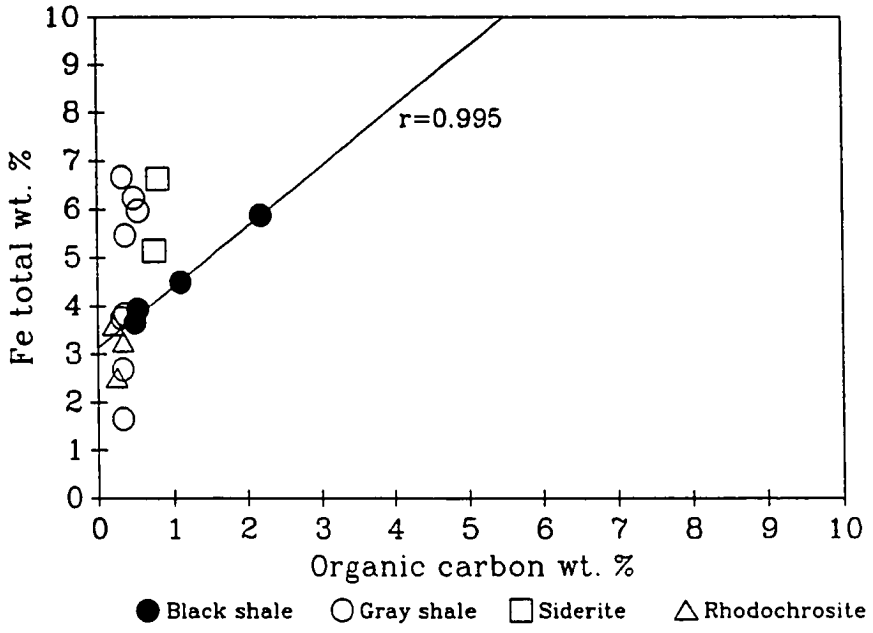

B. Manuel's River Manganese Prospect

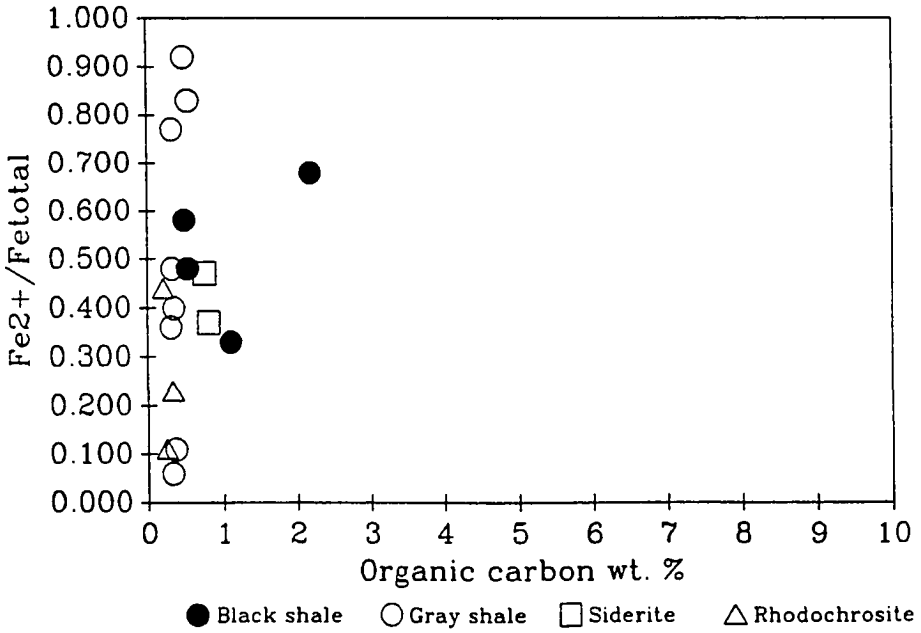

The rhodochrosite ores are red in color and occur as nodules with stromatolitic structure in the gray shales. These red rhodochrosite ores have low organic carbon (0.34 - 0.21%), low sulfide sulfur (0.05-0.02%) and very low DOP (0.01). The total reactive iron of rhodochrosite ores is high (2.51 - 3.60%) with a relatively low ratio of ferrous iron versus total reactive iron (0.11 - 0.44) which indicate perhaps the existence of Fe-oxides.

The red rhodochrosite ores are hosted by gray shales. These gray shales have low organic carbon (0.33 - 0.55%), low sulfide sulfur (0.03 -0.11%) and low DOP (0.01 - 0.02). The total reactive iron of these gray shales ranges from 1.65 to 6.67% and the ratio of ferrous iron versus total reactive iron ranges from 0.06 to 0.83. The TOC-S plots of both red rhodochrosite ores and the host gray shales are near the normal marine regression line (Fig. 76a). The pyrite formation of rhodochrosite ores and gray shales is limited by organic carbon and formed in normal marine environment.

The rocks above the rhodochrosite ore horizon are gray shales with siderite nodules and black shale. The gray shales contain low organic carbon (0.33 - 0.50%), low sulfide sulfur (0.01 - 0.08%) and low DOP (0.01 - 0.08). The total reactive iron of gray shales ranges from 2.69 to 5.46% and the ratio of ferrous iron versus total reactive

iron ranges from 0.11 to 0.77 (Fig. 77a,b). The siderite nodules of the gray shales have relatively higher organic carbon (0.76 - 0.80%), low sulfide sulfur (0.05 - 0.1%) and low DOP (0.01 - 0.02). The total reactive iron of siderite nodules ranges from 5.14 to 6.67% and the ratio of ferrous iron versus total reactive iron ranges from 0.47 - 0.48. The TOC-S plots of gray shale and siderite nodules are close to the normal marine regression line. The black shales have higher organic carbon (0.5 - 2.19%), sulfide sulfur (0.1 - 1.84%), and DOP (0.02 - 0.44). The total reactive iron of black shale ranges from 3.65 to 5.87% and the ratio of ferrous iron versus total reactive iron ranges from 0.33 - 0.68.

On the TOC-S plot, black shales are scattered and show a poorly correlated regression line which follows an euxinic environment pattern: $y = 0.231(x)+0.621$, $n = 4$, $r = 0.206$, which is not significant at 90% level (Fig. 76a). The DOP and the organic carbon of black shale have a negative correlation: $y = -0.019(x)+0.196$, $n = 4$, $r = 0.076$, which is not significant at 90% level (Fig. 76b). Both the total reactive iron and the ratio of ferrous iron versus total reactive iron of the black shale have a good correlation with organic carbon. Especially, the total reactive iron increases with the increasing organic carbon ($r = 0.995$; Fig. 77a). This indicates that the pyrite

formation of black shale was organic carbon limited and formed possibly in a semi-euxinic to near normal marine environment.

Summary

The TOC-S-Fe correlation of rhodochrosite ores and host rocks of the manganese deposits studied provides valuable information about depositional and diagenetic environments. The rocks below the rhodochrosite ore horizon are black shale (except the Manuel's River prospect, which consists of sideritic gray shales) and represent an euxinic ("Santiago" Formation, Molango Deposit, Xiangtan Deposit) or a semi-euxinic (Hule Formation and lower part of Modaoxi Formation, Taojiang Deposit) depositional environments.

Black shales and gray shales or gray mudstones occurring within rhodochrosite ore horizons (Taojiang Deposit and Manuel's River Deposit) represent near-normal marine (black shales) to normal marine (gray shales and gray mudstones) depositional environments. Thus during manganese mineralization, relatively more oxidized conditions were present.

In contrast to biogenic siliceous and calcium carbonate sediments which contain less reactive iron (Raiswell and Berner, 1986), the rhodochrosite ores as well as the limestones studied contain high reactive iron, low organic carbon and low sulfide sulfur contents (except the Pre-

Cambrian Xiangtan Deposit). The TOC-S correlations are poor and pyrite formation was partially limited by organic carbon content. The rhodochrosite ores of the Xiangtan manganese deposit have higher organic carbon and sulfide sulfur than younger deposits and shows a good correlation between them. It can be concluded that the pyrite formation in this case is limited by organic carbon.

Above the rhodochrosite ore horizon, the hosting rocks can be gray mudstones (upper Modaoxi Formation, Taojiang Deposit), or limestones with black shale interbeds (upper Chipoco facies, Molango Deposit) and represent normal marine or semi-euxinic to near-normal marine environments.

In contrast, the Manuel's River Deposit does not have a euxinic black shale lithofacies below the rhodochrosite ore horizon. The rhodochrosite ores occur as nodules hosted by gray shales that represent a normal marine environment. Above the ore horizon, gray shales with siderite nodules and black shales represent normal marine to semi-euxinic environments.

There are two limitations to the use of TOC-S-Fe correlation of samples in this research. First, the principles of using TOC-S and TOC-DOP plots to distinguish depositional environments are based on large numbers of data points. Smaller amounts of data like this research make it more difficult to obtain good correlations.

Second, the low organic carbon and low sulfide sulfur contents (less 1%) of gray shales, limestones, and rhodochrosite ores cause more difficulties for analyzing depositional environments.

CHAPTER 6. MANGANESE MINERALIZATION AND DEPOSITIONAL ENVIRONMENT

In order to synthesize the information for these four manganese deposits, in this chapter, details of the stratified basin margin model proposed by Cannon and Force (1983), Force and Cannon (1988), will be introduced first, and then the four manganese carbonate deposits studied will be compared and contrasted using this model.

Marine Geochemistry of Manganese and Iron

The formation of an economic manganese deposit requires that two general conditions be met: manganese must be concentrated to at least 200 times above its average crustal abundance of about 0.15 percent, and iron cannot be concentrated to any appreciable degree above its average crustal abundance of about 5 percent (Force and Cannon, 1988).

The solubility of iron and manganese compounds in aqueous solutions was determined by Hem (1963, 1972). In figure 78, which superimposes two of Hem's diagrams, it is evident that both Mn and Fe form virtually insoluble oxides or carbonates at Eh and pH conditions typical of modern ocean water.

Figure 78 also illustrates an important difference between Mn and Fe that is the key to the sedimentary fractionation of Mn and Fe. In a field of low Eh, iron

Figure. 78. Superimposed Eh-pH diagrams of manganese (screened line) and iron (solid) deposition, after Hem (1972). Phase boundaries are for concentrations of Mn, Fe, S, and CO_2 which approximate concentrations of present-day Black Sea anoxic water. Dashed line represents the Mn carbonate field at one order of magnitude greater P_{CO_2}. Shaded area is a field of soluble Mn and insoluble Fe. D and S represent deep and surface water of the Black Sea (Force and Cannon, 1988).

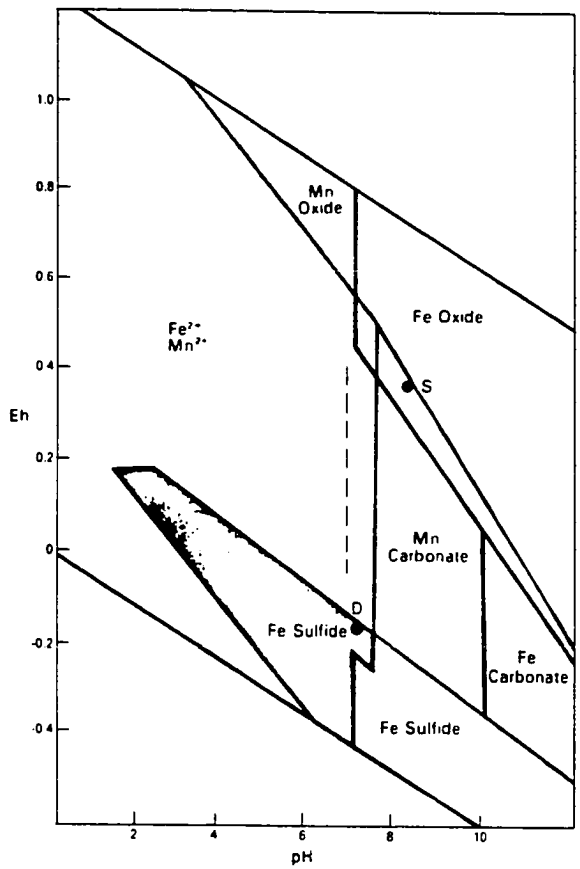

solubility is extremely low because iron sulfide precipitates, but manganese solubility is high because there is no comparable insoluble manganese sulfide. Iron and manganese in this Eh-pH field therefore will be extremely fractionated, with nearly all the iron going into sulfide and nearly all the manganese remaining in solution. Subsequent increase in Eh and/or pH of this water could cause deposition of manganese-rich, iron-poor chemical sediments. These solubility relations form the general basis for a stratified basin margin model -- low Eh conditions in one part of a marine basin result in manganese-rich, iron-depleted water from which a manganiferous precipitate can form in a more oxygenated portion of the basin.

In more detail, the fractionation by iron sulfide precipitation can occur by two somewhat different mechanisms:

1. If a basin attains truly euxinic conditions, in which H_2S is stable in the water column, the fractionation may occur in the water column itself with direct precipitation of iron sulfide from seawater.

2. During anoxic diagenesis, iron is fixed in pyrite during sulfate-reducing diagenetic reactions under low Eh conditions and manganese is mobilized toward the sediment-water interface by diffusion or by upward-moving pore

fluids. Where the overlying seawater also has a sufficiently low Eh to support high manganese solubility, the manganese remains in solution and contributes to the increasing reservoir of dissolved manganese.

In both cases, the fractionation of manganese and iron occurs by the formation of black pyritic muds under an anoxic or nearly anoxic water column in the deep basin. The seawater, now enriched in manganese and depleted in iron, can function as a dilute ore-forming solution.

In a practical sense, this model implies that marine sedimentary manganese deposits are contemporaneous with black pyritic shales. The facies may be spatially contiguous or spatially separated where rapid lateral circulation and/or sluggish Mn precipitation reactions cause deposition for most Mn away from the black shale.

Depositional Models

The sedimentary manganese deposits found in the world show evidence of having precipitated where interfaces between deep water with low Eh and shallow water with high Eh intersected shallow-marine substrates (Force and Cannon, 1988). Water column interfaces are places of precipitation because they juxtapose waters with dissolved elements in differing concentrations. Any mixing process, or diffusion, across the interface can cause precipitation, including biochemical precipitation, if a supersaturated

fluid is generated, i.e., the concentration of a compound in one body of water exceeds the effective solubility in the other (Force and Cannon, 1988).

For manganese, a particularly sharp solubility gradient exists along oxidation-reduction interfaces in water columns. Anoxic water may have dissolved manganese concentrations 1,000 times greater than those of oxidized water (Fig. 78, 79). Changes of pH and P_{CO_2} are also important influences on manganese solubility that occur locally along these interfaces. Where a water column is stratified such that near-surface water is oxic and lies above an anoxic water body, manganese oxide precipitates on the oxic side of the interface and dissolves as it falls into the lower anoxic water (Fig. 80; Maynard and May, 1988).

Preservation of this manganiferous precipitate occurs only where the redox interface intersects the ocean floor on basin margins or shoals so that the precipitate is deposited at or above the redox interface rather than sinking back below the interface where it would redissolve (Fig. 80).

There are two general depositional models for sedimentary manganese deposits: (1) oxic depositional model and (2) reduced and zoned depositional model (Cannon and Force, 1983).

Figure 79. Profiles of the Black Sea. (a). Values of dissolved (Mn^{+2}) and particulate (MnO_2) manganese and dissolved iron, from Brewer and Spencer (1974). Lightly shaded area may exceed saturation with respect to rhodochrosite. (b). Values of Eh and pH (from Cannon and Force, 1983).

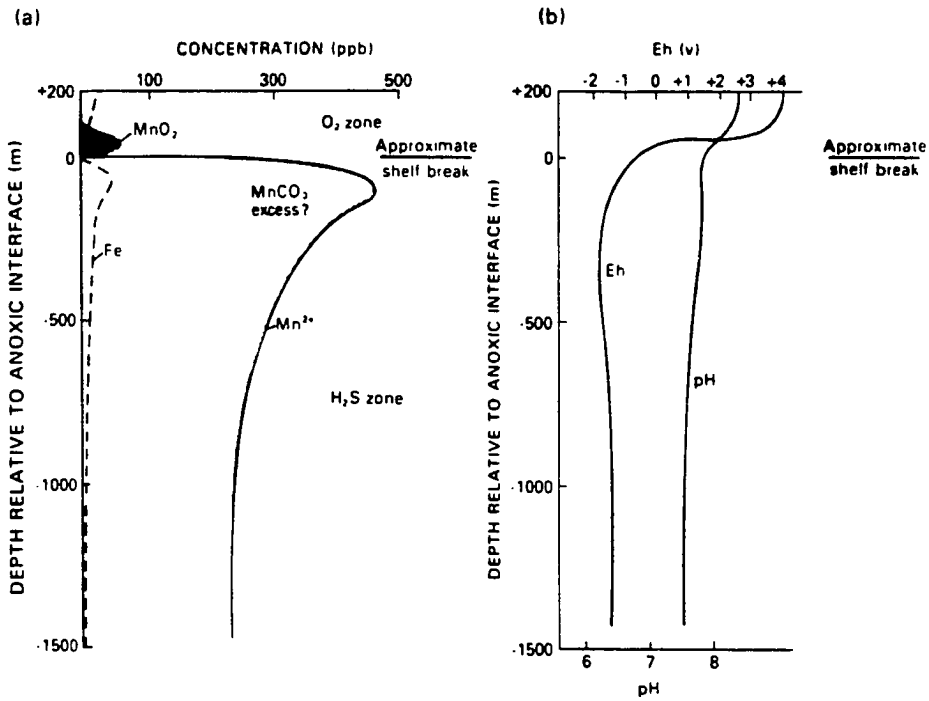

Figure 80. Euxinic basin model for $MnCO_3$ formation (Maynard and May, 1988).

Euxinic Basin Model for $MnCO_3$ Formation

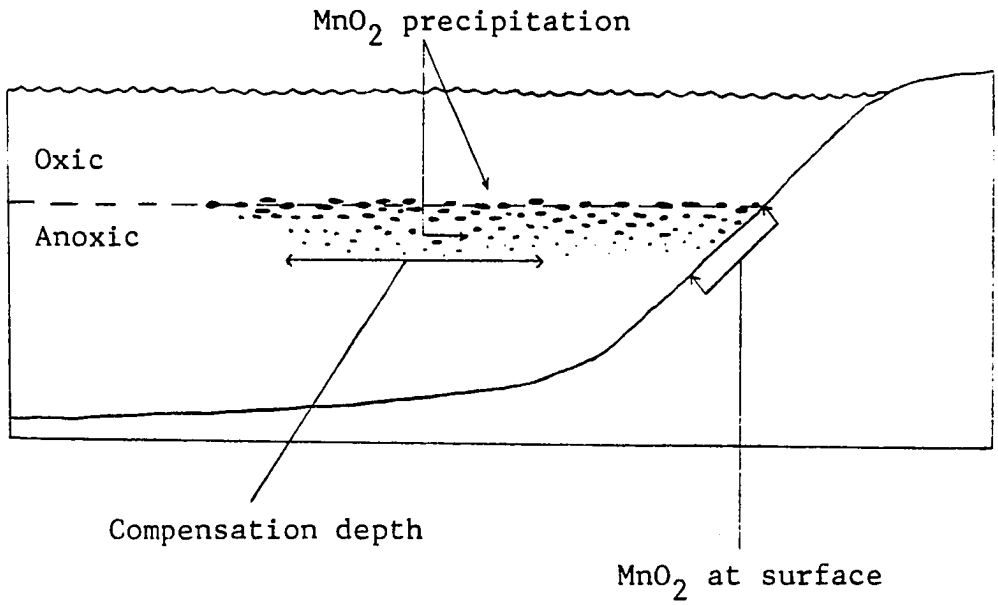

Within sediments:

$$2MnO_2 + CH_2O + CaCO_3 + 2H^+ =$$

$$2MnCO_3 + Ca^{2+} + 2H_2O$$

The oxic depositional model (Fig. 81.a) hypothesizes manganese deposition as oxide and/or carbonate facies on the oxygenated (landward) side of an oxic-anoxic interface intersecting the shelf of a stratified sea. Either or both facies of manganese deposits can form there because oxygenated surface waters of stratified seas may be near the boundary between manganese oxide and carbonate stability fields, where only slight changes in pH, Eh, or P_{CO_2} can favor one or the other of these facies. Oxide facies apparently is mostly primary sedimentary and carbonate facies mostly early diagenetic. The carbonate facies may predominate even where both facies are stable, because manganese oxide precipitation can be extremely slow. This variation of the model fits manganese deposits where oxide and/or carbonate facies show evidence of oxygenated bottom waters (e.g., benthic shell bed-hosted deposits). Primary sedimentary pisoliths or ooliths are also common in these deposits, in and adjacent to ore (Frakes and Bolton, 1984).

The model of reduced and zoned deposits (Fig. 81.b) differs from that for oxic deposits in the position of the manganese carbonate deposition relative to the redox interface and fits deposits with evidence of reduced facies carbonate deposition (e.g., laminated shallow-marine rhodochrosite-pyrite deposits). This variation treats the

Figure 81. Depositional models for stratified basin margin manganese. A. Oxic model, after Cannon and Force (1983). B. Zoned model. Analogous to A except for labeled features (from Force and Cannon, 1988).

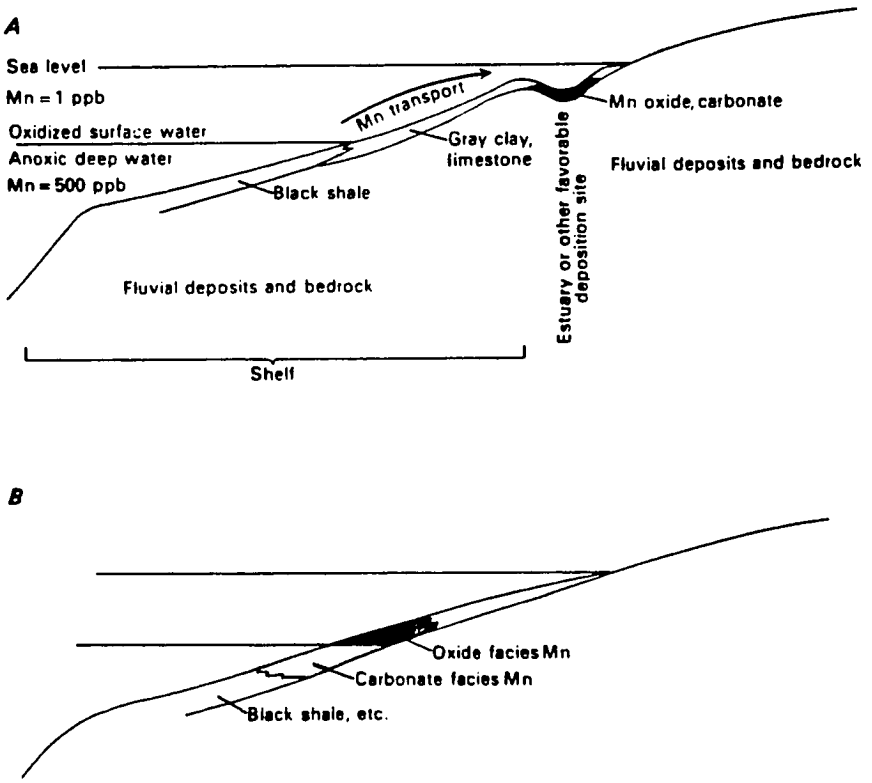

contact between carbonate and oxide facies of a manganese deposit as recording the position of the oxic-anoxic interface in the water column at the depositional site. Manganese carbonates in this assemblage would form mostly as replacements of primary carbonates, in a zone just below and seaward from the redox interface. Here anoxic water is saturated with respect to manganese carbonates due to redissolution of manganese oxides dropping through the interface. Carbonate facies deposits show a gradual transition by grade reduction of manganese to reduced basinal sediments.

Host rocks of sedimentary manganese deposits studied

Stratigraphic, petrographic, and TOC-S-Fe correlation features of host rocks of Taojiang, Xiangtan, and Molango sedimentary manganese deposits indicate that host rocks below the rhodochrosite ore zone consist of well-laminated, organic-rich, pyritic black shales formed in euxinic or semi-euxinic depositional environments. This feature fits the stratified basin margin model.

Stratigraphic features indicate that the black shale of the "Santiago" Formation in the Molango deposit is much thicker than that of the black shales of the Hule formation and the lower part of the Modaoxi Formation in the Taojiang deposit and than that of the black shales of the lower part of the Liantuo Formation in the Xiangtan deposit.

TOC-S-Fe correlations of these black shales also indicate that the "Santiago" Formation formed in a very typical euxinic environment by having high sulfur and relatively low carbon contents and high DOP values (Fig. 82.a,b). In this case, H_2S existed in the water column and iron went completely into pyrite formation. The manganese-rich and iron depleted ore-forming solution was well developed, and this process, considering the thickness of the "Santiago" Formation, possibly continued for a longer time.

The TOC-S plot of the black shales of the Taojiang deposit shows an euxinic to semi-euxinic condition evidenced by a lower sulfur content and a smaller intercept on the sulfur axis than for the Molango black shale. DOP values of these black shales are also lower than those of the Molango deposit and increase with increasing organic carbon, which indicates that additional diagenetic pyrite developed. In this case, a manganese-rich and iron-depleted solution formed in the water column and in sediments during early diagenesis, but the thickness of this black shale formation possibly indicates a poorly developed euxinic basin that limited the manganese ore-forming fluid for large Mn accumulation.

A few data points from the black shale of the Xiangtan deposit exhibit basically the same behavior as in the black

Figure 82. Comparison of TOC-S plots (A) and TOC-DOP plots (B) of hosting rocks below the ore zone of the manganese deposits studied.

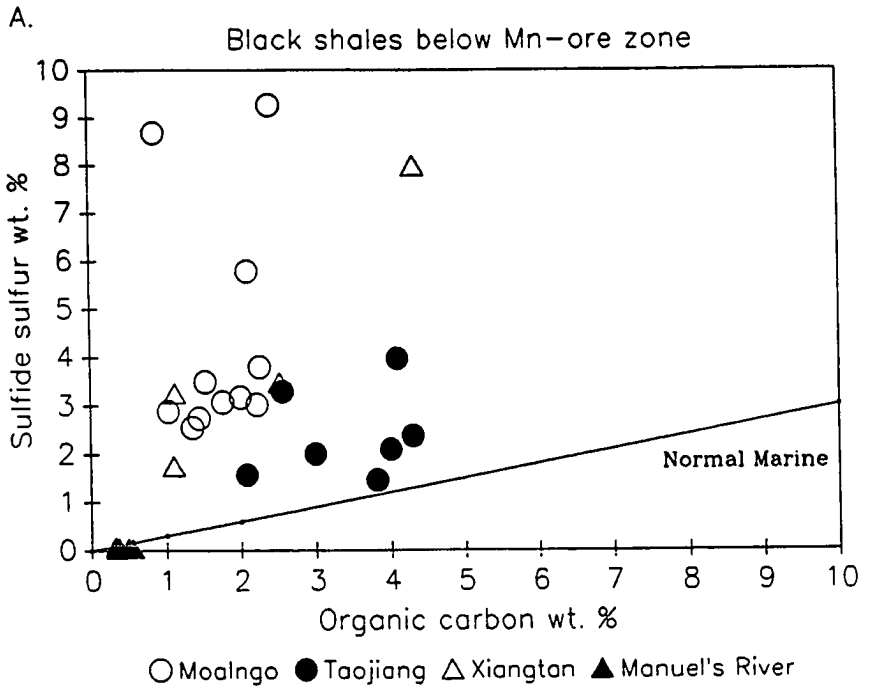

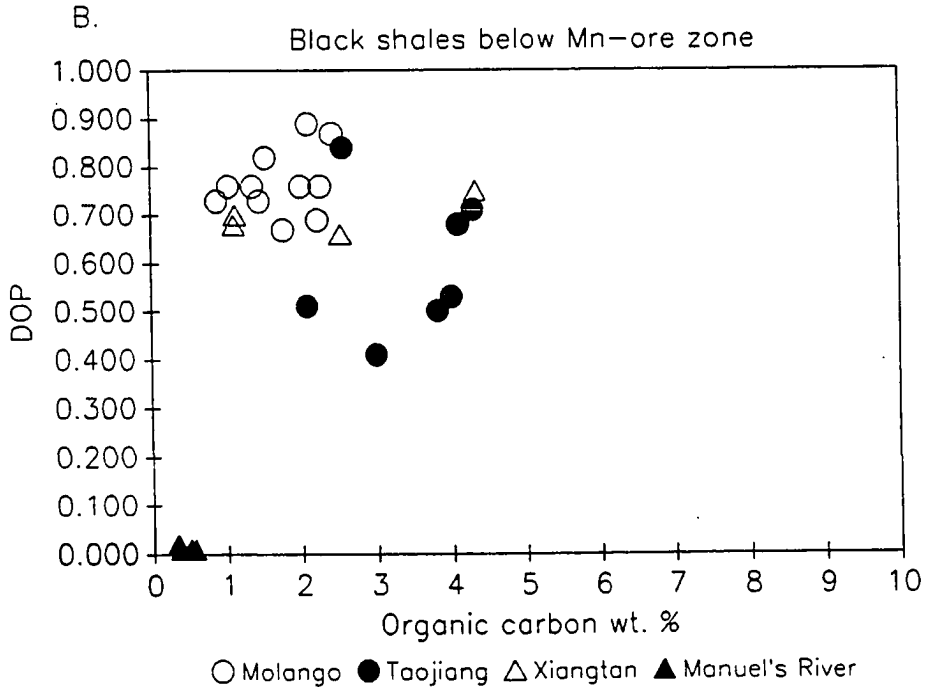

shales of the Molango deposit. The thin black shale formation below the ore zone may be a factor limiting the size of the subsequent manganese deposit. It can be concluded that well-developed euxinic conditions (indicated by the TOC-S-Fe correlation) and longer time (thicker black shale formation) should favor larger Mn-accumulations (Molango deposit). In contrast to the thick black shale formation of the Molango deposit, the black shales of the Taojiang and the Xiangtan deposits present semi-euxinic to euxinic conditions, but have a much smaller thickness. To a certain degree, this factor caused smaller Mn accumulation.

The host rocks below the manganese ore horizon in the Manuel's River prospect consist of green and gray shales with limestone interbeds. The TOC-S-Fe correlation from these rocks indicates normal marine conditions by having very low carbon and sulfur contents and low DOP values. Well-developed euxinic conditions did not exist, which caused very small amounts of Mn accumulation.

Host rocks above the ore zone present a more complex and different situation in these deposits. Petrographic and TOC-S-Fe correlation features indicate that rocks above the ore zone in the Taojiang deposit consist of fine-grained, organic-poor, gray mudstone with thin black shale interbeds which formed in a normal marine depositional

environment. The whole manganese ore-bearing sequence of the Taojiang deposit shows that the depositional environments changed from euxinic (pyritic black shales below the ore bed) to normal marine (gray mudstones above the ore bed), the rhodochrosite mineralization occurred at the transition.

In the Xiangtan deposit, rocks above the ore zone consist of well-laminated, organic-rich, pyritic black shale. TOC-S-Fe correlation of these black shales shows high carbon and sulfur contents and high DOP values which indicate an euxinic condition. Considering the rhodochrosite ores also contain relatively higher sulfur content, it can be concluded that the whole manganese ore-bearing sequence formed under continuous reducing conditions.

In contrast, the rocks above the ore zone of the Molango deposit consist of organic-rich limestone and thin black shale interbeds of the middle part of the Chipoco facies. TOC-S-Fe correlation shows that these limestones generally follow a semi-euxinic TOC-S plot pattern and have relatively higher DOP values. The interbedded black shales also represent a semi-euxinic condition. Compared with the black shale of the "Santiago" Formation of the Molango deposit, the limestones and the black shale interbeds of Chipoco facies represent relatively oxidized conditions,

but they did not reach normal marine conditions like the gray mudstone of upper Modaoxi Formation in the Taojiang deposit.

The rocks above the manganese ore zone of the Manuel's River prospect consist of gray shales and gray sideritic shales. TOC-S-Fe correlation shows that these gray shales formed in a normal marine environment. The whole ore-bearing sequence of the Manuel's River prospect shows a consistently oxidized, normal marine environment. Considering the oxic model mentioned above, Mn-carbonate could precipitate on the oxygenated side of the basin and separate from the euxinic source rock spatially. However, the information of this research does not provide any evidence for a reducing basin in the area.

Manganese Mineralization

Petrographic and whole rock X-ray diffraction analysis shows that each of these four manganese deposits consists of rhodochrosite as the main Mn-bearing mineral in the high grade portion of the ore body and kutnahorite, dolomite, Mn-calcite in the low grade portion. No manganese oxide phases, nor any petrographic evidence of replacement of manganese oxide by carbonates, were found. Based on the two depositional models proposed by Cannon and Force (1983) and Force and Cannon (1988), it is still very difficult to

answer the question why primary manganese oxides did not develop in these deposits.

Petrographic features of the rhodochrosite ores of these deposits are generally the same --- very fine grained and containing low organic carbon and sulfide sulfur contents. Rhodochrosite ores of both the Xiangtan and the Molango deposits are well-laminated. The ooliths and pisoliths in the ore zone of the Molango deposit may be evidence of early diagenetic manganese mineralization. However, the rhodochrosite ores of the other deposits do not show any petrographic evidence of replacement of primary carbonate by rhodochrosite. TOC-S-Fe correlations for the rhodochrosite ores as well as low grade ore zones follow a normal marine TOC-S pattern, as do the clastic rocks.

As mentioned in Chapter 5, TOC-S plots of carbonate rocks do not accurately reflect depositional environments, because the iron content of carbonate rocks is generally low. In addition, Aller and Rude (1988) in their recent work found that during physical or biological reworking of marine sediments, Mn oxides can be reduced to Mn carbonates under normal marine conditions at the same time oxidizing sulfides and organic matter. This is a possible way to explain the low sulfur and carbon contents of the rhodochrosite ore body if Mn oxides were originally present

and were then reduced. According to the reduced and zoned depositional model mentioned above, the rhodochrosite ore of these deposits may form at or slightly below the redox interface. Euxinic (Xiangtan) and semi-euxinic (Molango) environments above the ore zone caused by transgression of sea level could possibly provide a condition in which manganese oxides were reduced or Mn oxides precipitation was limited completely. This situation does not apply to the Taojiang deposit or the Manuel's River prospect where subsequent beds indicated oxidizing conditions under which primary Mn oxides should have been stable. More work needs to be done on regional basin analysis. Figure 83 shows a general summary of depositional environments and manganese mineralization of these deposits, except the Xiangtan deposit. All information of this research indicates that the Xiangtan deposit does not fit the Force and Cannon model. The data show that the whole manganese ore-bearing sequence formed under a continuously reducing conditions. Possibly, ore formation was related to glacial processes, as have been suggested for deposits of similar age in Brazil (Urban and Stribrny, 1985; Leeuwen and Graf, 1987). Further work should be done on this aspect of the Xiangtan deposit.

Figure. 83. Summarizing models of depositional environments and manganese mineralization of Molango and Taojiang deposits and the Manuel's River prospect.

(A) Well-developed euxinic basin is associated with thicker black shale formation below the manganese ore zone and larger manganese ore body (Molango deposit).

(B) Not well-developed euxinic basin is associated with thinner black shale formation below the manganese ore zone and smaller ore body (Taojiang deposit).

(C) The absence of euxinic black shale formation below the manganese ore zone is associated with sub-economic manganese (Manuel's River prospect).

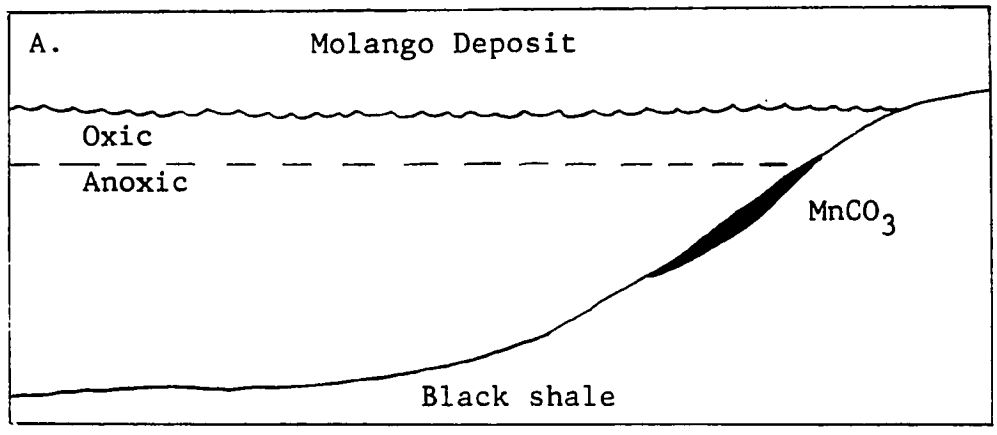

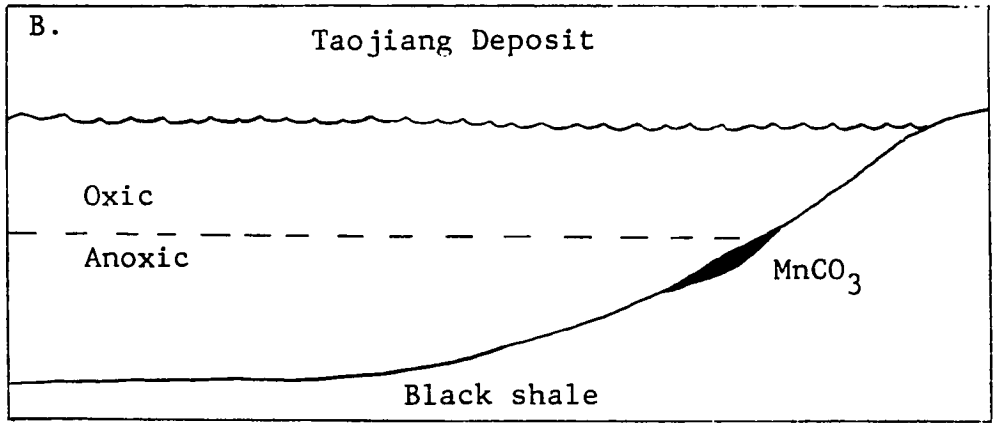

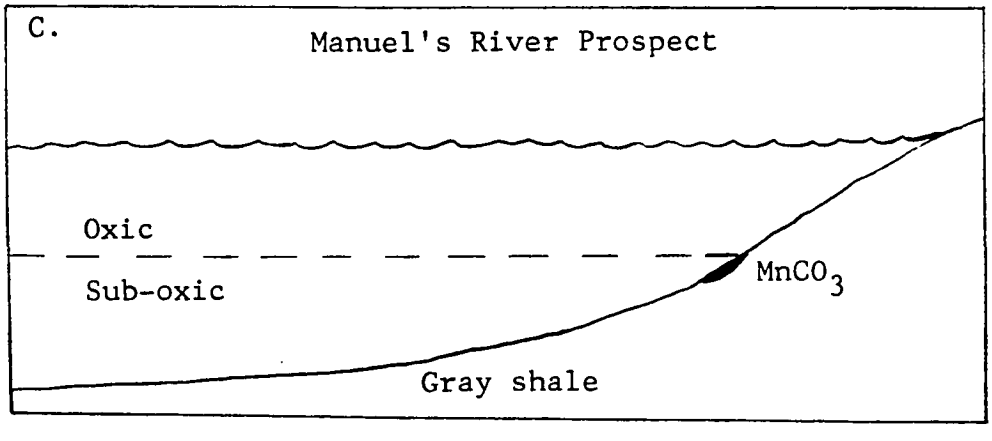

CHAPTER 7. CONCLUSION

(1) TOC-S-Fe correlation of shales hosting manganese carbonate deposits studied can be used to indicate their depositional environments. High S and TOC contents and high DOP values of the black shales below a rhodochrosite ore body indicate a euxinic to semi-euxinic environment. Low S and TOC contents and low DOP values of gray shales and limestones above a rhodochrosite ore body indicate a normal marine condition or a semi-euxinic condition.

(2) The size of the manganese carbonate deposits studied is related to the degree of development of a pre-existing euxinic basin. A well-developed euxinic basin can provide more iron depleted manganese ore-forming solution and form a larger manganese deposit (Molango). Thinner euxinic black shale formations below the ore body are associated with smaller manganese carbonate deposits (Taojiang and Xiangtan). A poorly developed manganese carbonate layer with associated nodules can be found in the normal marine depositional sequence (Manuel's River).

(3) The vertical successions of the ore-bearing sequences indicate that the manganese carbonate horizon occurs at the transition zone from euxinic or semi-euxinic to more oxidizing condition, normal marine depositional environment, except for the Xiangtan deposit.

(4) The rhodochrosite ores have low organic carbon and low sulfide sulfur contents and low DOP values (Taojiang and Molango). Some rhodochrosite may also have replaced pre-existing normal carbonate sediments during early diagenesis (Molango), but light carbon isotopes for both Taojiang and Molango imply an early diagenetic process similar to the oxidation of sulfide and organic matter by Mn^{4+}, described by Aller and Rude (1988) for modern sediments.

(5) Some rhodochrosite ores contain higher organic carbon and sulfide sulfur contents and higher DOP values, similar to their host rocks (Xiangtan). Possibly this kind of manganese carbonate was syngenetic.

(6) Rhodochrosite is the major Mn-bearing carbonate of the high grade ore zones. Lower grade ore is composed of Mn-dolomite and kutnahorite.

REFERENCES

Alexandri-R. R., and Martinez-V. A., 1986, Geologia del Dto. manganesifero de Molango, Hgo. In: G.P. Salas, Ed., Geologia Economica de Mexico. Fond de Cultire Economica, Mexico, p. 401 - 408.

Aller, R.C., and Rude, P.D., 1988, Complete oxidation of solid phase sulfides by manganese and bacteria in anoxic marine sediments, Geochimica et Cosmochimica Acta, v. 52, p. 751-765.

Analysis of Exploration and Mining Technology of Manganese Nodules, 1984, United Nations, Ocean Economics and Technology Branch, Seabed Mineral Series, v. 2, Graham and Trotman in co-operation with the U.N., 140 p.

Anderson, T.F., Kruger, J., and Raiswell, R., 1987, C-S-Fe relationships and the isotopic composition of pyrite in the New Albany Shale of the Illinois Basin, U.S.A., Geochimica et Cosmochimica Acta, v. 51, p. 2795-2805.

Assessment of Manganese Nodule Resources, 1982, United Nations, Ocean Economics and Technology Branch, Seabed Mineral Series, v. 2, Graham and Trotman in co-operation with the U.N., 79 p.

Berner, R.A., 1967, Thermodynamic stability of sedimentary iron sulfides, Am. Jour. Sci. v. 265, p. 773-785.

Berner, R.A., 1967, Diagenesis of iron sulfide in recent marine sediments, in Lauff, ed., Estuaries: Washington, D.C., Am. Assoc. Adv. Sci. Special Pub. 83, p. 268-272.

Berner, R.A., 1970, Sedimentary pyrite formation, Am. Jour. Sci., v.268, p. 1-23.

Berner, R.A., 1972, Sulfate reduction, pyrite formation, and the oceanic sulfur budget, In: D. Dyrssen, and D. Jagner, Eds., The changing Chemistry of the Oceans: Stokholm, Almquist and Wikcell, p. 347-361.

Berner, R.A., 1978, Sulfate reduction and the rate of

deposition of marine sediments, Earth Planet. Sci. Letters, v.37, p. 492-498.

Berner, R.A., 1981, A new geochemical classification of sedimentary environments, Jour. Sedimentary Petrology, v. 51, p. 359-365.

Berner, R.A., 1982, Burial of organic carbon and pyrite sulfur in the modern ocean: its geochemical and environmental significance, Amer. J. Sci., v. 282, p. 451-473.

Berner, R.A., 1984, Sedimentary pyrite formation: An up date, Geochim. Costomochim. Acta. v. 48. p. 605-615.

Berner, R.A., 1985, Sulfate reduction, organic matter decomposition and pyrite formation. In: G. Eglinton, Ed., Geochemistry of Buried Sediments, London, The Royak Society. p.25-38.

Berner, R.A. and Raiswell, R., 1983, Burial of organic carbon and pyrite sulfur in sediments over Phanerozoic time: a new theory, Geochim. Cosmochim. Acta., v. 47, p. 855-862.

Berner, R.A. and Raiswell, R., 1984, C/S method for distinguishing freshwater from marine sedimentary rocks. Geology, No. 12, p. 365-368.

Berner, R.A. and Westrich, J.T., 1985, Bioturbation and the early diagenesis of carbon and sulfur, Amer. J. Sci., v. 285, p. 193-206.

Bonatti, E., Kraeme, T., and Rydell, H.S., 1972, Classification and genesis of submarine iron-manganese deposits, In: D.R. Horn, Ed., Ferromanganese Deposits on the Ocean Floor, National Science Foundation, Washington, p. 159-166.

Canfield, D.E., Raiswell, R., Westrich, J.T., Reaves, C.M., and Berner,R.A., 1986, The use of chromium reduction in the analysis of reduced inorganic sulfur in sediments and shales, Chemical Geology, v. 54, p. 149-155.

Cannon, W.F., and Force, E.R., 1983, Potential for highgrade shallow-marine manganese deposits in North America, In: W. C. Shanks, Ed., Deposits,

Unconventional Mineral, American Institute of Mining, Metallurgical, and Petroleum Engineers, New York, p. 175-190.

Carver, R., 1971, Procedures in sedimentary petrology, Wiley-interscience, 653 p.

Davis, J. C., 1986, Statistics and data analysis in geology. John Wiley and Sons inc. 646 p.

DeYoung, J.H.Jr., Sutphin, D.M., and Cannon, W. F., 1984, International strategic minerals inventory summary report -- manganese , U.S., Geol. Surv. Circ. 930-A, 22 p.

Donnelly, T.H., Shergold, J.H., and Southgate, P.N., 1988, Pyrite and organic matter in normal marine sediments of Middle Cambrian age, southern Georgina Basin, Australia, Geochimica et Cosmochimica Acta, v. 52, p. 259-263.

Douglas, J., 1983, Geochemistry of the Cambrian Manganese deposits of Eastern Newfoundland, Ph.D. thesis, Memorial University, 250 p.

Fisher, I.St.J., 1986, Pyrite formation in bioturbated clays from the Jurassic of Britain, Geochimica et Cosmochimica Acta, v. 50, p. 517-523.

Fisher .I.St.J., and Hudson, J.D., 1987, Pyrite formation in Jurassic shales of contrasting biofacies, In: J. Brooks, and A. J. Fleet, Ed., Marine Petroleum Source Rocks, Geological Society Publication, No. 26, p. 69-78.

Force, E.R., and Cannon, W.F., 1988, Depositional model for shallow-marine manganese deposits around black shale basins, Economic Geology, v. 83, p. 93-117.

Frakes, L.A., and Bolton, B.R., 1984, Origin of manganese giants: Sea level change and anoxic-oxic history, Geology, v. 12, p. 83-86.

Garrels, R.M., and Perry, E.A., 1974, Cycling of carbon and oxygen through geological time, In: E. D. Geldbery, Ed., The Sea, v. 5, New York, Wiley, p. 569-655.

Garrels, R.M., and Lerman, A., 1984, Coupling of the sedimentary sulfur and carbon cycles -- an improved model, Amer. J. Science, v. 284, p. 989-1007.

Gautier, D.L., 1986, Cretaceous shales from the Western Interior of North America -- sulfur/carbon ratios and sulfur isotope composition, Geology, v. 14, p. 225-228.

Gautier, D.L., 1987, Isotopic composition of pyrite: relationship to organic matter and iron availability in some North American Cretaceous Shales, Chemical Geology, v. 65, p. 293-303.

Gibson, D.L., 1985, Pyrite-organic relationships: Currant Bush Limestone, Georgina Basin, Australia, Geochimica et Cosmochimica Acta, v. 49, p. 989-992.

Goldhaber, M.B., 1983, Experimental study of metastable sulfur oxidation formation during pyrite oxidation at pH 6-9 and 30 C, Amer. J. Sci., v. 283, p. 193-217.

Goldhaber, M.B., and Kaplan, J.R., 1974, The sulfur cycle, In: Goldberg, E.D., ed., The Sea, v. 5, New York, Wiley, p. 569-655.

Gryaznov, V.I., and Danilov, I.S., 1980, Oxidized Manganese ores of the Nikopol deposits, Ukranian SSR, In: I. M. Varensov, and G. Y. Grassely, Ed., Geology and Geochemistry of Manganese, Schweizerbart'sche Verlagsuchhanlung, Stuttgart, v.2. p. 403-416.

Hem, J.D., 1963, Chemical equilibria and rates of manganese oxidation, U.S. Geol. Survey Water Supply paper 1667A, 41 p.

Hem, J.D., 1972, Chemical factors that influence the availability of iron and manganese in aqueous systems, Geol. Soc. America Bull., v. 83, p. 443-450.

Hennessee, E.L., Blakeslee, P.J., and Hill, J.M., 1986, The distributions of organic carbon and sulfur in surficial sediments of the Maryland portion of Chesapeake Bay, Journal of Sedimentary Petrology, v. 56, N. 5, p. 674-683.

Jenkyns, H.C., 1986, Black shale and carbon isotopes in pelagic sediments from the Tethyan Lower Jurassic, Sedimentology, v. 33, p. 87-106.

Krom, M.D., and Berner, R.A., 1983, A rapid method for the determination of organic and carbonate carbon in geological samples, J. Sediment. Petrol., v. 53, p. 660-663.

Leeuwen, P., 1987, The Urucum-Mutun iron and manganese deposits, Mato Grosso do Sul, Brazil and Sta. Cruz, Bolivia, Part I. The region's potatial as an economic of iron and manganese, Geologie en Mijnbouw, v. 65, p. 317-325.

Leeuwen, P., and Graf, J.L., 1987, The Urucum-Mutun iron and manganese deposits, Mato Grosso do Sul, Brazil and Sta. Cruz, Bolivia, Part II. Stratigraphy, lithology and origin, Geologie en Mijnbouw, v. 65, p. 327-343.

Leventhal, J.S., 1983, An interpretation of carbon and sulfur relationships in Black Sea sediments as indicators of environments of deposition, Geochim. Cosmochim. Acta. V. 47, p. 133-138.

Leventhal, J.S., 1987, Carbon and sulfur relationships in Devonian shales from the Appalachian Basin as an indicator of environment of deposition, American Journal of Science, v. 287, p. 33-49.

Leventhal, J.S., Crock, J.G., and Malcolm, M.J., 1981, Geochemistry of trace elements and uranium in Devonian shales of the Appalachian Basin, U.S.G.S. Open File Report, p. 81-778.

Lewan, M.D., 1985, Evaluation of petroleum by hydrous pyrolysis experimentation, Phil. Trans. R. Sco. Lond. Part A, v. 315, P. 123-134.

Martino, O., 1986, The minerals industry of Mexico, in Minerals Yearbook 1984, v. 3, Area Reports: International, p. 553-573.

Maynard, J.B., 1982, Extension of Berner's "New geochemical classification of sedimentary environments" to ancient sediments, Jour. Sedimentary Petrology, v. 52, p. 1325-1331.

Maynard, I.B., and May, E.D., 1988, Sedimentary environment of manganese mineralization, Molango, Mexico. Intl. Assoc. Sedimentologists meeting, Beijing, China.

May, E., 1988, Petrographic and depositional environments of the Chipoco facies, Molango mining destrict, Molango, Sam Luis Potosi, Mexico. M.S. thesis, Department of Geology, University of Cincinnati, 102p.

McIntosh, J.L., Farag, J.S., and Slee, K.J., 1975, Groote Eylant manganese deposits, In: C.L. Knight, Ed., Economic Geology of Australia and Papua New Guinea, v. 1, Metals, Austral. Inst. of Mining and Metall., Monograph 5, p. 815-821.

National Materials Advisory Board, 1981, Manganese reserves and resources of the world and their industrial implications, Natl. Mater. Advis. Board Publication NMAB-374, 334 p.

Okita, P.M., 1987, Geochemistry and mineralogy of the Molango manganese orebody, Hidalgo State, Mexico, Ph.D. thesis, University of Cincinnati, 362 p.

Potter, P.E., Maynard, J.B., and Pryor, W.A., 1980, Sedimentology of shale, Spring-Verlag, New York, Heidelberg, Berlin, 305 p.

Raiswell, R., and Berner, R.A., 1985, Pyrite formation in euxinic and semi-euxinic sediments, American Journal of Science, v. 285, p. 710-724.

Raiswell, R., and Berner, R.A., 1986, Pyrite and organic matter in Phanerozoic normal marine shales, Geochimica et Cosmochimica Acta, v. 50, p. 1967-1976.

Raiswell, R., and Berner, R.A., 1987, Organic carbon losses during burial and thermal maturation of normal marine shales, Geology, v. 15, p. 853-856.

Rao, X., 1988, The diagenesis-mineralization of the Taojiang manganese ore deposit, M.S. thesis. Institute of Geology, Academia Sinica, 147 p. (in Chinese).

Roy, S., 1981, Manganese Deposits, Academic Press, New York, 458 p.

Rozanov, A.G., Volkov, I.I., and Yagodiskaya, T.A., 1974, Forms of iron in surface layer of Black Sea sediments: In: E. T. Degens, and D. A. Ross, Ed., The Black Sea -- Geology, Chemistry, and Biology, Amer. Assoc. Petrol. Geol. Mem. v. 20, p. 532-541.

Sandell, E.B., 1959, Colorimetric determination of traces of metals, New York, Intersci. Publishers, 1032 p.

Song, S., 1985, The characteristics of manganese deposits in Hunan Province, South China, In: Manganese Deposits of China, Geology Publication, p. 48-152, (in Chinese).

Sweeney, R.E., ms, 1972, Pyritization during diagnensis of marine sediments: Ph.D. thesis, Univ. California, Los Angeles, 184 p.

Sweeney, M., Turner, P., and Vaughan, D.J., 1987, The Marl Slate: a model for the precipitation of calcite, dolomite and sulfides in a newly formed anoxic sea, Sedimentology, v. 34, p. 31-48.

Taras, M.J., 1971, Standard Methods for the examination of water and wastwater, 13th, ed., Am. Public Health Assoc., 874 p.

Tavera, E., and Alexandri, R., 1972, Molango manganese deposits, Hidalgo, Mexico, Acta Mineralogica Petrographica, v. 20, p. 387-388.

Tissot, B.P., and Welte, D.H., 1984, Petroleum Formation and Occurrences, 2nd Ed. Spring-Verlay, New York, 699 p.

Urban, H., and Stribrny, B., 1985, The geology and genesis of the iron and manganese deposits of the Urucum district, Mato Grosso do Sul, Brazil. Zbl. Geol. Palaont. Teil I, H. 9/10, p 1515-1527.

Westrich, J.T., and Berner, R.A., 1984, The role of sedimentary matter in bacterial sulfate reduction: the G model tested. Limnol, Oceanogr., v. 29, p. 236 - 249.

Xu, X., 1980, The Ordovician manganese deposits of TaoJiang, Hunan Province, South China, Hunan Geology, p. 16-25, (in Chinese).

Ye L., Fan D., and Yang P., 1988, The characteristics of manganese ore deposits in China, Earth Science Review, in printing.

Zhabina, N.H., Volkov, I.I., 1978, A method of determination of various sulfur compounds in sea sediments and rocks, in Environmental Biogeochemistry and Geomicrobiology, v. 3, p. 735-745.

APPENDIX A

METHOD OF SULFIDE SULFUR MEASUREMENT

$CrCl_3$ EXTRACTION OF PYRITE

P.M. Okita, Eastern Mineral Resources, x6338*

This technique can be used to convert pyrite in a sample to silver sulfide which can then be converted to SO_2 for sulfur isotope analysis. The procedure is essentially the same as that described by Canfield, et al. (1985).

The chromous chloride digestion is said to be specific for pyrite. However, the first step required is acid digestion and this can liberate acid soluble sulfides. The typical setup usually vents the gases evolved by acid digestion, into the hood. I recommend bubbling these gases through a silver nitrate trap to (1) identify is acid soluble sulfides were released, (2) precipitate the sulfide in cases the amount can be weighed, and (3) to analyze the ^{34}S value if the quantity of silver sulfide is sufficient.

The procedure involves digesting 1 to 2 grams of samples into two steps. First, removal of carbonate and acid soluble sulfides is accomplished using hot 6N HCl. Second, conversion of pyrite to H_2S gas is performed by adding a solution of $CrCl_3$ reduced over zinc (a Jones Reductor) and heating for several hours. The evolved H_2S gas is bubbled into a silver nitrate solution and converted to silver sulfide. The entire process is carried out in a nitrogen atmosphere.

Several points should be kept in mind the setup and digestion:

A. All glassware must be very clean and dry. The last rinses should be done in good deionized water. Any chloride will cause white precipitates to form (silver chloride).

B. A tight seal is mandatory throughout the process. You must clamp shut the syringe injection hose before removing the syringe. Seals can be checked by squirting deionized water on the stopper assembly. Do not use any greases to insure seals.

C. Keep the nitrogen flow rate as slow as possible. This serves two purposes: (1) loss of precipitate from splashing, in the silver nitrate trap, will be minimized, and (2) complete conversion of the H_2S gas will occur before the bubble escapes the trap. Do not use an aerator in the silver nitrate trap as it will clog. I have started using pasteur pipettes because it gives a smaller bubble and the pipettes can be discarded after use.

CHEMICALS

-- 6N HCl

-- Ethanol

-- $AgNO_3$ Crystal (Fisher Chemical S - 181)

-- Zinc Shot (Fisher Chemical Z - 12)

-- Chromic Chloride (Fisher Chemical C - 325)

-- N_2 Gas

HARDWARE

-- Stirring hot plate

-- Stir bar

-- Ring stand

-- Three-finger clamps

-- 45 micron filters

-- Millipore filtering apparatus

GLASSWARE

Reaction Vessel

-- 250 ml wide month Erlenmeyer flask

-- 3-hole robber stopper

-- Water jacket condensing column

-- Glass tube long enough to reach almost to the bottom of flask when about 3 cm are left above the top of the robber stopper. This will be the N_2 inlet line.

-- Short piece of glass tubing. This should be long enough to pass through the rubber stopper and still have about 1 to 2 cm sticking above and below the stopper. This will be the port for injecting solutions via the syringe.

-- 50 cc, or greater, plastic syringe

-- Tygon tubing

Acid Trap

-- 125 ml aspirator flask

-- 1-hole robber stopper

-- Glass tube (a fritted glass aerator works best)

Silver Nitrate Trap

-- 50 ml (approximately) test tube

-- Pasteur pipettes

SETUP OF APPARATUS

Assemble the apparatus as shown in the figure 84. The 3 hole stopper is best made from a solid one in which you drill the holes. This allows you to space the holes as necessary to accommodate your condenser and glass tubing.

A short piece of flexible tubing should be place on the syringe inlet. Be sure the I.D. of the tubing is small enough to fit tightly in the syringe.

The $AgNO_3$ trap does not have to be fitted with a stopper, and I prefer that it isn't. It is much simpler to just place a pipette on the hose and allow it to hang in the trap. This way only a basic test tube is needed and the pipette can be thrown away after use.

The pH 4 buffer trap is optional. If you have trouble keeping acid from being carried from the flask to the trap you should use it.

PREPARATION OF SOLUTIONS

5% Silver Nitrate Solution:

5 g $AgNO_3$ crystals + 100 ml deionized water.

Make sure your water is "clean". If there is any

chloride in it you will see a white precipitate or cloud form in the solution. The solution must remain clear.

Chromous Chloride Solution:

2 g $CrCl_3$ + 50 ml 6N HCl.

Put the $CrCl_3$ in a 100 ml beaker and add the acid to it under the hood. Keep this solution under the hood at all times.

Reduction of Zinc Shot:

Put the zinc shot in a separator funnel (e.g. 250 ml or greater). Reduce the zinc pellets by adding a solution of 10 ml 6N + 60 ml deionized water.

BE CAREFUL : THIS IS VERY EXOTHERMIC -- add the acid solution slowly and carefully.

Allow this reaction to go on at least 3 minutes (it can't go on too long so don't rush to use it).

STEP BY STEP PROCEDURE

STEP 1 - Sample Setup

-- Place 1 or 2 g of sample in the 250 ml flask.

-- Add the stir bar.

-- Add 5 ml ethanol.

-- Fit the flask onto the rubber stopper.

-- Secure the vessel in the clamp and make sure you have a good seal and the syringe inlet hose is clamped shut.

STEP 2 - Purge Reaction Vessel

-- Turn on hot plate (but not stir bar).

-- Start the flow of N_2.

-- Wait about a minute for the flask to be purged of air.

-- Place pipette in silver nitrate solution and adjust flow rate so about 1 bubble per second is being release.

STEP 3 - Acid Digestion

-- Inject 25 ml of 6N HCl in to the flask. Be careful to inject the acid slowly. You will displace a volume of 25 cc in the flask which will be forced out at the $AgNO_3$ trap.

-- Clamp the inlet hose before removing the syringe.

-- Allow this stage of the reaction to continue for 10 minutes. Check your seals by squirting water on them. Also, adjust your N_2 flow rate is necessary.

**** If a measurable amount of sulfide has been produced you should change the $AgNO_3$ trap. Do not turn off the N_2.

STEP 3 A. Cool the sample before adding $CrCl_3$. This step is optional. The advantage to it is that the evolution of H_2S by the $CrCl_3$ will not take place quite so quickly. It is recommended if your acid solution is near boiling. If you do cool the apparatus, turn the nitrogen flow rate up so that silver nitrate (or air !!! If you do not have a trap on) is not sucked back into the line.

STEP 4 - $CrCl_3$ Digestion.

-- While the HCl digestion is going on, reduce the $CrCl_3$ solution by:

Drain the acid solution from the zinc shot.

Slowly add the $CrCl_3$ solution to the zinc shot.

Wait until the solution stops bubbling and turns blue.

-- Immediately drain the solution from the zinc and draw it into the syringe.

Do this quickly as the solution is very unstable in air.

If it begins to turn green reduce it again.

-- Place the syringe in the inlet hose and open the clamp the hose tightly before removing the syringe.

-- Adjust the flow rate of the N_2 gas.

-- Allow the reaction to run at least 2 hours or until the $AgNO_3$ solution turns clear.

STEP 5 - Recovering the Precipitates

-- Remove the $AgNO_3$ trap. NOTE: Do not turn off the N_2 gas until you remove the trap or the $AgNO_3$ solution may back wash.

-- Filter the $AgNO_3$ solution through the filter paper and wash with deionized water. If a white precipitate formed in your trap, it is silver chloride, rinse with ammonia.

-- Dry the filtrate overnight by placing the petri dish, with its lid half off, in a desiccator.

-- Weigh the petri dish + sample and calculate weight-percent sulfide.

Figure 84. A general setup scheme of sulfide sulfur determination (after Okita, 1987).

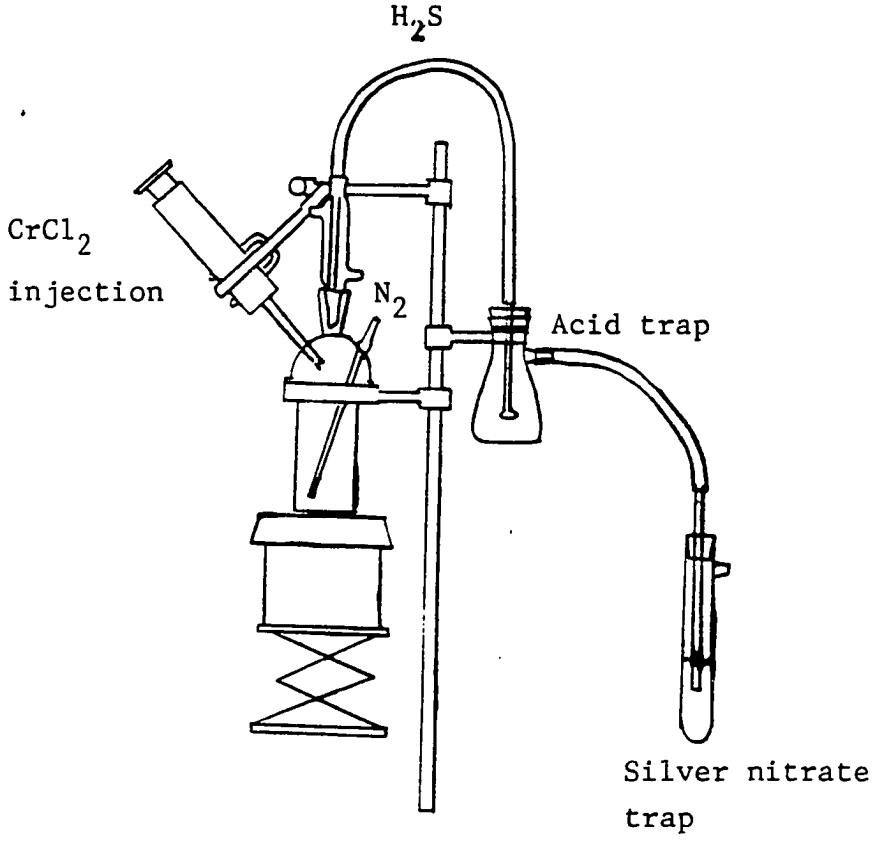

APPENDIX B

SAMPLE LOCATION FOR STRATIGRAPHIC COLUMN STUDIED

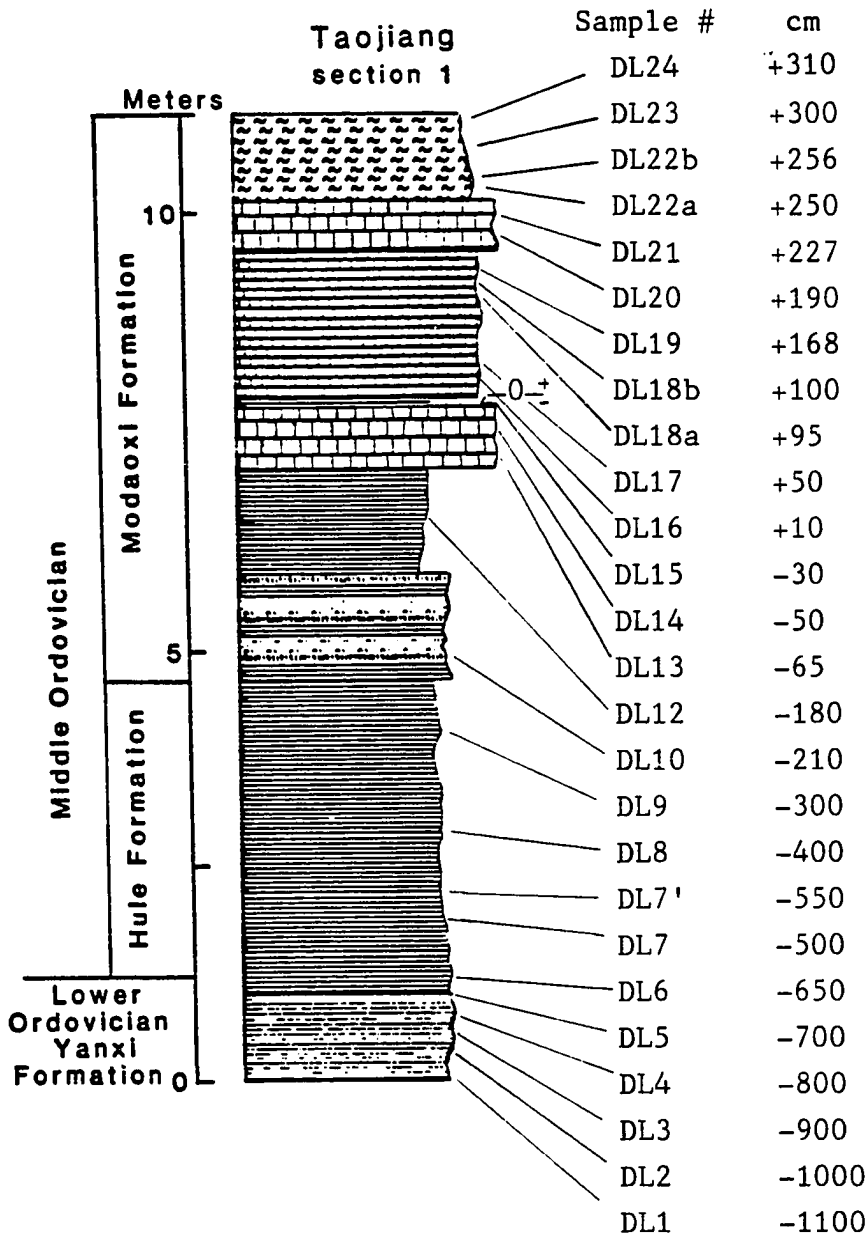

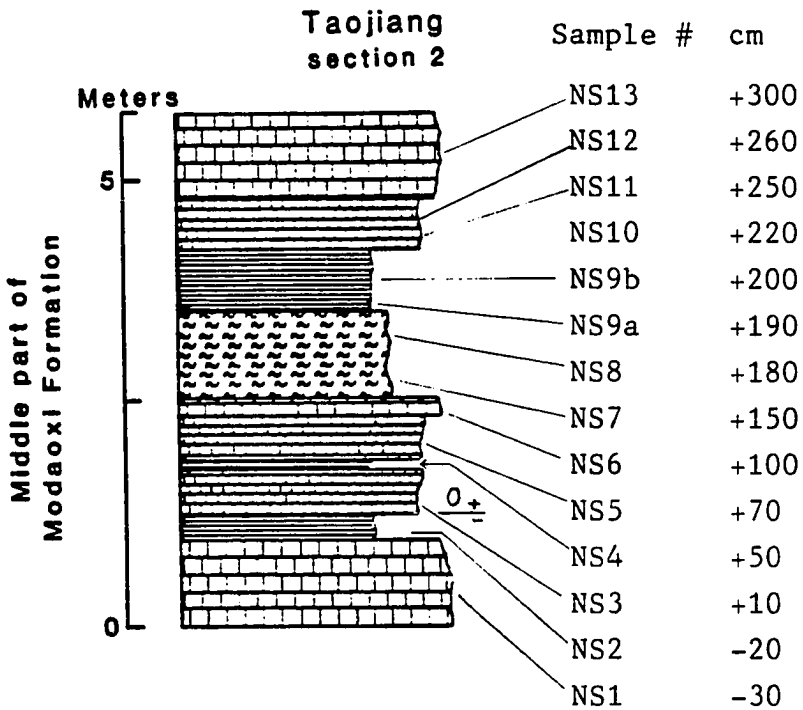

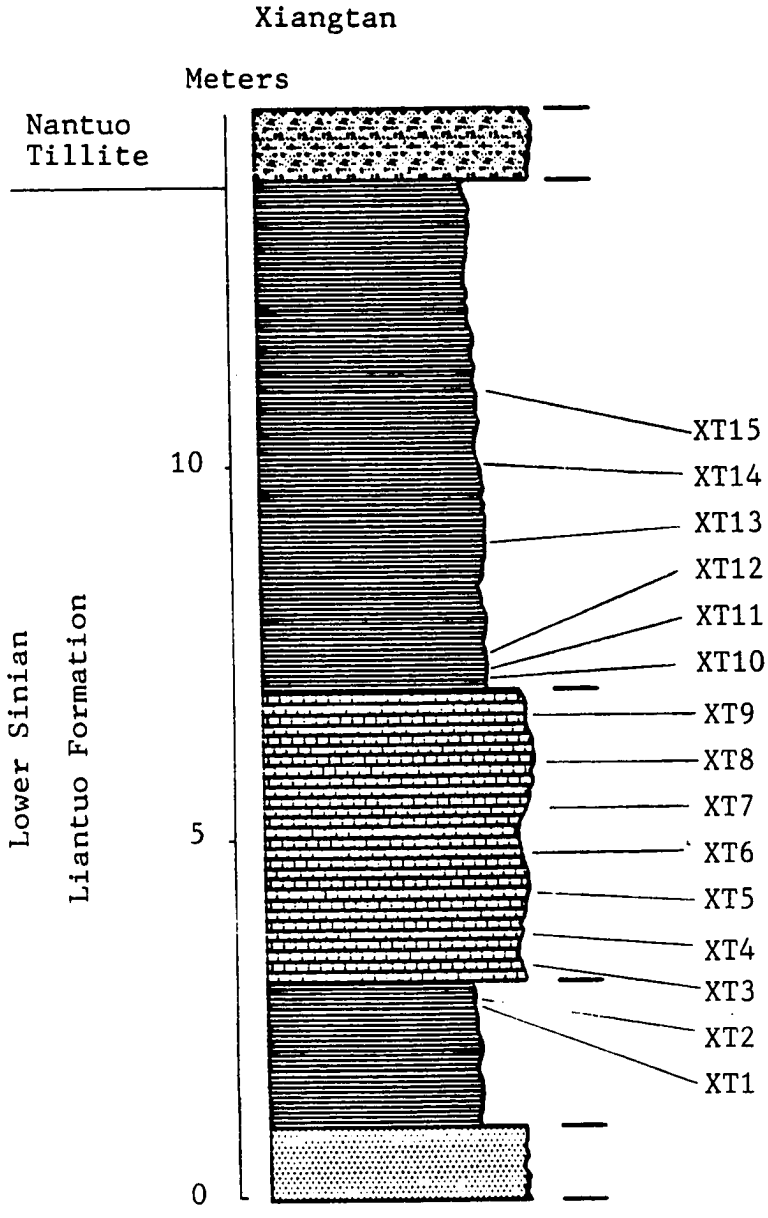

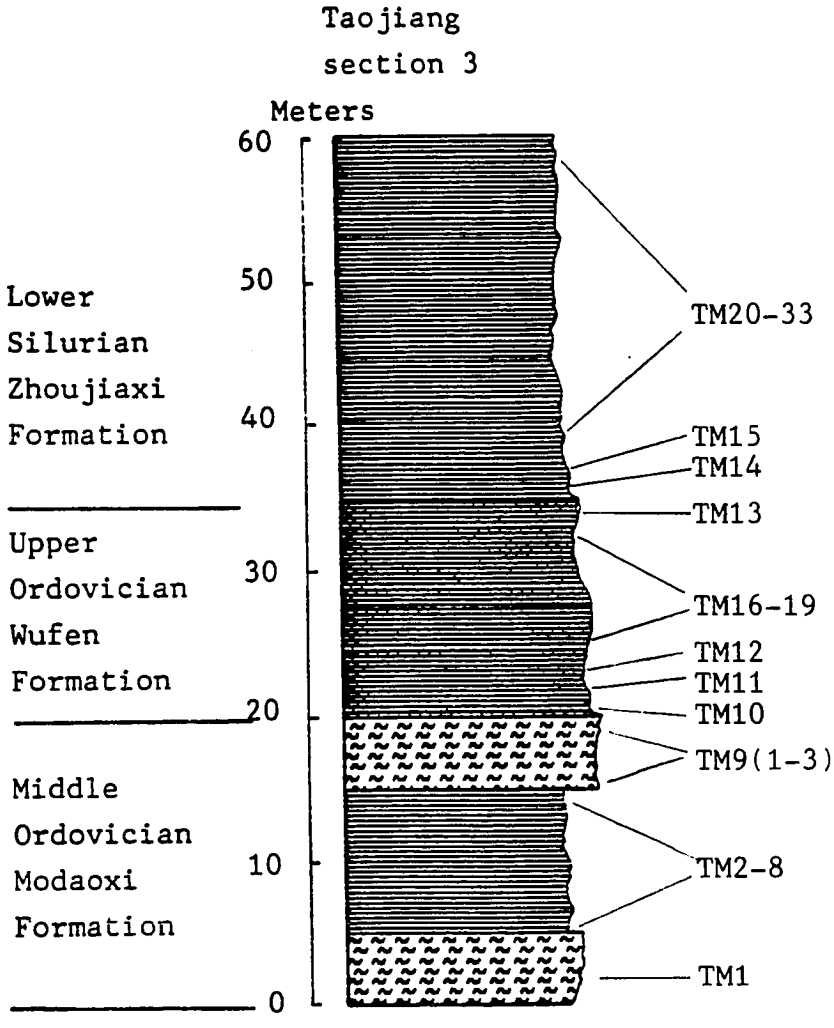

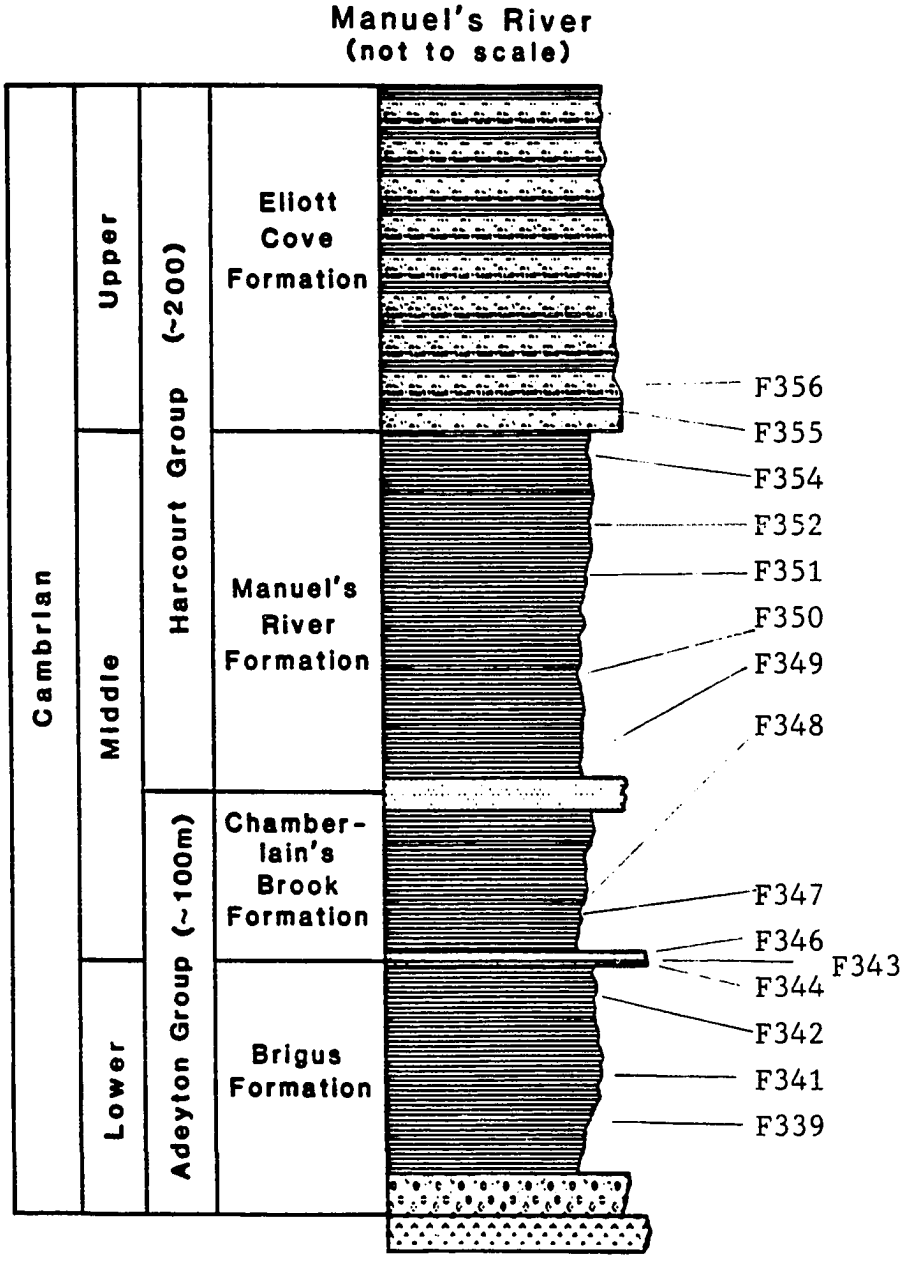

APPENDIX C

TOC-S-Fe DATA OF SAMPLES FROM THIS STUDY

Table 13. C-S-Fe data og the Taojiang Manganese Deposit (section 1), China

SAMPLE#	CARBONATE%	RESIDUE%	TOTAL C%	OC%	SS%	Fe total% acid	Fe++ % acid
DL1	2.20	97.80	0.65	0.60	0.09	1.87	1.81
DL2	29.17	70.83	2.58	0.52	0.08	1.28	0.53
DL3	14.75	85.24	1.06	0.72	0.22	2.33	1.15
DL4	63.34	35.66	0.84	0.79	0.12	3.85	2.14
DL5	55.88	44.12	7.23	0.93	0.10	1.07	0.27
DL6	9.52	90.48	3.15	3.00	2.00	2.50	0.62
DL7	4.55	95.54	4.26	4.00	2.09	1.62	1.48
DL7'	25.70	74.28	4.26	4.10	3.96	1.62	0.50
DL8	7.35	92.65	4.40	3.82	1.45	1.25	0.43
DL9	0.00	100.00	4.30	4.30	2.37	0.84	0.50
DL10	4.00	96.00	0.76	0.63	0.51	1.21	0.39
DL12	7.46	92.54	2.52	2.09	1.56	1.31	0.16
DL13	67.50	32.50	8.18	0.42	0.28	0.69	0.52
DL14	66.07	33.93	8.06	0.34	0.15	2.10	0.95
DL15	3.77	96.23	3.71	2.57	3.28	0.54	0.04
DL16	76.12	23.88	9.22	0.32	0.47	0.67	0.23
DL17	72.55	27.45	8.90	0.39	0.06	0.88	0.47
DL18A	41.86	58.41	2.78	0.44	0.51	2.03	1.25
DL18B	86.36	13.64	9.27	0.46	1.00	1.99	1.13
DL19	51.35	48.65	5.70	0.75	0.21	3.62	1.66
DL20	68.35	31.65	7.00	0.71	0.13	4.48	3.19
DL21	75.61	24.39	7.61	0.76	0.12	2.58	1.49
DL22A	0.00	100.00	0.87	0.87	0.06	2.46	1.58
DL22B	13.04	86.96	1.54	0.42	0.05	3.50	1.54
DL23	3.40	96.60	0.93	0.42	0.42	1.20	0.08
DL24	8.57	91.43	1.00	0.53	0.14	2.73	2.41

Table 14. C-S-Fe data of the Taojiang Manganese Deposit (section 2), China

SAMPLE#	CARBONATE%	RESIDUE%	TOTAL C%	OC%	SS%	Fe total% acid	Fe++ % acid
NS1	77.55	22.45	9.94	0.93	0.04	0.25	0.03
NS2	11.11	88.89	3.25	2.72	1.86	1.55	0.57
NS3	78.75	21.43	8.71	0.39	0.11	0.68	0.22
NS4	41.56	58.44	4.09	0.74	1.15	2.67	2.01
NS5	89.74	10.26	8.89	0.15	0.05	0.54	0.13
NS6	70.21	29.79	7.36	0.33	0.06	1.01	0.62
NS7	34.42	65.58	2.44	0.27	0.06	3.10	1.86
NS8	8.00	92.00	1.14	0.49	0.05	1.98	1.47
NS9A	2.08	97.92	1.43	1.19	0.41	1.74	0.58
NS9B	50.49	49.51	5.35	0.31	0.19	2.23	0.99
NS10	54.35	45.65	5.42	1.12	0.68	1.43	0.57
NS11	17.74	82.26	2.70	0.58	0.13	1.66	0.57
NS12	76.47	23.53	8.53	0.40	0.06	0.42	0.18
NS13	74.51	25.49	8.90	0.58	0.05	1.39	0.80

Table 15. C-S-Fe data of the Taojiang Manganese Deposit (section 3), China

SAMPLE#	CARBONATE%	RESIDUE%	TOTAL C%	OC%	SS%	Fe total% acid	Fe++ % acid
TM1	7.84	92.16	0.93	0.67	0.03	4.38	2.29
TM2	3.33	96.67	4.56	4.29	0.04	0.90	0.68
TM3	5.26	94.74	4.90	4.70	0.14	0.54	0.27
TM4	0.00	100.00	4.69	4.69	0.17	0.29	0.09
TM5	0.00	100.00	4.56	4.56	0.08	0.21	0.12
TM6	0.00	100.00	1.63	1.63	0.07	1.11	0.25
TM7	0.00	100.00	1.01	1.01	0.05	1.63	0.08
TM8	5.60	94.40	0.83	0.78	0.01	4.24	2.10
TM9A	0.00	100.00	0.37	0.37	0.02	0.85	0.08
TM9B	0.00	100.00	0.48	0.48	0.02	3.23	0.41
TM9C	0.00	100.00	0.57	0.57	0.03	3.06	0.01
TM10	0.00	100.00	1.26	1.26	0.03	3.87	0.20
TM11	0.00	100.00	0.67	0.67	0.11	0.11	0.08
TM12	0.00	100.00	1.66	1.66	0.04	1.70	0.18
TM14	0.00	100.00	4.34	4.34	0.04	0.28	0.09
TM15	10.91	89.09	4.61	4.34	0.07	3.46	1.54
TM16	0.00	100.00	1.35	1.35	0.29	0.42	0.03
TM17	0.00	100.00	0.99	0.99	0.05	0.34	0.00
TM18	11.43	88.57	2.07	0.97	0.08	0.63	0.05
TML9	0.00	100.00	0.67	0.67	0.05	0.37	0.24
TM20	0.00	100.00	5.51	5.51	0.06	0.19	0.01
TM21	0.00	100.00	0.93	0.93			
TM22	11.63	88.37	4.91	4.21	0.06	0.29	0.06
TM23	0.00	100.00	4.68	4.68	0.06	0.25	0.00
TM24	10.00	90.00	4.68	4.14	0.09	0.19	0.02
TM25	12.50	87.50	4.60	4.23	0.04	0.27	0.04
TM26	28.13	71.87	4.95	3.84	0.04	0.64	0.16
TM27	10.64	89.36	4.39	3.67	0.48	0.37	0.06
TM28	7.13	92.86	4.42	3.59	1.56	0.73	0.16
TM29	8.82	91.18	3.78	3.23	1.46	0.99	0.14
TM30	0.00	100.00	4.99	4.98	0.16	0.35	0.11
TM31	7.69	92.31	3.78	3.67	0.86	1.07	0.43
TM32	0.00	100.00	0.50	0.50		0.17	0.00
TM33	17.24	82.76	1.56	1.01	0.05	3.98	0.86

Table 16. C-S-Fe data of the Xiangtan manganese deposit, China

SAMPLE#	CARBONATE%	RESIDUE%	TOTAL C%	OC%	SS%	Fe total% acid	Fe++ % acid
XT1	47.54	52.46	5.77	1.11	1.75	0.72	0.66
XT2	26.56	73.44	3.59	1.13	3.25	1.23	0.72
XT3	3.57	96.43	4.88	4.33	7.98	2.33	0.60
XT4	48.28	51.72	4.50	2.53	3.47	1.57	0.28
XT5	72.13	28.87	6.38	0.75	0.45	1.19	0.47
XT7	62.96	37.04	8.28	3.34	2.47	2.02	0.67
XT8	64.47	35.53	7.97	1.83	1.16	1.15	0.16
XT9	47.27	52.73	6.13	1.66	1.52	1.03	0.20
XT10	9.43	90.57	4.96	4.80	2.57	0.91	0.14
XT11	66.67	33.33	11.66	4.63	0.62	0.30	0.05
XT12	4.48	95.52	6.29	5.41	2.78	0.33	0.04
XT13	6.98	93.02	3.70	3.60	2.31	1.04	0.13
XT15	8.14	91.86	3.42	3.30	1.69	1.13	0.13

Table 17. C-S-Fe data of the Molango Manganese Deposit, Mexico

SAMPLE#	CARBONATE%	RESIDUE%	TOTAL C%	OC%	SS%	Fe total% acid	Fe++ % acid
T1-24.9	40.29	59.71	6.21	1.36	2.54	0.69	0.47
T1-20.4	27.14	72.86	5.29	2.23	3.01	1.20	0.37
T1-20.3	35.71	64.29	5.35	2.27	3.79	1.05	0.15
T1-20.35	25.00	75.00	1.99	0.88	8.68	2.80	0.41
T1-19.0	69.77	30.23	7.65	1.04	2.87	0.78	0.21
T1-17.1	51.35	48.65	5.86	1.77	3.06	1.29	0.31
T1-13.8	41.46	58.54	5.55	1.45	2.73	0.89	0.33
T1-7.2	31.25	68.75	5.47	2.01	3.17	0.88	0.31
T1-3.9	45.45	54.55	6.11	1.54	3.48	0.66	0.27
T1-0.1	40.82	59.18	6.02	2.11	5.78	0.62	0.12
T1+0.0	39.29	60.71	6.87	2.43	9.27	1.17	0.13
T1+0.1	79.59	20.41	10.19	0.94	0.88	0.30	0.15
T1+0.45	72.00	28.00	6.01	0.31	5.93	4.54	1.30
T1+0.5	82.35	17.65	11.06	1.13	0.11	5.81	0.80
T1+1.5	86.05	13.95	8.85	0.54	1.02	0.95	0.42
T1+2.0	71.93	28.07	7.73	1.06	0.05	11.12	5.56
T1+2.5	76.09	23.91	6.58	0.96	0.10	4.16	2.29
T1+3.0	88.57	11.43	7.26	0.46	0.36	4.43	1.73
T1+3.4	77.14	22.86	7.35	0.93	0.12	5.69	2.41
T1+4.0	79.07	20.93	7.03	0.79	0.38	5.48	2.84
T1+4.5	75.86	24.14	7.25	1.04	0.10	8.42	3.30
T1+5.9	85.11	14.89	7.55	0.66	0.15	4.31	1.50
T1+8.5	93.85	6.15	9.66	0.67	4.65	0.90	0.25
T1+8.9	74.58	25.42	9.00	0.63	0.38	0.91	0.70
T1+12.5	79.16	20.84	8.46	0.92	0.95	3.56	2.04
T1+19	66.25	33.75	8.24	0.97	0.94	0.88	0.08
T1+21.7	66.66	33.34	7.87	0.44	0.54	0.70	0.17
T1+22.2	21.80	78.20	2.74	0.88	0.45	0.83	0.12
T1+22.3	60.29	39.71	7.37	0.73	3.29	1.81	0.20
T1+27.5	6.84	93.16	1.67	0.90	1.38	0.51	0.05
T1+38.7	70.50	29.50	8.38	1.01	1.26	0.51	0.07
T1+45.3	80.14	19.86	10.36	0.91	0.44	0.20	0.04
T1+58.4	34.16	65.84	5.90	3.16	2.88	0.26	0.01
T1+71.5	59.57	40.43	8.26	1.24	2.09	0.41	0.02
T1+87.9	56.86	43.14	8.18	1.39	2.55	0.36	0.05
T1+101	53.98	46.02	7.05	1.74	2.75	0.56	0.04
T1+102.6	64.19	35.18	7.28	3.32	1.75	0.51	0.01
T1+124	66.66	33.34	8.41	0.89	2.54	0.41	0.17
T1+135	54.30	45.70	7.50	2.39	1.69	2.06	0.22
T1+151.8	70.49	29.51	9.12	1.81	1.38	0.72	0.05
T1+161.5	90.10	9.90	10.36	0.25	0.15	0.23	0.04
T1+130.6	67.57	32.43	7.55	0.99	1.31	0.38	0.02
T1+140.6	63.95	36.05	7.70	0.28	0.29	0.40	0.05
T1+171	79.07	20.93	8.54	0.43	0.24	0.32	0.05
T1+223.5	79.41	20.86	9.66	0.50	0.36	9.43	4.35

Table 18. C-S-Fe data of the Manuel's River Prospect, Noewfoundland, Canada

SAMPLE#	CARBONATE%	RESIDUE%	TOTAL C%	OC%	SS%	Fe total% acid	Fe++ % acid
F339	4.17	95.83	0.42	0.36	0.06	3.78	1.48
F341	11.43	88.57	0.95	0.32	0.08	3.68	1.27
F342	20.00	80.00	1.46	0.49	0.05	6.20	5.72
F343 red	88.45	11.55	8.02	0.21	0.04	3.56	1.54
F343 frey	30.00	70.00	2.70	0.33	0.03	1.62	0.06
F344	9.31	90.69	0.68	0.55	0.04	5.93	4.91
F346 red	77.12	22.88	6.85	0.25	0.02	2.49	0.27
F347 red	45.48	54.52	4.20	0.34	0.05	3.21	0.70
F347 grey	55.82	44.18	4.50	0.33	0.11	6.57	3.12
F348	17.07	82.93	0.92	0.80	0.05	6.59	2.43
F349	13.64	86.36	0.73	0.54	0.10	3.85	1.79
F350	14.28	85.72	1.67	1.11	0.14	4.36	1.34
F351	17.78	82.22	1.04	0.76	0.10	5.05	2.34
F352	15.38	84.62	0.59	0.37	0.08	5.39	0.51
F354	39.06	60.94	4.09	2.19	1.41	4.64	2.79
F355	0.00	100.00	0.33	0.33	0.23	2.49	1.87
F356	7.50	92.50	0.57	0.50	1.84	2.05	0.51

APPENDIX D

X-RAY DIFFRACTION PATTERNS OF SAMPLES

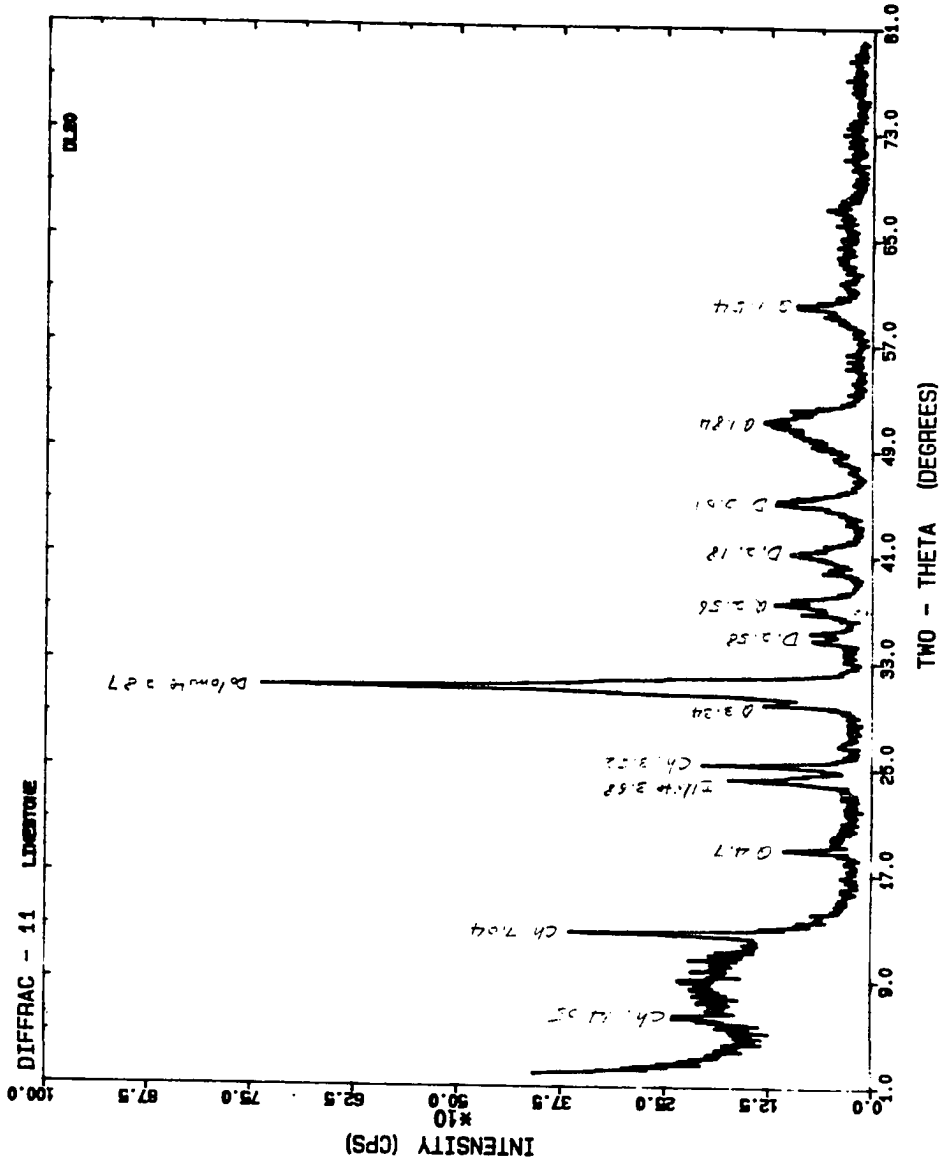

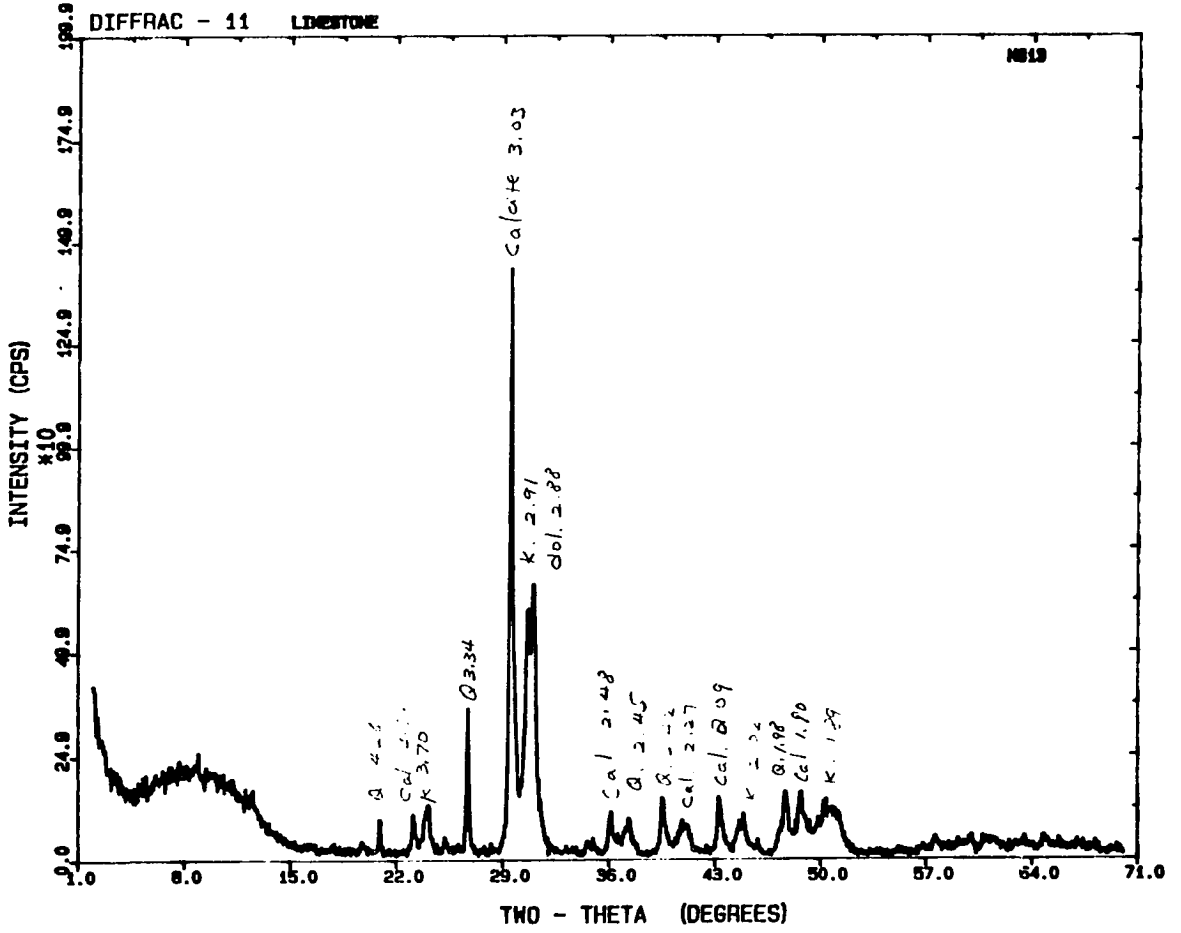

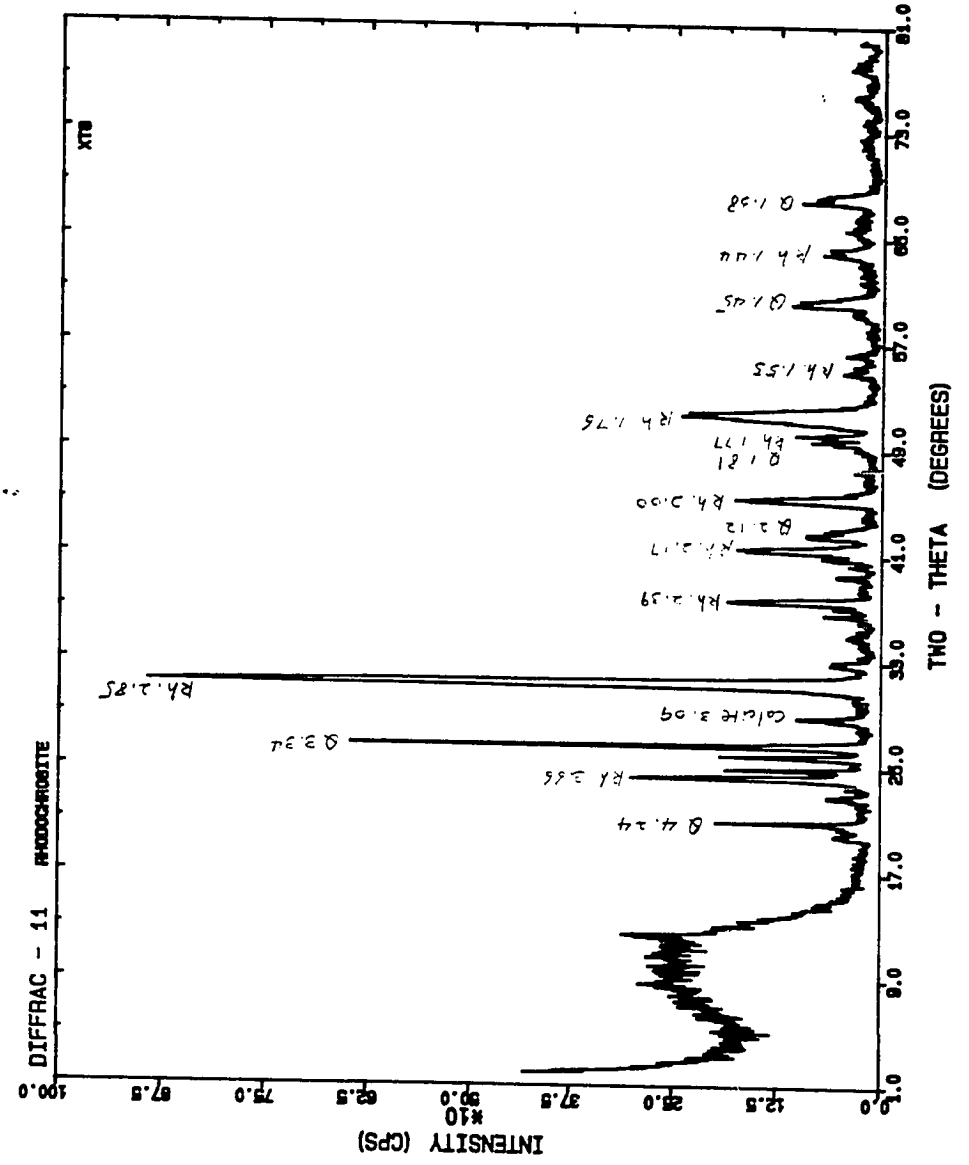

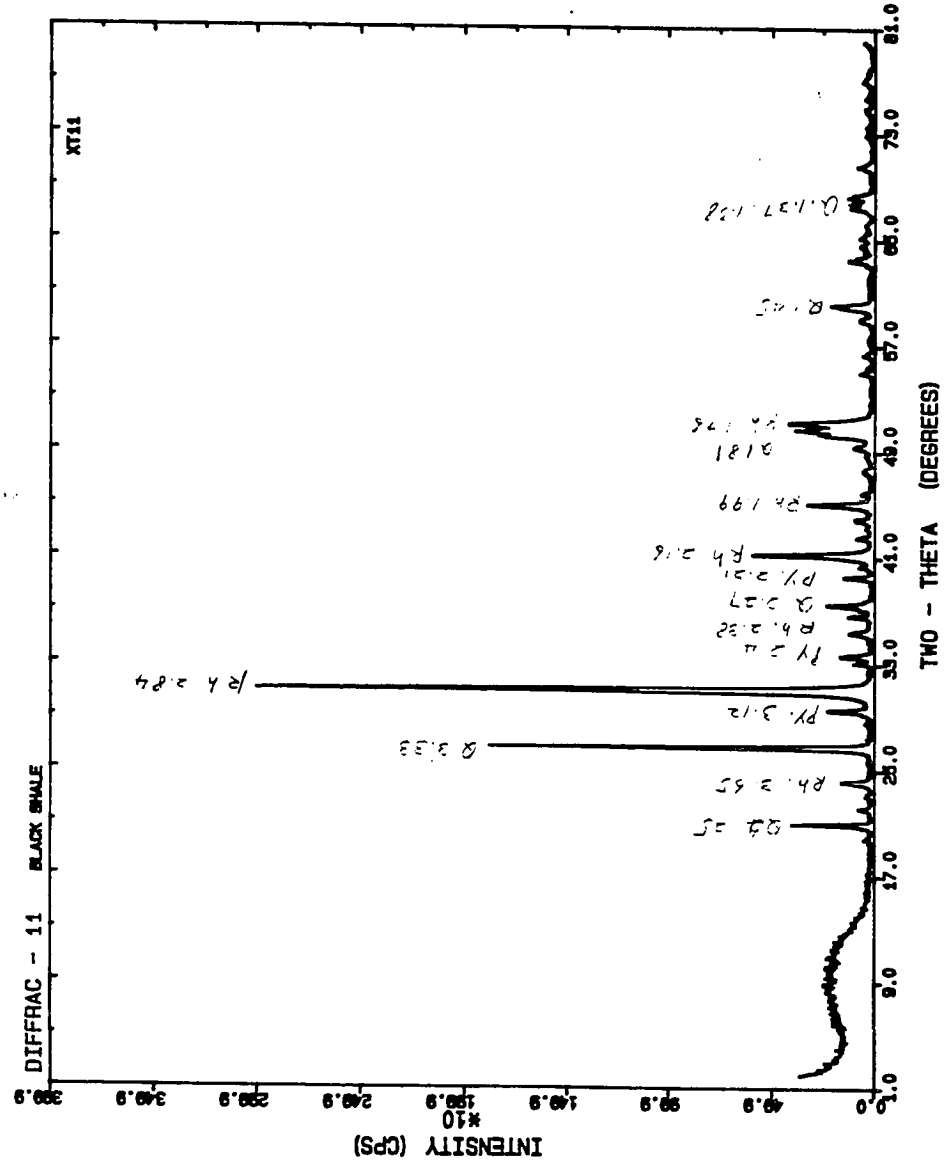

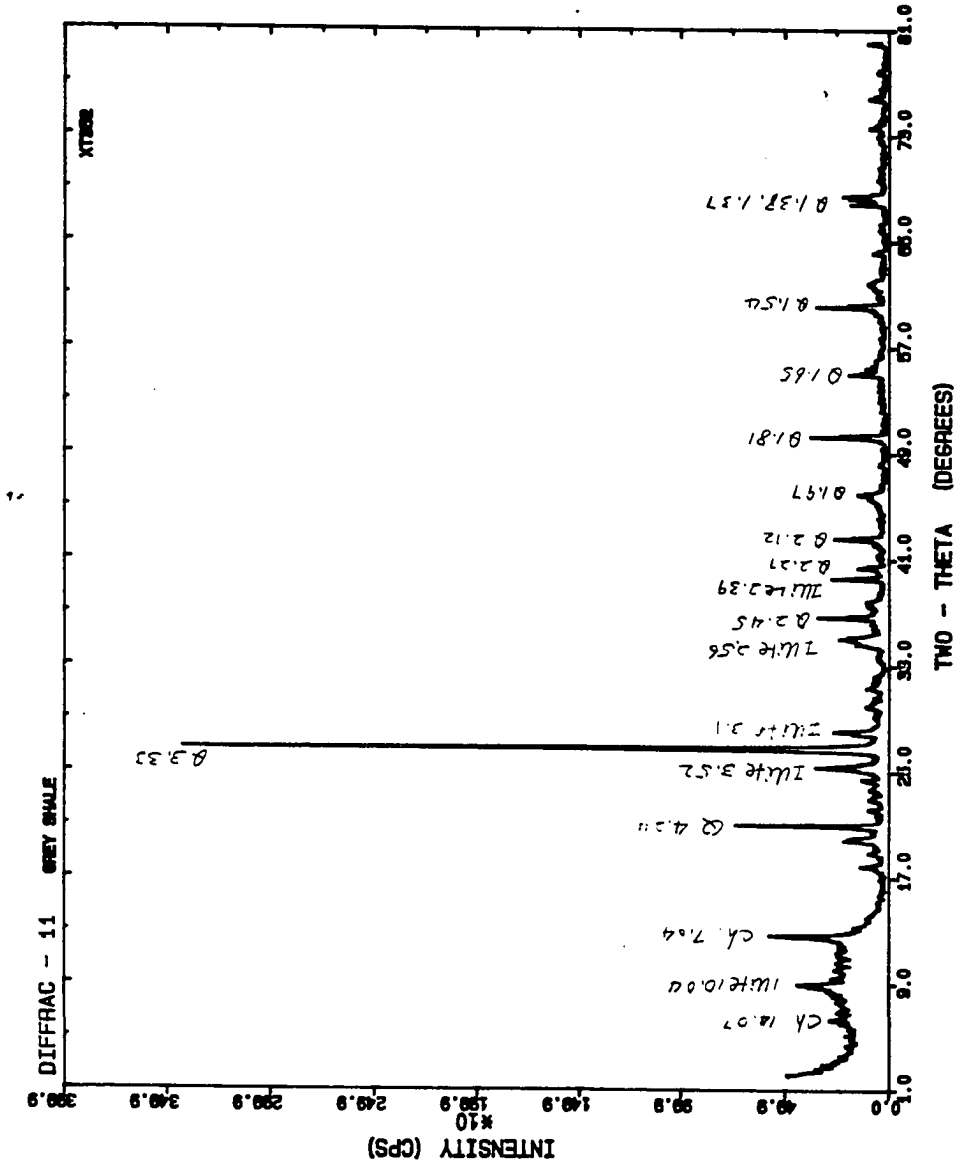

VITA

Tiebing Liu, was born in Beijing, People's Republic of China on November 2, 1950. He received his middle school education in Beijing. During the "Culture Revolution", he worked in a small country village, North China for five years and finished basic high school courses by himself.

In the Fall of 1973, Tiebing enrolled in the Nanking University and received the Bachelor of Science degree in the fields of geology. His bachelor thesis dealt with the stratigraphy and petrology of Precambrian Iron Formation in Shanxi Province, Northwest China.

In September, 1978, he enrolled in the graduate program at the Science and Technology of University of China and received the Master of Science degree in October, 1981. His thesis research was a study of a siderite ore deposit at Hubei Province, South China.

Tiebing Liu entered the Ph.D. program at the University of Cincinnati during the Fall of 1984.

At present he is a assistant professor in the Branch of sedimentology at the Institute of Geology, Academia Sinica, Beijing, People's Republic of China.

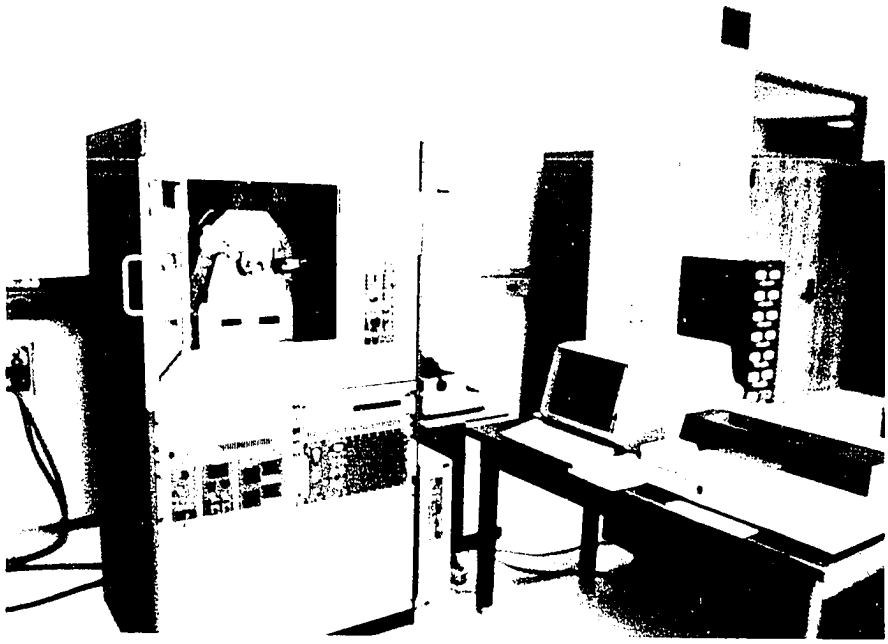

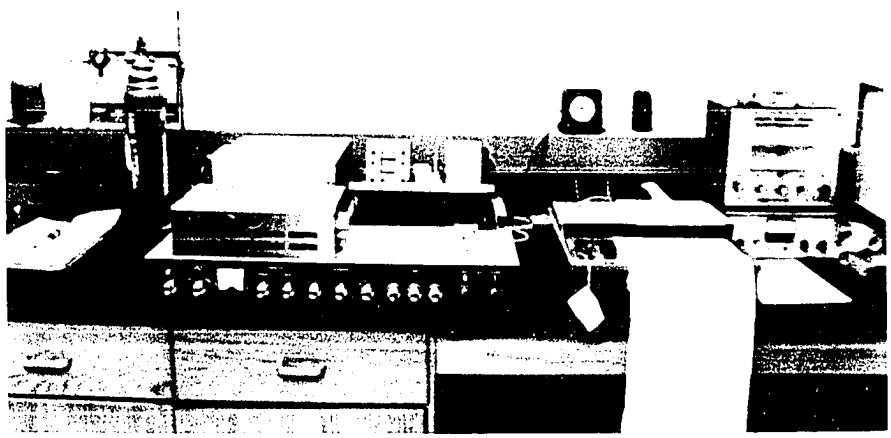

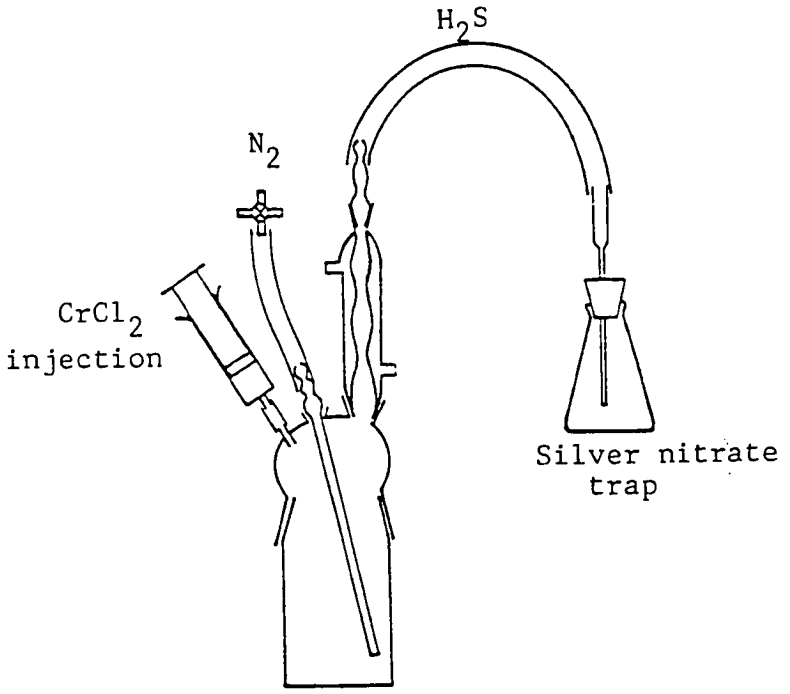

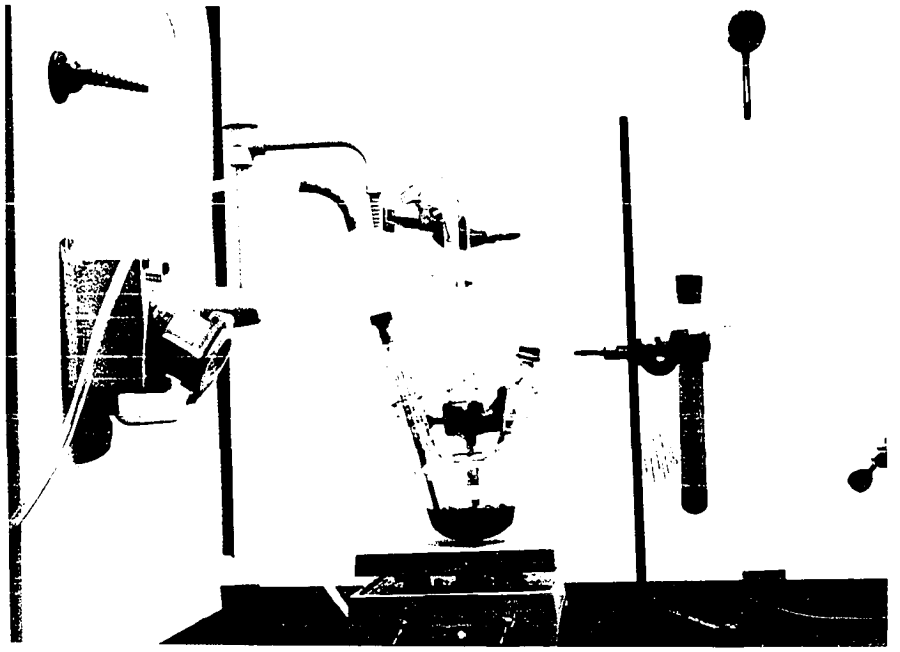

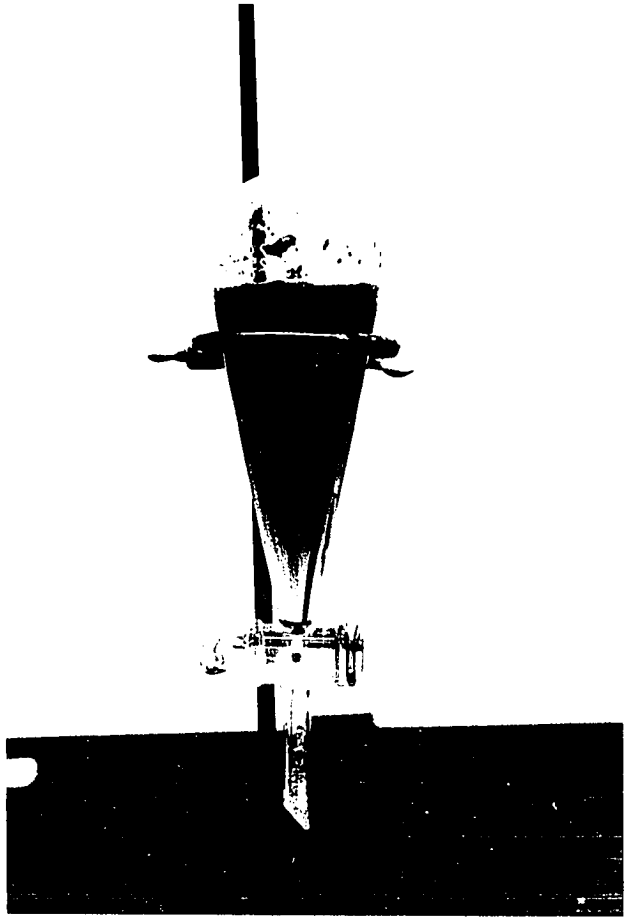

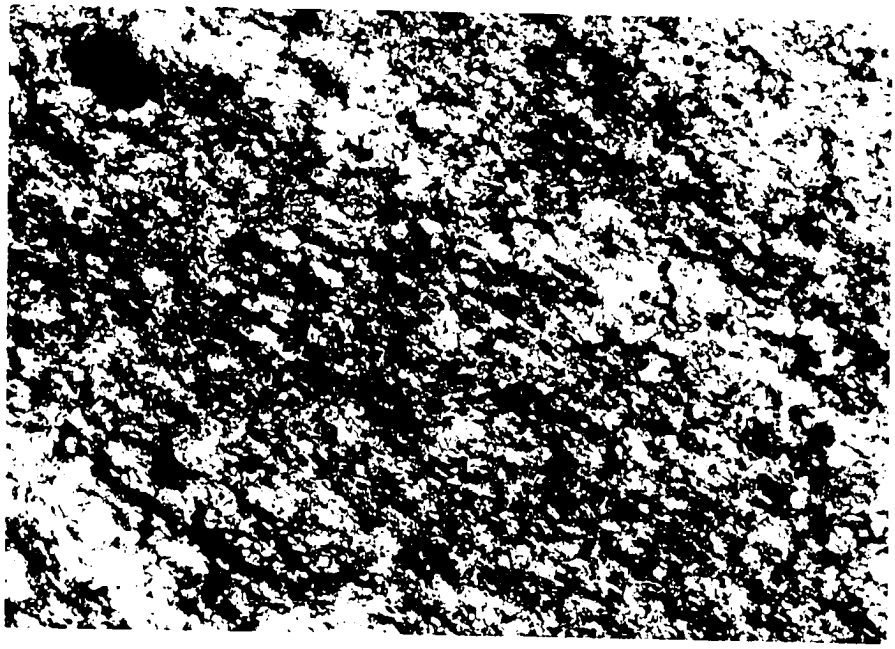

0.2mm

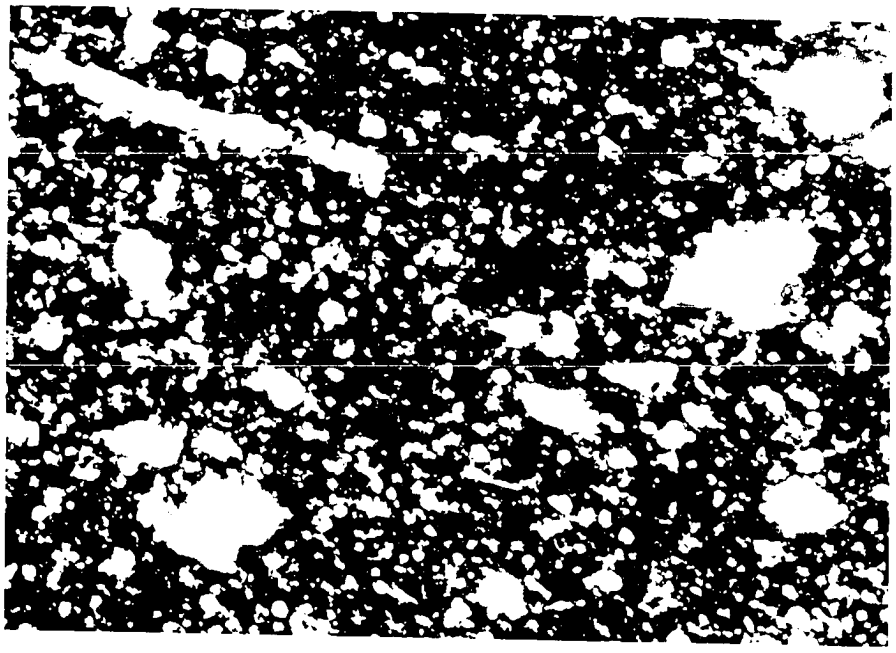

0.2mm

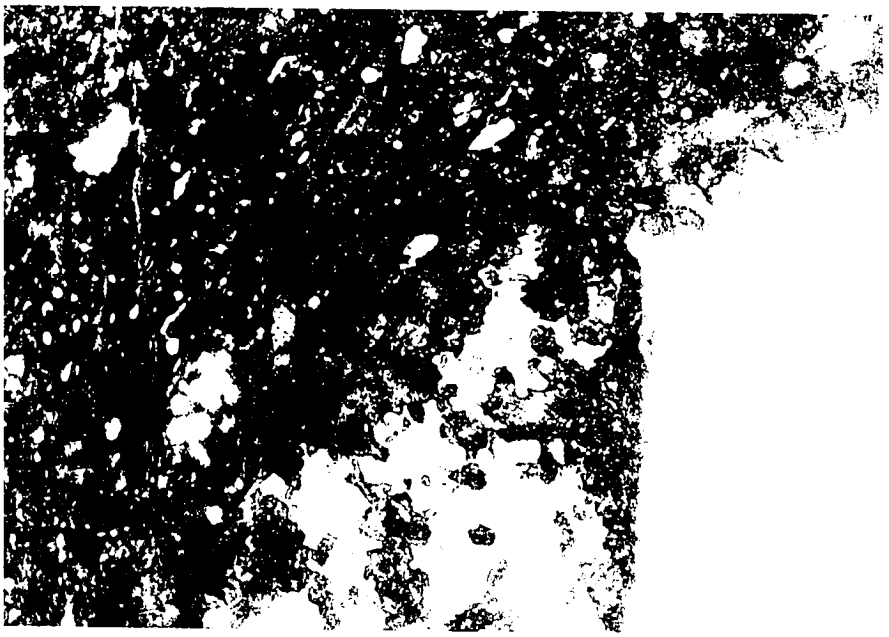

0.2mm

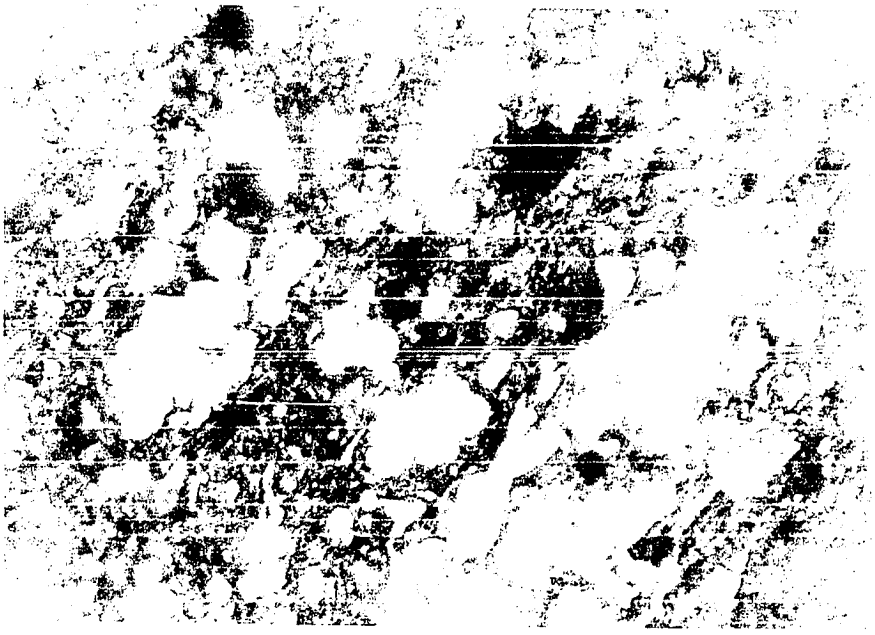

0.2mm

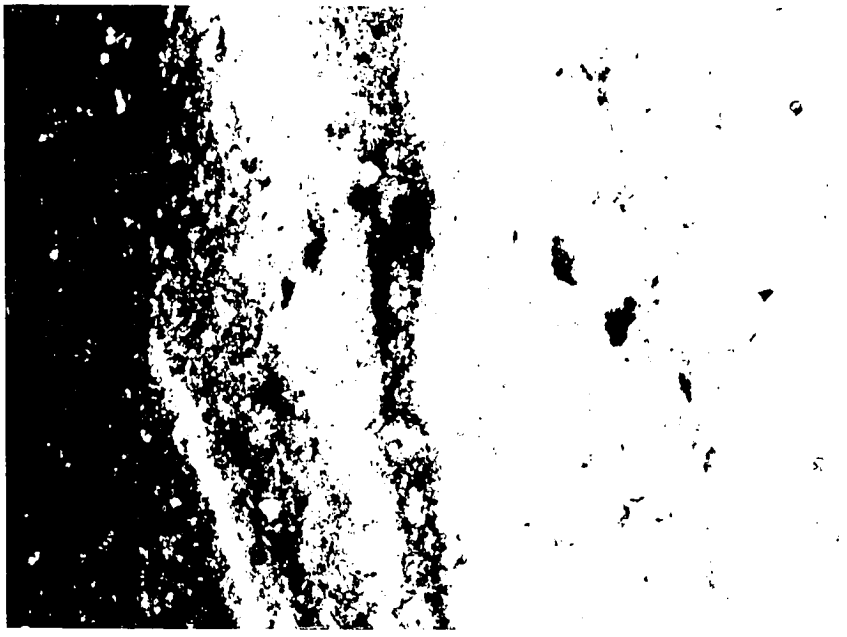

0.2mm

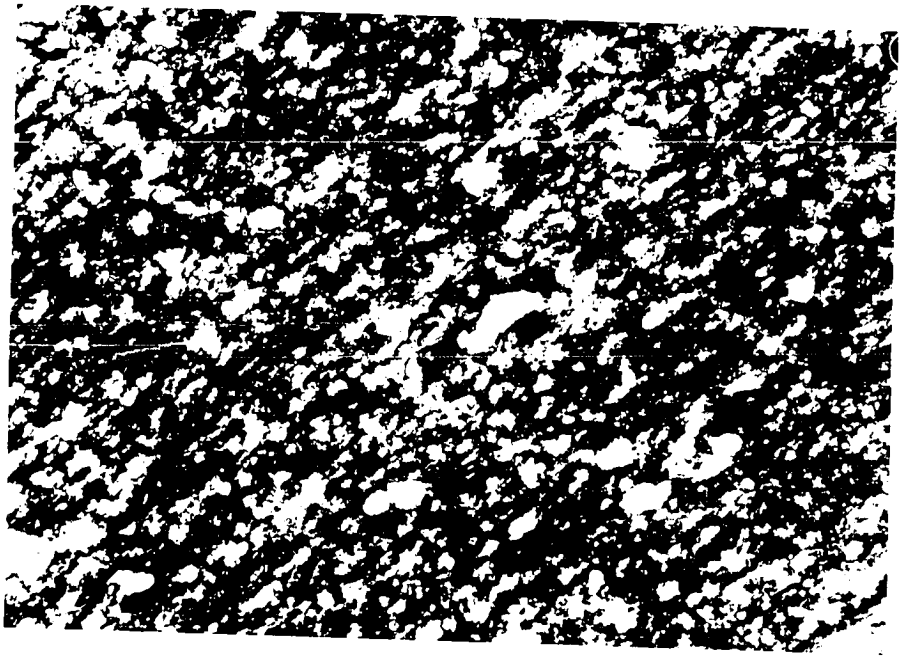

0.2mm

0.2mm

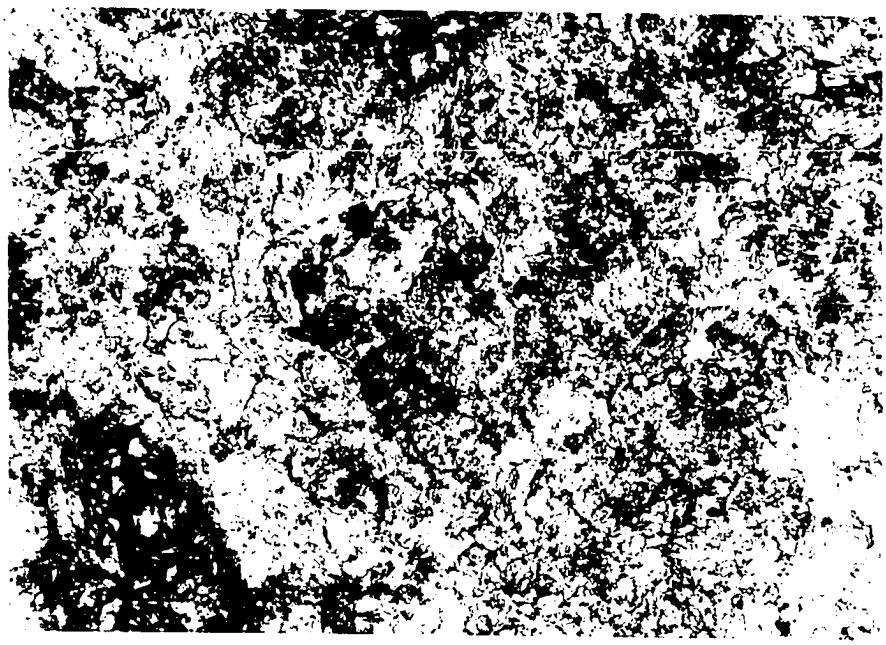

0.2mm

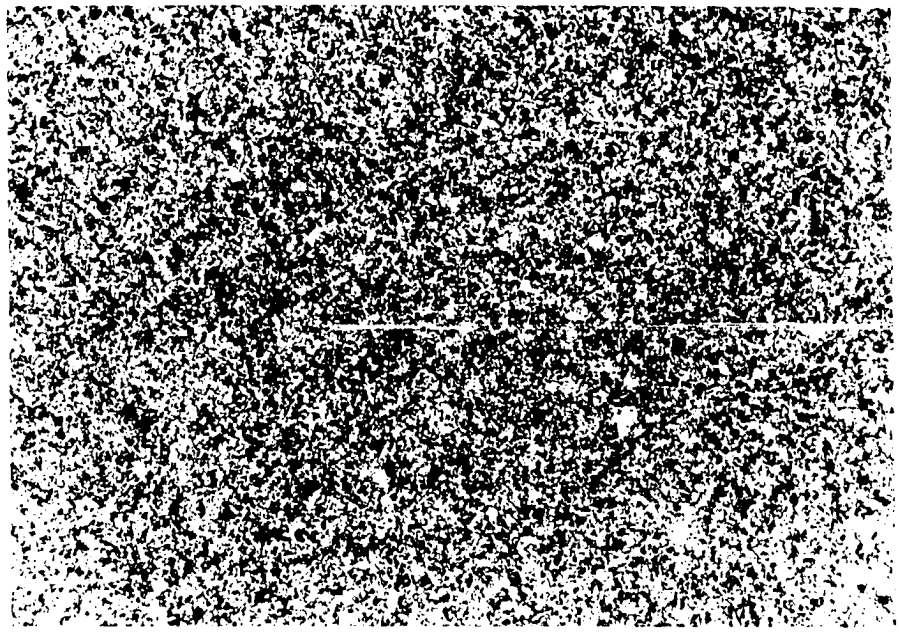

0.2mm

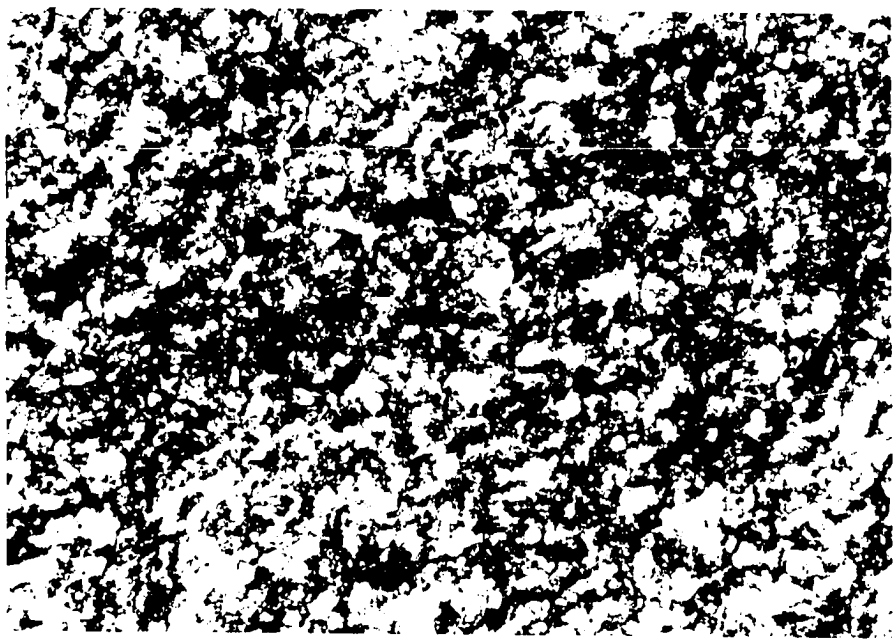

0.2mm

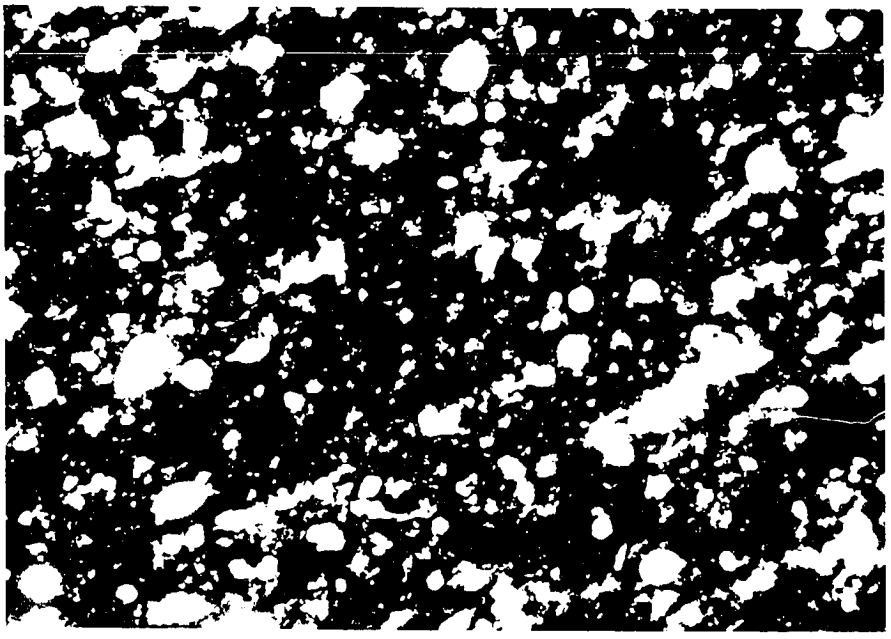

0.2mm

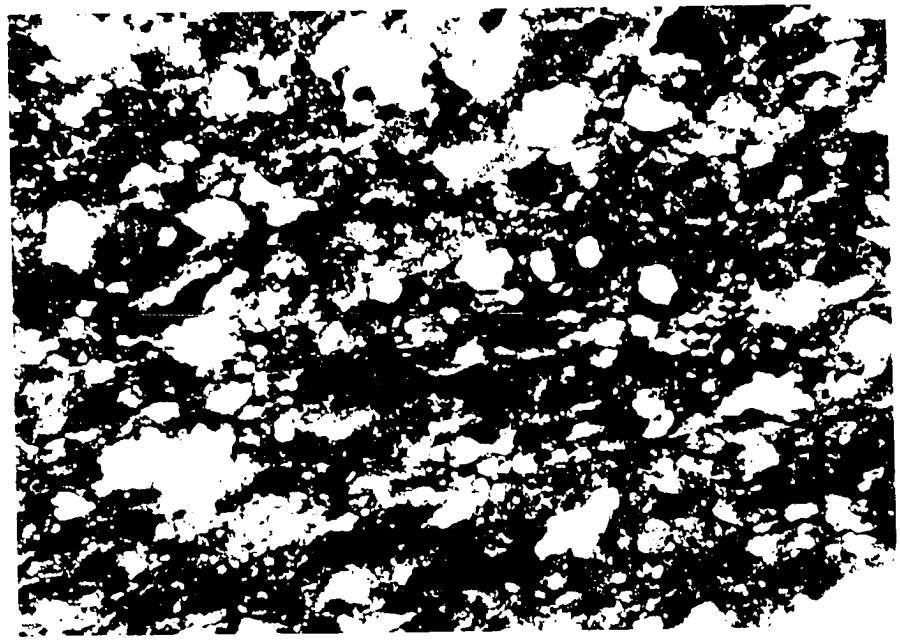

0.2mm

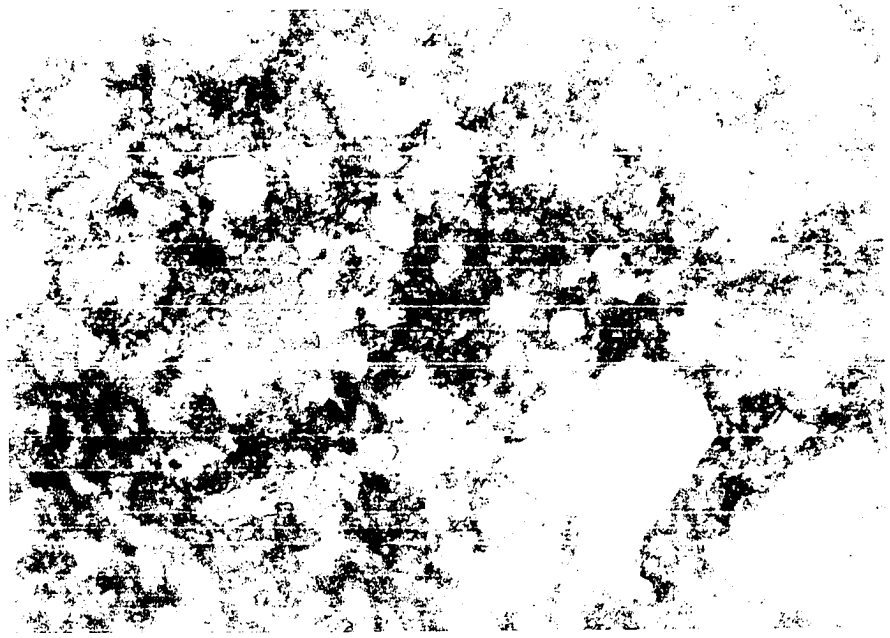

0.04mm

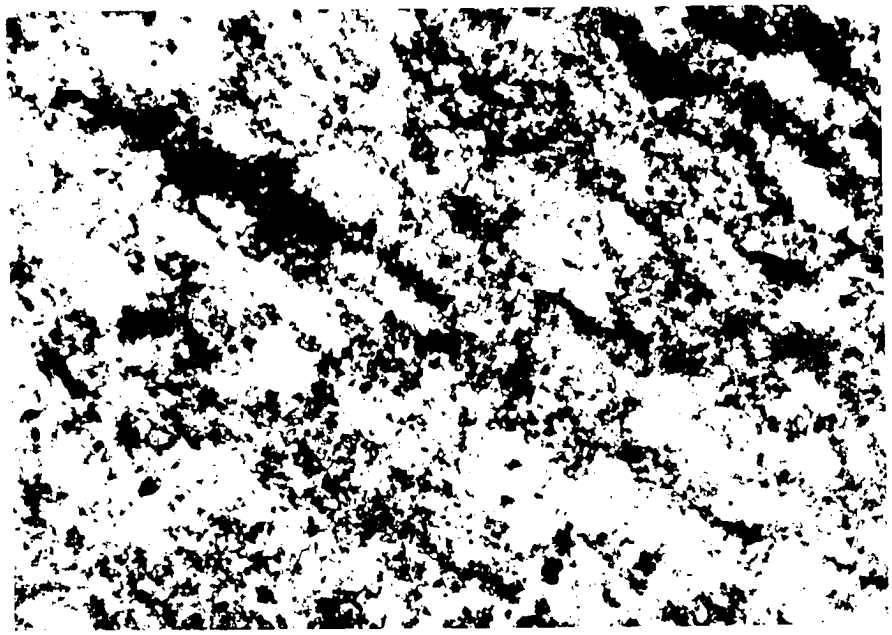

0.2mm

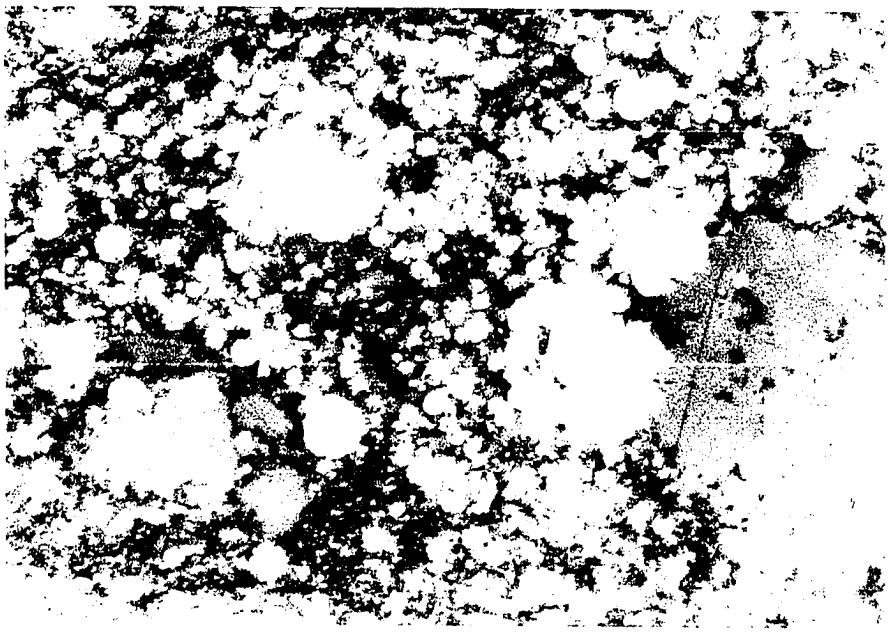

0.04mm

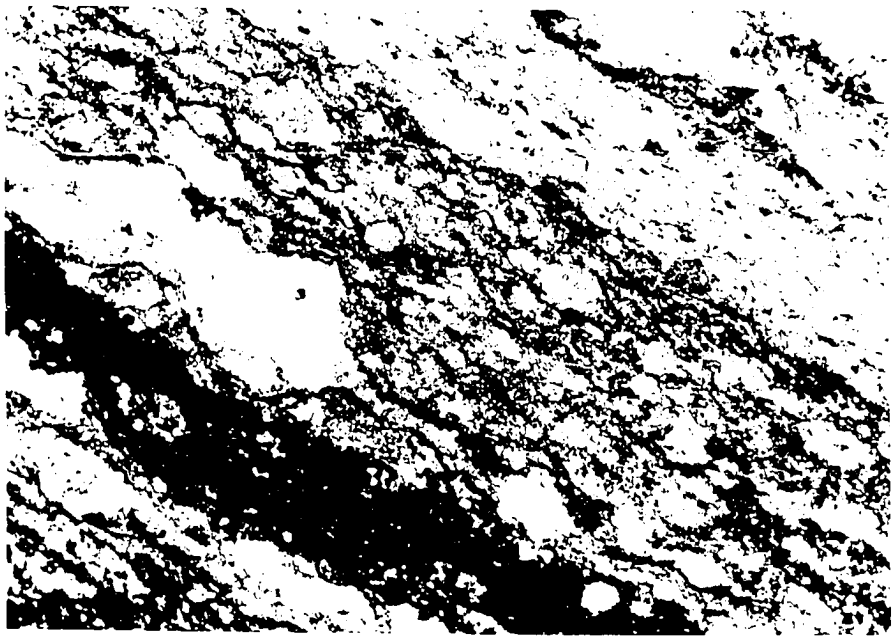

0.2mm

0.2mm

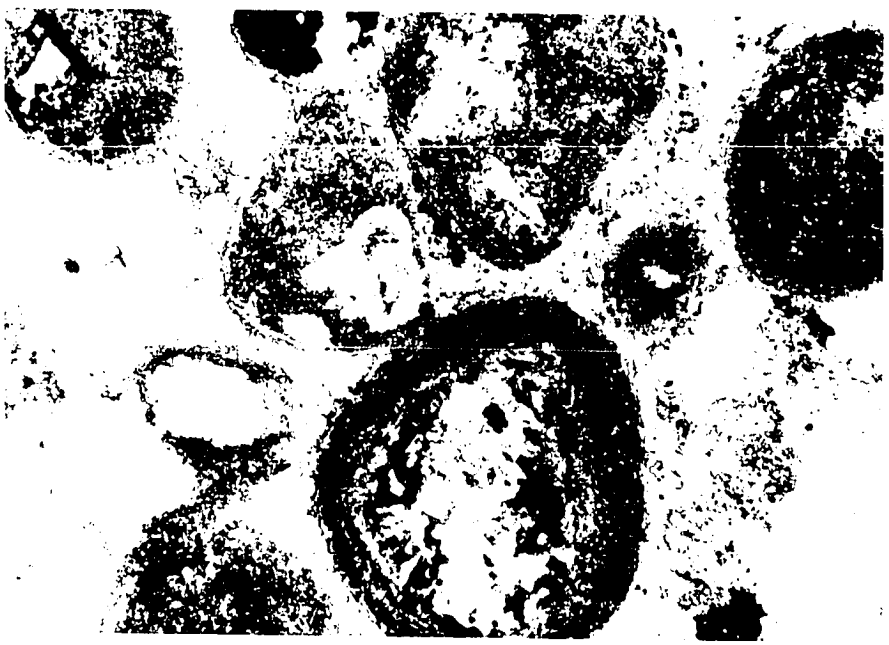

0.2mm

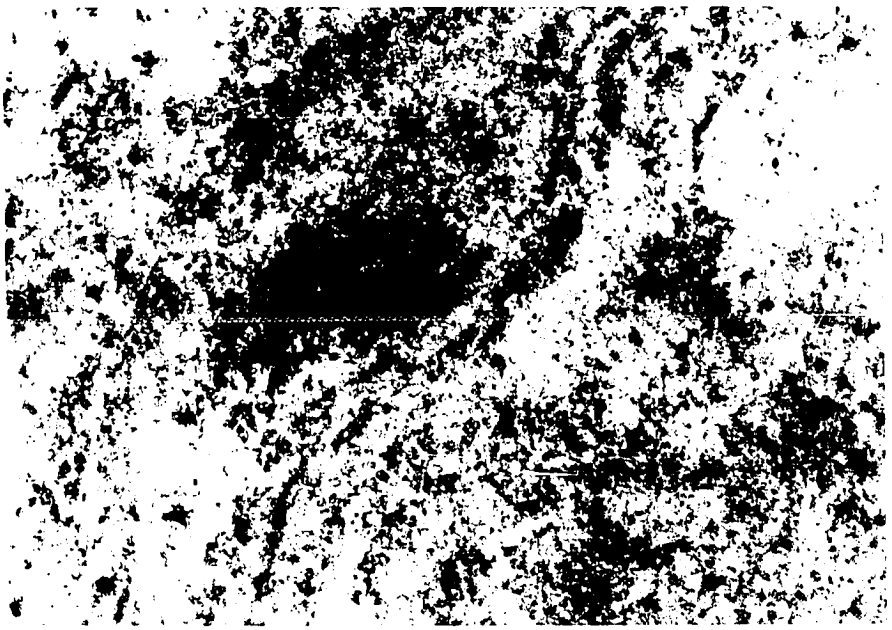

0.2mm

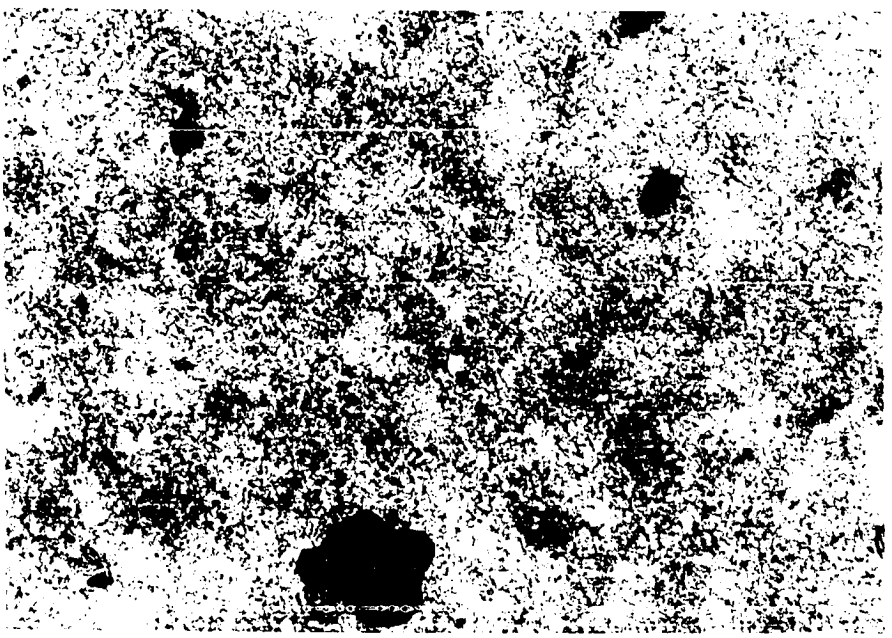

0.2mm